Aus der
Klinik und Poliklinik für Allgemein-, Viszeral-, Thorax- und Gefäßchirurgie
des Universitätsklinikums Bonn
Direktor: Prof. Dr. med. Jörg C. Kalff

Diagnostische, prognostische und therapeutische Bedeutung der Tumormutationslandschaft und des umgebenden Tumormikromilieus im duktalen Adenokarzinom des Pankreas

Habilitationsschrift
zur
Erlangung der venia legendi
der Hohen Medizinischen Fakultät
der Rheinischen Friedrich-Wilhelm-Universität
für das Lehrgebiet
„Chirurgie“

vorgelegt von
Dr. med. Alexander Semaan
wissenschaftlicher Assistent
an der Rheinischen Friedrich-Wilhelms-Universität Bonn

Bonn 2022

Datum des Habilitationskolloquiums
27. Januar 2022

TO MY PARENTS
for raising me to believe that
anything was possible

TO MY WIFE
for making everything possible

AND TO MY CHILDREN
for opening my eyes
to what is *possible*

Inhaltsverzeichnis

Auflistung der publizierten Arbeiten, die der Schrift zu Grunde liegen 1

1. Einleitung 2

2. Ergebnisteil 14

2.1: Diagnostic value of digital droplet polymerase chain reaction and digital multiplexed detection of single nucleotide variants in pancreatic cytology specimens collected by EUS-guided FNA 14

2.2: Defining the Comprehensive Genomic Landscapes of Pancreatic Ductal Adenocarcinoma Using Real World Endoscopic Aspiration Samples 16

2.3: Characterization of circulating tumor cell phenotypes identifies a partial-EMT subpopulation for clinical stratification of pancreatic cancer 19

2.4: Single-Cell Transcriptomics of Pancreatic Cancer Precursors Demonstrates Epithelial and Microenvironmental Heterogeneity as an Early Event in Neoplastic Progression 21

3. Diskussion 24

4. Zusammenfassung 32

5. Überlappung aufgrund kumulativer Arbeiten 34

6. Bibliographie 35

7. Danksagung 44

8. Erklärung 45

9. Vollständige Kopie der publizierten eigenen Arbeiten, die dem zusammenfassenden Text zu Grunde liegen 46

Auflistung der publizierten Arbeiten, die der Schrift zu Grunde liegen

I. Cazacu IM*, **Semaan A***, Stephens BM, Swartzlander DB, Guerrero PA, Singh BS, Cherciu Harbiyeli IF, Streata I, Popescu C, Saftoiu A, Roy-Chowdhuri S, Maitra A, Bhutani MS. Diagnostic value of digital droplet polymerase chain reaction and digital multiplexed detection of single nucleotide varients in pancreatic cytology specimens collected by EUS-guided FNA.
Gastrointestinal Endoscopy, 2021 May;93(5):1142-1151.e2, PMID: 33058885, doi: 10.1016/j.gie.2020.09.051, *equal contribution, Impact factor (6,8)

II. **Semaan A***, Bernard V*, Lee JJ*, Wong J, Huang J, Swartzlander DB, Stephens BM, Monberg ME, Weston BR, Bhutani MS, Chang K, Scheet PA, Maitra A, Jakubek YA, Guerrero PA: Defining the Comprehensive Genomic Landscapes of Pancreatic Ductal Adenocarcinoma Using Real World Endoscopic Aspiration Samples
Clinical Cancer Research, 2021;27:1082–93, PMID: 33188144, doi: 10.1158/1078-0432.CCR-20-2667, *equal contribution, Impact factor (10.1)

III. Bernard V*, **Semaan A***, Huang J, San Lucas A, Mulu F, Stephens B, Guerrero P, Kamyabi N, Sen S, Scheet P, Taniguchi CM, Tzeng M, Katz MH, Singhi AD, Maitra A, Alvarez HA: Single Cell Transcriptomics of Pancreatic Cancer Precursors Demonstrates Epithelial and Microenvironmental Heterogeneity as an Early Event in Neoplastic Progression
Clinical Cancer Research, 2019 April 1; 25 (7), 2194-2205, PMID: 30385653, doi: 10.1158/1078-0432.CCR-18-1955, *equal contribution, Impact factor (10.1)

IV. **Semaan A***, Bernard V*, Kim DU, Lee JJ, Huang J, Kamyabi N, Stephens BM, Qiao W, Varadhachary GR, Katz MH, Shen MU, San Lucas FA, Gascoyne P, Alvarez HA, Maitra A, Guerrero PA: Characterization of circulating tumor cell phenotypes identifies a partial-EMT subpopulation for clinical stratification of pancreatic cancer
British Journal of Cancer, 2021 March 30; Article in press, PMID: 33785875, doi: 10.1038/s41416-021-01350-9, *equal contribution, Impact factor (5.8)

1. Einleitung

Das Duktale Adenokarzinom des Pankreas (PDAC) zählt zu den aggressivsten Malignomen des Gastrointestinaltrakts und ist einer der wenigen soliden Tumore mit einer steigenden Inzidenz. Aktuell ist jeder vierte, krebsassoziierte Todesfall in den USA und Europa durch ein PDAC bedingt und es wird geschätzt, dass bis zum Jahr 2030 jeder zweite Krebspatient an dieser Entität versterben wird (Siegel et al., 2019), obwohl nur ca. 3 % der gesamten Tumorneuerkrankungen durch ein Pankreaskarzinom verursacht werden (Abbildung 1). Trotz intensiver Forschung in den letzten Dekaden haben Patienten mit PDAC eine fast unveränderte 5-Jahres-Überlebensrate von unter 10%. Ein Hauptproblem in der Behandlung ist die Tatsache, dass über 80% der Patienten erst in einem fortgeschrittenen Stadium mit inoperablem Primärtumor oder bereits vorhandenen Metastasen diagnostiziert werden (Ryan et al., 2014). Diese ist durch eine geringe klinische Symptomatik v.a. früher Tumorstadien bedingt. Zu möglichen klinischen Symptomen zählen dabei ein schmerzloser Ikterus, eine B-Symptomatik, eine exokrine bzw. endokrine Pankreasinsuffizienz sowie unspezifische abdominelle Beschwerden. Die Masse der Pankreastumore ist dabei im Pankreaskopf lokalisiert, wohingegen Tumore im Pankreasschwanz und -korpus seltener vorkommen.

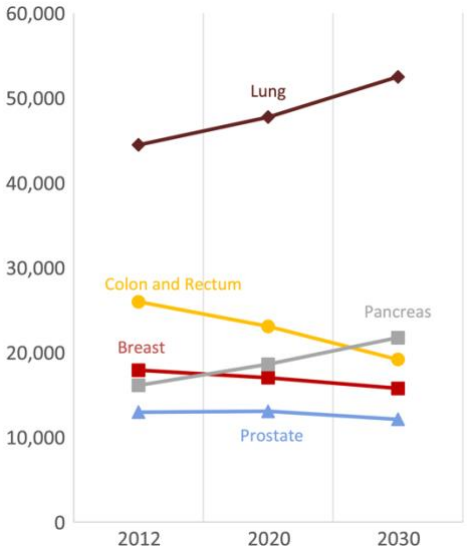

Abbildung 1: Vorhergesagte Krebs-assoziierte Todeszahlen in Deutschland bis zum Jahre 2020 und 2030 {Quante:2016fc}

Histopathologisch ist ein Großteil der malignen Pankreastumore durch ein PDAC und nur ein geringer Anteil durch neuroendokrine Tumore, Azinuszellkarzinome, muzinös-zystische Tumore oder seröse Zystadenome verursacht (Haeberle and Esposito, 2019). Als primärer Risikofaktor der Erkrankung gilt neben einem Alkohol- und Nikotinabusus eine (chronische) Pankreatitis. Es existieren daneben eine Reihe von Syndromen und genetischen Mutationen, die mit einem erhöhten PDAC-Risiko einhergehen. Dazu zählen das Peutz-Jeghers-Syndrom mit einer Mutation des Tumorsuppressorgens der Serin-Threonin-Kinase *STK11/LKB1*, das Familiäre Atypische Multiple Muttermal- und Melanomsyndrom (FAMMM) mit einer *SDKN2A* Mutation, das Lynch-Syndrom mit einer Mutation eines Gens der DNA-Reparaturmaschinerie (*MSH1*, *MSH2*, *MSH6* und *PMS2*) und eine hereditäre chronische Pankreatitis mit einer Mutation im *PRSS1* Gen (Grover et al., 2010). Klinisch am bedeutsamsten sind Patienten mit einem familiären Mamma- und Ovarialkarzinom-Syndrom, welches mit einer Mutation in den Tumorsuppressorgenen *BRCA1/2* oder *PALP2* zusammenhängt. Diese Mutationen spielen eine wichtige Rolle in der zellulären Reparatur von DNA-Doppelstrangbrüchen und sind bei ca. 7% der PDAC Patienten pathogen mutiert (Holter et al., 2015).

Das PDAC entsteht größtenteils aus pathologisch gut charakterisierten Vorläuferläsionen (Hezel et al., 2006; Kleeff et al., 2016). Die Mehrzahl der Tumore ist dabei solide und bildet sich aus Pankreatischen Intraepithelialen Neoplasien, sog. PanIN. Diese durchlaufen im Rahmen einer malignen Progression - ähnlich zu anderen Tumorentitäten - mehrere Dysplasiestufen vor Ausbildung einer invasiven Komponente (Lee et al., 2019; Ryan et al., 2014). Die zunehmende Progression geht einher mit der Akkumulation von charakteristischen genetischen Veränderungen (Abbildung 2). Bereits in frühen Stadien zeigen sich Mutationen im Protoonkogen „Kirsten Rat Sarcoma Viral Oncogene Homolog“ (*KRAS*). Dieses auf dem Chromosom 12p12.1 lokalisierte Gen zählt zu den häufigsten mutierten Genen menschlicher Tumore und wird in ca. 20-30% aller Karzinome nachgewiesen (Uprety and Adjei, 2020). Nichtsdestotrotz sind bisher multiple Versuche gescheitert, sich die molekularen Veränderungen dieses Gens für eine effektive Therapie zunutze zu machen. Viele Autoren bezeichnen *KRAS* Mutationen daher als „undruggable“ (Uprety and Adjei, 2020). *KRAS* codiert mehrere Isoformen des Ras Proteins, welches membrangebunden ist und eine GTPase Aktivität aufweist, die durch eine Vielzahl von Stimuli angeregt werden kann. In seiner aktiven GTP gebundenen Form aktiviert es multiple intrazelluläre Signalwege, die u.a. für die Zellproliferation, das Zellwachstum und die Angiogenese kritisch sind. Eine *KRAS* Mutation versetzt das Ras Protein in einen daueraktiven Zustand und wirkt durch eine von Erk-Kinasen vermittelte Phosphorylierung von intranukleären Transkriptionsfaktoren pro-tumorigen (sog. RAS/MAPK Signalweg) (Moore et al., 2020). Mit fortschreitender PDAC Progression akkumulieren dann weitere Mutationen in den Tumorsuppressorgenen wie *CDKN2A*, *TP53* und *SMAD4* (Hosoda et al., 2017).

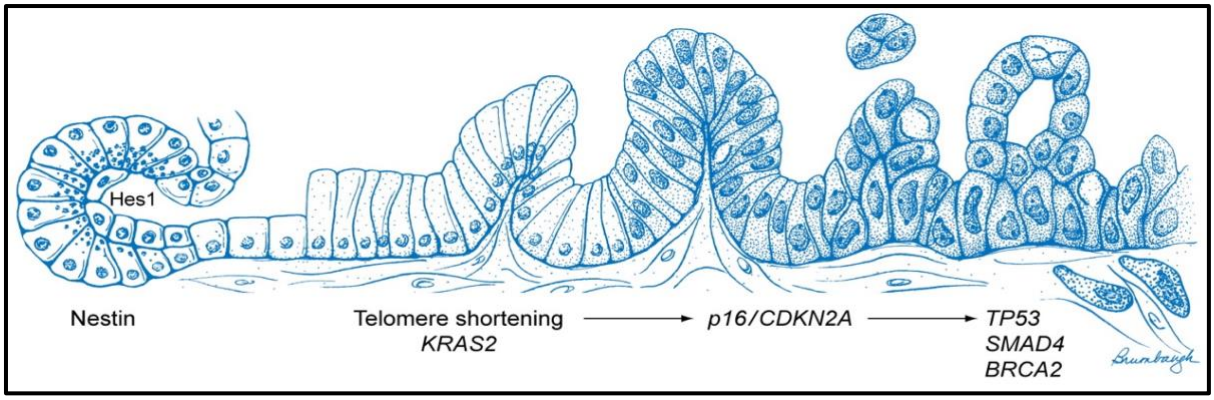

Abbildung 2 : Schematische Darstellung der stufenweisen Akkumulation von Mutationen in PDACs (Maitra and Hruban, 2008)

Eine zweite Gruppe von PDAC Vorläuferläsionen umfasst die Gruppe der zystischen Läsionen des Pankreas. Dabei werden zwischen Intraduktalen Papillären Muzinösen Neoplasien (IPMN), Muzinös-Zystischen Neoplasien (MCN) und Serös-Zystischen Neoplasien (SCN) unterschieden. IPMNs treten gehäuft mit dem Alter auf und sind bei bis zu 10% der über 70-jährigen Bevölkerung nachweisbar (Kleeff et al., 2016). Häufig fallen sie inzidentell im Rahmen einer Schnittbildgebung auf. Histologisch werden auch IPMNs hinsichtlich ihres Dysplasiegrades in wenig dysplastische (low grade) und hochgradig dysplastische (high grade) Läsionen

unterteilt. Genetisch zeigen sie neben Mutationen im *KRAS* Gen in mehr als 2/3 der Fälle Mutationen im *GNAS* Gen, welches Teil des Adenylyl-Cyclase Signalweges ist und dem *RNF43* Gen. Beide Mutationen sind in großen Sequenzierungsstudien bereits sehr früh in der Karzinogenese nachzuweisen (Biankin et al., 2012; Jones et al., 2008; Matthaei et al., 2011; Siegel et al., 2014).
Anatomisch unterscheidet man bei IPMNs aufgrund ihres Anschlusses an den Hauptausführungsgang des Pankreas, dem Ductus Wirsungianus, zwischen einem sogenannten Hauptgangtyp, einem Nebengangtyp sowie Mischformen (Machado et al., 2015). Gerade Hauptgang-IPMNs haben ein erhöhtes Risiko einer malignen Entartung (Choi et al., 2017). Zur radiologischen Evaluation wurde über die Jahre versucht, radiologische Kriterien zu etablieren, die für eine maligne Entartung sprechen. Diese sogenannten „worrisome features“ sind in den Sendai und Fukuoka Kriterien zusammengefasst und beinhalten u.a. eine Zystengröße von $\geq$ 3 cm, einen Größenprogress, solide murale Anteile, eine wandständige Kontrastmittelanreicherung und eine Kaliberschwankung des Pankreasganges (Tanaka et al., 2017). Trotz modernster Schnittbildverfahren haben die Sendai und Fukuoka Kriterien in aktuellen Analysen gerade bei Hochrisikopatienten eine unzureichende Sensitivität von nur 40-60% bei moderater Spezifität von ca. 80% für die Detektion eines invasiven Tumors in zystischen Läsionen des Pankreas (Dbouk et al., 2021). Aus diesem Grund werden auxilliäre Methoden und Kriterien zur verbesserten Beurteilung einer möglichen Malignität dieser Läsionen dringend benötigt.

Die Biomarkerforschung zur Frühdiagnose und zum Therapiemonitoring des PDAC ist hochaktiv. Derzeit ist CA-19-9 der einzige von der amerikanischen Food and Drug Administration (FDA) zugelassene, serumbasierte Test für das Rezidivmonitoring, jedoch nicht die Initialdiagnose beim PDAC. Das Glykoprotein besitzt bei unklarer Pankreasraumforderung eine Sensitivität und Spezifität von ca. 70-90% für die Erkennung eines PDAC (Jones et al., 2008; Wood, 2013). Jedoch sind ca. 30-45% aller Menschen Lewis-Antigen negativ und können per se kein CA-19-9 im Serum exprimieren (Hamada et al., 2012). In der Vergangenheit wurde das Biomarkerpotential weiterer Serumproteine evaluiert, ohne dass eine relevante Alternative zu CA-19-9 etabliert werden konnte (Kanda et al., 2012).
Eine Großteil der Biomarker beruht auf spezifischen Mutationsmustern der verschiedenen Tumorentitäten, die im Zuge umfassender Tumorsequenzierungsstudien nachgewiesen wurden (Bettegowda et al., 2014; Bidard et al., 2013; Thierry et al., 2014; Vogelstein et al., 2013). Somatische Alterationen des Erbguts besitzen daher ein hohes Potential für die Tumordiagnose, das Therapiemonitoring und die personalisierte Krebstherapie. Neben gewebebasierten Nachweismethoden existiert auch die Möglichkeit Tumor-DNA aus Körperflüssigkeiten zu isolieren. Diese neuartigen Diagnoseverfahren werden unter dem Begriff „liquid biopsy“ zusammengefasst (siehe Reviewartikel in (Corcoran and Chabner, 2018;

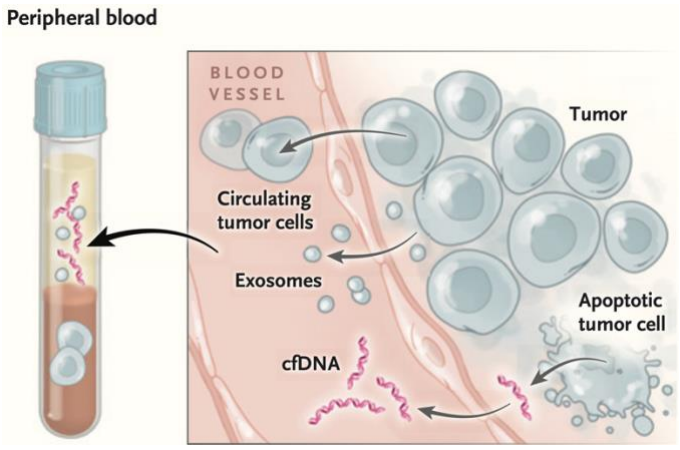

Abbildung 3: Schematische Darstellung der drei liquid biopsy Kompartimente {Corcoran:2018iv}

Ignatiadis et al., 2021)). Liquid biopsies können dabei aus drei Quellen im Blut gewonnen werden (Abbildung 3) (Bidard et al., 2013; Brinton et al., 2015; Corcoran and Chabner, 2018):

1. Zirkulierende Tumorzellen (CTC) sind intakte Zellen, die aus dem Blut isoliert werden können. Trotz modernster molekularbiologischer Methoden ist es weiterhin eine technische Herausforderung, die wenigen CTCs aus der Gesamtheit an zirkulierenden Zellen zu isolieren (Bidard et al., 2013; Tsujiura et al., 2014).
2. Zirkulierende, zellfreie Tumor-DNA (cfDNA) sind Nukleinsäurefragmente, die ohne assoziierte zelluläre Bestandteile im Blut nachgewiesen werden können. Hochsensitive Assays können DNA-Mutationen auch bei PDAC-Patienten identifizierten (Bettegowda et al., 2014). Seit einigen Jahren sind erstmals auch cfDNA Assays für personalisierte Chemotherapien durch die FDA zugelassen (Ignatiadis et al., 2021).
3. Exosomale Tumor DNA (exoDNA) beschreibt aktiv von (Tumor-)zellen sezernierte Vesikel, die einen wichtigen Stellenwert in der Zell-Zell-Kommunikation besitzen (Brinton et al., 2015) und ihren Inhalt durch eine Lipid-Doppelmembran vor Degradation besonders schützen.

Das Pankreaskarzinom ist insgesamt wenig sensibel auf einen Großteil gängiger Therapieoptionen, inklusive Strahlen-, Chemo- und Immuntherapie. Dies ist u.a. auf die folgenden Faktoren zurückzuführen: Erstens handelt es sich beim PDAC um sehr stromareiche Tumore. So liegt der durchschnittliche Tumorzellanteil nur bei ca. 10-20% (Kleeff et al., 2016). Die wenigen Tumorzellen sind von dichtem, kollagenösem Stroma umgeben. Dieses Stroma besteht sowohl aus extrazellullären Matrixproteinen wie Kollagen, Fibronectin und Laminin als auch aus nicht-kollagenösen Proteinen wie Glycoproteinen, Proteoglycanen und Glycosaminenoglycanen. Von zellulärer Seite beinhaltet das Stroma v.a. Pankreassternzellen, die in aktiviertem Zustand auch als krebs-assoziierte Fibroblasten bezeichnet werden und einen Großteil der extrazellulären Matrix produzieren. Dieses „dichte“ Stroma macht das PDAC außerordentlich strahlenresistent (Chin et al., 2018). Zudem finden sich auch infiltrierende Immunzellen (T-Zellen (größtenteils $CD4^+$)), myeloide Suppressorzellen (MDSC), Mastzellen, Makrophagen, Endothelzellen und neurogene Zellen im peritumoralen Stroma. In seiner Gesamtheit wird das Tumorstroma auch als Tumormikromilieu oder „tumor micro enviroment“ (TME) bezeichnet. Das TME spielt eine entscheidende Rolle in der Entwicklung, der Progression und der Chemoresistenz des PDAC. Ebenso ist die Entwicklung eines immunsuppressiven TME enorm wichtig für die Tumorentwicklung, da dieses eine

Immunevasion der Tumorzellen begünstigt. Bei diesem Prozess scheinen maßgeblich regulatorische CD4⁺-Zellen beteiligt zu sein (Gan et al., 2020). Zweitens handelt es sich bei PDAC um genetisch sehr heterogene Tumore. In der genetischen Mutationslandschaft dominieren nur wenige wiederkehrende Mutationen (sog. driver mutations) (Dreyer et al., 2017). Über 90% der PDAC weisen eine *KRAS* Mutation auf, die sich v.a. in den Codons 12, 13 und 61 befindet. Inaktivierende Mutationen in den Tumorsuppressorgenen *TP53*, *SMAD4* und *CDKN2A* finden sich in ca. 50-80% der Tumore. Mutationen in den Genen *ARDI1A*, *TGFBR2* und *MLL3* sind in ca. 10% der Tumore existent. Demgegenüber steht eine Myriade von weiteren genetischen Mutationen, die extrem heterogen sind und meist in nicht mehr als 1-2% der PDAC vorkommen (Abbildung 4).

Interessanterweise scheint die Zeitspanne von der ersten Mutation im Pankreasepithel bis zur Entstehung eines invasiv wachsenden PDAC fast 20 Jahre zu betragen (Siegel et al., 2014; Yachida et al., 2010). Diese lange Zeitspanne gibt Hoffnung für die Entwicklung effektiver Frühdiagnosestrategien zur Behandlung der Erkrankung im kurablen Stadium. Zahlreiche Studien konnten in diesem Zusammenhang belegen, dass die Diagnose eines PDAC im frühen operablen Stadium mit einer deutlich besseren Prognose einhergeht (Matthaei et al., 2011; Ryan et al., 2014).

Aufgrund der bisher weitgehend frustranen Versuche, PDACs durch eine (Immun-)Therapie zu behandeln (Herbst and Zheng, 2019), existieren nur wenige etablierte Chemotherapie-Regime. Dazu zählen zum einen Gemcitabin oder 5-Fluorouracil basierte und zum anderen

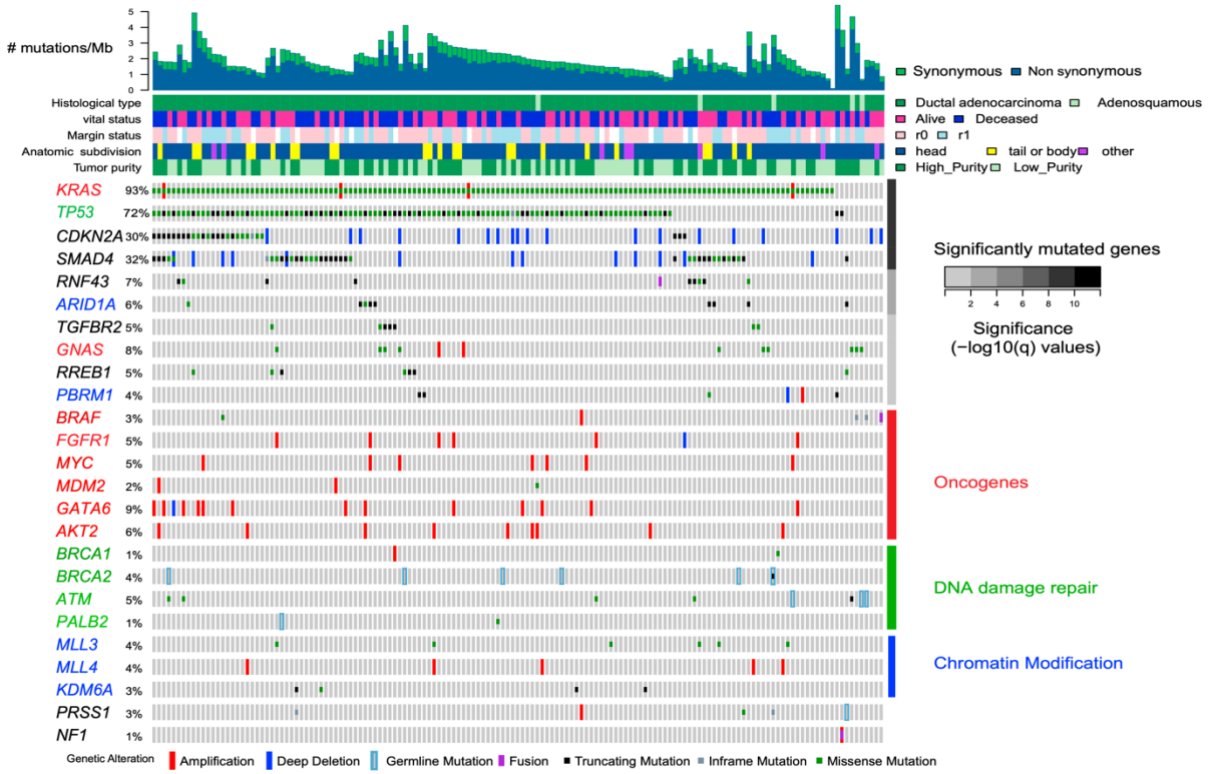

Abbildung 4: Repräsentative Heatmap häufiger genetischer Alterationen im PDAC organisiert nach ihren funktionellen Klassen. Histopathologische und demographische Charakteristika sind als Balken über der Heatmap dargestellt {Raphael:2017kl}

Platinum-basierte Therapieansätze (FOLFOX, FOLFIRI(NOX)). Letztere werden aufgrund ihres verstärkten Nebenwirkungsspektrums meist bei Patienten mit einem guten Allgemeinzustand eingesetzt. Im Gegensatz zu vielen anderen Tumorerkrankungen wie dem Melanom oder Lungentumoren, wird die Auswahl der Chemotherapie bei PDAC Patienten bis heute meist immer noch rein klinisch gefällt (Conroy et al., 2018). Wichtig ist in diesem Zusammenhang, dass Platinum-basierte Chemotherapien oftmals besser in HR-defizienten (Homologous Recombination Deficiency) Tumoren wirken. Ein HRD Phänotyp ist dabei durch eine gestörte Reparatur von DNA-Doppelstrangbrüchen charakterisiert (Davies et al., 2017). Zu den bekanntesten HRD Genen gehören *BRCA1/2* und *PALP2*. Neben Punktmutationen (single nucleotid variant, SNV) (Holter et al., 2015) können auch andere, schwerer detektierbare Veränderungen wie z.B. DNA-(Promoter)-Hypermethylierung, Amplifikationen, Indels und chromosomale Rearrangements einen HRD-Phänotyp verursachen. Bei Ovarial- und Mammakarzinomen hat die Bestimmung des HRD-Phänotyps eine große Bedeutung für die Auswahl der Therapie. Hier zeigt sich eine deutliche Prognoseverbesserung durch die prä-therapeutische Selektion potentiell sensibler Tumore (Staaf et al., 2019). Interessant ist hierbei, dass selbst Tumore, die keine Veränderungen in bekannten HRD-assoziierten Regionen aufweisen mithilfe von sogenannten Mutationssignaturen und genomischen Mustern als potentiell HR-defizient klassifiziert werden können (Davies et al., 2017). Mutationssignaturen beschreiben dabei die Analyse von charakteristischen globalen „Mutationsmustern“, die sich aus einer spezifischen Mutagenese ergeben. Diese werden in den sogenannten COSMIC Signaturen zusammengefasst (Alexandrov et al., 2020). Beispielhaft ist hier die COSMIC Signatur 4 zu nennen, die durch die DNA-schädigende Wirkung von nikotinhaltigem Zigarettenrauch entsteht und durch eine Schädigung von Guanin charakterisiert ist. Diese Signatur ist daher signifikant häufiger in Lungenkarzinomen nachweisbar. Durch die Analyse dieser Muster konnten letztlich auch Patienten ohne bekannte SNV aber einem HRD-typischen Muster identifiziert und erfolgreich einer Platinum-basierten Therapie unterzogen werden (Staaf et al., 2019).

Auch in aktuellen Studien wird angenommen, dass >10% der PDACs einen HRD-Typ aufweisen und potentiell auf eine Platinum-basierte Chemotherapie sensibel sein könnten. In diesem Zusammenhang beschrieben Waddell et al. 2015 erstmals einen genomisch instabilen PDAC Subtyp („unstable genome“), der einem HRD-Typ ähnlich ist. Für diese Studie sequenzierte das Forscherteam das gesamte Genom (whole genome sequencing, WGS) von 100 PDAC Tumoren und wertete sowohl die Mutationslandschaft als auch strukturelle Aberrationen (somatic copy number alterations (SCNA)) aus (Waddell et al., 2015). Speziell durch die Analyse der SCNA konnten die untersuchten PDAC in 4 Subtypen unterteilt werden: „stable“, „locally rearranged“, „scattered“ und „unstable“. Der instabile Subtyp, der in 14% der Tumore vorlag, war dabei durch eine hohe Anzahl an großen strukturellen Aberrationen charakterisiert. Ebenso war ein instabiles Genom signifikant assoziiert mit Mutationen in bekannten DNA-Reparaturgenen (s.o.) sowie Mutationssignaturen, die auf eine gestörte DNA-

Reparaturmaschinerie hindeuten (COSMIC SBS3). Korrespondierend zu den oben beschriebenen Daten zeigten besonders Patienten mit einem instabilen Phänotyp ein klinisches Ansprechen auf eine Platinum-basierte Therapie. Jedoch wiesen nur rund 50% der Tumore mit instabilem Genom eine detektierbare Mutation im BRCA-Signalweg auf. Die restlichen Tumore zeigten nur vereinzelt Veränderungen in Genen, die mit der Aufrechterhaltung der DNA-Stabilität assoziiert sein können (z.B. *ATM*, *FANCM*, *XRCC4* und *XRCC6*). Diese Ergebnisse im PDAC korrelieren gut mit HRD-Phänotypen in anderen Tumorentitäten und unterstreichen die Komplexität der genomischen Vorgänge sowie die klinisch relevanten Subtypisierungen der Tumore.

Neben den oben beschriebenen DNA-Signaturen wurde in den letzten Jahren auch die transkriptionelle Landschaft im PDAC mit verschiedenen, teils überlappenden Subtypen beschrieben (Bailey et al., 2016; Collisson et al., 2019; 2011; Moffitt et al., 2015; Raphael, 2017). Validierungsstudien zeigten jedoch, dass einige der initial publizierten PDAC-Subtypen keine „echten" Subtypen sind. So sind der „ADEX" (Bailey et al., 2016) und der „exocrine-like" Subtyp (Collisson et al., 2011) v.a. durch eine Kontamination mit infiltrierenden Immunzellen als eigene Subtypen klassifiziert. 2017 und 2019 führten weitere Arbeiten, die PDACs auch epigenetisch untersuchten, letztlich zu der Klassifikation in zwei große transkriptionelle Subtypen (Collisson et al., 2019; Guo et al., 2021): 1. Den sogenannten „classical-pancreatic" Subtyp und 2. den „basal/squamous" Subtyp. Ersterer zeichnet sich durch seine Ähnlichkeit zu pankreatischen Vorläuferläsionen aus, die die embryonale Entwicklung des Pankreas nachahmen. Der klassische Subtyp scheint dabei *GATA6*-getriggert zu sein und zeigt v.a. Veränderungen in Genen der epithelialen und der endodermalen Differenzierung. Im Gegensatz dazu ist der basal/squamous Subtyp durch Veränderungen in Genen der Chromatinmodifikation wie *MLL2*, *MLL3* und *KDM6A* charakterisiert, welche letztlich zu einer endodermalen Entdifferenzierung der (Pankreas-)zellen führen. Ebenso zeigt dieser Subtyp eine deutlich erhöhte Laminin- und Keratin-Expression und ähnelt damit teilweise vorbeschriebenen Subtypen in Brust- und Blasenkarzinomen (Guo et al., 2021). Der basal/squamous Subtyp ist zudem mit einer deutlich schlechteren Prognose verbunden.

Trotz großer Fortschritte in der medikamentösen Tumorbehandlung und auch ersten Schritten in der individualisierten Tumorbehandlung bleibt die einzig kurative Therapieoption eines PDACs die vollständige chirurgische Resektion (Kleeff et al., 2016). Bei Tumoren im Pankreaskopf ist die Operation der Wahl entweder eine pyloruserhaltende Pankreatikoduodenektomie nach Traverso und Longmire, oder eine partielle Duodenopankreatektomie nach Kausch-Whipple. Tumore im Schwanzbereich werden durch eine Pankreaslinksresektion inklusive Splenektomie entfernt (Strobel et al., 2019). Bedingt durch ein verbessertes perioperatives Management, einer Behandlung der Patienten an Pankreaszentren und Verbesserungen in der OP-Technik konnte die hohe Mortalitätsrate dieser Operationen auf ca. 3% gesenkt werden (Strobel et al., 2019). Zudem ist in den letzten Jahren das 5 Jahres Überleben nach R0 Resektion und adjuvanter Chemotherapie deutlich

gestiegen und nähert sich bei diesen Patienten der 30% Marke an (Neoptolemos et al., 2017). Innerhalb von klinischen Studien werden aktuell auch neoadjuvante Therapiekonzepte zum Downstaging von lokal fortgeschrittenen, sog. „borderline resectable“ Tumore eruiert (Oba et al., 2020). Trotz aller Fortschritte in der operativen Technik ist die Pankreaschirurgie jedoch weiterhin mit einer hohen Morbidität von ca. 20-25% assoziiert(Strobel et al., 2019), so dass die Indikation zur Resektion gerade bei zystischen Läsionen sehr sorgfältig abgewogen werden muss.

Im Fall einer chirurgischen Irresektabilität kann eine palliative Chemotherapie begonnen werden. Die aktuellen deutschen Leitlinien für das exokrine Pankreaskarzinom {Leitlinienprogramm Onkologie Deutsche Krebsgesellschaft:wx}, sowie internationale Leitlinien (AJCC) fordern jedoch eine histologische Sicherung vor Beginn jeder systemischen Chemotherapie. Aufgrund der retroperitonealen Pankreaslage ist dieses für eine transkutane Biopsie nur eingeschränkt zugänglich. Aus diesem Grund hat sich die endoskopische Feinnadelbiopsie (endoscopic ultrasound-guided fine needle aspiration, EUS-FNA) als Standard zur prätherapeutischen Gewebegewinnung durchgesetzt. Bei dieser Technik wird mithilfe eines endoskopisch eingebrachten Ultraschallkopfes der Pankreas über das Duodenum oder den distalen Magen dargestellt. Tumore können dann mit einer feinen, über das Endoskop eingeführten Hohlnadel, punktiert werden. Das gewonnene Gewebe wird mithilfe einer Unterdruckansaugung aus dem Gewebe mobilisiert. Die verwendete Nadel hat dabei standardmäßig einen Außendurchmesser von ca. 0,95-0,46mm (20-25 Gauge), so dass nur geringe Gewebemengen selbst durch mehrfache Punktion gewonnen werden können. Standardmäßig wird das durch EUS-FNA gewonnene Gewebe dann histologisch als „Ausstrich-Zytologie“ untersucht und beim Nachweis von malignen Zellen in der Hämatoxylin-Eosin-Färbung zur Diagnose eines PDAC verwendet. Trotz vieler technischer Verbesserungen der letzten Jahre ist die EUS-FNA eine untersucherabhängige Technik, so dass der Anteil von nicht-diagnostischen EUS-FNA immer noch bei ca. 10-15% liegt (Hewitt et al., 2012; Layfield et al., 2014; Puli et al., 2013). Zudem ist eine EUS-FNA Punktion trotz der kaliberschwachen Feinnadel mit einer nicht unerheblichen Komplikationsrate verbunden (Nassour et al., 2018; Patel et al., 2020). Versuche, diese Aspirationsbiopsien für eine detaillierte Tumorcharakterisierung zu nutzen, waren aufgrund der geringen Gewebemenge bzw. der eingeschränkten Qualität bisher selten erfolgreich. (Aguirre et al., 2018; Alix-Panabières and Pantel, 2014; Raphael, 2017).

Zur Identifikation von somatischen Aberrationen gilt die DNA- und RNA-Sequenzierung (next generation sequencing, NGS) aktuell als Goldstandard. Diese Techniken haben unser Verständnis der Tumorbiologie revolutioniert. So wurde mithilfe der DNA Sequenzierung beispielsweise die schrittweise Akkumulation von genetischen Alterationen im Rahmen der Adenom-Karzinom Sequenz im Kolorektalen Karzinom 1990 durch Fearon und Vogelstein beschrieben (Fearon and Vogelstein, 1990).

Trotz dieser bahnbrechenden Entdeckung haben herkömmliche Sequenzierungsmethoden

den Nachteil, dass sie teils entscheidende genetische Varianten und Subpopulationen aufgrund der Nachweisgrenze nicht mit ausreichender Genauigkeit detektieren können. Speziell im stromareichen PDAC, welches eine hohe genetische Diversität und gleichzeitig einen Tumorzellanteil von oftmals nur 10-15% aufweist, bleibt mit der NGS Methodik oftmals selbst die epitheliale Tumorsignatur unterhalb der Nachweisgrenze. So werden in klinisch validierten Sequenzierungsanalysen meist nur Mutationen mit einer Allelfrequenz (MAF, mutant allel frequency) von 5-10% gewertet (Johnson et al., 2010). Viele NGS Studien im PDAC haben daher nur Karzinome mit einem Tumorzellanteil von >30% in die Analysen eingeschlossen (Raphael, 2017).

Eine Technik zur Verbesserung sowohl der Detektionsrate als auch der Fehlerquote in der NGS Sequenzierung ist die Verwendung von sogenannten „unique molecular identifiers“ (UMI). Diese auch Barcodes genannten UMIs erlauben es PCR-Amplifikations- (Polymerase Chain reaction) und Sequenzierungs-Artefakte, die zu potentiell falsch-positiven Genvarianten führen, effektiv zu reduzieren (Kivioja et al., 2011). So wird bei der klassischen Sequenzierung abhängig von der Leselänge, dem verwendeten Algorithmus und der Art der genetischen Veränderungen eine Fehlerrate bei der Sequenzierung von 0,05-1% angenommen (Kinde et al., 2011). Zur Reduktion derartiger Artefakte wird bei diesem ultrasensitiven Sequenzierungsansatz zu Beginn der sogenannten „Library“ Präparation eine individuelle UMI-Sequenz von ca. 8-12 Basenpaaren-Länge an die originären DNA-Fragmente ligiert. Bei diesen UMIs handelt es sich um vollkommen zufällig erzeugte Basensequenzen, die letztlich als einzigartiges Identifikationsmerkmal des jeweiligen DNA-Stückes dienen. Während der Library Präparation werden von den ursprünglichen DNA-Segmenten durch Amplifikationsschritte unzählige Kopien angefertigt, die dann später in ihrer Gesamtheit sequenziert werden. Durch bioinformatische Algorithmen können dann nach der Sequenzierung diese Kopien anhand der UMIs zweifelsfrei „Ursprungsgruppen“ zugeordnet werden. Dabei wird bioinformatisch abgeglichen, ob alle Kopien, die anhand desselben UMI zu einer Ursprungsgruppe zusammengefasst wurden, an gleicher Stelle eine identische Mutation aufweisen oder ob nur Teile der Ursprungsgruppen eine Mutation aufweisen (Abbildung 5). Im ersten Fall wird von einer echten Mutation, im zweiten Fall von einem Artefakt ausgegangen.

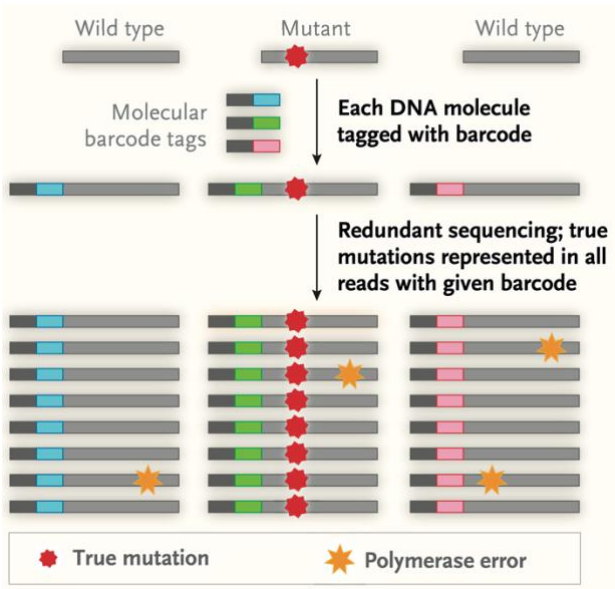

Abbildung 5: Prinzip der UMI Sequenzierung zur Reduktion von PCR und Sequenzierungsartefakten{Corcoran:2018iv}

Zur ultrasensitiven Detektion spezifischer Punktmutationen kann alternativ die droplet digital PCR (ddPCR) verwendet werden. Bei dieser Methode werden Nukleinsäuren in ein volumetrisch definiertes Wasser-Öl Gemisch eingeschlossen (Hindson et al., 2013), um parallel multiple PCR Reaktionen in räumlich getrennten Kompartimenten durchzuführen (Abbildung 6). Dies gewährleistet im Vergleich zur analogen, klassischen real-time PCR und NGS eine verbesserte Detektionsrate von 1 zu 100.000 Mutationen (0.001%). Der Vorteil dieser Methode ist seine enorme Detektionssensitivität in heterogenem Probenmaterial.

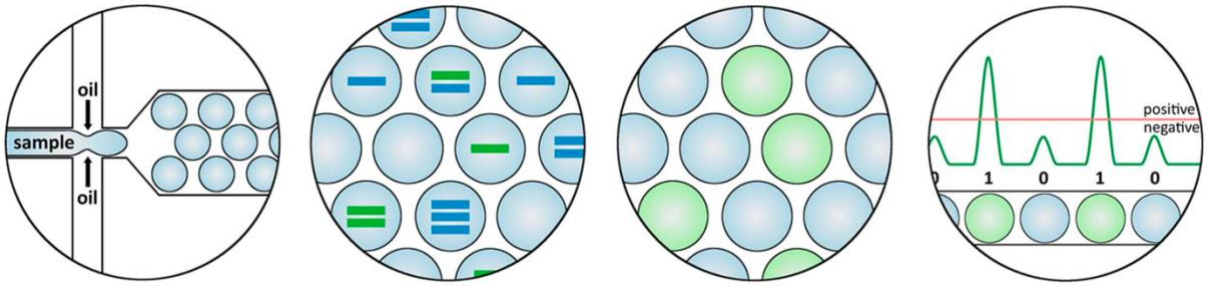

Abbildung 6: Prinzip der ddPCR Methode zur ultrasensitiven SNVDetektion {Verheul:2016be}

Eine weitere bedeutende technologische Entwicklung der letzten Jahre, die das Verständnis der Tumorbiologie maßgeblich vorangebracht hat, ist die Entwicklung der sogenannten Einzelzellsequenzierung (single cell RNA sequencing, scRNA) (Vitak et al., 2017). Im Vergleich zur klassischen Sequenzierung eines gesamten Tumorstückes, welches eine Vielzahl von unterschiedlichen Zelltypen enthält, hat die scRNA-Analyse den großen Vorteil, dass durch die individuelle Sequenzierung der Einzelzellen auch kleine, aber wichtige Zellpopulationen genau charakterisiert werden können. Bei der Massensequenzierung hingegen gehen diese kleine Zellpopulationen im allgemeinen Signal der dominierenden Zellpopulationen unter. Gerade Subpopulationen besonders resistenter Zellen haben jedoch häufig eine therapeutische Relevanz, da diese oft die „Keimzelle“ für spätere Rezidive oder Metastasen bilden (Hong et al., 2019). Selektive Beschreibungen der genetischen Tumorlandschaft waren daher oftmals nur durch eine aufwendige und zeitintensive Lasermikrodissektion von hunderten bis tausenden gepoolten Einzelzellen möglich. Eine zunehmende Zahl von hochpublizierten Arbeiten zeigt durch scRNA-Analysen eine ausgesprochene intra-tumorale Heterogenität und ermöglicht detaillierte neue Einblicke in die Tumorformation und -evolution (Gawad et al., 2016). Exemplarisch wurden vor kurzem durch die scRNA-Analyse von mehr als 50.000 Einzelzellen von 24 PDAC und 11 gesunden Pankreaskontrollen mehrere unterschiedliche Subpopulationen der epithelialen Tumorzellen beschrieben, die sich transkriptional deutlich voneinander unterscheiden (Peng et al., 2019). Einige Subpopulationen fanden sich dabei in einem Großteil der Tumore wohingegen andere nur in einzelnen Patienten nachweisbar waren, was eine inter-individuelle Tumorentwicklung betont.

Technisch muss das Tumorgewebe zu Beginn jeder scRNA-Analyse durch mechanische und enzymatische Dissoziation in eine Einzelzelllösung aufgelöst werden. Aufgrund des hohen

Gehaltes an Verdauungsenzymen in der Bauchspeicheldrüse, die zu einer schnellen Schädigung der Zellen führen, sind bisher noch keine allgemein empfohlenen Dissoziationsprotokolle für das Pankreas veröffentlicht. Im Gegensatz dazu wurden für viele andere solide Tumore Protokolle für die Herstellung einer Einzelzellsuspension veröffentlicht (Slyper et al., 2019). Die eigentliche Library Präparation läuft dann methodisch folgendermaßen ab: In einem ersten Schritt werden sogenannte „GEMs“ (Gel Beads-in-emulsion) in einem Mikro-Chip erzeugt (Abbildung 7). Diese GEMs enthalten jeweils eine individuelle, nanomillimetergroße Gel-Sphäre, die mit einer einzigartigen, diesem GEM zuzuordnenden Nukleotidsequenz (Barcode) und einer Standard-Primersequenz überzogen ist. GEMs werden dann jeweils mit einer Einzelzelle beladen. Nach der GEM Erzeugung erfolgt als nächstes die Freisetzung der an die Gel-Sphäre gebundenen Oligonucleotide und die Lyse der in den GEMs vorhandenen Einzelzellen unter Beibehaltung der äußeren GEM-Hülle. Durch die räumliche Trennung der einzelnen Zellen innerhalb einzelner GEMs können alle Zelllysate anhand der individuellen GEM Barcodes später jeweils einer einzigen Zelle zugeordnet werden. Nach Lyse der Zellen innerhalb der GEMs wird die freigesetzte poly-adenylierte mRNA in vollständige cDNA umgeschrieben. Nachfolgend werden die GEMs aufgelöst und die vollständige, zell-individuell markierte cDNA amplifiziert.

Nachfolgend durchläuft die so markierte cDNA dann ein Standard NGS Library Protokoll. Die scRNA Sequenzierungsdaten werden anhand von mathematischen Algorithmen prozessiert, die u.a. berechnen wie ähnlich die Transkriptome der Einzelzellen sind. Dadurch bilden sich Zellcluster, die verschiedenen Zellpopulationen entsprechen und anhand der exprimierten Gene charakterisiert und weiter analysiert werden können.

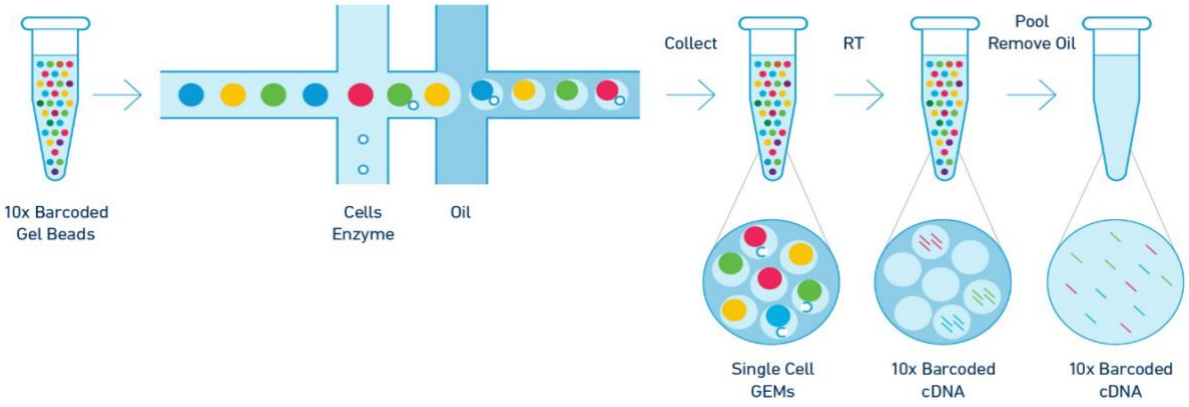

Abbildung 7: Schematische Darstellung des scRNA-Workflows (Single Cell 3' Reagent Kits v2 User Guide, 10x)

Insgesamt besteht jedoch trotz immer detailreicheren Charakterisierungsmöglichkeiten von Tumoren die größte Herausforderung in der klinischen Implementierung der Analyseergebnisse. In diesem Zusammengang sind auch im PDAC zunehmend Versuche unternommen worden, prätherapeutisches Tumormaterial für eine klinische Charakterisierung und Diagnosesicherung zu nutzen (Aguirre et al., 2018), die allerdings aufgrund der schwierigen Biopsietechnik nur eingeschränkt erfolgreich waren.

Aus diesem Grund evaluierten wir in dieser Arbeit die diagnostische, prognostische und

therapeutische Bedeutung der Tumormutationslandschaft und des umgebenden Tumormikromilieus im duktalen Adenokarzinom des Pankreas. Aufgrund der vorliegenden wissenschaftlichen Arbeiten und Hypothesen resultieren folgende Fragestellungen sowie Zielsetzungen:

I. Kann eine genetische Diagnostik von EUS-FNA die Diagnosesicherheit dieser Proben erhöhen?
II. Ist prätherapeutisch eine detaillierte, genetische Charakterisierung des limitierten EUS-FNA Probenmaterials möglich und besitzt diese einen prognostischen oder prädiktiven Stellenwert im PDAC?
III. Kann durch ein serielles, prospektives Therapiemonitoring das Therapieansprechen und die Prognose im PDAC vorhergesagt werden?
IV. Weisen zystische Vorläuferläsionen und solide Tumore ein vergleichbares Progressionsmuster zum invasiven Pankreaskarzinom auf?

2. Ergebnisteil

2.1: Diagnostic value of digital droplet polymerase chain reaction and digital multiplexed detection of single nucleotide variants in pancreatic cytology specimens collected by EUS-guided FNA

Aufgrund der Notwendigkeit einer histologischen PDAC Sicherung vor Beginn einer Chemotherapie und der bekannten diagnostischen Unsicherheit von EUS-FNA Proben beschäftigen wir uns in dieser Studie mit Möglichkeiten einer Diagnoseverbesserung mittels Molekulardiagnostik. Durch die retroperitoneale Lage des Pankreas ist eine transkutane Biopsie nur schwer möglich, so dass in einem Großteil der Fälle die histologische Tumordiagnose durch eine EUS-FNA erbracht wird. Trotz einer in Metaanalysen gezeigten hohen Sensitivität und Spezifität der EUS-FNA (Hewitt et al., 2012; Hébert-Magee et al., 2013; Puli et al., 2013) variiert die diagnostische Genauigkeit der Methodik stark zwischen Zentren und wird außerdem von benutzer- und tumorabhängigen Faktoren beeinflusst. Aus vorangegangenen Gründen ist die Rate an falsch negativen Befunden in einigen Kliniken weiterhin hoch (Trisolini et al., 2017).

Wir evaluierten daher den diagnostischen Zusatznutzen einer ultrasensitiven *KRAS* und Multi-Gen-Mutationsbestimmung aus 31 EUS-FNA Proben (22 PDAC, 7 chronische Pankreatitiden und 2 pankreatische neuroendokrine Tumore), die an einem kommunalen Krankenhaus in Craiova (Rumänien) während einer Standard EUS-FNA bei klinischem Verdacht auf ein PDAC entnommen worden sind. Alle Patienten der Kohorte wurden für mindestens 6 Monate nachverfolgt. Die Diagnosestellung erfolgt nach internationalen Standards mittels Ausstrichzytologie. Aus einer Feinnadelbiopsie-Probe wurde DNA isoliert und sowohl mittels ddPCR basierter Multiplex *KRAS* Testung (n=31) als auch mit einem digitalen Multiplex-Detektionskit analysiert (n=24). Bei Letzterem handelt es sich um ein 24 Gene umfassendes Genpanel (NanoString Vantage 3D DNA SNV Solid Tumor Panel, Nanostring), welches nach spezieller Anreicherung und multiplex PCR auf der nCounter Plattform von Nanostring analysiert wurde. Diese Plattform ist in der Lage, genetische Mutationen bis zu einer MAF von 5% zu detektieren.

Die Sensitivität und Spezifität der klinisch-zytologischen Ausstrichuntersuchung in unserer Kohorte lag bei 63% bzw. 100%. Durch die Ergebnisse der ddPCR basierten *KRAS* Detektion konnte die Sensitivität deutlich auf 90% erhöht werden. Jedoch verringerte sich die Spezifität gleichzeitig auf 87%. Der Multiplex-Genpanel ermöglichte den Nachweis von zwei zusätzlichen PDACs durch die Detektion von – in der ddPCR nicht inkludierten - Q61 *KRAS* Mutationen. Interessanterweise konnte mittels des Nanostring Genpanels in allen suspekten oder atypischen FNA Proben, die von einem PDAC entnommen worden waren, mindestens eine pathogene Genmutation detektiert werden, während alle Proben aus chronischen Pankreatitiden negativ waren. Die Sensitivität des Nanostring Genpanels lag daher bei 94%

mit einer Spezifität von 80%. Durch Kombination der Ergebnisse beider molekularer Analysemethoden mit der histologischen Untersuchung, konnte die diagnostische Präzision der EUS-FNA von 74% auf insgesamt 91% angehoben werden.

Zusammenfassend liefern beide hier vorgestellten auxilliären, molekularen Analysemethoden besonders in histologisch nicht eindeutigen EUS-FNA Fällen eine wertvolle und objektive Zusatzinformation zur Diagnose eines PDAC und stellen daher eine sinnvolle Ergänzung zur Erhöhung der Diagnosesicherheit der EUS-FNA v.a. in zytologisch nicht eindeutigen Befunden dar.

2.2: Defining the Comprehensive Genomic Landscapes of Pancreatic Ductal Adenocarcinoma Using Real World Endoscopic Aspiration Samples

Ziel dieser Studie war es, die technische Machbarkeit einer detaillierten genetischen Analyse aus EUS-FNA Proben zu untersuchen und ihren klinischen Nutzen zu evaluieren.

Wir kombinierten zur Verbesserung der molekularen Diagnostik aus diesen qualitativ limitierten Proben zwei neue Techniken. Erstens reicherten wir die Tumorzellen mittels „epithelial cell adhesion molecule“ (EpCAM) beschichteter, magnetischer Mikrosphären an (Oberflächenmarker von Epithelzellen) und zweitens verwendeten wir einen ultrasensitiven Sequenzierungsansatz (UMI, siehe Einleitung für Details, S. 10).

In einer initialen Pilotphase testeten wir unseren Versuchsansatz sowohl an transkutanen Hohlnadelbiopsien von PDAC Metastasen (n=4) als auch resezierten Primärtumoren mit einem Tumoranteil von <10% (n=5). Durch die Anreicherung zeigte sich dabei eine deutliche Verbesserung der Detektierbarkeit von genetischen Veränderungen. So stellten wir eine signifikante Erhöhung der mittels ddPCR bestimmten *KRAS* MAF im Vergleich zu nicht angereicherten Proben fest (21.7% vs. 4.3%, p=0,049) (Abbildung 8 a/b). Zusätzlich zeigten die Proben ein identisches Mutationspektrum wie bisherige Fallserien (Aguirre et al., 2018; Raphael, 2017; Singhi et al., 2019; Waddell et al., 2015) und den entsprechenden validierten Mutationsreporten (CLIA Standard) der untersuchten Patienten. Durch den erhöhten Anteil an malignen Zellen am Gesamtzelllysat war zudem die Charakterisierung der genetischen Veränderungen im Vergleich zu nicht angereicherten Proben enorm vereinfacht und präzisiert.

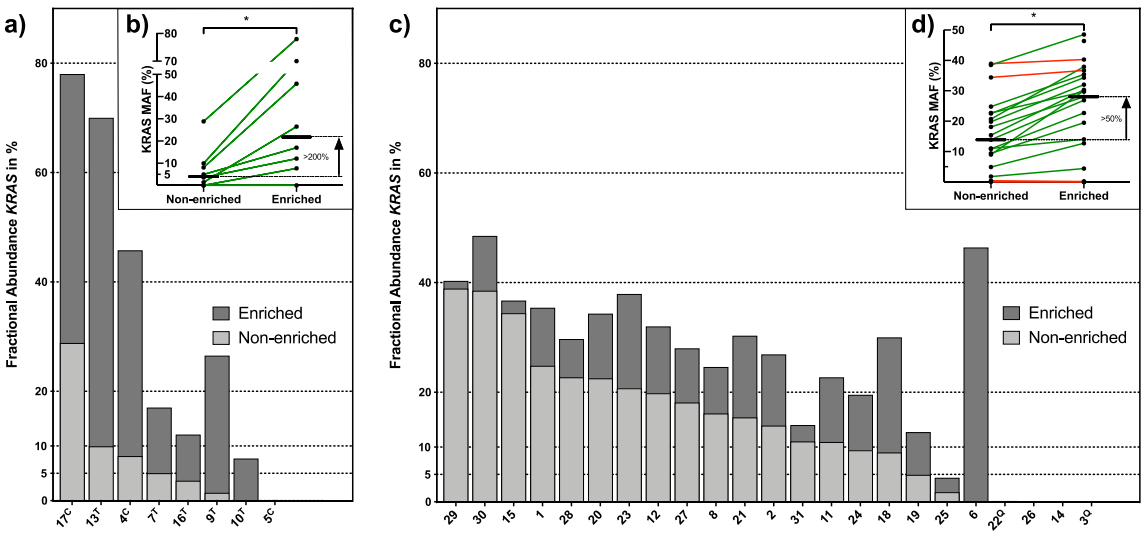

Abbildung 8: Nachweis von *KRAS* Mutationen in Hohlnadelbiopsien - markiert mit ^{C} - und resezierten Primärtumoren - markiert mit ^{T} - (a) und b)) und EUS-FNA (c) und d)). a) und c) zeigen die *KRAS* MAF von angereicherten (dunkelgrau) und nicht angereicherten (hellgrau) Proben. b) und d) zeigen die Veränderung der *KRAS* MAF zwischen angereicherten und nicht angereicherten Proben. Grüne Linien zeigen dabei eine Veränderung von >10%, rote Linien eine Veränderung <10%. Proben markiert mit ^{Q} weisen Tumore mit einer *KRAS* Mutation in Q61 aus.

In einem zweiten Schritt wendeten wir diese Technik dann in klinischen EUS-FNA Proben von weiteren 23 PDAC Patienten an. Auch hier zeigte sich ein signifikanter Anstieg der *KRAS* MAF durch die oben beschriebene Anreicherungsmethode (28.0% vs. 13.9%, p=0.03) (Abbildung 8 c/d). Ebenso war der Patientenanteil mit spezifischen Mutationen, die für eine gezielte Krebs- oder Immuntherapie nutzbar sind (7/23 Patienten) identisch mit einschlägigen Publikationen (Aguirre et al., 2018; Aung et al., 2018; Singhi et al., 2019). Es zeigte sich zudem, dass die Gesamtanzahl an vorliegenden Mutationen eng mit Mutationen in bekannten DNA-Reparaturgenen oder Mismatch-Repaturgenen korrelierten, was für den Einschluss von Patienten in klinische Studien, die ebendiese Reparaturmechanismen zum Ziel haben, zunehmend an Bedeutung gewinnt.

Neben Punktmutationen konzentrierten wir uns auch auf chromosomale bzw. strukturelle Aberrationen, die durch ihre schiere Größe eine Vielzahl von Genen verändern können. Besonders interessant sind hierbei Veränderungen, die ganze Chromosomenarme umfassen, da diese eine zunehmende genomische Instabilität anzeigen (Taylor et al., 2018). Die Menge von SCNA auf Chromosomenarmebene fassten wir in einem modifizierten „Aneuploidie Score“ (AS) zusammen (Abbildung 9 a). Dabei zeigte sich, dass eine höhere genetische Instabilität - unabhängig - vom Tumorstadium eine deutliche prognostische Signifikanz sowohl im Gesamtüberleben (OS) als auch für das progressionsfreie Überleben (PFS) besitzt (Abbildung 9 b-e). Zusätzlich zeigten alle drei nicht metastasierten Patienten, die einen hohen AS aufwiesen, einen frühen Progress unter neoadjuvanter Therapie. Diese Ergebnisse sprechen dafür, dass eine hohe genomische Instabilität, die indirekt durch den AS gemessen werden kann, als prognostische Variable im klinischen Kontext dienen kann und deren prognostische Bedeutung in einer unabhängigen Kohorte aus dem Dana-Farber Cancer Institute (DFCI) kreuzvalidiert werden konnte.

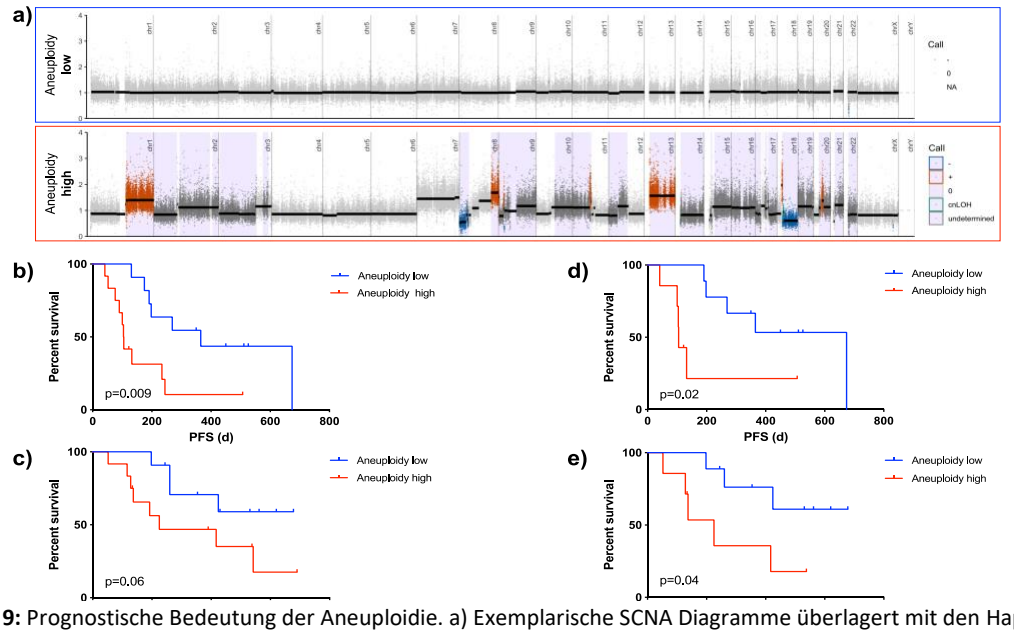

Abbildung 9: Prognostische Bedeutung der Aneuploidie. a) Exemplarische SCNA Diagramme überlagert mit den HapLOHseq-Daten (pinker Hintergrund) von Patienten mit niedriger (oben) und hoher Aneuploidie. b) -e) Kaplan Meier Kurven, die das progressions-freie Überleben (PFS) oder Gesamtüberleben (OS) von allen Patienten (linksseitig) bzw. lokalisierten Tumoren (rechtsseitig) vergleichen

Zudem zeigte ein neu entwickelter „Complexity Score“ (CS), der als einfacher Marker für einen HRD-Phänotyp verwendet werden kann, ein prädiktives Potential für die Vorhersage der Wirksamkeit von Platinum-basierter Chemotherapie. Der Versuch diesen CS in der DFCI Kohorte zu validieren, war aufgrund fehlender Responder auf eine Platinum-basierte Therapie leider nicht möglich.

Zusammengefasst konnten wir mit dieser Arbeit zeigen, dass selbst kleinste Probenmengen, die während einer EUS-FNA entnommen wurden, nach entsprechender Anreicherung geeignet sind für hochdetaillierte und prognostisch relevante, genomische Tumorcharakterisierungen. Durch die fortwährend kostengünstigeren Analyseverfahren und zunehmend anwenderfreundlichen Analysemethoden können diese Verfahren mehr und mehr in den klinischen Alltag und die Therapieentscheidung integriert werden, um zusätzliche wertvolle Informationen zur Therapieverbesserung des Pankreaskarzinoms zu erlangen.

2.3: Characterization of circulating tumor cell phenotypes identifies a partial-EMT subpopulation for clinical stratification of pancreatic cancer

Neben der Charakterisierung von Tumorgewebe spielen „liquid biopsy“ Ansätze zunehmend eine klinische Rolle (siehe Einleitung). In diesem Projekt analysierten wir daher die prognostische und prädiktive Signifikanz von zirkulierenden Tumorzellen (CTC) im PDAC. Der große Vorteil von CTCs besteht in der vollständig erhaltenen Integrität dieser Zellen, wohingegen andere Biomarker wie z.B. zellfreie DNA (cfDNA) nur fragmentiert vorliegen. Problematisch bei der Erforschung von CTCs ist jedoch die Isolation der Zellen, da CTCs nur in extrem geringen Mengen im Blutkreislauf zirkulieren (ca. 1–10 CTCs/10 mL Blut) (Alix-Panabières and Pantel, 2014).

Unsere Gruppe entwarf daher eine neue epitop-unabhängige Isolationsmethode, die auf dem unterschiedlichen Membranpotential der CTCs im Vergleich zu normalen Blutzellen (PBMC) beruht und dem Prinzip der Dielektrophorese folgt. Dabei erfolgt die Trennung der CTCs von anderen Blutzellen ähnlich einer Chromatographie in speziell konzipierten Kammern, auf Basis des Membranpotentials (sog. „dielectrophoresis-field flow fractionation“, DEP-FFF). Im Gegensatz zu gängigen Isolationsverfahren (Alix-Panabières and Pantel, 2014), die hauptsächlich Oberflächenantigene zur Isolation nutzen und daher oftmals nur spezifische CTC Subpopulationen anreichern, kann die DEP-FFF eine Vielzahl von CTC Populationen isolieren. Die erfolgreiche CTC Isolation dieser neuartigen Methode wiesen wir mittels Titrationsversuchen nach (Isolationsrate 89,1%), bei denen Zellkulturzellen in PBMC von gesunden Probanden zugegeben wurden (1-1200 CTCs, R^2=0.99).

Folgend ı rsuchten wir die prognostische Bedeutung von CTCs in einer prospektiven Kohorte von 74 PDAC Patienten (n=272 sequenzielle Blutproben). CTCs konnten hier in >75% der Patienten nachwiesen werden. Zur Charakterisierung der isolierten Zellen färbten wir diese immunhistochemisch mittels CD45 (Leukozytenmarker), EpCAM und Cytokeratin (CK, epitheliale Marker), Vimentin (mesenchymaler Marker), CD133 (Stammzellmarker) und DAPI (DNA-Marker). Die gefärbten CTC wurden dann in einem Vielfarben-Durchflusszytometer analysiert. Diese Technik verbindet die Geschwindigkeit und Sensibilität der Durchflusszytometrie mit der detaillierten Bildgebung eines Mikroskops und ermöglicht daher die genaue Charakterisierung von Zellen in einem hohen Durchsatz. Entsprechend der Proteinexpression wurde die CTC als epitheliale CTC (E-CTC), mesenchymale CTC (M-CTC), stammzellähnliche CTC (SC-CTC) oder im Sinne einer partiellen epithelialen-mesenchymalen Transition (pEMT-CTC) kategorisiert (Abbildung 10). Interessanterweise war der Anteil von pEMT-CTCs in metastasierten, therapienaiven Patienten signifikant erhöht im Vergleich zu nicht metastasierten Patienten (52.4% vs 28.4%, p = 0,004). Zudem hatten Patienten, die

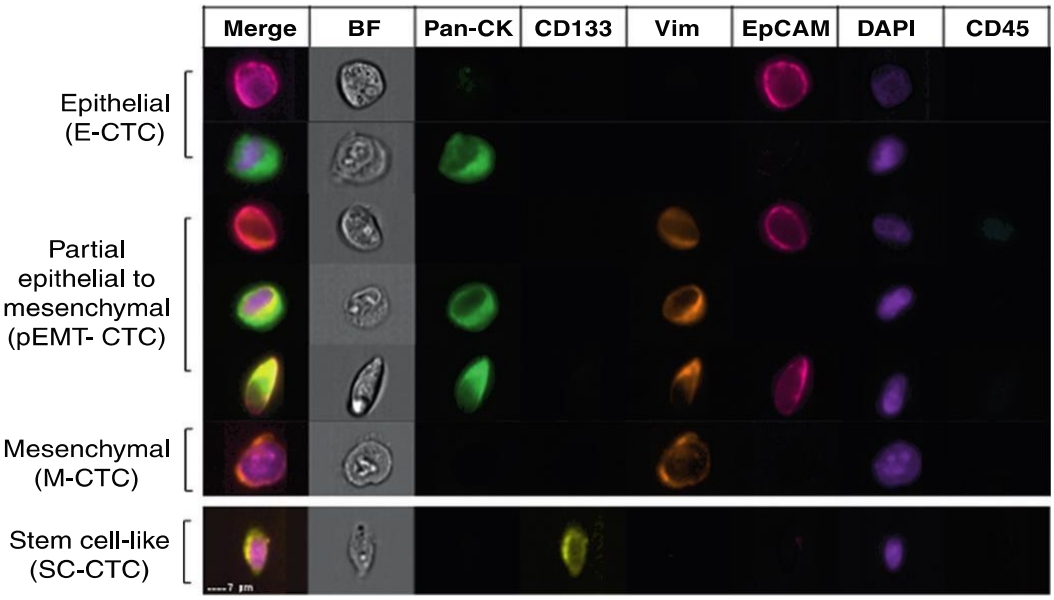

Abbildung 10: Mikroskopische Hellfeld (BF) und Immunofluoreszenz Bilder der mittels Imagestream Flow-Cytometrie anhand der Oberflächenmarker analysierten CTCs

einen > 50%igen Anteil von pEMT-CTC aufwiesen ein schlechteres progressionsfreies Überleben, (677 Tage vs. undef., p = 0,01), ein früheres Rezidiv nach Resektion (4/7 (57.1%) vs. 1/15 (6.7%), p=0,02 und ein verschlechtertes Gesamtüberleben (Abbildung 11). Bei metastasierten Patienten zeigte sich zudem ein deutlich schlechteres Gesamtüberleben, wenn mindestens ein pEMT-CTC nachgewiesen werden konnte (325.2 Tage vs. 731.0 Tage, p<0,001). Wir konnten durch die Einzelzellanalyse mittels ddPCR zeigen, dass alle CTC Subpopulationen inklusive der M- und pEMT-CTC eine *KRAS* Mutation aufwiesen und daher „echte“ Tumorzellen im Blut sind, was von einigen Gruppen bislang angezweifelt wurde.

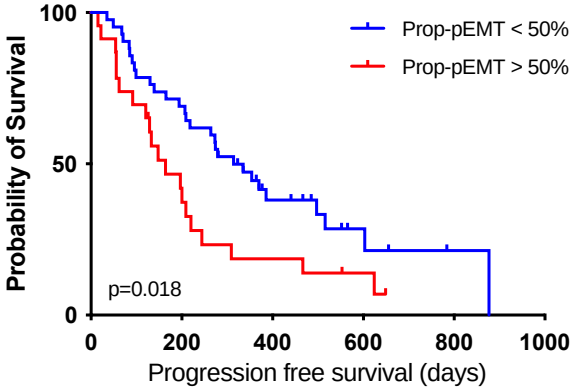

Abbildung 11: Kaplan Meier Kurve des Progression-freien Überlebens von Patienten mit mehr bzw. weniger als 50% Prop-pEMT

Zusammenfassend zeigt diese Arbeit, dass auch liquid biopsy Ansätze eine zunehmende prätherapeutische Bedeutung in der Risikostratifizierung von PDAC Patienten besitzen.

2.4: Single-Cell Transcriptomics of Pancreatic Cancer Precursors Demonstrates Epithelial and Microenvironmental Heterogeneity as an Early Event in Neoplastic Progression

Ziel des Projektes war die detaillierte Charakterisierung von IPMN bis auf Einzelzellebene zur Evaluation von ggf. abweichenden Progressionsmechanismen im Vergleich zu soliden PDACs und deren Bedeutung für die klinische Behandlung. Ein Fokus wurde dabei neben der Analyse der Tumorzellen auch auf das TME gelegt.

Aufgrund eines bis dato fehlenden Protokolls zur Herstellung einer Einzelzellsuspension in Pankreasgewebe erfolgte in einem ersten Schritt die systematische Optimierung und Validierung desselben für PDAC und IPMN. Folgend analysierten wir Gewebe von insgesamt 6 Patienten: jeweils zwei IPMNs mit geringgradigen Dysplasien (LG-IPMN), hochgradigen Dysplasien (HG-IPMN) und tumortragenden IPMNs (I-PDAC).

Zur Validierung unserer scRNA Daten verglichen wir diese in einem ersten Schritt mit Transkriptomdaten aus einer parallelen Massensequenzierung desselben Gewebes und fanden eine exzellente Korrelation der exprimierten Gene (r_s > 0.9). Bei der Analyse der insgesamt 5.403 Einzelzellen konnte, korrelierend zu Mausmodellen, eine deutliche Heterogenität aller Zellpopulationen (epithelialen Tumorzellen, Immun- und Stromazellen) während des Progresses von IPMN zu I-PDAC gezeigt werden. Insgesamt charakterisierten wir 10 individuelle Zellpopulationen: drei LG-IPMN-, eine HG-IPMN, zwei I-PDAC, zwei Immunzell- und zwei Stromazell-Populationen (Abbildung 12).

Zur detaillierten Subanalyse der einzelnen Zelltypen führten wir eine sog. virtuelle Mikrodissektion durch. Bei dieser Technik werden durch spezielle Algorithmen nur bestimmte Zellpopulationen herausgefiltert und dann erneut hinsichtlich ihrer Ähnlichkeit zueinander analysiert. Unsere Ergebnisse sind im Folgenden zur besseren Übersicht nach Zellklassen aufgeteilt:

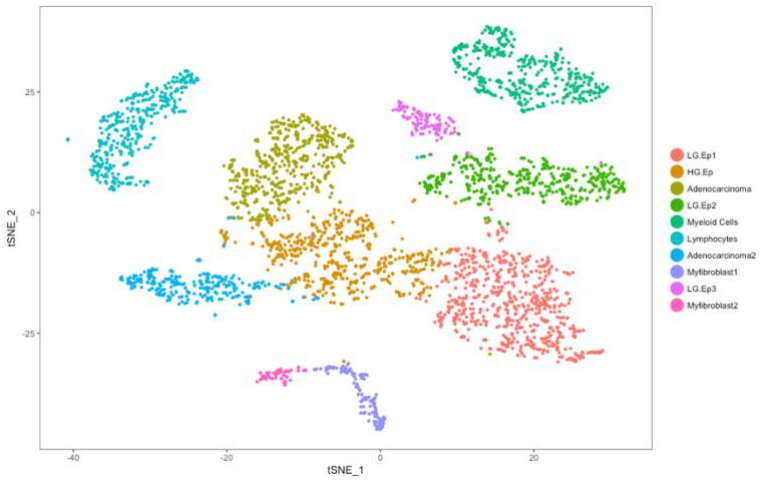

Abbildung 12: tSNE Plot aller 5.403 Zellen der 6 Läsionen annotiert nach Zellsubtypen (Ep = duktale Epithelzellen)

Epithelzellen exprimierten unter Progression von LG- über HG-IPMN zu I-PDAC zunehmend einen aggressiveren Phänotyp und verloren u.a. multiple Tumorsuppressorgene wie z.B. *RAP1GAP* (Zhang et al., 2006). Ebenso nahm die Fraktion spätproliferativer Epithelzellen deutlich zu. Auch zeigten Epithelzellen im Vergleich von HG-IPMN vs. LG-IPMN, sowie I-PDAC vs. HG-IPMN eine Zunahme von tumorassoziierten „canonical“ Signalwegen, wie z.B. den

Wnt/B-Catenin, Axonal guidance, Apoptose und Zellzyklusregulator-Signalwegen. I-PDAC Epithelzellen zeigten zudem eine zunehmende Dysregulation von DNA-Reparaturgenen, der TGF-B und der SAPK/JNK Signalkaskade. Überraschenderweise enthielten jedoch bereits LG-IPMN kleine Populationen von Zellen, die ein erhöhtes Entartungspotential besitzen und eher HG oder sogar I-PDAC Zellen ähnelten (Abbildung 13). Wir spekulierten daher, dass diese auffällig aggressiveren Zellpopulationen in LG-IPMN bereits den Ursprung von späteren Tumoren bilden könnten. Durch die hochsensitive scRNA-Technik können solche Populationen nun erstmals beschrieben und charakterisiert werden, was aufgrund von Überlagerung in der klassischen Massensequenzierung bisher nicht möglich war.

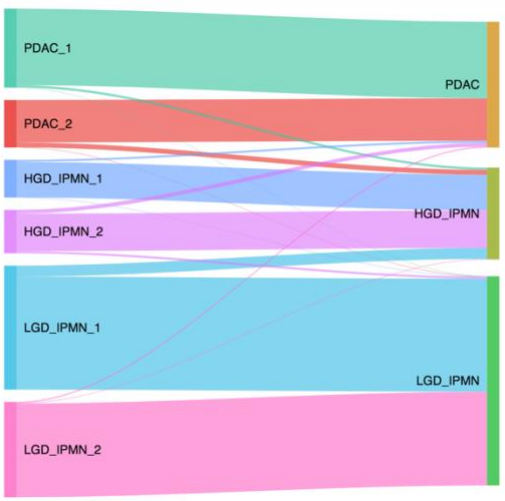

Abbildung 13: Sankey Diagramm, welches die Zuordnung von Epithelzellen zu den Subtypen (links) zu den jeweiligen Läsionstypen (rechts) zeigt

Aufgrund der kritischen Rolle des TME in der Tumorprogression beim PDAC (Ligorio et al., 2019) untersuchten wir dieses mittels virtueller Mikrodissektion genauer und wiesen sieben Immunzell-, fünf Stromazell- und zwei Fibroblastenpopulationen nach. Zusammengefasst zeigten IPMN deutliche Unterschiede des TME im Vergleich zu PDACs (Abbildung 14).

So sind LG und HG-IPMN z.B. von deutlich mehr $CD8^+$, aktivierten $CD4^+$ T-Zellen und dentritischen Zellen infiltriert. Außerdem zeigten LG-IPMN im Vergleich zu HG-IPMN und I-PDAC einen höheren Anteil von zytotoxischen $CD8^+$ T Zellen, während sowohl LG- als auch HG-IPMN im Vergleich zu I-PDAC praktisch keine Myeloide Suppressorzellen (MDSC) aufwiesen. Dies mag darauf hinweisen, dass einige IPMN-assoziierte Karzinome im Gegensatz zu soliden PDACs auf eine Therapie mit Vakzinen oder Immunotherapien ansprechen könnten.

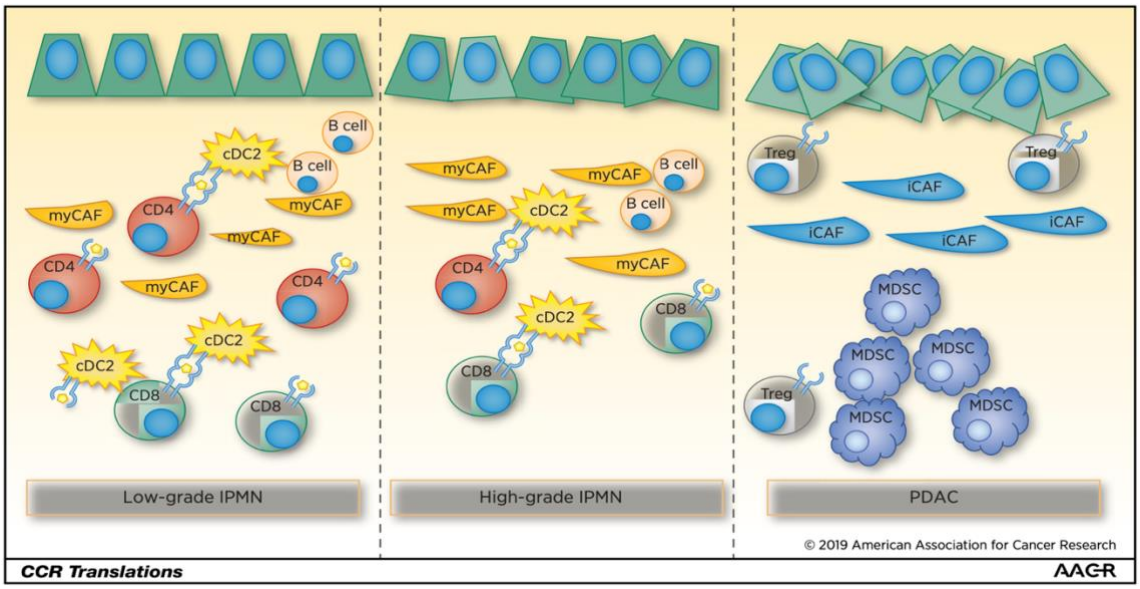

Abbildung 14: Schematische Darstellung der nachgewiesenen immunologischen und stromalen Einzelzellen in LG-, HG-IPMNs und I-PDACs {HernandezBarco:2019ij}

Bei der Analyse der Fibroblastencluster konnten wir mehrere Populationen nachvollziehen, die durch andere Gruppen beschrieben worden sind und eine hohe Relevanz für die Tumorprogression zeigen (myCAF and iCAF) (Öhlund et al., 2017). Interessanterweise kamen iCAFs ausschließlich in den PDAC Läsionen vor und überexprimierten v.a. Signalwege, die mit fortschreitender Metastasierung und Aggressivität von Tumoren assoziiert sind. Im Gegensatz dazu waren myCAF hauptsächlich in nichtmalignen IPMNs anzutreffen. Unsere Ergebnisse weisen auf eine tragende Rolle des umgebenden TME bei der Progression zystischer Pankreasläsionen hin, die sich teils gravierend von bekannten Mechanismen bei soliden PDAC unterscheiden.

Zusammenfassend schließt unsere Arbeit eine Wissenslücke zur Tumorprogression in zystischen Pankreasläsionen. Die Ergebnisse unserer Studie wurde zudem vom Clinical Cancer Research in einem Editorial zusammengefasst, was den Wert und die Bedeutung der Arbeit noch einmal unterstreicht (Hernandez-Barco et al., 2019).

3. Diskussion

Die Krebstherapie hat in den letzten Jahrzehnten einen tiefgreifenden Wandel durchlaufen. Bedingt durch innovative Techniken zur genetischen Charakterisierung von Tumoren, die unser Verständnis zum Tumorprogress und seiner Interaktion mit dem Immunsystem revolutioniert haben sowie technischen Errungenschaften in der operativen Therapie hat sich die Prognose der meisten Tumorentitäten deutlich verbessert. Im Gegensatz dazu zeigt das duktale Adenokarzinom des Pankreas trotz intensiver Forschung weiterhin nur eine Überlebensrate von unter 10%.
Ziel dieser kumulativen Habilitationsschrift ist daher die Evaluation neuer Analysemethoden zur Verbesserung der frühen Diagnose, Prognose und Therapiestratifizierung im PDAC.

In den vorgestellten Arbeiten konnten wir zeigen, dass

1. die diagnostische Genauigkeit einer PDAC Diagnose aus EUS-FNA Proben durch die Verwendung von axillären molekularen Testverfahren verbessert werden kann.
2. eine effektive, reproduzierbare und qualitativ hochwertige genetische Analyse zur prätherapeutischen Tumorcharakterisierung auch aus limitierten Gewebeproben möglich ist.
3. die prätherapeutische Tumorcharakterisierung prädiktives und prognostisches Potential besitzt und
4. sich das TME von zystischen IPMN signifikant von bekannten Progressionsmodellen solider PDAC unterscheidet.

Aufgrund der späten Diagnosestellung der meisten PDAC und der Tatsache, dass aktuelle Leitlinien eine histologische Sicherung vor Beginn einer systemischen Chemotherapie fordern, kommt der zuverlässigen Diagnosebestätigung ein hoher Stellenwert zu. In einem Großteil der Fälle erfolgt die histologische Sicherung durch eine EUS-FNA (siehe Einleitung, S. 10). Insgesamt weist diese laut Literatur eine ca. 80-90%ige Sensitivität zur Diagnose eines PDAC auf, jedoch zeigt die histologische Auswertung in bis zu 25% der Fälle nicht konklusive Fälle (beschrieben als suspekt für PDAC, atypisch oder nicht-diagnostisch) (Jani et al., 2016).
In diesem Zusammenhang konnten unsere und weitere Studien zeigen, dass die Diagnosesicherheit einer EUS-FNA auch durch genetische Untersuchungen verbessert werden. Aufgrund der hohen Prävalenz der *KRAS* Mutation im PDAC eignet sich diese Mutation dafür besonders und viele Arbeiten sowie entsprechende Metaanalysen zeigen den diagnostischen Zusatznutzen des *KRAS*-Status zur Diagnose des PDAC in EUS-FNA, was v.a. für histologisch nicht eindeutige EUS-FNA Proben gilt (Fuccio et al., 2013; Xu et al., 2014). Kritisch muss angemerkt werden, dass dabei in den analysierten Arbeiten hauptsächlich qPCR-basierte oder (Sanger) Sequenzierungs-Methoden zur *KRAS*-Detektion verwendet wurden. Jedoch bestätigen auch neuere Manuskripte mit aktualisierten Analysemethoden die

potentiellen diagnostischen Zusatzgewinne einer *KRAS*-Detektion (Gleeson et al., 2016; Ishizawa et al., 2020; Kameta et al., 2016; Ono et al., 2020; Sho et al., 2017).

Insgesamt ist bisher eine große Anzahl von Analyseverfahren zum Nachweis einer *KRAS* Mutation in diesem Zusammenhang getestet worden (Fuccio et al., 2013; Ishizawa et al., 2020; Jani et al., 2016; Ono et al., 2020), jedoch bietet die von uns verwendete ddPCR entscheidende Vorteile. So besitzt sie eine niedrige Nachweisgrenze (theoretische Detektion bis zu einer MAF von 0,01%), eine einfache Handhabung und benötigt zudem nur eine geringe DNA-Menge. Limitiert wird die Diagnosesicherheit des in dieser Arbeit verwendeten Multiplex *KRAS*-Panels durch die fehlende Detektion der Mutationen im Q61 Exon, die ca. 1% der KRAS Mutationen ausmachen (Lu et al., 2016) und der Tatsache, dass ca. 10% der Patienten generell keine *KRAS*-Mutation aufweisen (Singhi et al., 2019). Es existieren zwar spezielle ddPCR-Sonden für Q61 *KRAS*-Mutationen, jedoch erhöht der Einschluss weiterer SNV Assays die diagnostische Komplexität und auch die notwendige DNA-Konzentration. Die DNA-Menge ist jedoch gerade in EUS-FNA Proben niedrig. Ebenso ist die Tumorzellfraktion aus dem pauci-zellulären EUS-FNA Gewebe niedrig, was noch zusätzlich den Mutationsnachweis erschwert. Auch das Probenmaterial hat hier einen direkten Einfluss auf den *KRAS*-Nachweis. Grundsätzlich kann DNA direkt aus frischen EUS-FNA, den Ausstrichpräparaten oder nach Fixierung aus FFPE-Blöcken gewonnen werden. FFPE-Blöcke weisen dabei eine signifikant schlechtere DNA-Qualität auf als frisch prozessierte oder in entsprechenden Medien schockgefrorene Proben (Hartley et al., 2017). Insgesamt lieferten in unserer Studie 2/31 (6,5%) EUS-FNA Proben keine ausreichende DNA-Menge für eine weitergehende Untersuchung, was sich mit Ergebnissen vorheriger Studien deckt (Fuccio et al., 2013; Hewitt et al., 2012; Layfield et al., 2014).

Im Vergleich zur ddPCR besitzen NGS-Verfahren eine um ca. 2 Potenzen schlechtere, untere Nachweisgrenze und sind in diesem Punkt der ddPCR deutlich unterlegen (Corcoran and Chabner, 2018). Ebenso sind Sequenzierungsverfahren generell deutlich aufwändiger hinsichtlich Material, Kosten und Zeit, so dass eine Implementierung gerade in kleineren Krankenhäusern fraglich erscheint. Auf der anderen Seite können NGS-Genpanels nicht nur einzelne SNV sondern eine Vielzahl von Mutationen nachweisen, was die diagnostische Sicherheit erhöhen kann.

Eine weitere Schwierigkeit bei der Interpretation des *KRAS*-Mutationsstatus als auxiliärer Diagnosemarker sind falsch-positive Befunde. So weisen z.B. Patienten mit einer chronischen Pankreatitis in bis zu 20% der Fälle ebenfalls *KRAS*-Mutation auf (Rashid et al., 2018; Rivera et al., 1997). Hier müssen radiologische Hinweise für das Vorliegen einer Pankreatitis wie z.B. Kalzifikationen oder Auffälligkeiten im Ductus Wirsungianus bei der Auswertung berücksichtigt werden (Tirkes et al., 2019).

Zum direkten Vergleich verwendeten wir in unserem Versuchsaufbau daher zusätzlich ein Genpanel-basiertes Verfahren. Dadurch gehört diese Arbeit zu den wenigen, die verschiedene Verfahren unmittelbar gegenübergestellt hat. Im direkten Vergleich zeigt sich dabei ein leichter diagnostischer Vorteil für das Genpanel basierte Verfahren, v.a. aufgrund der

breiteren „Abdeckung“ von pathologisch erachteten Mutationen trotz verringerter Nachweisgrenze. Aufgrund der geringen Fallzahl sollte jedoch eine weitere Validierung der Ergebnisse in entsprechenden Kohorten erfolgen.
Eine weitere Möglichkeit zur Verbesserung der diagnostischen Präzision besteht in der „rapid on-site evaluation“ (ROSE). Sie bezeichnet ein zyto-morphologisches Schnellverfahren, das während der laufenden endoskopischen Untersuchung durchgeführt werden kann. Innerhalb von Minuten können dabei durch einen Zytopathologen EUS-FNA Probenqualität bestimmt und mittels Schnellfärbung auch eine vorläufige Diagnose gestellt werden. Die ROSE kann dabei zu einer 10-15%igen Verbesserung der diagnostischen Sicherheit führen. Jedoch ist sie limitiert durch eine eingeschränkte Verfügbarkeit außerhalb großer Zentren (Erickson et al., 2000; Larghi et al., 2014).
Letztlich bleibt als Hauptdiagnosekriterium der histologische Nachweis eines PDACs. Die erwähnten molekularen Marker kommen hauptsächlich dann zum Tragen, wenn die histologische Diagnose unsicher ist. In diesem Fall können sie, wie in unseren und weiteren Arbeiten gezeigt, die diagnostische Sicherheit der PDAC Diagnose erhöhen. Besonders problematisch bleiben in diesem Zusammenhang z.B. PDAC Verdachtsfälle bei Patienten mit einer chronischen Pankreatitis, für die trotz aller analytischen Fortschritte weiterhin eine hohe Diagnoseunsicherheit besteht.
Alternativ zu EUS-FNA wird in den letzten Jahren die Verwendung neuer endoskopischer Biopsiemethoden diskutiert. Diese als EUS Feinnadelbiopsie (EUS-FNB) bezeichneten Verfahren verwenden kein Aspirationsverfahren, sondern speziell geschliffene Punktionshohlnadeln, die ähnlich einer transkutanen Biopsie Gewebe-Stanzzylinder gewinnen. EUS-FNB zeigen in mehreren Arbeiten Vorteile sowohl hinsichtlich einer histologischen PDAC Diagnose als auch eine signifikant höhere DNA-Menge und Qualität (Bang et al., 2018; Elhanafi et al., 2018). Nichtsdestotrotz existieren auch Arbeiten, die keinen Vorteil der neuen Biopsietechnik dokumentieren (Asokkumar et al., 2019). EUS-FNB könnten daher einen wichtigen Beitrag bei der PDAC Diagnoseverbesserung liefern, gehen jedoch mit einer deutlichen Kostensteigerung einher, was einen flächendeckenden Einsatz bisher verhindert hat. Trotz aller diskutierten Probleme ist speziell in Hinblick auf die komplikationsreiche Pankreaschirurgie und die nebenwirkungsreiche Chemotherapie eine maximale prätherapeutische Diagnosesicherung auch unter Verwendung molekularer oder alternativer Biopsieverfahren anzustreben. Welche Methode sich hierbei in Zukunft durchsetzen wird, bleibt abzuwarten.

Das EUS-FNA Material einer einzigen Aspiration kann jedoch nicht nur zur Diagnose verwendet werden, sondern erlaubt auch - unter Verwendung entsprechender Techniken - eine deutlich detailliertere Tumoranalyse. So konnten wir als eine der ersten Gruppen zeigen, dass selbst limitierte EUS-FNA Proben auch für WES-Sequenzierungen geeignet sind (Semaan et al., 2020; Aguirre et al., 2018; Aung et al., 2018; Dreyer et al., 2019). Unsere Studie (Semaan et al., 2020)

zeigt, dass die Probenqualität der EUS-FNA durch innovative Verbesserungen der Tumoranalyse eine valide und detaillierte genetische Analyse erlaubt. Ein essentieller Bestandteil besteht dabei in der prä-analytischen Anreicherung der Epithelzellen, welche effektiv und sicher durchgeführt werden kann. Unsere Ergebnisse bestätigten sich zudem in einer unabhängigen Kohorte des Dana-Farber Cancer Institute (DFCI).
Jede Anreicherung birgt jedoch die Gefahr, dass es durch diesen zusätzlichen Schritt der Probenaufarbeitung zu einem irreversiblen Verlust von Tumorzellen kommt. Das von uns eingesetzte Anreicherungsverfahren muss unmittelbar an frischen Proben durchgeführt werden, was eine breite klinische Anwendung des Verfahrens limitieren kann. Die Sequenzierung des gesamten Tumorexoms vor Therapiebeginn bringt dabei einen enormen prädiktiven und prognostischen Zugewinn.
Bisher scheiterte eine prätherapeutische PDAC Evaluation häufig an der Unmöglichkeit, bekannte PDAC Subtypen aus EUS-FNA Proben überhaupt zu klassifizieren, da in anderen Studien meist nur targeted Panels oder Einzelmutationen in EUS-FNA Proben erfolgreich verwendet wurden (Aguirre et al., 2018; Alix-Panabières and Pantel, 2014; Raphael, 2017).
Ein weiteres Problem aller Sequenzierungstechniken ist der zeitliche Aufwand der Probenprozessierung und Datenauswertung. Letztlich kann mit einer ROSE Evaluation die Diagnose eines PDAC unmittelbar gestellt werden, wohingegen jede weitere molekulare Diagnostik einen Therapiebeginn verzögert. Bei der ddPCR kann die Analyse hierbei in ca. 1-2 Tagen durchgeführt werden. Ein WES, scRNA oder transkriptionelle Analyse benötigt im Schnitt ca. einen Monat (Probenaufbereitung, Library Präparation, Sequenzierung, Datenprozessierung und Datenauswertung/Interpretation) (Aguirre et al., 2018). Diese zusätzliche Zeit verzögert den Beginn einer gezielten Therapie und es muss evaluiert werden, inwieweit sich eine unmittelbare Therapieeinleitung vs. einer verzögerten aber molekular gesteuerten Therapieeinleitung auf die PDAC Prognose auswirkt.
Ein Großteil der Therapieentscheidungen wird weiter alleine aufgrund von klinischen Gesichtspunkten getroffen, obwohl es inzwischen klare Hinweise in unseren wie auch weiteren Studien für ein verbessertes Ansprechen von PDAC Patienten mit einem HRD-Phänotyp, einem instabilen bzw. einem basalen Subtyp gibt (Aguirre et al., 2018; Aung et al., 2018; Waddell et al., 2015). Laufende Studien wie z.B. der COMPASS Trial (NCT02750657) werden dabei in Zukunft wichtige Informationen für den Stellenwert detaillierter präoperativer Tumorcharakterisierungen im PDAC liefern (Aung et al., 2018).

Heutzutage werden in einigen Tumorentitäten bereits standardmäßig molekulare Analysen auf therapierelevante Alterationen durchgeführt. Patienten mit malignen Melanomen oder Mammakarzinomen werden z.B. auf eine *BRAF* V600 Mutation bzw. ihren HER2 Status untersucht und einer entsprechenden Therapie zugeführt (Chapman et al., 2011; Slamon et al., 2001). Ein Großteil der Tumore wird jedoch weiterhin „klassisch“ anhand der histologischen Entität und dem UICC Stadium behandelt. Ein alternativer Weg in der

Tumortherapie ist die Verwendung von sogenannten Master Protocol Studien (Umbrella- oder Basket-Trials). Diese beschreiben eine Therapieauswahl alleine basierend auf dem Nachweis spezifischer Alterationen unabhängig von der jeweiligen Tumorentität. In den letzten Jahren hat die Zahl solcher Studien deutlich zugenommen (Park et al., 2019; Woodcock and LaVange, 2017). Beispielhaft sei hier die 2015 erschienene Studie von Hyman et al. zitiert, die in einem Phase II Basket Trial das Ansprechen von Vemurafenib in Nicht-Melanom Tumoren mit einer nachgewiesenen *BRAF* V600 Mutation evaluierten. Dabei zeigte sich, dass einige, aber nicht alle Tumorarten deutlich auf diese experimentelle Therapie ansprachen, so dass vermutet werden muss, dass neben spezifischen SNVs auch die Tumorentität und das lokale TME eine entscheidende Rolle für die Wirksamkeit spielen.

Neben der Therapiestratifizierung ist das nicht-invasive Therapiemonitoring eine weitere große Errungenschaft der molekularen Diagnostik. Dabei hat sich in multiplen Arbeiten gezeigt, dass liquid biopsy Ansätze wertvolle Informationen zur Behandlungskontrolle bieten können (Corcoran and Chabner, 2018). Grundlage hierfür ist die Annahme, dass sich Tumore unter dem Evolutionsdruck einer Chemotherapie verändern und zunehmend Resistenzen entwickeln (McGranahan and Swanton, 2017). Eine einzelne Biopsie kann erstens bei metastasiertem Tumorleiden nicht die Gesamtheit der verschiedenen Tumorklonalität abbilden und zweitens ist eine serielle bioptische Probenentnahme meist aufgrund des akkumulierten Komplikationsrisikos nicht möglich. Blutbasierte Tests hingegen können diese Hürden überwinden (Bardelli and Pantel, 2017).
Der Vorteil von CTC im Gegensatz zu cfDNA ist, dass CTC intakte Zellen repräsentieren, wohingegen cfDNA aus fragmentierter DNA von untergegangenen Tumorzellen besteht. Leider ist die Detektion von CTC gerade im PDAC aufgrund der generell geringen CTC-Anzahl besonders anspruchsvoll (Martini et al., 2019). Es existiert letztlich nur ein durch die FDA zugelassenes Isolationssystem (Cell Search, Menarini Silicon Biosystems). Dieses reichert CTC epitopabhängig an und hat daher den Nachteil nur CTCs zu isolieren, welche die Oberflächenproteine EpCAM/Zytokeratin 18/19 tragen. Wir und andere Gruppen konnten indes zeigen, dass viele CTCs durch diesen Isolationsansatz nicht erfasst werden (Aiello and Kang, 2019; Alix-Panabières and Pantel, 2014; Gemenetzis et al., 2018; Porter et al., 2019; Poruk et al., 2016; Ting et al., 2014). Durch das von uns entwickelte DEP-FFF System kann diese wichtige Hürde überwunden werden und CTCs unabhängig von ihren Oberflächeneigenschaften isoliert werden.
Neben dem DEP-FFF Isolationssystem existieren einige weitere epitop-unabhängige CTC Isolationssysteme, die jedoch alle nur in Studien getestet wurden (Gemenetzis et al., 2018; Poruk et al., 2016; 2017; Ting et al., 2014). Diese isolieren CTCs basierend auf ihrer Größe (ISET: Isolation by Size of Epithelial Tumor) (Kulemann et al., 2017; Poruk et al., 2016; 2017), durch Immunofluoreszenz (Gemenetzis et al., 2018) oder die Mikromanipulation von Zellen (Ting et al., 2014). Verschiedene Studien konnten im Vergleich zum Cell Search System in

anderen Tumorentitäten zeigen, dass epitop-unabhängige CTC-Isolationsverfahren dem Cell Search System überlegen sind (Andreopoulou et al., 2012; Maertens et al., 2017; Zavridou et al., 2020). Insgesamt existieren jedoch keine Vergleichsstudien zwischen unterschiedlichen epitop-unabhängigen CTC Isolationssystemen v.a. aufgrund des bisher hauptsächlich experimentellen Charakters der Isolationsmethoden und der daher schwierigen Vergleichbarkeit (Martini et al., 2019).
Neben der Isolation von CTCs mit eher mesenchymalem Charakter, die von uns ebenso wie in vielen Studien als Ausdruck einer erhöhten epithel-zu-mensenchymal Transition (EMT) gewertet worden sind (Aiello and Kang, 2019; Nieto et al., 2016), besteht mit dem von uns vorgestellten DEP-FFF System auch die Möglichkeit für die Anlage von CTC Organoidkulturen. Dies ist möglich, da die CTCs im Gegensatz zum CellSearch System nicht fixiert werden müssen (Tiriac et al., 2018). Organoidmodelle können in der personalisierten Medizin zur Prädiktion eines patienten-individuellen Therapieansprechens verwendet werden (Bengtsson et al., 2021). Dabei wird das Patienten-Organoid in-vivo hinsichtlich seines Ansprechens auf unterschiedliche Chemotherapeutika und deren Kombinationen evaluiert (Driehuis et al., 2019).
Letztlich muss jedoch betont werden, dass die Isolation von CTCs auch mit unserer DEP-FFF Methode einen deutlichen Personal- und Zeitaufwand darstellt, der in Relation mit den zu erwartenden Ergebnissen gesetzt werden muss. Zudem ist die verwendete Blutmenge zur Isolation von CTCs höher verglichen mit der notwendigen Plasmamenge zur cfDNA Analyse (Ignatiadis et al., 2021). Auch erfolgten in den letzten Jahren zunehmend klinische Zulassungen für cfDNA Anwendungen, wie z.B. 2016 die Zulassung eines cfDNA Assays zur Therapiestratifizierung von nicht-kleinzelligen Bronchialkarzinomen (Kwapisz, 2017; Leighl et al., 2019) oder 2020 die Zulassung im Ovarial-, dem Mamma- und dem Prostatakarzinom. Insgesamt bleibt abzuwarten, welches Kompartiment der liquid biopsy sich als Methode der Wahl für ein nicht-invasives Therapiemonitoring durchsetzt.

Wie bereits in der Einleitung ausgeführt, hat die Einzelzellsequenzierung unser Verständnis der Tumorbiologie entscheidend verändert. Durch die erstmalige Charakterisierung des Tumorprogresses auf der Einzelzellebene in humanen IPMNs konnten wir dazu einen wichtigen Beitrag leisten. Bisherige Studien haben nur in autochtonen Mausmodellen eine große Heterogenität in fortgeschrittenen I-PDAC beschrieben (Ting et al., 2014). Wir konnten diese Ergebnisse bestätigen und zeigen, dass im Menschen eine ausgeprägte Heterogenität der humanen IPMN Tumorzellen besteht. Unsere Ergebnisse weisen dabei auf eine tragende Rolle des TME bei der IPMN Progression hin, welche sich teils von bekannten Mechanismen bei soliden PDACs unterscheidet. Solide PDACs entwickeln sich aus PanIN und sind charakterisiert durch ihr immunsuppressives TME. So findet man im TME solider PDACs v.a. myeloide Suppressorzellen (MDSC), Tregs und tumorassozierte Makrophagen (TAM) (Daley et al., 2016). Dabei spielen scheinbar Tregs als Treiber der Tumorprogression durch eine

verminderte Aktivierung und Infiltration des Tumors mit zytotoxischen T-Zellen eine tragende Rolle. Dieses immunsuppressive TME wird maßgeblich durch die Interaktion von Tregs mit dendritischen Zellen vermittelt (Jang et al., 2017). Im Gegensatz zur PanIN-PDAC Sequenz, welche schon in frühen Läsionen durch eine signifikante Reduktion von CD8-positiven T-Zellen gekennzeichnet ist, weisen LG-IPMN Läsionen - laut unseren Daten - einen hohen Anteil dieser zytotoxischen T-Zellen im Vergleich zu HG-IPMN und I-PDAC auf. Interessanterweise sind hingegen MDSCs praktisch nicht in LG- und HG-IPMN vorhanden, wohingegen sie in I-PDAC vermehrt vorkommen, was sich mit dem Progressionsmuster im TME von soliden PDAC deckt. Weiterhin konnten wir zeigen, dass sowohl LG- als auch HG-IPMN aktivierte CD4-positive T-Zellen und dendritische Zellen des sogenannten DC2-Typs aufweisen. Das Vorhandensein sowohl von zytotoxischen CD8-positiven T-Zellen, aktivierten CD4-positive T-Zellen und dendritischen Zellen unterscheidet ein IPMN dabei substantiell vom TME in PanINs. Basierend auf Arbeiten zur Charakterisierung des stromalen Kompartments in soliden PDACs (Öhlund et al., 2017) konnten wir sowohl Myofibroblasten (myCAF) als auch inflammatorische iCAF nachweisen. MyCAF waren dabei v.a in den Vorläuferläsionen lokalisiert, wohingegen die entzündungsfördernden und protumoriogenen iCAF ausschließlich in den I-PDAC gefunden wurden und Gene, wie z.B. *CXCL12* und *COL3A1* exprimierten, die in vielen Tumorarten mit einer systemischen Metastasierung assoziiert sind (Tsai et al., 2015). Ultimativ könnten I-PDAC und seine zystischen Vorläuferläsionen - basierend auf unseren Ergebnissen - aufgrund eines „aktiveren“ Immunkompartments möglicherweise besser auf Immuntherapien oder Chemopräventionsstrategien reagieren.

Überraschenderweise enthielten zudem bereits LG-IPMN kleine Populationen von Zellen, die I-PDAC ähneln. Wir mutmaßen daher, dass es sich bei diesen Zellen, ggf. um Keimzellen der späteren Tumore handelt, was jedoch durch unseren Versuchsaufbau nicht eindeutig bewiesen werden konnte und in einer größeren, unabhängigen Kohorte validiert werden muss.

Die „nächste Stufe“ zum Verständnis der Tumorbiologie repräsentieren aktuell räumliche Sequenzierungsverfahren, wie z.B. der „digital spatial profiler“ von Nanostring oder Spatial Visium Plattform von 10x Genomics. Diese ermöglichen die Evaluation von quantitativen Sequenzierungsdaten mit der räumlichen Anordnung der Zelltypen im Gewebe (Larsson et al., 2021). Diese Techniken werden uns mit großer Wahrscheinlichkeit weitere wichtige Details zur Tumorbiologie liefern können und steigern das biologische Verständnis durch die räumliche Komponente enorm (Marx, 2021).

Zusammenfassend konnten wir verschiedene neuartige Methoden entwickeln, die eine detaillierte Charakterisierung von Pankreaskarzinomen auch aus limitierten Gewebeproben ermöglichen und zur Verbesserung der Diagnostik und Prognose verwendet werden können. Blutplasmabasierte, serielle liquid biopsies können zudem bei der Therapiestratifizierung behilflich sein. Ebenso wiesen wir durch Einzelzellsequenzierung erstmals nach, dass sich das

Tumormikromilieu zystischer Pankreastumoren deutlich von soliden Tumoren unterscheidet und potentielle neue Angriffspunkte für neuartige Therapieverfahren besitzt. Letztlich muss das Ziel weiterer Bemühungen die klinische Etablierung dieser Techniken zur Individualisierung der Behandlung beim Pankreaskarzinom sein. Die fortwährende Erforschung der Tumorbiologie und die prätherapeutische, genetische Charakterisierung des PDAC kann dabei die Basis für die Etablierung molekularer Tumorboards bilden. In diesen könnten zur Therapieindividualisierung genetische Alterationen und Muster als auxilliäre Prognose- und Prädiktionsmarker angewandt werden, um hoffentlich in Zukunft das Outcome der Patienten mit dieser Erkrankung signifikant zu verbessern.

4. Zusammenfassung

Das duktale Adenokarzinom des Pankreas (PDAC) hat unter allen Tumorerkrankungen eine der schlechtesten Überlebensraten und weist eine steigende Inzidenz auf. Die einzige kurative Möglichkeit besteht in der kompletten Resektion, jedoch ist diese aufgrund einer oftmals späten Diagnosestellung nur selten möglich. Leitlinien fordern vor dem Einsatz einer systemischen Therapie die histologische Diagnosesicherung. Aufgrund der anatomischen Lage des Pankreas ist jedoch nur eine endoskopische Feinnadel-Aspirationsbiopsie (EUS-FNA) möglich, die in ihrer Qualität stark abhängig vom Untersucher ist und zudem schwierig in der diagnostischen Aufarbeitung. Trotz zunehmender Hinweise einer Therapierelevanz der genetischen Tumor-Landschaft für das Ansprechen von Zytostatika auch im PDAC erfolgt die Chemotherapieentscheidung weiterhin v.a. nach klinischen Gesichtspunkten.

Wir beschäftigten uns daher mit der Evaluation des prognostischen und prädiktiven Wertes genetischer Charakterisierungen im PDAC. In insgesamt vier Arbeiten beleuchteten wir dabei verschiedene Aspekte der Fragestellung.

So wiesen wir in unserer ersten Arbeit nach, dass durch die auxilliäre Verwendung des *KRAS*-Mutationsstatus bzw. eines Genpanels die Diagnosesicherheit von EUS-FNA v.a. bei histologisch nicht eindeutigen Befunden signifikant verbessert werden kann. Auch zählt unsere Arbeit zu den wenigen, die einen Vergleich verschiedener Methoden beinhaltet.

In einer zweiten Arbeit konnten wir durch die Verwendung einer innovativen Anreicherungsstrategie und einer ultrasensitiven Sequenzierung des gesamten Genoms zeigen, dass EUS-FNA Proben - entgegen bisheriger Arbeiten - auch für eine detaillierte, prätherapeutische Tumorcharakterisierung verwendet werden können. Die dadurch bestehende neue Möglichkeit einer prätherapeutischen Analyse der genetischen Tumorlandschaft eröffnet so neue Möglichkeiten zur individualisierten Therapie.

In der dritten hier vorgestellten Arbeit entwickelten und validierten wir einen neuen, epitop-unabhängigen Isolationsansatz für zirkulierende Tumorzellen (CTC). Mit diesem war die Isolation von mesenchymalen CTC-Populationen möglich, die in einer großen prospektiven und seriellen PDAC Kohorte eine hohe prognostische Bedeutung besitzt.

Zum genaueren Verständnis der Tumorbiologie und des umgebenden Tumormikromilieus (TME) untersuchten wir in der letzten Arbeit zystische Vorläuferläsionen des PDACs, sogenannte intraduktale papillär-muzinöse Neoplasien (IPMN). Durch die Verwendung neuester Einzelzellsequenzierungs-Techniken konnten wir erstmals Besonderheiten der IPMN Progression auf der Einzelzellebene beschreiben. Unsere Ergebnisse weisen auf eine tragende

Rolle des TME bei der IPMN Progression hin, die sich teils von bekannten Mechanismen bei soliden PDACs unterscheiden. Zudem fanden wir heraus, dass bereits IPMN mit geringgradigen Dysplasien kleine Populationen von Zellen beinhalten, die den späteren invasiven Tumorzellen ähneln und diese frühen Keimzellen des späteren Tumors entsprechen könnten.

Zusammenfassend zeigen diese Arbeiten den hohen diagnostischen, prognostischen und prädiktiven Nutzen genetischer Analysen im PDAC, die zur Verbesserung der Patientenversorgung zunehmend in den klinischen Alltag integriert werden sollten.

5. Überlappung aufgrund kumulativer Arbeiten

Eine Überlappung durch die gemeinsamen Autorschaften, die in dieser kumulativen Habilitationsschrift aufgeführt sind, ist ausgeschlossen, da keiner der Koautoren im deutschsprachigen Raum zu habilitieren gedenkt.

6. Bibliographie

Aguirre, A.J., Nowak, J.A., Camarda, N.D., Moffitt, R.A., Ghazani, A.A., Hazar-Rethinam, M., Raghavan, S., Kim, J., Brais, L.K., Ragon, D., et al. (2018). Real-time Genomic Characterization of Advanced Pancreatic Cancer to Enable Precision Medicine. Cancer Discov *8*, 1096–1111.

Aiello, N.M., and Kang, Y. (2019). Context-dependent EMT programs in cancer metastasis. J. Exp. Med. *216*, 1016–1026.

AJCC, A.J.C.O.C. NCCN Guidelines Version 1.2015 Pancreatic Adenocarinoma.

Alexandrov, L.B., Kim, J., Haradhvala, N.J., Huang, M.N., Tian Ng, A.W., Wu, Y., Boot, A., Covington, K.R., Gordenin, D.A., Bergstrom, E.N., et al. (2020). The repertoire of mutational signatures in human cancer. Nature *578*, 94–101.

Alix-Panabières, C., and Pantel, K. (2014). Challenges in circulating tumour cell research. Nat Rev Cancer *14*, 623–631.

Andreopoulou, E., Yang, L.-Y., Rangel, K.M., Reuben, J.M., Hsu, L., Krishnamurthy, S., Valero, V., Fritsche, H.A., and Cristofanilli, M. (2012). Comparison of assay methods for detection of circulating tumor cells in metastatic breast cancer: AdnaGen AdnaTest BreastCancer Select/Detect™ versus Veridex CellSearch™ system. Int J Cancer *130*, 1590–1597.

Asokkumar, R., Yung Ka, C., Loh, T., Kah Ling, L., Gek San, T., Ying, H., Tan, D., Khor, C., Lim, T., and Soetikno, R. (2019). Comparison of tissue and molecular yield between fine-needle biopsy (FNB) and fine-needle aspiration (FNA): a randomized study. Endosc Int Open *7*, E955–E963.

Aung, K.L., Fischer, S.E., Denroche, R.E., Jang, G.H., Dodd, A., Creighton, S., Southwood, B., Liang, S.-B., Chadwick, D., Zhang, A., et al. (2018). Genomics-Driven Precision Medicine for Advanced Pancreatic Cancer: Early Results from the COMPASS Trial. Clin. Cancer Res. *24*, 1344–1354.

Bailey, P., Chang, D.K., Nones, K., Johns, A.L., Patch, A.-M., Gingras, M.-C., Miller, D.K., Christ, A.N., Bruxner, T.J.C., Quinn, M.C., et al. (2016). Genomic analyses identify molecular subtypes of pancreatic cancer. Nature *531*, 47–52.

Bang, J.Y., Hebert-Magee, S., Navaneethan, U., Hasan, M.K., Hawes, R., and Varadarajulu, S. (2018). EUS-guided fine needle biopsy of pancreatic masses can yield true histology. Gut *67*, 2081–2084.

Bardelli, A., and Pantel, K. (2017). Liquid Biopsies, What We Do Not Know (Yet). Cancer Cell *31*, 172–179.

Bengtsson, A., Andersson, R., Rahm, J., Ganganna, K., Andersson, B., and Ansari, D. (2021). Organoid technology for personalized pancreatic cancer therapy. Cell Oncol (Dordr) *44*, 251–260.

Bettegowda, C., Sausen, M., Sausen, M., Leary, R.J., Kinde, I., Kinde, I., Wang, Y., Wang, Y., Agrawal, N., Bartlett, B.R., et al. (2014). Detection of circulating tumor DNA in early- and late-stage human malignancies. Sci Transl Med *6*, 224ra24.

Biankin, A.V., Waddell, N., Waddell, N., Kassahn, K.S., Kassahn, K.S., Gingras, M.-C., Gingras, M.-C., Muthuswamy, L.B., Muthuswamy, L.B., Johns, A.L., et al. (2012). Pancreatic cancer genomes reveal aberrations in axon guidance pathway genes. Nature *491*, 399–405.

Bidard, F.-C., Weigelt, B., and Reis-Filho, J.S. (2013). Going with the flow: from circulating tumor cells to DNA. Sci Transl Med *5*, 207ps14.

Brinton, L.T., Sloane, H.S., Kester, M., and Kelly, K.A. (2015). Formation and role of exosomes in cancer. Cell Mol Life Sci *72*, 659–671.

Chapman, P.B., Chapman, P.B., Hauschild, A., Hauschild, A., Robert, C., Robert, C., Haanen, J.B., Haanen, J.B., Ascierto, P., Ascierto, P., et al. (2011). Improved survival with vemurafenib in melanoma with BRAF V600E mutation. N Engl J Med *364*, 2507–2516.

Chin, V., Nagrial, A., Sjoquist, K., O'Connor, C.A., Chantrill, L., Biankin, A.V., Scholten, R.J., and Yip, D. (2018). Chemotherapy and radiotherapy for advanced pancreatic cancer. Cochrane Database Syst Rev *3*, CD011044.

Choi, S.H., Park, S.H., Kim, K.W., Lee, J.Y., and Lee, S.S. (2017). Progression of Unresected Intraductal Papillary Mucinous Neoplasms of the Pancreas to Cancer: A Systematic Review and Meta-analysis. Clin. Gastroenterol. Hepatol. *15*, 1509–1520.e4.

Collisson, E.A., Bailey, P., Chang, D.K., and Biankin, A.V. (2019). Molecular subtypes of pancreatic cancer. Nat Rev Gastroenterol Hepatol *16*, 207–220.

Collisson, E.A., Sadanandam, A., Olson, P., Gibb, W.J., Truitt, M., Gu, S., Cooc, J., Weinkle, J., Kim, G.E., Jakkula, L., et al. (2011). Subtypes of pancreatic ductal adenocarcinoma and their differing responses to therapy. Nat Med *17*, 500–503.

Conroy, T., Hammel, P., Hebbar, M., Ben Abdelghani, M., Wei, A.C., Raoul, J.-L., Choné, L., Francois, E., Artru, P., Biagi, J.J., et al. (2018). FOLFIRINOX or Gemcitabine as Adjuvant Therapy for Pancreatic Cancer. N Engl J Med *379*, 2395–2406.

Corcoran, R.B., and Chabner, B.A. (2018). Application of Cell-free DNA Analysis to Cancer Treatment. N Engl J Med *379*, 1754–1765.

Daley, D., Zambirinis, C.P., Seifert, L., Akkad, N., Mohan, N., Werba, G., Barilla, R., Torres-Hernandez, A., Hundeyin, M., Mani, V.R.K., et al. (2016). γδ T Cells Support Pancreatic Oncogenesis by Restraining αβ T Cell Activation. Cell *166*, 1485–1499.e15.

Davies, H., Glodzik, D., Morganella, S., Yates, L.R., Staaf, J., Zou, X., Ramakrishna, M., Martin, S., Boyault, S., Sieuwerts, A.M., et al. (2017). HRDetect is a predictor of BRCA1 and BRCA2 deficiency based on mutational signatures. Nat Med *23*, 517–525.

Dbouk, M., Brewer Gutierrez, O.I., Lennon, A.M., Chuidian, M., Shin, E.J., Kamel, I.R., Fishman, E.K., He, J., Burkhart, R.A., Wolfgang, C.L., et al. (2021). Guidelines on management of pancreatic cysts detected in high-risk individuals: An evaluation of the 2017 Fukuoka guidelines and the 2020 International Cancer of the Pancreas Screening (CAPS) consortium statements. Pancreatology.

Dreyer, S.B., Chang, D.K., Bailey, P., and Biankin, A.V. (2017). Pancreatic Cancer Genomes: Implications for Clinical Management and Therapeutic Development. Clin. Cancer Res. *23*, 1638–1646.

Dreyer, S.B., Jamieson, N.B., Evers, L., Duthie, F., Cooke, S., Marshall, J., Beraldi, D., Knight, S., Upstill-Goddard, R., Dickson, E.J., et al. (2019). Feasibility and clinical utility of endoscopic ultrasound guided biopsy of pancreatic cancer for next-generation molecular profiling. Chin Clin Oncol *8*, 16–16.

Driehuis, E., van Hoeck, A., Moore, K., Kolders, S., Francies, H.E., Gulersonmez, M.C., Stigter, E.C.A., Burgering, B., Geurts, V., Gracanin, A., et al. (2019). Pancreatic cancer organoids recapitulate disease and allow personalized drug screening. Proc Natl Acad Sci USA *116*, 26580–26590.

Elhanafi, S., Mahmud, N., Vergara, N., Kochman, M.L., Das, K.K., Ginsberg, G.G., Rajala, M., and Chandrasekhara, V. (2018). Comparison of endoscopic ultrasound tissue acquisition methods for genomic analysis of pancreatic cancer. J. Gastroenterol. Hepatol. *16*, 318.

Erickson, R.A., Sayage-Rabie, L., and Beissner, R.S. (2000). Factors predicting the number of EUS-guided fine-needle passes for diagnosis of pancreatic malignancies. Gastrointest. Endosc. *51*, 184–190.

Fearon, E.R., and Vogelstein, B. (1990). A genetic model for colorectal tumorigenesis. Cell *61*, 759–767.

Fuccio, L., Hassan, C., Laterza, L., Correale, L., Pagano, N., Bocus, P., Fabbri, C., Maimone, A., Cennamo, V., Repici, A., et al. (2013). The role of K-ras gene mutation analysis in EUS-guided FNA cytology specimens for the differential diagnosis of pancreatic solid masses: a meta-analysis of prospective studies. Gastrointest. Endosc. *78*, 596–608.

Gan, L.-L., Hii, L.-W., Wong, S.-F., Leong, C.-O., and Mai, C.-W. (2020). Molecular Mechanisms and Potential Therapeutic Reversal of Pancreatic Cancer-Induced Immune Evasion. Cancers (Basel) *12*, 1872.

Gawad, C., Koh, W., and Quake, S.R. (2016). Single-cell genome sequencing: current state of the science. Nat. Rev. Genet. *17*, 175–188.

Gemenetzis, G., Groot, V.P., Yu, J., Ding, D., Teinor, J.A., Javed, A.A., wood, L.D., Burkhart, R.A., Cameron, J.L., Makary, M.A., et al. (2018). Circulating Tumor Cells Dynamics in Pancreatic Adenocarcinoma Correlate With Disease Status: Results of the Prospective CLUSTER Study. Ann Surg *268*, 408–420.

Gleeson, F.C., Kerr, S.E., Kipp, B.R., Voss, J.S., Minot, D.M., Tu, Z.J., Henry, M.R., Graham, R.P., Vasmatzis, G., Cheville, J.C., et al. (2016). Targeted next generation sequencing of endoscopic ultrasound acquired cytology from ampullary and pancreatic adenocarcinoma has the potential to aid patient stratification for optimal therapy selection. Oncotarget *7*, 54526–54536.

Grover, S., Grover, S., and Syngal, S. (2010). Hereditary pancreatic cancer. Gastroenterology *139*, 1076–80–1080.e1–2.

Guo, J.A., Hoffman, H.I., Weekes, C.D., Zheng, L., Ting, D.T., and Hwang, W.L. (2021). Refining the Molecular Framework for Pancreatic Cancer with Single-cell and Spatial Technologies. Clin. Cancer Res.

Haeberle, L., and Esposito, I. (2019). Pathology of pancreatic cancer. Transl Gastroenterol Hepatol *4*, 50.

Hamada, E., Taniguchi, T., Baba, S., and Maekawa, M. (2012). Investigation of unexpected serum CA19-9 elevation in Lewis-negative cancer patients. Ann. Clin. Biochem. *49*, 266–272.

Hartley, C.P., Mahajan, A.M., Selvaggi, S.M., and Rehrauer, W.M. (2017). FNA smears of pancreatic ductal adenocarcinoma are superior to formalin-fixed paraffin-embedded tissue as a source of DNA: Comparison of targeted KRAS amplification and genotyping in matched preresection and postresection samples. Cancer Cytopathol *125*, 838–847.

Herbst, B., and Zheng, L. (2019). Precision medicine in pancreatic cancer: treating every patient as an exception. The Lancet Gastroenterology & Hepatology *4*, 805–810.

Hernandez-Barco, Y.G., Bardeesy, N., and Ting, D.T. (2019). No Cell Left Unturned: Intraductal Papillary Mucinous Neoplasm Heterogeneity. Clin. Cancer Res. *25*, 2027–2029.

Hewitt, M.J., McPhail, M.J.W., Possamai, L., Dhar, A., Vlavianos, P., and Monahan, K.J. (2012). EUS-guided FNA for diagnosis of solid pancreatic neoplasms: a meta-analysis. Gastrointest. Endosc. *75*, 319–331.

Hezel, A.F., Kimmelman, A.C., Stanger, B.Z., Bardeesy, N., and DePinho, R.A. (2006). Genetics and biology of pancreatic ductal adenocarcinoma. Genes Dev. *20*, 1218–1249.

Hébert-Magee, S., Bae, S., Varadarajulu, S., Ramesh, J., Frost, A.R., Eloubeidi, M.A., and Eltoum, I.A. (2013). The presence of a cytopathologist increases the diagnostic accuracy of endoscopic ultrasound-guided fine needle aspiration cytology for pancreatic adenocarcinoma: a meta-analysis. Cytopathology *24*, 159–171.

Hindson, C.M., Hindson, C.M., Chevillet, J.R., Chevillet, J.R., Briggs, H.A., Briggs, H.A., Gallichotte, E.N., Gallichotte, E.N., Ruf, I.K., Ruf, I.K., et al. (2013). Absolute quantification by droplet digital PCR versus analog real-time PCR. Nat. Methods *10*, 1003–1005.

Holter, S., Borgida, A., Dodd, A., Grant, R., Semotiuk, K., Hedley, D., Dhani, N., Narod, S., Akbari, M., Moore, M., et al. (2015). Germline BRCA Mutations in a Large Clinic-Based Cohort of Patients With Pancreatic Adenocarcinoma. J. Clin. Oncol. *33*, 3124–3129.

Hong, S.P., Chan, T.E., Lombardo, Y., Corleone, G., Rotmensz, N., Bravaccini, S., Rocca, A., Pruneri, G., McEwen, K.R., Coombes, R.C., et al. (2019). Single-cell transcriptomics reveals multi-step adaptations to endocrine therapy. Nature Communications *10*, 3840–14.

Hosoda, W., Chianchiano, P., Griffin, J.F., Pittman, M.E., Brosens, L.A., Noë, M., Yu, J., Shindo, K., Suenaga, M., Rezaee, N., et al. (2017). Genetic analyses of isolated high-grade pancreatic intraepithelial neoplasia (HG-PanIN) reveal paucity of alterations in TP53 and SMAD4. J. Pathol. *242*, 16–23.

Ignatiadis, M., Sledge, G.W., and Jeffrey, S.S. (2021). Liquid biopsy enters the clinic - implementation issues and future challenges. Nat Rev Clin Oncol 1–16.

Ishida, Y., Agata, Y., Shibahara, K., and Honjo, T. (1992). Induced expression of PD-1, a novel member of the immunoglobulin gene superfamily, upon programmed cell death. Embo J *11*, 3887–3895.

Ishizawa, T., Makino, N., Matsuda, A., Kakizaki, Y., Kobayashi, T., Ikeda, C., Sugahara, S., Tsunoda, M., and Ueno, Y. (2020). Usefulness of rapid on-site evaluation specimens from endoscopic ultrasound-guided fine-needle aspiration for cancer gene panel testing: A retrospective study. PLoS ONE *15*, e0228565.

Jang, J.-E., Hajdu, C.H., Liot, C., Miller, G., Dustin, M.L., and Bar-Sagi, D. (2017). Crosstalk between Regulatory T Cells and Tumor-Associated Dendritic Cells Negates Anti-tumor Immunity in Pancreatic Cancer. Cell Rep *20*, 558–571.

Jani, B.S., Rzouq, F., Saligram, S., Lim, D., Rastogi, A., Bonino, J., and Olyaee, M. (2016). Endoscopic Ultrasound-Guided Fine-Needle Aspiration of Pancreatic Lesions: A Systematic Review of Technical and Procedural Variables. N Am J Med Sci *8*, 1–11.

Johnson, A.D., Bhimavarapu, A., Benjamin, E.J., Fox, C., Levy, D., Jarvik, G.P., and O'Donnell, C.J. (2010). CLIA-tested genetic variants on commercial SNP arrays: potential for incidental findings in genome-wide association studies. Genet Med *12*, 355–363.

Jones, S., Jones, S., Zhang, X., Zhang, X., Parsons, D.W., Parsons, D.W., Lin, J.C.-H., Lin, J.C.-H., Leary, R.J., Angenendt, P., et al. (2008). Core signaling pathways in human pancreatic cancers revealed by global genomic analyses. Science *321*, 1801–1806.

Kameta, E., Sugimori, K., Kaneko, T., Ishii, T., Miwa, H., Sato, T., Ishii, Y., Sue, S., Sasaki, T., Yamashita, Y., et al. (2016). Diagnosis of pancreatic lesions collected by endoscopic ultrasound-guided fine-needle aspiration using next-generation sequencing. Oncol Lett *12*, 3875–3881.

Kanda, M., Matthaei, H., Wu, J., Hong, S.-M., Yu, J., Borges, M., Hruban, R.H., Maitra, A., Kinzler, K., Kinzler, K., et al. (2012). Presence of somatic mutations in most early-stage pancreatic intraepithelial neoplasia. Gastroenterology *142*, 730–733.e739.

Kinde, I., Wu, J., Papadopoulos, N., Kinzler, K.W., and Vogelstein, B. (2011). Detection and quantification of rare mutations with massively parallel sequencing. Proc Natl Acad Sci USA *108*, 9530–9535.

Kivioja, T., Vähärautio, A., Karlsson, K., Bonke, M., Enge, M., Linnarsson, S., and Taipale, J. (2011). Counting absolute numbers of molecules using unique molecular identifiers. Nat. Methods *9*, 72–74.

Kleeff, J., Korc, M., Apte, M., La Vecchia, C., Johnson, C.D., Biankin, A.V., Neale, R.E., Tempero, M., Tuveson, D.A., Hruban, R.H., et al. (2016). Pancreatic cancer. Nat Rev Dis Primers *2*, 16022.

Kulemann, B., Rösch, S., Seifert, S., Timme, S., Bronsert, P., Seifert, G., Martini, V., Kuvendjiska, J., Glatz, T., Hussung, S., et al. (2017). Pancreatic cancer: Circulating Tumor Cells and Primary Tumors show Heterogeneous KRAS Mutations. Sci Rep *7*, 4510.

Kwapisz, D. (2017). The first liquid biopsy test approved. Is it a new era of mutation testing for non-small cell lung cancer? Ann Transl Med *5*, 46–10.

Larghi, A., Eguia, V., Hassan, C., Verna, E.C., Tarantino, I., and Gonda, T.A. (2014). Economic crisis: the right time to widen endoscopic ultrasound utilization. Endoscopy *46*, 80–81.

Larsson, L., Frisén, J., and Lundeberg, J. (2021). Spatially resolved transcriptomics adds a new dimension to genomics. Nat. Methods *18*, 15–18.

Layfield, L.J., Schmidt, R.L., Hirschowitz, S.L., Olson, M.T., Ali, S.Z., and Dodd, L.L. (2014). Significance of the diagnostic categories "atypical" and “suspicious for malignancy” in the cytologic diagnosis of solid pancreatic masses. Diagn Cytopathol *42*, 292–296.

Leach, D.R., Krummel, M.F., and Allison, J.P. (1996). Enhancement of antitumor immunity by CTLA-4 blockade. Science *271*, 1734–1736.

Lee, A.Y.L., Dubois, C.L., Sarai, K., Zarei, S., Schaeffer, D.F., Sander, M., and Kopp, J.L. (2019). Cell of origin affects tumour development and phenotype in pancreatic ductal adenocarcinoma. Gut *68*, 487–498.

Leighl, N.B., Page, R.D., Raymond, V.M., Daniel, D.B., Divers, S.G., Reckamp, K.L., Villalona-Calero, M.A., Dix, D., Odegaard, J.I., Lanman, R.B., et al. (2019). Clinical Utility of Comprehensive Cell-free DNA Analysis to Identify Genomic Biomarkers in Patients with Newly Diagnosed Metastatic Non-small Cell Lung Cancer. Clin. Cancer Res. *25*, 4691–4700.

Ligorio, M., Sil, S., Malagon-Lopez, J., Nieman, L.T., Misale, S., Di Pilato, M., Ebright, R.Y., Karabacak, M.N., Kulkarni, A.S., Liu, A., et al. (2019). Stromal Microenvironment Shapes the Intratumoral Architecture of Pancreatic Cancer. Cell *178*, 160–175.e27.

Lin, W., Noel, P., Borazanci, E.H., Lee, J., Amini, A., Han, I.W., Heo, J.S., Jameson, G.S., Fraser, C., Steinbach, M., et al. (2020). Single-cell transcriptome analysis of tumor and stromal compartments of pancreatic ductal adenocarcinoma primary tumors and metastatic lesions. Genome Med *12*, 80–14.

Lu, S., Jang, H., Nussinov, R., and Zhang, J. (2016). The Structural Basis of Oncogenic Mutations G12, G13 and Q61 in Small GTPase K-Ras4B. Sci Rep *6*, 1–15.

Machado, N.O., Qadhi, Al, H., and Wahibi, Al, K. (2015). Intraductal Papillary Mucinous Neoplasm of Pancreas. N Am J Med Sci *7*, 160–175.

Maertens, Y., Humberg, V., Erlmeier, F., Steffens, S., Steinestel, J., Bögemann, M., Schrader, A.J., and Bernemann, C. (2017). Comparison of isolation platforms for detection of circulating renal cell carcinoma cells. Oncotarget *8*, 87710–87717.

Maitra, A., and Hruban, R.H. (2008). Pancreatic cancer. Annu Rev Pathol *3*, 157–188.

Malhotra, N., Jackson, S.A., Freed, L.L., Styn, M.A., Sidawy, M.K., Haddad, N.G., and Finkelstein, S.D. (2014). The added value of using mutational profiling in addition to cytology in diagnosing aggressive pancreaticobiliary disease: review of clinical cases at a single center. BMC Gastroenterol *14*, 135.

Martini, V., Timme-Bronsert, S., Fichtner-Feigl, S., Hoeppner, J., and Kulemann, B. (2019). Circulating Tumor Cells in Pancreatic Cancer: Current Perspectives. Cancers (Basel) *11*, 1659.

Marx, V. (2021). Method of the Year: spatially resolved transcriptomics. Nat. Methods *18*, 9–14.

Matthaei, H., Schulick, R.D., Hruban, R.H., and Maitra, A. (2011). Cystic precursors to invasive pancreatic cancer. Nat Rev Gastroenterol Hepatol *8*, 141–150.

McGranahan, N., and Swanton, C. (2017). Clonal Heterogeneity and Tumor Evolution: Past, Present, and the Future. Cell *168*, 613–628.

Moffitt, R.A., Marayati, R., Flate, E.L., Volmar, K.E., Loeza, S.G.H., Hoadley, K.A., Rashid, N.U., Williams, L.A., Eaton, S.C., Chung, A.H., et al. (2015). Virtual microdissection identifies distinct tumor- and stroma-specific subtypes of pancreatic ductal adenocarcinoma. Nat. Genet. *47*, 1168–1178.

Moore, A.R., Rosenberg, S.C., McCormick, F., and Malek, S. (2020). RAS-targeted therapies: is the undruggable drugged? Nat Rev Drug Discov *19*, 533–552.

Nassour, I., Wang, S.C., Christie, A., Augustine, M.M., Porembka, M.R., Yopp, A.C., Choti, M.A., Mansour, J.C., Xie, X.-J., Polanco, P.M., et al. (2018). Minimally Invasive Versus Open Pancreaticoduodenectomy: A Propensity-matched Study From a National Cohort of Patients. Ann Surg *268*, 151–157.

Neoptolemos, J.P., Palmer, D.H., Ghaneh, P., Psarelli, E.E., Valle, J.W., Halloran, C.M., Faluyi, O., O'Reilly, D.A., Cunningham, D., Wadsley, J., et al. (2017). Comparison of adjuvant gemcitabine and capecitabine with gemcitabine monotherapy in patients with resected pancreatic cancer (ESPAC-4): a multicentre, open-label, randomised, phase 3 trial. Lancet *389*, 1011–1024.

Nieto, M.A., Huang, R.Y.-J., Jackson, R.A., and Thiery, J.P. (2016). EMT: 2016. Cell *166*, 21–45.

Oba, A., Ho, F., Bao, Q.R., Al-Musawi, M.H., Schulick, R.D., and Del Chiaro, M. (2020). Neoadjuvant Treatment in Pancreatic Cancer. Front Oncol *10*, 245.

Ono, Y., Hayashi, A., Maeda, C., Suzuki, M., Wada, R., Sato, H., Kawabata, H., Okada, T., Goto, T., Karasaki, H., et al. (2020). Time-saving method for directly amplifying and capturing a minimal amount of pancreatic tumor-derived mutations from fine-needle aspirates using digital PCR. Sci Rep *10*, 12332–10.

Öhlund, D., Handly-Santana, A., Biffi, G., Elyada, E., Almeida, A.S., Ponz-Sarvise, M., Corbo, V., Oni, T.E., Hearn, S.A., Lee, E.J., et al. (2017). Distinct populations of inflammatory fibroblasts and myofibroblasts in pancreatic cancer. Journal of Experimental Medicine *214*, 579–596.

Park, J.J.H., Siden, E., Zoratti, M.J., Dron, L., Harari, O., Singer, J., Lester, R.T., Thorlund, K., and Mills, E.J. (2019). Systematic review of basket trials, umbrella trials, and platform trials: a landscape analysis of master protocols. Trials *20*, 572–10.

Patel, B.Y., White, L., Gavriilidis, P., Satyadas, T., Frampton, A.E., and Pai, M. (2020). A systematic review into patient reported outcomes following pancreaticoduodenectomy for malignancy. Eur J Surg Oncol *82*, 111.

Peng, J., Sun, B.-F., Chen, C.-Y., Zhou, J.-Y., Chen, Y.-S., Chen, H., Liu, L., Huang, D., Jiang, J., Cui, G.-S., et al. (2019). Single-cell RNA-seq highlights intra-tumoral heterogeneity and malignant progression in pancreatic ductal adenocarcinoma. Cell Res. *29*, 725–738.

Porter, R.L., Magnus, N.K.C., Thapar, V., Morris, R., Szabolcs, A., Neyaz, A., Kulkarni, A.S., Tai, E., Chougule, A., Hillis, A., et al. (2019). Epithelial to mesenchymal plasticity and differential response to therapies in pancreatic ductal adenocarcinoma. Proc Natl Acad Sci USA *116*, 26835–26845.

Poruk, K.E., Blackford, A.L., Weiss, M.J., Cameron, J.L., He, J., Goggins, M., Rasheed, Z.A., Wolfgang, C.L., and wood, L.D. (2017). Circulating Tumor Cells Expressing Markers of Tumor-Initiating Cells Predict Poor Survival and Cancer Recurrence in Patients with Pancreatic Ductal Adenocarcinoma. Clin. Cancer Res. *23*, 2681–2690.

Poruk, K.E., Valero, V., Saunders, T., Blackford, A.L., Griffin, J.F., Poling, J., Hruban, R.H., Anders, R.A., Herman, J., Zheng, L., et al. (2016). Circulating Tumor Cell Phenotype Predicts Recurrence and Survival in Pancreatic Adenocarcinoma. Ann Surg *264*, 1073–1081.

Puli, S.R., Bechtold, M.L., Buxbaum, J.L., and Eloubeidi, M.A. (2013). How good is endoscopic ultrasound-guided fine-needle aspiration in diagnosing the correct etiology for a solid pancreatic mass?: A meta-analysis and systematic review. Pancreas *42*, 20–26.

Quante, A.S., Ming, C., Rottmann, M., Engel, J., Boeck, S., Heinemann, V., Westphalen, C.B., and Strauch, K. (2016). Projections of cancer incidence and cancer-related deaths in Germany by 2020 and 2030. Cancer Med *5*, 2649–2656.

Raphael, B.J. (2017). Integrated Genomic Characterization of Pancreatic Ductal Adenocarcinoma. Cancer Cell *32*, 185–203.e13.

Rashid, S., Singh, N., Gupta, S., Rashid, S., Nalika, N., Sachdev, V., Bal, C.S., Datta Gupta, S., Chauhan, S.S., and Saraya, A. (2018). Progression of Chronic Pancreatitis to Pancreatic Cancer: Is There a Role of Gene Mutations as a Screening Tool? Pancreas *47*, 227–232.

Rivera, J.A., Rall, C.J., Graeme-Cook, F., Fernández-del Castillo, C., Shu, P., Lakey, N., Tepper, R., Rattner, D.W., Warshaw, A.L., and Rustgi, A.K. (1997). Analysis of K-ras oncogene mutations in chronic pancreatitis with ductal hyperplasia. Surgery *121*, 42–49.

Ryan, D.P., Ryan, D.P., Hong, T.S., Hong, T.S., Bardeesy, N., and Bardeesy, N. (2014). Pancreatic adenocarcinoma. N Engl J Med *371*, 2140–2141.

Semaan, A., Bernard, V., Lee, J.J., Wong, J.W., Huang, J., Swartzlander, D.B., Stephens, B.M., Monberg, M.E., Weston, B., Bhutani, M.S., et al. (2020). Defining the Comprehensive Genomic Landscapes of Pancreatic Ductal Adenocarcinoma Using Real World Endoscopic Aspiration Samples. Clin. Cancer Res. clincanres.2667.2020.

Sho, S., Court, C.M., Kim, S., Braxton, D.R., Hou, S., Muthusamy, V.R., Watson, R.R., Sedarat, A., Tseng, H.-R., and Tomlinson, J.S. (2017). Digital PCR Improves Mutation Analysis in Pancreas Fine Needle Aspiration Biopsy Specimens. PLoS ONE *12*, e0170897.

Siegel, R.L., Miller, K.D., and Jemal, A. (2019). Cancer statistics, 2019. CA Cancer J Clin *69*, 7–34.

Siegel, R., Ma, J., Zou, Z., and Jemal, A. (2014). Cancer statistics, 2014. CA Cancer J Clin *64*, 9–29.

Singhi, A.D., George, B., Greenbowe, J.R., Chung, J., Suh, J., Maitra, A., Klempner, S.J., Hendifar, A., Milind, J.M., Golan, T., et al. (2019). Real-time Targeted Genome Profile Analysis of Pancreatic Ductal Adenocarcinomas Identifies Genetic Alterations that Might be Targeted with Existing Drugs or Used as Biomarkers. Gastroenterology.

Slamon, D.J., Leyland-Jones, B., Shak, S., Fuchs, H., Paton, V., Bajamonde, A., Fleming, T., Eiermann, W., Wolter, J., Pegram, M., et al. (2001). Use of chemotherapy plus a monoclonal antibody against HER2 for metastatic breast cancer that overexpresses HER2. N Engl J Med *344*, 783–792.

Slyper, M., Porter, C.B.M., Ashenberg, O., Waldman, J., Drokhlyansky, E., Wakiro, I., Smillie, C., Smith-Rosario, G., Wu, J., Dionne, D., et al. (2019). A single-cell and single-nucleus RNA-seq toolbox for fresh and frozen human tumors. bioRxiv *13*, 761429.

Staaf, J., Glodzik, D., Bosch, A., Vallon-Christersson, J., Reuterswärd, C., Häkkinen, J., Degasperi, A., Amarante, T.D., Saal, L.H., Hegardt, C., et al. (2019). Whole-genome sequencing of triple-negative breast cancers in a population-based clinical study. Nat Med *25*, 1526–1533.

Strobel, O., Neoptolemos, J., Jäger, D., and Büchler, M.W. (2019). Optimizing the outcomes of pancreatic cancer surgery. Nat Rev Clin Oncol *16*, 11–26.

Tanaka, M., Fernández-del Castillo, C., Kamisawa, T., Jang, J.-Y., Levy, P., Ohtsuka, T., Salvia, R., Shimizu, Y., Tada, M., and Wolfgang, C.L. (2017). Revisions of international consensus Fukuoka guidelines for the management of IPMN of the pancreas. Pancreatology *17*, 738–753.

Taylor, A.M., Shih, J., Ha, G., Gao, G.F., Zhang, X., Berger, A.C., Schumacher, S.E., Wang, C., Hu, H., Liu, J., et al. (2018). Genomic and Functional Approaches to Understanding Cancer Aneuploidy. Cancer Cell *33*, 676–689.e3.

Thierry, A.R., Mouliere, F., Messaoudi, El, S., Messaoudi, El, S., Mollevi, C., Mollevi, C., Lopez-Crapez, E., Lopez-Crapez, E., Rolet, F., Rolet, F., et al. (2014). Clinical validation of the detection of KRAS and BRAF mutations from circulating tumor DNA. Nat Med *20*, 430–435.

Ting, D.T., Wittner, B.S., Ligorio, M., Vincent Jordan, N., Shah, A.M., Miyamoto, D.T., Aceto, N., Bersani, F., Brannigan, B.W., Xega, K., et al. (2014). Single-cell RNA sequencing identifies extracellular matrix gene expression by pancreatic circulating tumor cells. Cell Rep *8*, 1905–1918.

Tiriac, H., Bucobo, J.C., Tzimas, D., Grewel, S., Lacomb, J.F., Rowehl, L.M., Nagula, S., Wu, M., Kim, J., Sasson, A., et al. (2018). Successful creation of pancreatic cancer organoids by means of EUS-guided fine-needle biopsy sampling for personalized cancer treatment. Gastrointest. Endosc. *87*, 1474–1480.

Tirkes, T., Shah, Z.K., Takahashi, N., Grajo, J.R., Chang, S.T., Venkatesh, S.K., Conwell, D.L., Fogel, E.L., Park, W., Topazian, M., et al. (2019). Reporting Standards for Chronic Pancreatitis by Using CT, MRI, and MR Cholangiopancreatography: The Consortium for the Study of Chronic Pancreatitis, Diabetes, and Pancreatic Cancer. Radiology *290*, 207–215.

Trisolini, E., Armellini, E., Paganotti, A., Veggiani, C., Bozzola, C., Frattini, M., Pizio, C., Mancuso, G., Andorno, S., and Boldorini, R. (2017). KRAS mutation testing on all non-malignant diagnosis of pancreatic endoscopic ultrasound-guided fine-needle aspiration biopsies improves diagnostic accuracy. Pathology *49*, 379–386.

Tsai, M.-F., Chang, T.-H., Wu, S.-G., Yang, H.-Y., Hsu, Y.-C., Yang, P.-C., and Shih, J.-Y. (2015). EGFR-L858R mutant enhances lung adenocarcinoma cell invasive ability and promotes malignant pleural effusion formation through activation of the CXCL12-CXCR4 pathway. Sci Rep *5*, 13574–14.

Tsujiura, M., Ichikawa, D., Konishi, H., Komatsu, S., Shiozaki, A., and Otsuji, E. (2014). Liquid biopsy of gastric cancer patients: circulating tumor cells and cell-free nucleic acids. World J Gastroenterol *20*, 3265–3286.

Uprety, D., and Adjei, A.A. (2020). KRAS: From undruggable to a druggable Cancer Target. Cancer Treat. Rev. *89*, 102070.

Verheul, R.C., van Deutekom, J.C.T., and Datson, N.A. (2016). Digital Droplet PCR for the Absolute Quantification of Exon Skipping Induced by Antisense Oligonucleotides in (Pre-)Clinical Development for Duchenne Muscular Dystrophy. PLoS ONE *11*, e0162467.

Vitak, S.A., Torkenczy, K.A., Rosenkrantz, J.L., Fields, A.J., Christiansen, L., Wong, M.H., Carbone, L., Steemers, F.J., and Adey, A. (2017). Sequencing thousands of single-cell genomes with combinatorial indexing. Nat. Methods *14*, 302–308.

Vogelstein, B., Papadopoulos, N., Velculescu, V.E., Zhou, S., Diaz, L.A., and Kinzler, K.W. (2013). Cancer genome landscapes. Science *339*, 1546–1558.

Waddell, N., Pajic, M., Patch, A.-M., Chang, D.K., Kassahn, K.S., Bailey, P., Johns, A.L., Miller, D., Nones, K., Quek, K., et al. (2015). Whole genomes redefine the mutational landscape of pancreatic cancer. Nature *518*, 495–501.

Wood, L. (2013). Pancreatic cancer genomes: toward molecular subtyping and novel approaches to diagnosis and therapy. Mol Diagn Ther *17*, 287–297.

Woodcock, J., and LaVange, L.M. (2017). Master Protocols to Study Multiple Therapies, Multiple Diseases, or Both. N Engl J Med *377*, 62–70.

Xu, Y., Hu, D., Zhu, Q., and Sun, Y. (2014). Performance of K-ras mutation analysis plus endoscopic ultrasound-guided fine-needle aspiration for differentiating diagnosis of pancreatic solid mass: a meta-analysis. Chin Med J (Engl) *127*, 3296–3301.

Yachida, S., Jones, S., Bozic, I., Bozic, I., Antal, T., Antal, T., Leary, R., Leary, R., Fu, B., Kamiyama, M., et al. (2010). Distant metastasis occurs late during the genetic evolution of pancreatic cancer. Nature *467*, 1114–1117.

Zavridou, M., Mastoraki, S., Strati, A., Koutsodontis, G., Klinakis, A., Psyrri, A., and Lianidou, E. (2020). Direct comparison of size-dependent versus EpCAM-dependent CTC enrichment at the gene expression and DNA methylation level in head and neck squamous cell carcinoma. Sci Rep *10*, 6551–6559.

Zhang, L., Chenwei, L., Mahmood, R., van Golen, K., Greenson, J., Li, G., D'Silva, N.J., Li, X., Burant, C.F., Logsdon, C.D., et al. (2006). Identification of a putative tumor suppressor gene Rap1GAP in pancreatic cancer. Cancer Res *66*, 898–906.

7. Danksagung

Mein Dank gilt all meinen Kollegen/innen, die mich während meines beruflichen und wissenschaftlichen Werdegangs immer motiviert und unterstützt haben.

Während meiner Doktorarbeit hat Herr Prof. Holland-Cunz mir erstmals wissenschaftliches Arbeiten nähergebracht, jedoch haben erst Herr Prof. Dr. Thomas Boemers, Dr. med. Reza Vahdad und Dr. Tobias Klein neben meiner klinischen kinderchirurgischen Arbeit mein Interesse an der klinischen Forschung geweckt und gefördert.

Nach meinem Wechsel in die „Erwachsenenchirurgie“ an der Universitätsklinik Bonn wurde ich von Herrn Prof. Kalff weiter in meiner klinischen und wissenschaftlichen Laufbahn tatkräftig unterstützt. Er war dabei gleichzeitig ein exzellenter chirurgischer Lehrer sowie ein Vorbild als „Clinician Scientist“ und steht mir allzeit mit Rat und Tat zur Seite.
Auch Herrn PD Dr. Matthaei und PD Lingohr gilt mein besonderer Dank, da diese mich in ihre produktive, interdisziplinäre und hochmotivierte Arbeitsgruppe aufgenommen und unglaublich gefördert haben. Ich hoffe, dass wir auch in Zukunft über die klinische Tätigkeit hinaus freundschaftlich verbunden bleiben.

Während meines Postdoctoral Fellowship in Houston durfte ich mich dann erstmals voll und ganz auf meine Forschungstätigkeit konzentrieren. Hier möchte ich zuerst meinem PI Herrn Prof. Maitra danken, der mich in allen Belangen unterstützt hat und mir die eigenständige Verfolgung meiner Forschungsideen ermöglichte. Zudem möchte ich speziell Frau Paola Guerrero, PhD für Ihre Geduld und Anleitung, Herrn Vincent Bernard, PhD und Herrn James Jaewon Lee, PhD für die großartige Kollegialität sowie dem gesamten Team des Labors für meine unvergessliche Zeit in Houston danken.

Meinen immer nachsichtigen, loyalen und sehr konstruktiven Kollegen Herrn PD Dr. Dimo Dietrich, Herrn Dr. Vittorio Branchi, Herrn Dr. Jonas Dohmen, Herrn Dr. Jonas Henn und Herrn Dr. Daniel Weissinger gilt ebenso mein Dank. Mit ihnen beruflich sowie freundschaftlich verbunden zu bleiben, ist mir ein großes Anliegen.

Ein besonderer Gedanke gilt den Patienten und ihren Familien, die mit der Diagnose und der Prognose dieser Erkrankung leben müssen. Ihnen wünsche ich, dass unsere Forschung und die Forschung aller Kollegen in naher Zukunft einen Durchbruch bei der effektiven Behandlung des Pankreaskarzinoms bringen wird.

8. Erklärung

Hiermit bestätige ich, dass ich die Richtlinien zur guten wissenschaftlichen Praxis der Universität Bonn, laut Habil-Ordnung, zur Kenntnis genommen habe und ich versichere, dass ich sie beim Verfassen der Habilitationsschrift beachtet habe. Insbesondere versichere ich, dass ich alle in der Habilitationsschrift benutzten Quellen und Hilfsmittel angegeben habe.

Bonn, den 28.05.2021

Dr. Alexander Semaan

9. Vollständige Kopie der publizierten eigenen Arbeiten, die dem zusammenfassenden Text zu Grunde liegen

ORIGINAL ARTICLE

Diagnostic value of digital droplet polymerase chain reaction and digital multiplexed detection of single-nucleotide variants in pancreatic cytology specimens collected by EUS-guided FNA

Irina M. Cazacu, MD, PhD,[1,4,*] Alexander Semaan, MD, PhD,[2,*] Bret Stephens, M.S,[2] Daniel B. Swartzlander, M.S,[2] Paola A. Guerrero, PhD,[2] Ben S. Singh, M.S,[1] Cristian Virgil Lungulescu, MD, PhD,[3] Mihaela Maria Danciulescu, MD, PhD,[3] Irina F. Cherciu Harbiyeli, MD, PhD,[4] Ioana Streata, MD, PhD,[4] Carmen Popescu, MD,[4] Adrian Saftoiu, MD, PhD,[4] Sinchita Roy-Chowdhuri, MD, PhD,[5] Anirban Maitra, MBBS,[2*] Manoop S. Bhutani, MD[1]

Houston, Texas, USA; Craiova, Romania

Background and Aims: EUS-guided FNA is recommended as a first-line procedure for the histopathologic diagnosis of pancreatic cancer. Molecular analysis of EUS-FNA samples might be used as an auxiliary tool to strengthen the diagnosis. The current study aimed to evaluate the diagnostic performances of K-*ras* testing using droplet digital polymerase chain reaction (ddPCR) and a novel single-nucleotide variant (SNV) assay performed on pancreatic EUS-FNA samples.

Methods: EUS-FNA specimens from 31 patients with pancreatic masses (22 pancreatic ductal adenocarcinomas, 7 chronic pancreatitis, and 2 pancreatic neuroendocrine tumors) were included in the study. K-*ras* testing was initially performed by ddPCR. In addition, mutational status was evaluated using an SNV assay by NanoString technology, using digital enumeration of unique barcoded probes to detect 97 SNVs from 24 genes of clinical significance.

Results: The overall specificity and sensitivity of cytologic examination were 100% and 63%, respectively. K-*ras* mutation testing was performed using ddPCR, and the sensitivity increased to 87% with specificity 90%. The SNV assay detected at least 1 variant in 90% of pancreatic ductal adenocarcinoma samples; the test was able to detect 2 K-*ras* codon 61 mutations in 2 cases of pancreatic ductal adenocarcinoma, which were missed by ddPCR. The overall diagnostic accuracy of the cytologic examination alone was 74%, and it increased to 91% when the results of both molecular tests were considered for the cases with negative and inconclusive results.

Conclusions: The current study illustrated that integration of K-*ras* analysis with cytologic evaluation, especially in inconclusive cases, can enhance the diagnostic accuracy of EUS-FNA for pancreatic lesions. (Gastrointest Endosc 2020;■:1-10.)

Abbreviations: CI, confidence interval; CP, chronic pancreatitis; ddPCR, droplet digital polymerase chain reaction; FFPE, formalin-fixed paraffin-embedded; FNB, fine-needle biopsy; LOD, limit of detection; NPV, negative predictive value; PDAC, pancreatic ductal adenocarcinoma; pNET, pancreatic neuroendocrine tumor; PPV, positive predictive value; ROSE, rapid on-site evaluation; SNV, single-nucleotide variant.

DISCLOSURE: *Dr Maitra recevied royalties from Cosmo Wisdom Biotechnology and a license from Thrive Earlier Detection. All other authors disclosed no financial relationships.*

*Drs Cazacu and Semaan contributed equally to this article.

0016-5107/$36.00
https://doi.org/10.1016/j.gie.2020.09.051

Received March 31, 2020. Accepted September 29, 2020.

Current affiliations: Department of Gastroenterology, Hepatology and Nutrition, The University of Texas, MD Anderson Cancer Center, Houston, Texas (1); Sheikh Ahmed Pancreatic Cancer Research Center, The University of Texas, MD Anderson Cancer Center, Houston, Texas, USA (2); Department of Oncology, University of Medicine and Pharmacy, Craiova (3); Research Center of Gastroenterology and Hepatology, Craiova, Romania (4); Department of Pathology, The University of Texas MD Anderson Cancer Center, Houston, Texas, USA (5).

Reprint requests: Manoop S. Bhutani, MD, Department of Gastroenterology, Hepatology and Nutrition-Unit 1466, UT MD Anderson Cancer Center, 1515 Holcombe Boulevard, Houston, TX 77030-4009; Anirban Maitra, MBBS, Sheikh Ahmed Bin Zayed Al Nahyan Center for Pancreatic Cancer Research, Department of Pathology and Translational Molecular Pathology, UT MD Anderson Cancer Center, 1515 Holcombe Boulevard, Houston, TX 77030-4009.

INTRODUCTION

Pancreatic ductal adenocarcinoma (PDAC) is one of the leading causes of cancer-related mortality with an increasing incidence across the world.[1-3] Margin-free surgical resection is considered the only curative option, but less than 20% of patients with PDACs are diagnosed at a resectable stage.

Proof of malignancy via biopsy is not required for resectable tumors; however, a biopsy is necessary before administration of any systemic therapy in a neoadjuvant or palliative setting.[4]

EUS-guided sampling is recommended as a first-line procedure when a histopathologic diagnosis is required. Alternatively, percutaneous sampling may be considered in cases of metastatic disease. EUS-guided FNA/fine-needle biopsy (FNB) is preferable to CT-guided FNA in patients with resectable disease because of better diagnostic yield, safety, and potentially lower risk of peritoneal seeding with EUS-FNA/FNB compared with the percutaneous approach.[4]

EUS-FNA is accurate and reliable for determining malignancy, with sensitivity ranging from 85% to 89% and specificity between 96% and 99% for the diagnosis of solid pancreatic lesions, according to 3 meta-analyses.[5-7] However, the diagnostic accuracy of EUS-FNA varies widely, and it is affected by several factors, including tumor-related factors (size and location of the pancreatic mass) or procedure-related factors (use of suction and stylet, fanning and capillary technique, number of needle passes). Moreover, EUS-FNA is an operator-dependent technique, and it is highly influenced by the experience and technical expertise of the endoscopist and the cytopathologist. A definitive diagnosis is frequently challenging for pathologists because of suboptimal EUS-FNA sample quality and low cellularity yield. Furthermore, because of the overlap of cytologic features between neoplastic and reactive ductal epithelium, it is difficult to distinguish between well-differentiated adenocarcinoma and chronic pancreatitis (CP), especially in its pseudo tumoral form.

Given all the above-mentioned factors, the rate of false-negative and inconclusive EUS-FNA results (atypical or suspicious categories according to the Papanicolaou Society of Cytopathology classification) still remains high in several institutions.[8] This may result in unnecessary resection for benign diseases or cause delay in treatment for patients with PDAC. Pancreatic masses with an atypical or suspicious cytology can be a challenge for clinicians with regard to the correct clinical management. To reduce the number of nondiagnostic samples, rapid on-site evaluation (ROSE) was introduced with a 10% to 15% gain in diagnostic accuracy.[9] However, the limited availability of ROSE in many centers throughout the world, and a limited perceived utility of EUS has created a barrier to the dissemination of the procedure in the community and in many countries.[10,11]

In such a scenario, molecular analysis of the limited EUS-FNA samples to aid the diagnosis of PDAC may be extremely useful. In the past decade, the mutational landscape of PDAC has been well characterized.[12-17] Activating mutations in K-*ras* are observed in >90% of patients with PDAC.[18] High-throughput molecular analysis has demonstrated that in addition to K-*ras* mutation, inactivation of *TP53*, *SMAD4*, and *CDKN2A* are the pivotal molecular alterations that define the development and progression of PDAC. Despite common deleterious mutations in *TP53*, *CDKN2A*, and *SMAD4*, PDACs show a remarkable heterogeneity, but other genetic alterations are only found at frequencies below 10%.[18]

Current methods for mutation detection have varying diagnostic accuracies and limitations.[19] Considering that cytologic material obtained from EUS-FNA is often composed of heterogeneous cell populations, it is crucial to use a molecular test that is both sensitive and quantitative to detect even a small proportion of mutated cells in a background of normal wild-type cells. Droplet digital polymerase chain reaction (ddPCR), based on water-oil emulsion droplet technology, has improved the analytical sensitivity of mutation detection because it can identify hotspot mutations at frequencies <1%.[20,21] This methodology has proven useful for the evaluation of archival tumor tissues, where poor DNA quality and limited specimens volume are major obstacles for standard methods, providing less subjective and more automated quantitative results.[22] In the context of PDAC, where >90% of cases harbor a hotspot oncogenic mutation in K-*ras*,[23] ddPCR can serve as an ideal first pass screening test to document the presence of mutant cell clones. At the same time, ddPCR is restricted to one or a few hotspots (eg, the multiplex assay that we used only detected K-*ras* codon 12/13 mutations but not codon 61). Thus, there may be a value in expanding the panel of mutations that can be detected on cytology specimens from both a diagnostic standpoint, as well as from the context of identifying potentially actionable mutations. Accordingly, to be able to detect multiple single-nucleotide variants (SNVs) simultaneously would be of pivotal importance for the molecular diagnostics of PDAC. NanoString's optical barcoding technology now enables detection of small genomic sequence changes such as SNVs and insertion-deletions.

The current study aimed to evaluate, and for the first time, conduct a head to head comparison of the respective diagnostic performances of the widely used ddPCR multiplex assay versus a novel multi-gene SNV assay by NanoString Technologies, performed on pancreatic specimens obtained through EUS-FNA.

METHODS

Patient cohort

The study was performed in accordance with standard ethical guidelines approved by the institutional review

board (123/16.05.2016) and in accordance with the Declaration of Helsinki. Thirty-one treatment-naive patients with a pancreatic mass who underwent EUS-FNA at The Research Center of Gastroenterology and Hepatology Craiova (Romania) between 2016 and 2017 were retrospectively analyzed. Clinicopathologic characteristics were analyzed by chart review, and patients were followed for at least 6 months after initial EUS-FNA. The final diagnosis was established based on the FNA cytology results (for the cases interpreted as unequivocally positive or negative for malignancy), histologic examination of the surgically resected specimens or clinical/radiologic follow-up of at least 6 months (nonmalignant defined as spontaneous improvement or lack of progression on follow-up).

EUS-FNA procedure

The EUS-FNA procedures were routinely performed as part of the clinical work-up; they followed the institutional standard protocols with a linear echoendoscope and a 22-gauge or 25-gauge FNA needle with the patient under propofol sedation. At least 3 passes were made for diagnosis. The aspirated material was smeared onto slides, hematoxylin and eosin staining was performed, and a pathologist later reviewed the slides; rapid on-site evaluation was not performed. An additional pass was performed, and the aspirated material was stored in RNA Later (Life Technologies, Grand Island, New York, USA) tubes at −80°C for subsequent DNA extraction.

Cytologic examination

Cytologic examination was performed by an experienced pathologist (C.P.). Samples were divided into 5 diagnostic categories according to the Papanicolaou Society of Cytopathology Guidelines[18]: (1) negative for malignancy, (2) positive for malignancy, (3) suspicious for malignancy, (4) atypical cells present, and (5) nondiagnostic.

DNA extraction and mutational analysis

DNA was extracted from the EUS-FNA material using a DNeasy Blood and Tissue Kit (QIAGEN, Hilden, Germany; catalog no./ID 69506), according to the manufacturer's instructions.

Several techniques are currently being used to detect K-*ras* mutations, such as Sanger sequencing, next-generation sequencing, mutant-enriched PCR, COLD-PCR, or digital PCR.[24] These techniques have different lower limits of detection (LOD) and specificity. For instance, direct sequencing has a reported LOD of approximately 20% mutant alleles,[25] whereas next-generation sequencing is able to detect mutant alleles at levels as low as 2% to 6%.[26] On the other hand, mutant-enriched PCR and COLD-PCR have better sensitivity for detecting K-*ras* mutations, with a LOD of 0.1%.[27,28]

Partitioning of PCR reactions via ddPCR provides a high sensitivity and specificity for detection and quantification of K-*ras* mutations even in limited samples with a high wild-type background. Accordingly, ddPCR has been reported to have a K-*ras* mutation limit of detection of 0.01%.[24,29,30] All samples were initially analyzed for their K-*ras* mutational status by digital droplet PCR. This method uses fluorescently labeled probes to detect the presence of hotspot mutations in the DNA sequences.[31] The DNA strands are encapsulated in droplets created from a water-in-oil emulsion and undergo PCR amplification. The QX200 Droplet Digital PCR System (Bio-Rad, Hercules, Calif, USA) was used to generate 20,000 droplets in each sample, which enhances the detection of low allele frequency variants and produces a high sensitivity of 0.001%. The ddPCR K-*ras* G12/G13 screening kit (Bio-Rad, Pleasanton, Calif, USA) was used as the fluorescently labeled probe to identify the 7 most common K-*ras* mutations (G12A, G12C, G12D, G12R, G12S, G12V, and G13D) within the DNA sequence. Negative and positive controls (Panc1 cell lines) were used to distinguish the wild-type alleles. Interpretation of the ddPCR results was done in accordance with Bio-Rad Rare Mutation Detection Best Practice Guidelines for Droplet Digital PCR. Data analysis was performed using QuantaSoft v1.7.4 software (Bio-Rad).

One of the biggest advantages of ddPCR is the necessity of a lower DNA input, making it a valuable choice for the molecular analysis of EUS-FNA samples. We performed K-*ras* mutant DNA (Panc-1 cells) titration experiments to determine the minimal input of DNA needed for ddPCR detection of K-*ras* mutations. According to our results, the lowest level of detection was at 0.08 ng/μL DNA (Supplementary Fig. 1A and B, available online at www.giejournal.org).

Digital multiplexed detection of single-nucleotide variants by NanoString technology

In addition, we evaluated the mutational status of EUS-FNA samples with a targeted gene panel (24 genes, Vantage 3D DNA SNV Solid Tumor Panel) on a NanoString platform. This technique analyzes 97 single-nucleotide variants (SNVs) from a DNA input level as low as 5 ng, using a modified version of the nCounter barcode chemistry enabling the detection of sequence variants after targeted enrichment by multiplex PCR. The assay enables sensitive and specific characterization of mutant allele sequences levels with a lower LOD of 5%.[32-34] Twenty-four FNA samples of the 31 included in the study were selected for SNV analysis.

Briefly, 5 ng of tumor-derived DNA was prepared as per the manufacturer's instructions and subjected to hybridization of variant-specific probes to unique fluorescent barcodes at the MD Anderson Cancer Center core facility. Results were analyzed with nSolve Analysis Software 4.0 Advanced Analysis. Positive variant calls were defined as meeting the following criteria according to the manufacturer's recommendations: (1) raw digital count levels

TABLE 1. Baseline characteristics of the study patients and details of the EUS-FNA procedure

Final diagnosis	PDAC	CP	pNET
Patients, n	22	7	2
Age (years), mean (range)	63.4 (46-78)	66.8 (48-86)	49
Female/male, n	9/13	2/5	2/0
Lesion size (cm), mean (range)	3.64 (1.8-6.5)	3.6 (1.9-5)	5.35
Lesion location, n (%)			
Pancreatic head	18 (82)	5 (71)	1
Pancreatic body	1 (4.5)	–	1
Pancreatic tail	3 (13.5)	2	–
Smoking, n (%)	15 (68)	10	–
Diabetes mellitus	8 (36)	3	1
Family history of pancreatic cancer, n (%)	1(4.5)	1	0
Needle size, n			
22 gauge	19 (86)	5 (71)	1
25 gauge	3 (14)	2 (29)	1
No. of passes, mean (range)	3.8 (3-5)	4 (3-5)	3

PDAC, Pancreatic ductal adenocarcinoma; *CP*, chronic pancreatitis; *pNET*, pancreatic neuroendocrine tumor.

above 200, (2) raw-count fold-change above the reference DNA sample greater than 2.0, and (3) a statistical significance of $P < .01$.

The approximate cost of ddPCR per sample is U.S.$22, whereas the cost of the SNV panel is ∼U.S.$200 per sample.

Statistical analysis

The diagnostic parameters along with the 95% confidence intervals (CI) were calculated using both MedCalc and Excel XLSTAT.

RESULTS

Clinical and demographic characteristics of the patients

Thirty-one patients (18 male and 13 female) with a mean age of 63 years (range, 46-80 years) underwent EUS-FNA. The lesions were mainly located in the pancreatic head (77%), and the mean size measured by EUS was 3.75 cm (range, 1.8-6.5 cm). Among the 31 patients, the final diagnoses were as follows: 22 (71%) PDAC, 7 (22%) CP, and 2 (6%) pancreatic neuroendocrine tumor (pNET). The main clinical characteristics of the patients included in the study are summarized in Table 1.

Cytologic evaluation

After cytologic examination, 15 (49%) FNA samples were classified as positive for malignancy. Five samples (16%) were classified as negative for malignancy and 11 (35%) were considered inconclusive: 7 (22%) suspicious and 4 (13%) atypical results (Table 2).

If the inconclusive results were considered negative for malignancy, the sensitivity of the cytologic examination was 63% (95% CI, 41%-82%) and the specificity was 100% (95% CI, 62%-100%). The negative likelihood ratio was 0.37 (95% CI, 0.22-0.62). The overall accuracy, positive predictive value (PPV), and negative predictive value (NPV) were 74% (95% CI, 55%-88%), 100% (95% CI, 73%-100%), and 53% (95% CI, 28%-76%), respectively.

If the inconclusive cases were interpreted by placing suspicious cases in the positive group and the atypical cases in the negative group, the diagnostic parameters of the cytologic examination were as follows: sensitivity 91% (95% CI, 72%-98%), specificity 88% (95% CI, 47%-99%), PPV 95% (95% CI, 77%-99%), NPV 77% (95% CI, 47%-93%), and overall accuracy 90% (95% CI, 74%-98%). The negative likelihood ratio was 0.10 (95% CI, 0.03-0.38) and the positive likelihood ratio was 7.3 (95% CI, 1.17-46).

K-*ras* mutation analysis using ddPCR

Two EUS-FNA samples were excluded from further analysis due to low DNA yields. A total of 18 of 29 (62%) cases were positive for K-*ras*.

K-*ras* mutations were found in 79% (11 of 14) of samples diagnosed as positive for malignancy, in 71% (5 of 7) of the cases suspicious for malignancy, in 25% (1 of 4) of atypical results, and in 16% (1 of 6) of cases considered negative for malignancy. According to the final diagnosis, a K-*ras* mutation was detected in 77% (17 of 22) of cases of PDAC and in 14% (1 of 7) cases of CP, whereas no mutation was observed in the cases of pNET.

The diagnostic value of K-*ras* mutation in combination with cytologic examination of the EUS-FNA samples was further analyzed. If the cytopathologic results were definite and sufficient for evaluation, we did not consider the results of K-*ras* mutation analysis to determine the final

TABLE 2. Diagnostic accuracy of cytologic examination of pancreatic specimens obtained by EUS-FNA

	PDAC	Other pancreatic pathologies*
Positive for malignancy	14	1 (pNET)
Atypical	1	3 (CP)
Suspicious	6	1 (pNET)
Negative	1	4 (CP)
Total	22	9

pNET, Pancreatic neuroendocrine tumor; *CP*, chronic pancreatitis; *PDAC*, pancreatic ductal adenocarcinoma.
*The category of other pancreatic pathologies includes chronic pancreatitis (n = 7) and pancreatic neuroendocrine tumors (n = 2).

diagnosis. Consequently, we considered the K-*ras* results only for the inconclusive and negative FNA samples. Cases with a positive K-*ras* mutation were assumed to be malignant, and those negative for the K-*ras* mutation were assumed to be benign. When this approach was used, the diagnostic parameters were as follows: sensitivity 90% (95% CI, 69%-98%), specificity 87% (95% CI, 47%-99%), PPV 95% (95% CI,75%-99%), NPV 77% (95% CI, 47%-93%), overall accuracy 90% (95% CI, 72%-97%). The positive likelihood ratio was 7.24 (95% CI, 1.15-45) and the negative likelihood ratio was 0.11 (95% CI, 0.03-0.42).

The 2 samples excluded due to low DNA yield were 1 case of pNET (interpreted as suspicious on cytology) and 1 case of PDAC (cytology positive). With the 2 samples included, the diagnostic accuracy of cytology + K-*ras* testing was as follows: sensitivity 95% (95% CI, 77%-99%), specificity 87% (95% CI, 47%-99%), PPV 95% (95% CI, 77%-99%), NPV 87% (95% CI, 50%-97%), and overall accuracy 93% (95% CI, 77%-99%).

Digital multiplexed detection of single-nucleotide variants by NanoString technology

Mutational status was evaluated using the NanoString Vantage 3D DNA SNV Solid Tumor Panel, in a cohort of 24 EUS-FNA samples including 19 cases of PDAC and 5 cases of CP.

According to the final diagnosis, the SNV assay detected at least 1 variant in 90% (17 of 19) of PDAC samples and in 20% (1 of 5) of cases with CP. Among the 19 PDAC samples, K-*ras* variants were detected in 17 (90%) cases; of these, 7 (41%) had G12V, 6 (35%) had G12D, 2 (12%) had G12R, 1 (6%) had Q61H, and 1 (6%) had Q61L mutations. One case of PDAC harbored 3 SNVs (*EGFR*, E746_A750delELREA; K-*ras*, G12D; *PIK3CA*[*E545G*]).

The SNV assay detected at least 1 variant in all FNA samples interpreted as suspicious or atypical and had a final diagnosis of PDAC; no variant was detected in the atypical specimens with a final diagnosis of CP.

The diagnostic performance of cytology examination combined with the SNV assay results (considered only for the negative and inconclusive samples) was further calculated. The sensitivity was 94% (95% CI, 74%-99%), specificity 80% (95% CI, 28%-99%), and the overall accuracy was 91% (95% CI,73%- 98%). The negative likelihood ratio was 0.07 (95% CI, 0.01-0.47) and the positive likelihood ratio was 4.47 (95% CI, 0.82-27.43).

ddPCR multiplex assay versus the SNV assay by NanoString technology

A comparison of the diagnostic performances of the ddPCR multiplex assay versus the SNV assay by NanoString technology was further performed. As previously mentioned, 24 EUS-FNA samples were analyzed using both molecular tests. The multi-gene SNV assay was able to detect 2 K-*ras* codon 61 mutations (Q61L, Q61H) in 2 cases of PDAC, which were missed by ddPCR. Ninety-five percent (16 of 17) of the K-*ras* codon 12/13 mutations detected by ddPCR were confirmed by the NanoString SNV panel. Both ddPCR and the NanoString test detected a K-*ras* mutation (G12D) in a patient with CP.

The diagnostic parameters of the cytologic examination, ddPCR multiplex assay, and the SNV assay are reported in Table 3. The overall diagnostic accuracy of the cytologic examination alone was 74%, and it increased to 91% ($P = .01$) when the results of both molecular tests were considered for the cases with negative and inconclusive results.

Follow-up of patients after the EUS-FNA procedure

All patients were followed up for at least 6 months or until time of death. The mean follow-up time was 298 days, and median follow-up time was 251 days (range, 49-951 days).

All patients with a definite diagnosis after the EUS-FNA procedure (samples interpreted as positive for malignancy) were managed according to their clinical condition (chemotherapy, n = 11; best supportive care, n = 3; surgical resection for pNET, n = 1). Patients with EUS-FNA samples interpreted as negative for malignancy (benign) were also followed up, and the final diagnosis was CP in 4 of 5 cases (spontaneous improvement or lack of progression on follow-up CT scans). For the other patient with negative cytology, the autopsy performed 3 months after the EUS-FNA procedure revealed PDAC; no mutation was detected for this patient.

Of the 7 samples interpreted as suspicious for malignancy, the final diagnosis was PDAC in 6 cases (diagnosis confirmed after a second EUS-FNA procedure in 4 cases, CT-guided biopsy of liver metastasis in 1 case, and based on patient medical record data in 1 case) and pNET in 1 case (diagnosis confirmed after surgical resection). A K-*ras* mutation was detected by ddPCR in 5 of 6 suspicious samples with a final diagnosis of PDAC; the SNV test detected a K-*ras* mutation in all suspicious samples.

Of the 4 samples interpreted as atypical after cytologic examination, the final diagnosis was CP in 3 cases (follow-up CT scans) and PDAC in 1 case (based on patient

TABLE 3. Comparison of the diagnostic parameters for pancreatic cancer among cytologic examination, K-*ras* mutation analysis by ddPCR, and the SNV assay for the 24 EUS-FNA samples

	Sensitivity (%), n/N (95% CI)	Specificity (%), n/N (95% CI)	Positive predictive value (%) (95% CI)	Negative predictive value (95% CI)	Positive likelihood ratio (95% CI)	Negative likelihood ratio (95% CI)	Accuracy (%), n/N (95% CI)
FNA cytology*	63, 12/19 (38-83)	100, 5/5 (47-100)	100 (69-100)	41 (28-56)	–	0.37 (0.2-0.6)	71,17/24 (49-87)
FNA cytology†	89, 17/19 (66-98)	100, 5/5) (47-100)	100	71 (40-90)	–	0.11 (0.03-0.4)	91, 22/24 (73-98)
Cytology + K-*ras*	89, 17/19 (66-99)	80, 4/5 (28-99)	94 (74-99)	66 (33-88)	4.47 (0.7-26)	0.13 (0.03-0.52)	87, 21/24 (67-97)
Cytology + SNV assay	94, 18/19 (74-99)	80, 4/5 (28-99)	94 (75-99)	80 (36-96)	4.74 (0.8-27)	0.07 (0.01-0.5)	91, 22/24 (73-98)
Cytology + ddPCR + SNV assay	94, 18/19 (74-99)	80, 4/5 (28-99)	94 (75-99)	80 (36-96)	4.74 (0.8-27)	0.07 (0.01-0.5)	91, 22/24 (73-98)

CI, Confidence interval; *SNV*, single-nucleotide variant; *ddPCR*, droplet digital polymerase chain reaction.
*Suspicious and atypical categories were interpreted as negative results.
†Suspicious categories were considered positive for malignancy and atypical categories were interpreted as negative results.

medical record data). Both ddPCR and the SNV test detected a K-*ras* mutation in the case with a final diagnosis of PDAC (Fig. 1).

DISCUSSION

EUS-FNA has greatly improved the preoperative diagnosis of PDAC; however, in a subset of cases, the diagnosis remains inconclusive. The current study illustrated that integration of the analysis of genetic markers with EUS-FNA and cytologic evaluation, especially in inconclusive cases, can increase the diagnostic accuracy of pancreatic lesions, thus preventing repeat biopsies or delay in the care of patients with PDAC.

In the present study, there was a high percentage of inconclusive results (35%) after cytologic evaluation, and this could be attributed to the absence of the on-site cytopathologist during the EUS-FNA procedures, which were performed in Romania. However, data regarding the accuracy of cytologic diagnosis with or without rapid on-site cytopathology examination are conflicting. Several studies have shown that ROSE increases the diagnostic yield, reducing the rate of false-negative and nondiagnostic results.[35,36] On the other hand, Wani et al[37] reported no differences in terms of nondiagnostic, atypical, and suspicious specimens as well as in the sensitivity and specificity of EUS-FNA with or without ROSE. Even in the presence of ROSE increasing the diagnostic yield, EUS-FNA does not have 100% sensitivity, specificity, and accuracy in diagnosing pancreatic masses, and cytology results can still be inconclusive or negative despite strong clinical suspicion of PDAC. Thus, further molecular testing as outlined in our approach could help in clinical decision making.

A retrospective study[38] including more than 4000 patients found that inconclusive pathologic diagnoses were made in 14% of the cases and consisted of atypical (1 of 3) and suspicious for malignancy (2 of 3) categories, and these carried a malignancy risk of 79% and 96%, respectively. Therefore, the authors have recommended classifying results suspicious for malignancy as malignant to optimize the diagnostic performance of EUS-FNA.[38] These results were in line with our study; when suspicious categories were interpreted as malignant, the sensitivity of EUS-FNA cytologic examination increased from 63% to 91%. In clinical practice, the management of a patient with inconclusive cytology has not yet been clearly standardized; in most cases, if a biopsy is interpreted as suspicious or atypical, at least 1 repeat biopsy is performed, although retrospective studies have shown that the repetition of EUS-FNA may give a correct diagnosis in only about 60% to 80% of cases.[39,40]

For the molecular analysis of EUS-FNA samples, 2 major barriers have been documented. First, the pauci-cellular FNA specimens do not always provide an adequate amount of DNA for molecular analysis. Two of the 31 samples included in our study had nonamplifiable tumor DNA and could not be used for molecular testing. A former study published in 2014 found that only 21 of 169 (12.4%) EUS-FNA specimens obtained from malignant solid pancreatic masses had adequate cellularity for theranostic studies.[41] However, this area has greatly improved in recent years. For example, Hartley et al[42] showed that FNA smears yielded more DNA per nuclear area compared with formalin-fixed paraffin-embedded (FFPE) tissue taken from Whipple resection specimens. K-*ras* codon 12 mutations were detected in 77% of the samples compared with 57% of matched FFPE samples, with FNA retrieving a higher DNA yield compared with FFPE. Moreover, the way the samples are stored might also affect DNA extraction efficiency. For instance, Berry et al[43] proved how the K-*ras* mutation frequency in the same patients was significantly lower (45%) when using DNA extracted from EUS-FNA-derived FFPE blocks compared with EUS-FNA samples that were snap frozen (80%), as were the samples in our study. The problem of

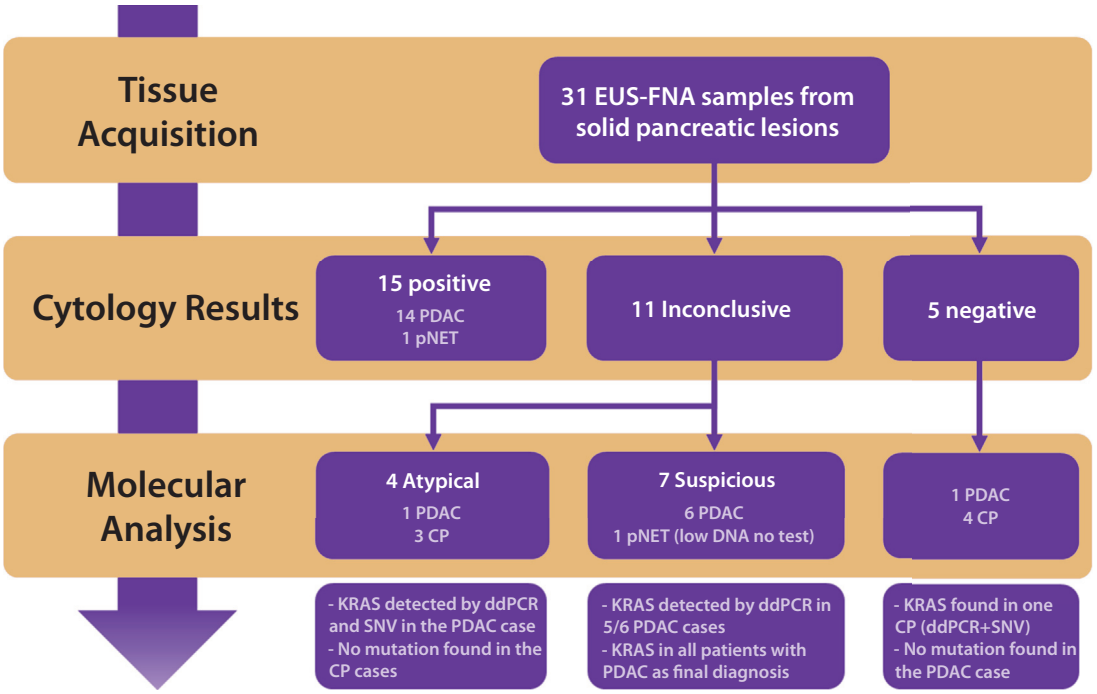

Figure 1. Diagnostic flow and follow-up data. CP, Chronic pancreatitis; *ddPCR*, droplet digital polymerase chain reaction; *PDAC*, pancreatic ductal adenocarcinoma; *SNV*, single nucleotide variant.

low DNA in the FNA samples could be overcome with the use of EUS-guided FNB, which in general leads to more tissue acquisition. However, the use of EUS-FNA versus EUS-FNB samples for genomic analysis is still a matter of debate. Some studies suggest that EUS-FNA samples have a higher concentration of pure tumor cells and seem to be a more reliable source of DNA.[44] On the other hand, others consider that the cellular material obtained using EUS-FNA is often graded to be insufficient, contaminated, composed of poor-quality DNA, and suboptimal for genetic analysis. Moreover, a study by Kandel et al[45] showed that more DNA can be extracted from the tumor tissue using FNB needles. They demonstrated that 74% of EUS-FNB samples of pancreatic cancer were adequate for whole-exome sequencing compared with 54% of EUS-FNA samples.[45]

Second, the low tumor cellularity complicates FNA of many PDAC masses, given the overshadowing of tumor cells by the abundant normal cells. Droplet digital PCR has the potential to overcome these difficulties. This technique can perform highly sensitive mutation detection with minimal template DNA input, enabling accurate and sensitive genotyping using tumor biopsy samples that are limited in both quantity and tumor cell purity.[22] There is limited information so far for PDAC; the ddPCR methodology has been used mainly for the detection of K-*ras* mutations in circulating tumor DNA in patients with early-stage pancreatic cancer.[31,46,47]

Accurate determination of K-*ras* mutation status from pancreas EUS-FNA biopsy specimens has important clinical implications for the diagnostic, prognostic, and therapeutic aspects of the care of patients with PDAC.[48,49] To date, numerous studies have investigated the diagnostic role of adding K-*ras* mutation analysis to biopsy specimens.[48] With the improved K-*ras* mutation detection facilitated by ddPCR, K-*ras* analysis in EUS-FNA can be performed more accurately, even in FNA specimens previously thought to be inadequate for molecular analysis. ddPCR can be easily implemented in the routine assessment of pancreatic EUS-FNA samples to quickly provide information on K-*ras* mutational status that can supplement cytologic evaluation. In our study, we combined cytology results with ddPCR results only for indeterminate and negative cytology samples, hypothesizing that mutation analysis is useful only in these categories (the diagnosis is definite for the samples that are positive for malignancy). Our follow-up data suggested that the detection of K-*ras* gene mutations could supplement cytopathology by improving the positive rate in indeterminate cases. However, there is a risk of false-positive results as was the case for the patient with CP included in our study, where both ddPCR and the SNV test found a G12D K-*ras* mutation. Previous studies have shown that K-*ras* mutations develop in a subset of CP, and this could provide a genetic basis for the potential progression of CP to pancreatic cancer.[50] Therefore, molecular testing poses the risk of false-positive results. Clinicians should be aware that the reduction in the false-negative rate with molecular testing is counterbalanced by a relatively small increase in the false-positive rate. Consequently, molecular testing should always be interpreted cautiously within the clinical context.

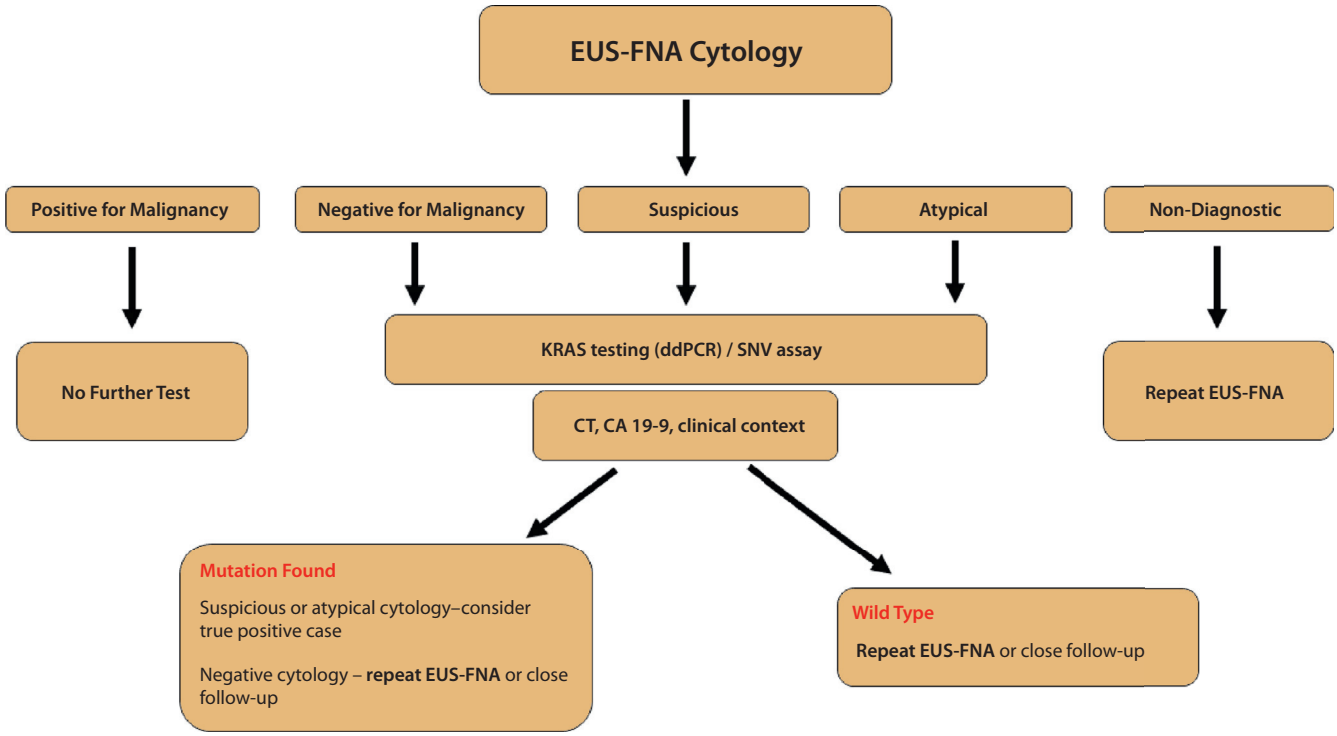

Figure 2. Diagnostic work-up of pancreatic EUS-FNA samples. *ddPCR*, Droplet digital polymerase chain reaction; *SNV*, single nucleotide variant.

Consequently, the combination of cytology and molecular testing is a double-edge sword: on the one hand, it increases the sensitivity compared with EUS-FNA cytology alone (63% vs 94%), but on the other hand, it decreases the specificity (100% vs 80%). Given the grim prognosis of PDAC, a high sensitivity is extremely important for any clinical assay, because fewer cased of PDAC will be missed. This increased sensitivity is bought about by a higher rate of false-positive cases, which highlight once again the need for a multidimensional diagnostic approach in patients with pancreatic masses.

The rationale for using ddPCR to analyze K-*ras* frequency in the EUS-FNA samples was to avoid high costs and time-consuming library preparations for next-generation sequencing. Furthermore, ddPCR is a highly sensitive method and is easy to use.

PDAC is a molecularly heterogeneous disease, and the use of wide gene panels can significantly improve the clinical sensitivity and specificity, minimizing the risk of false-positive results. The SNV assay by NanoString can detect SNVs from as little as 5 ng of DNA. By combining the SNV assay with cytology results only for indeterminate and negative cytology samples, we obtained a sensitivity of 94% and a specificity of 80% for the diagnosis of PDAC. The diagnostic performance of the SNV assay and ddPCR was similar (overall accuracy 91% vs 87%). The SNV test was able to detect 2 K-*ras* codon 61 mutations missed by ddPCR. Several studies have reported the usefulness of wide cancer gene panel testing on EUS-FNA-samples. Kameta et al[51] used a next-generation sequencing assay including 50 cancer-related genes on EUS-FNA samples from pancreatic cancer and detected K-*ras* mutations (96%), TP53 mutations (44%), CDKN2A mutations (11%), and SMAD4 mutations (7%). All the K-*ras* mutations were also confirmed using TaqMan PCR analysis. Gleeson et al[52] performed next-generation sequencing using a 160 cancer gene panel on pancreatic EUS-FNA and detected K-*ras* mutations in 93% of cases with a final diagnosis of PDAC. All the mutations detected on EUS-FNA samples were consistent with the mutations detected on surgical specimens. Ishizawa et al[53] compared K-*ras* mutation detection with cancer gene panel testing by next-generation sequencing performed on ROSE EUS-FNA specimens and K-*ras* mutation analysis by PCR. On the cancer gene panel testing, K-*ras* mutations were detected in 92% cases of PDAC, and 3 FNA samples showed K-*ras* mutations in cancer gene panel testing but not in K-*ras* mutation analysis by PCR. These previous studies have demonstrated that K-*ras* mutations (in addition to a diverse number of other mutations) can be adequately detected on EUS-FNA samples. The SNV test used in our study was able to detect K-*ras* mutations in 90% of cases of PDAC. In addition to those studies, K-*ras* mutation analysis was applied to clinical decision making, specifically in the diagnostic work-up of pancreatic solid lesions.

According to our data, cytologic examination of the EUS-FNA samples is highly specific for the diagnosis of PDAC and therefore, when a cytologic diagnosis of

malignancy is certain (positive for malignancy), further investigations are not needed. On the other hand, in cases with inconclusive cytology (suspicious/atypical) and in negative cases with a high clinical and radiologic suspicion of malignancy, molecular testing could be useful. The synergism between EUS-FNA and K-*ras* testing in these cases could help to limit the repetition of EUS-FNA only to those cases that are K-*ras* wild-type, while considering cases in which K-*ras* is found after inconclusive EUS-FNA results as true positives. Furthermore, in cases with negative cytology but a positive K-*ras* mutation, close follow-up or repeat EUS-FNA would be the preferred approach (Fig. 2).

The National Comprehensive Cancer Network guidelines have recently been updated to recommend testing for all patients with advanced PDAC.[4] Given the low DNA input, digital data output, and rapid turnaround time, NanoString technology may be instrumental in the preoperative molecular diagnosis of pancreatic lesions. Moreover, efforts are needed to obtain a more complete diagnostic profile for each patient to exploit all potential therapeutic opportunities in this lethal disease. Clinicians should bear in mind that tumor biopsies represent not only the standard for cancer diagnosis but also the primary method for molecular testing to guide the selection of personalized therapies. The gene panel we have used in this study includes some actionable mutations that could lead to a treatment that is not currently a standard of care chemotherapy for pancreatic cancer (*BRCA1/2*-platinum chemotherapy, *PARP* inhibitor, *PIK3CA-PICK3CA* inhibitor, *STK11-mTOR* inhibitor, etc).

Limitations of this study include the small sample size and the fact that the SNV panel did not include SMAD4 and CDKN2A, which represent frequent molecular alterations in PDAC. Moreover, the 95% CIs were wide for most measures reported in the current study, and this could be attributed to the small sample size. Accordingly, further studies with larger sample size are needed to validate our results. However, this is the first study to assess the diagnostic value of K-*ras* analysis using ddPCR on EUS-FNA samples and to conduct a head to head comparison, of the diagnostic performances of the ddPCR multiplex assay versus the multi-gene SNV assay by NanoString technology.

CONCLUSIONS

The current study illustrated that integration of K-*ras* analysis with EUS-FNA and cytologic evaluation, especially in inconclusive cases, can increase the diagnostic accuracy of pancreatic lesions, thus preventing repeat biopsies or delay in the care of patients with PDAC. K-*ras* analysis using ddPCR is a highly sensitive and cost-effective method to increase the diagnostic accuracy of EUS-FNA. However, mutation testing should always, as any other similar modality, be interpreted cautiously within the clinical context.

ACKNOWLEDGMENT

This work was supported by a grant of Ministry of Research and Innovation, CNCS-UEFISCDI, project "Pathogenic mechanisms and personalized treatment in pancreatic cancer using multi-omic technologies"—PANCNGS, code PN-III-P1-1.2-PCCDI2017-0797, within PNCDI III.

REFERENCES

1. Ferlay J, Colombet M, Soerjomataram I, et al. Cancer incidence and mortality patterns in Europe: estimates for 40 countries and 25 major cancers in 2018. Eur J Cancer 2018;103:356-87.
2. Howlader N, Noone A, Krapcho M, et al. SEER cancer statistics review, 1975-2013. Bethesda, MD: National Cancer Institute; 2016.
3. Rahib L, Smith BD, Aizenberg R, et al. Projecting cancer incidence and deaths to 2030: the unexpected burden of thyroid, liver, and pancreas cancers in the United States. Cancer Res 2014;74:2913-21.
4. Tempero MA. NCCN guidelines updates: pancreatic cancer. J Natl Compr Cancer Netw 2019;17:603-5.
5. Hewitt MJ, McPhail MJ, Possamai L, et al. EUS-guided FNA for diagnosis of solid pancreatic neoplasms: a meta-analysis. Gastrointest Endosc 2012;75:319-31.
6. Hebert-Magee S, Bae S, Varadarajulu S, et al. The presence of a cytopathologist increases the diagnostic accuracy of endoscopic ultrasound-guided fine needle aspiration cytology for pancreatic adenocarcinoma: a meta-analysis. Cytopathology 2013;24:159-71.
7. Puli SR, Bechtold ML, Buxbaum JL, et al. How good is endoscopic ultrasound-guided fine-needle aspiration in diagnosing the correct etiology for a solid pancreatic mass? A meta-analysis and systematic review. Pancreas 2013;42:20-6.
8. Trisolini E, Armellini E, Paganotti A, et al. KRAS mutation testing on all non-malignant diagnosis of pancreatic endoscopic ultrasound-guided fine-needle aspiration biopsies improves diagnostic accuracy. Pathology 2017;49:379-86.
9. Erickson RA, Sayage-Rabie L, Beissner RS. Factors predicting the number of EUS-guided fine-needle passes for diagnosis of pancreatic malignancies. Gastrointest Endosc 2000;51:184-90.
10. Kalaitzakis E, Panos M, Sadik R, et al. Clinicians' attitudes towards endoscopic ultrasound: a survey of four European countries. Scand J Gastroenterol 2009;44:100-7.
11. Larghi A, Eguia V, Hassan C, et al. Economic crisis: the right time to widen endoscopic ultrasound utilization. Endoscopy 2014;46:80-1.
12. Bailey P, Chang DK, Nones K, et al. Genomic analyses identify molecular subtypes of pancreatic cancer. Nature 2016;531:47-52.
13. Moffitt RA, Marayati R, Flate EL, et al. Virtual microdissection identifies distinct tumor- and stroma-specific subtypes of pancreatic ductal adenocarcinoma. Nat Genet 2015;47:1168-78.
14. Waddell N, Pajic M, Patch A-M, et al. Whole genomes redefine the mutational landscape of pancreatic cancer. Nature 2015;518:495.
15. Witkiewicz AK, McMillan EA, Balaji U, et al. Whole-exome sequencing of pancreatic cancer defines genetic diversity and therapeutic targets. Nat Commun 2015;6:6744.
16. Aguirre AJ, Nowak JA, Camarda ND, et al. Real-time genomic characterization of advanced pancreatic cancer to enable precision medicine. Cancer Discov 2018;8:1096-111.
17. Pishvaian MJ, Bender RJ, Halverson D, et al. molecular profiling of patients with pancreatic cancer: initial results from the know your tumor initiative. Clin Cancer Res 2018;24:5018-27.
18. Jones S, Zhang X, Parsons DW, et al. Core signaling pathways in human pancreatic cancers revealed by global genomic analyses. Science 2008;321:1801-6.

19. Sho S, Court CM, Kim S, et al. Digital PCR improves mutation analysis in pancreas fine needle aspiration biopsy specimens. PLoS ONE 2017;12:e0170897.
20. Decraene C, Silveira AB, Bidard F-C, et al. Multiple hotspot mutations scanning by single droplet digital PCR. Clin Chem 2018;64:317-28.
21. Vanova B, Kalman M, Jasek K, et al. Droplet digital PCR revealed high concordance between primary tumors and lymph node metastases in multiplex screening of KRAS mutations in colorectal cancer. Clin Exp Med 2019;19:219-24.
22. Olmedillas-López S, García-Arranz M, García-Olmo D. Current and emerging applications of droplet digital PCR in oncology. Mol Diagn Ther 2017;21:493-510.
23. Cancer Genome Atlas Research Network. Integrated genomic characterization of pancreatic ductal adenocarcinoma. Cancer Cell 2017;32:185-203.e13.
24. Dong L, Wang S, Fu B, et al. Evaluation of droplet digital PCR and next generation sequencing for characterizing DNA reference material for KRAS mutation detection. Sci Rep 2018;8:1-9.
25. Isler JA, Vesterqvist OE, Burczynski ME. Analytical validation of genotyping assays in the biomarker laboratory. Pharmacogenomics 2007;8:353-68.
26. Lin M-T, Mosier SL, Thiess M, et al. Clinical validation of KRAS, BRAF, and EGFR mutation detection using next-generation sequencing. Am J Clin Pathol 2014;141:856-66.
27. How Kit A, Mazaleyrat N, Daunay A, et al. Sensitive detection of KRAS mutations using enhanced-ice-COLD-PCR mutation enrichment and direct sequence identification. Hum Mutat 2013;34:1568-80.
28. Li J, Makrigiorgos GM. COLD-PCR: a new platform for highly improved mutation detection in cancer and genetic testing. Biochem Soc Trans 2009;37(Pt 2):427-32.
29. Taly V, Pekin D, Benhaim L, et al. Multiplex picodroplet digital PCR to detect KRAS mutations in circulating DNA from the plasma of colorectal cancer patients. Clin Chem 2013;59:1722-31.
30. Allenson K, Castillo J, San Lucas F, et al. High prevalence of mutant KRAS in circulating exosome-derived DNA from early-stage pancreatic cancer patients. Ann Oncol 2017;28:741-7.
31. Bernard V, Kim DU, San Lucas FA, et al. Circulating nucleic acids are associated with outcomes of patients with pancreatic cancer. Gastroenterology 2019;156:108-18.e4.
32. Houghton AM, Meredith G, Kargl J, et al. Simultaneous detection of activating somatic DNA mutations and expressed fusion transcripts from lung tumor FFPE samples. Cancer Res 2017;77(13 suppl):2422.
33. Parris B, Meredith G, Ross P, et al. Digital multiplexed detection of single nucleotide variants (SNV) in non-small cell lung cancer using NanoString technology. J Thorac Oncol 2017;12:S2099.
34. Lausted C, Zhou Y, Lee J, et al. NanoString 3D Biology™ technology: simultaneous digital counting of DNA, RNA and protein. Cancer Res 2017;77(13 suppl):2421.
35. Iglesias-Garcia J, Lariño-Noia J, Abdulkader I, et al. Rapid on-site evaluation of endoscopic-ultrasound-guided fine-needle aspiration diagnosis of pancreatic masses. World J Gastroenterol 2014;20:9451.
36. Ecka RS, Sharma M. Rapid on-site evaluation of EUS–FNA by cytopathologist: an experience of a tertiary hospital. Diagn Cytopathol 2013;41:1075-80.
37. Wani S, Mullady D, Early DS, et al. The clinical impact of immediate on-site cytopathology evaluation during endoscopic ultrasound-guided fine needle aspiration of pancreatic masses: a prospective multicenter randomized controlled trial. Am J Gastroenterol 2015;110:1429-39.
38. Layfield LJ, Schmidt RL, Hirschowitz SL, et al. Significance of the diagnostic categories "atypical" and "suspicious for malignancy" in the cytologic diagnosis of solid pancreatic masses. Diagn Cytopathol 2014;42:292-6.
39. Téllez-Ávila FI, Martínez-Lozano JA, Rosales-Salinas A, et al. Repeat endoscopic ultrasound fine needle aspiration after a first negative procedure is useful in pancreatic lesions. Endosc Ultrasound 2016;5:258-62.
40. Eloubeidi MA, Varadarajulu S, Desai S, et al. Value of repeat endoscopic ultrasound-guided fine needle aspiration for suspected pancreatic cancer. J Gastroenterol Hepatol 2008;23:567-70.
41. Navina S, McGrath K, Chennat J, et al. Adequacy assessment of endoscopic ultrasound-guided, fine-needle aspirations of pancreatic masses for theranostic studies: optimization of current practices is warranted. Arch Pathol Lab Med 2014;138:923-8.
42. Hartley CP, Mahajan AM, Selvaggi SM, et al. FNA smears of pancreatic ductal adenocarcinoma are superior to formalin-fixed paraffin-embedded tissue as a source of DNA: comparison of targeted KRAS amplification and genotyping in matched preresection and postresection samples. Cancer Cytopathol 2017;125:838-47.
43. Berry W, Algar E, Kumar B, et al. Endoscopic ultrasound-guided fine-needle aspirate-derived preclinical pancreatic cancer models reveal panitumumab sensitivity in KRAS wild-type tumors. Int J Cancer 2017;140:2331-43.
44. Kandel P, Wallace MB. Recent advancement in EUS-guided fine needle sampling. J Gastroenterol 2019;54:377-87.
45. Kandel P, Nassar A, Graddy C, et al. Mo1345 whole exome sequencing and genomic profiling of pancreas tumor tissue obtained with a novelfork-tipped eus guided fine needle core biopsy: a randomized controlled trial [abstract]. Gastrointest Endosc 2018;87:AB455-6.
46. Demuth C, Spindler K-LG, Johansen JS, et al. Measuring KRAS mutations in circulating tumor DNA by droplet digital PCR and next-generation sequencing. Transl Oncol 2018;11:1220-4.
47. Brychta N, Krahn T, von Ahsen O. Detection of KRAS mutations in circulating tumor DNA by digital PCR in early stages of pancreatic cancer. Clin Chem 2016;62:1482.
48. Fuccio L, Hassan C, Laterza L, et al. The role of K-ras gene mutation analysis in EUS-guided FNA cytology specimens for the differential diagnosis of pancreatic solid masses: a meta-analysis of prospective studies. Gastrointest Endosc 2013;78:596-608.
49. Ogura T, Yamao K, Hara K, et al. Prognostic value of K-ras mutation status and subtypes in endoscopic ultrasound-guided fine-needle aspiration specimens from patients with unresectable pancreatic cancer. J Gastroenterol 2013;48:640-6.
50. Rashid S, Singh N, Gupta S, et al. Progression of chronic pancreatitis to pancreatic cancer: is there a role of gene mutations as a screening tool? Pancreas 2018;47:227-32.
51. Kameta E, Sugimori K, Kaneko T, et al. Diagnosis of pancreatic lesions collected by endoscopic ultrasound-guided fine-needle aspiration using next-generation sequencing. Oncol Lett 2016;12:3875-81.
52. Gleeson FC, Kerr SE, Kipp BR, et al. Targeted next generation sequencing of endoscopic ultrasound acquired cytology from ampullary and pancreatic adenocarcinoma has the potential to aid patient stratification for optimal therapy selection. Oncotarget 2016;7:54526.
53. Ishizawa T, Makino N, Matsuda A, et al. Usefulness of rapid on-site evaluation specimens from endoscopic ultrasound-guided fine-needle aspiration for cancer gene panel testing: a retrospective study. PLoS ONE 2020;15:e0228565.

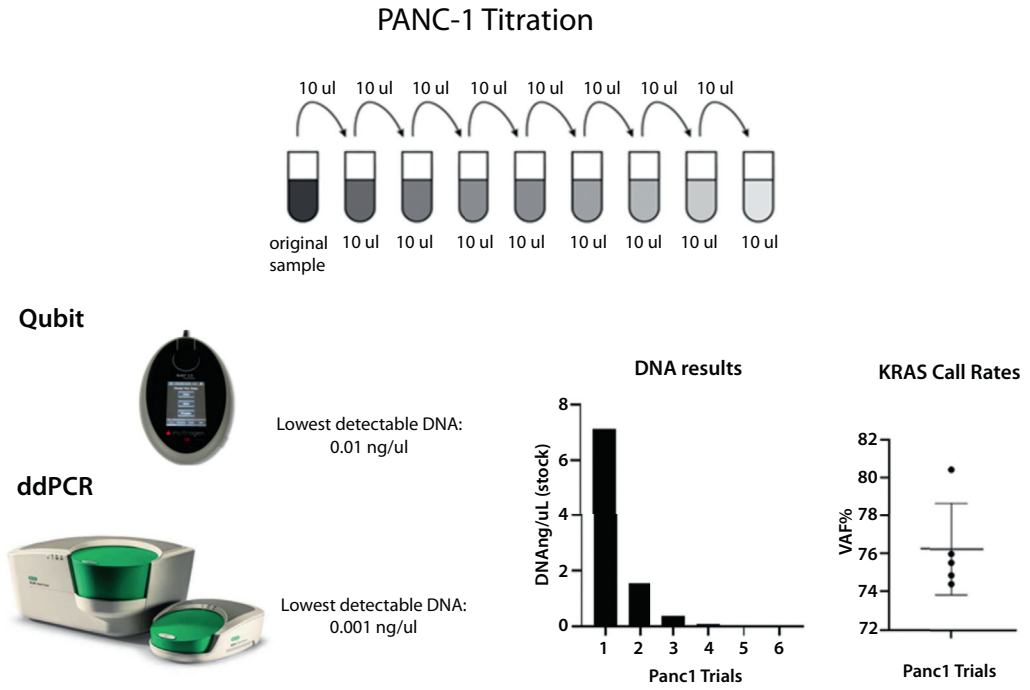

Supplementary Figure 1. A, Panc-1 titration experiment. The samples are labeled according to the numbers on the ddPCR graphs (**B**). K-*ras* mutations could be detected at levels as low as 0.004 ng/μL (graph no. 8); however, there are not enough wild-type DNA droplets (*green dots*). Therefore, that K-*ras* frequency cannot be called with 100% accuracy. The lowest level of detection is at 0.08 ng/μL (graph no. 6); there are enough wild-type DNA droplets suggesting that there was plenty of DNA loaded into the sample. *ddPCR*, Droplet digital polymerase chain reaction.

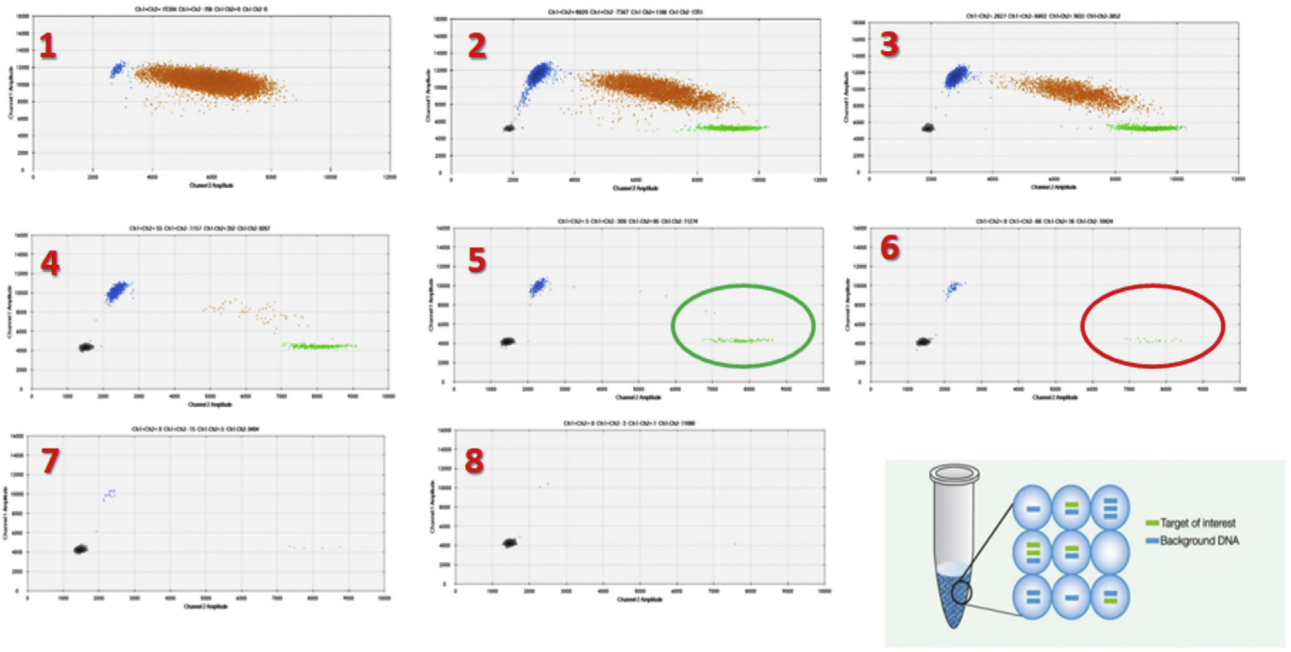

Sample	1	2	3	4	-	5	-	6	-	7	-	-	8
Qubit (ng/ul)	61.4	33.2	16.8	9.6	-	2.3	-	-	-	0.184	-	-	-
Predicted (ng/ul)	-	30	15	7.5	3.75	2	1	0.5	0.25	0.12	0.06	0.03	0.001
ddPCR (8x)	Too High	24.6	13.4	7.2	-	1.5	-	0.08	-	0.02	-	-	0.004

Supplementary Figure 1. Continued.

Published OnlineFirst November 13, 2020; DOI: 10.1158/1078-0432.CCR-20-2667

Defining the Comprehensive Genomic Landscapes of Pancreatic Ductal Adenocarcinoma Using Real-World Endoscopic Aspiration Samples

Alexander Semaan[1,2], Vincent Bernard[1,2], Jaewon J. Lee[1,2,3], Justin W. Wong[1], Jonathan Huang[2], Daniel B. Swartzlander[1,2], Bret M. Stephens[1,2], Maria E. Monberg[1,2], Brian R. Weston[4], Manoop S. Bhutani[4], Kyle Chang[5], Paul A. Scheet[5], Anirban Maitra[1,2], Yasminka A. Jakubek[5], and Paola A. Guerrero[1,2]

ABSTRACT

Purpose: Most patients with pancreatic ductal adenocarcinoma (PDAC) present with surgically unresectable cancer. As a result, endoscopic ultrasound–guided fine-needle aspiration (EUS-FNA) is the most common biospecimen source available for diagnosis in treatment-naïve patients. Unfortunately, these limited samples are often not considered adequate for genomic analysis, precluding the opportunity for enrollment on precision medicine trials.

Experimental Design: Applying an epithelial cell adhesion molecule (EpCAM)-enrichment strategy, we show the feasibility of using real-world EUS-FNA for in-depth, molecular-barcoded, whole-exome sequencing (WES) and somatic copy-number alteration (SCNA) analysis in 23 patients with PDAC.

Results: Potentially actionable mutations were identified in >20% of patients. Further, an increased mutational burden and higher aneuploidy in WES data were associated with an adverse prognosis. To identify predictive biomarkers for first-line chemotherapy, we developed an SCNA-based complexity score that was associated with response to platinum-based regimens in this cohort.

Conclusions: Collectively, these results emphasize the feasibility of real-world cytology samples for in-depth genomic characterization of PDAC and show the prognostic potential of SCNA for PDAC diagnosis.

Introduction

Pancreatic ductal adenocarcinoma (PDAC) is a disease with a dire prognosis and one of the few cancers with a rising incidence, leading to estimates of it becoming the second leading cause of cancer-related death in the United States within the next decade (1). A series of studies on large-scale molecular characterization of PDAC have elucidated the comprehensive genomic landscape of this neoplasm, including the so-called "long tail" of potentially actionable mutations (many at as low prevalence rates as ∼1%), which may form the basis for precision oncology and clinical trial inclusion (2–6). Most of these prior "discovery" studies have used archival surgically resected specimens with optimal tumor cellularity (e.g., >60% for The Cancer Genome Atlas cohort), limiting much of our current knowledge to localized, and therefore resectable tumors (3, 4). Nonetheless, the majority of patients with PDAC (∼80%–85%) are diagnosed with locally advanced or metastatic disease, precluding surgical options, which, in turn, restricts many patients from the opportunity for in-depth genomic analyses from resected specimens (1, 7).

All patients with PDAC, irrespective of disease stage, are required to have histologic or cytological confirmation of their underlying diagnosis prior to onset of therapy (7). The two most common avenues for obtaining diagnostic biospecimens in advanced disease include either endoscopic ultrasound–guided fine-needle aspiration (EUS-FNA) of the primary tumor, performed by a gastroenterologist, or a percutaneous core biopsy of a biopsy-amenable metastatic lesion, when possible, the latter performed by an interventional radiologist. Overall, with the gastroenterology clinic being the typical "portal of entry" for symptomatic individuals, an EUS-FNA represents one of the most common, if not the most common, sample type obtained in patients with PDAC at the time of *de novo* presentation. Although both sources of biopsies are comprised of minimal tissue material, the challenges of using EUS-FNA from PDAC for next-generation sequencing (NGS) studies are unique. In contrast to the generally high cellularity of metastatic samples obtained by core biopsy, EUS-FNA samples of desmoplastic primary PDAC tend to be hypocellular, and potentially contaminated with nonneoplastic gastric and duodenal mucosa, replete with mucosal inflammatory cells, which can "drown" cancer-associated alterations (8). Further, the limited neoplastic DNA yield from EUS-FNA samples often precludes the use of even the currently available targeted NGS panels, let alone more comprehensive whole-exome sequencing (WES). Consequently, most published studies have been limited to assessing a few common "hotspot" mutations in PDAC, such as *KRAS* or *BRAF* (9). At the same time, it is worth noting that the currently available targeted NGS panels are geared toward common actionable genes, and not included are the aforementioned low-frequency alterations (so-called "long tail").

[1]Department of Translational Molecular Pathology, The University of Texas MD Anderson Cancer Center, Houston, Texas. [2]Sheikh Ahmed Center for Pancreatic Cancer Research, The University of Texas MD Anderson Cancer Center, Houston, Texas. [3]Department of Surgical Oncology, The University of Texas MD Anderson Cancer Center, Houston, Texas. [4]Department of Gastroenterology, Hepatology, and Nutrition, The University of Texas MD Anderson Cancer Center, Houston, Texas. [5]Department of Epidemiology, The University of Texas MD Anderson Cancer Center, Houston, Texas.

Note: Supplementary data for this article are available at Clinical Cancer Research Online (http://clincancerres.aacrjournals.org/).

A. Semaan, V. Bernard, and J.J. Lee contributed equally to this article.

Corresponding Authors: Paola A. Guerrero, Department of Translational Molecular Pathology, The University of Texas MD Anderson Cancer Center, Houston, TX 77030. Phone: 713-745-3386; E-mail: paguerrero@mdanderson.org; and Yasminka A. Jakubek, Department of Epidemiology, The University of Texas MD Anderson Cancer Center, Houston, TX 77030. Phone: 832-703-8634; E-mail: yjakubek@mdanderson.org

Clin Cancer Res 2021;27:1082–93

doi: 10.1158/1078-0432.CCR-20-2667

Published OnlineFirst November 13, 2020; DOI: 10.1158/1078-0432.CCR-20-2667

Translational Relevance

Genomic characterization of pancreatic ductal adenocarcinoma is infeasible in most patients mainly due to limited tissue availability and quality. Using an enrichment protocol combined with molecular-barcoded whole-exome sequencing, we demonstrate feasibility, prognosis and predictive value of genomic characterization from limited fine-needle aspiration samples.

Third, the most commonly used first-line, and by some measures, most efficacious therapy in advanced PDAC is FOLFIRINOX, a platinum-containing multidrug regimen (10). Although preclinical data support that patients with PDAC with homologous recombination repair defects (HRD) are likely to bear greatest susceptibility to platinum agents like oxaliplatin (an integral component of FOLFIRINOX), the targeted NGS panels only interrogate a fraction of HRD, such as the approximately 5% of patients with deleterious *BRCA1/2* mutations. Yet, prior studies have suggested that the full compendium of HRD in PDAC, as reflected in the "unstable genome" phenotype comprised of multiple structural abnormalities, might be several fold higher in prevalence (3). As a result, most first-line therapy decisions in the advanced disease setting are made empirically, warranting strategies that can provide improved treatment prediction information from the PDAC genome.

In this study, we use real-world limited biospecimens obtained via EUS-FNA, almost all in the diagnostic "first encounter" that a patient with PDAC has with their gastroenterologist, for in-depth genomic analysis of PDAC. Applying a relatively facile enrichment strategy, we were able to significantly increase neoplastic cell fraction, which allowed us to detect actionable mutations using molecularly barcoded WES for clinical decision-making. Further, we demonstrate the ability to use the WES information paired with bioinformatics pipelines to determine potential HRD status in the cases, which can help guide the choice of first-line regimen in a clinically feasible timeline. Our data establish the feasibility for WES in the most commonly obtained diagnostic biospecimen in PDAC, EUS-FNA samples, with consistent results compared with previous studies.

Materials and Methods

Patient cohort

Investigators obtained written informed consent under MD Anderson protocol Lab00–396 from each patient prior to tissue and blood sampling. The study was performed in accordance with standard ethical guidelines approved by the Institutional Review Board and in accordance with the Declaration of Helsinki. All patients had clinically and histologically confirmed localized or metastatic PDAC. In the pilot phase, resected tissue specimens were only included if tumor cellularity was below 10% (Supplementary Fig. S1B). All biopsies (CT-guided core or EUS-FNA) were taken within routine clinical procedures. No EUS-FNB (fine-needle biopsy) samples have been included. All research passes harvested were sampled after routine diagnostic EUS-FNA passes and ROSE-rapid on-site cytology assessment which showed adequate cellularity in diagnostic specimens.

No complications have been reported in any tissue sampling.

Tissue digestion and EpCAM pulldown

Biopsy samples were mechanically and enzymatically digested into single-cell suspension as described before (11). The cell suspension was then processed using the EasySepTM Human EpCAM Positive Selection Kit (Stemcell, cat#18356) following the manufacturer's protocol to enrich for epithelial cell adhesion molecule (EpCAM)-positive epithelial cells. In brief, cell suspensions were incubated with EpCAM antibodies and magnetic beads, followed by subsequent clean-up steps using magnetic separation (Supplementary Fig. S1C).

DNA isolation, quality control, and digital droplet PCR analysis

Bulk genomic DNA was extracted from enriched and nonenriched cell suspensions using the QIamp DNA Micro Kit (Qiagen, cat#56304) and DNeasy Blood & Tissue Kit for peripheral blood mononuclear cells (PBMC; Qiagen, cat#69506) following the manufacturer's protocol. At least two different quantification methods for DNA quality and quantity were performed in parallel using a QubitTM dsDNA BR Assay Kit (Thermo Fisher, cat#Q32853), a NanoDropTM 2000/2000c spectrophotometers (Thermo Fisher, cat#ND2000), and/or high sensitivity D1000 screentape (HSD1000) with a Tapestation 2200 system (Agilent, cat#5067–5584). Digital droplet PCR (ddPCR) was performed for validation of KRAS mutations and MYC amplification as described in the Supplementary Materials.

Library construction and sequencing

A median of 160 ng of enriched tumor DNA or 200 ng of matched PBMC DNA was diluted in a total volume of 52 μL low TE buffer and fragmented to 150 to 200 bq using a Covaris LE 220 ultrasonicators system (Covaris). The following optimized settings were used: Duty Factor 30%, Peak Incident Power (PIP) W 450, cycles per burst 200, time 300 seconds, temperature 7°C, and water level 6. Adequate fragmentation was documented using HSD1000. Molecular-barcoded libraries were constructed following the SureSelect XT HT–targeted enrichment protocol (Version A1, July 2017). In brief, end repair and dA-tailing were followed by ligating individual molecular barcoding to each strand, PCR amplification, and bead-based cleaning. Libraries were then hybridized and incubated with a whole-exome capture library (SureSelect Clinical Research Exome V2; Agilent, cat#5190–9492), captured to streptavidin-coated beats, washed, and amplified. Libraries were multiplexed, denatured, and diluted to a final concentration of 1.8 pmol/L for sequencing and cluster generation as per the manufacturer's recommendation. Clustered flow cells were sequenced on the Illumina NextSeq 500 instrument (Illumina) using standard Illumina paired-end primers and chemistry. A median of 74,991,096 reads/PBMC (range, 25,067,034–251,278,724 reads) and 144,308,769 reads/enriched tumor (range, 25,451,842–236,573,016 reads) was detected. Median on-target coverage reached 56x (range, 23–157x) for matched PBMC and 108x (range, 14–177x) for enriched tumor samples for family size of 1 library.

Sequencing data analysis

Sequencing data were processed as detailed in the Supplementary Materials. Three algorithms were used for single-nucleotide variant (SNV) calling, and these were filtered as detailed in the Supplementary Materials. Of note, the median mutational burden of non–PBMC-paired samples ($n = 5$) was higher than in paired samples but did not reach statistical significance (4.89 mut/Mb; range, 0.72–23.91 vs. 1.63 mut/Mb; range, 0.29–21.46; $P = 0.06$) and seemed to had no impact on our ability to identify patients with increased tumor mutational burden (TMB; Supplementary Fig. S3C).

When available, Clinical Laboratory Improvement Amendments (CLIA) reports were used for SNV validation. These reports were generated from resected or core biopsied tissue samples during the

Published OnlineFirst November 13, 2020; DOI: 10.1158/1078-0432.CCR-20-2667

course of treatment. Reports were available for 1 core biopsy patient (pilot phase) and for 4 FNA patients (second phase). Four of the CLIA reports were generated in-house at MD Anderson Cancer Center (MDACC) with a PCR-based sequencing platform and assembled using GRCh37/hg19 builds. MDACC CLIA reports included a panel of 134 individual genes (Solid Tumor Genomic Assay V1 report). The fifth patient report was performed by an outside CLIA-certified laboratory using a company-specific gene panel (Perthera).

Dana-Farber Cancer Institute (DFCI) cohort data were processed using the same bioinformatics pipeline used in our study with the exception of unique molecular identifiers (UMI)-specific processing.

Actionable mutation

We evaluated each sample for presence of 24 potentially targetable genes/alterations and SCNAs: *BRCA1*, *BRCA2*, *PALP2*, *FGFR1*, *FGFR2*, *FGFR3*, *FGFR4*, *PDGFR*, *c-Kit/CD117*, *ROS1* (fusion), *MET*, *NOTCH1*, *JAK1*, *JAK2*, *JAK3*, *mTOR*, *BRAF*, *RNF43*, *PI3K/PIK3CA*, *AKT*, *NTRK*, *MYC*, *KRAS* wild-type, and *HER2* amplification.

Tumor mutational burden

TMB was defined by the sum of all synonymous SNV, nonsynonymous SNV, stopgain, stoploss, frameshifts, or indels per sample that passed filter criteria as described above. For PBMC-matched samples, germline mutations called by HaplotypeCaller were excluded but for mutations in important PDAC genes like, e.g., *BRCA1/2, PALB2*, or *ATM* (12). Non–PBMC-matched samples are indicated in the analysis workflow and throughout results. TMB was then calculated by dividing the total number of mutations/patient by the coding region target of the SureSelect Clinical Research Exome V2 panel used (67.3 Mb).

Mutational signatures

Mutational signature analysis of FNAs was performed using MutationalPatterns following the steps outlined for cancer/Catalog of Somatic Mutations in Cancer (COSMIC) signature analysis (13). Only FNA samples with a matched germline control (PBMC sample) and those from treatment-naïve tumors were included in the mutational analysis.

Detection of chromosomal alterations

Two algorithms were used for detection and classification of somatic copy-number alterations [SCNA; amplifications, deletions, and copy-neutral LOH (cnLOH)]. HapLOHseq was used for detection of genomic regions exhibiting allelic imbalance (AI). Results from this algorithm were combined with output from standard $\log_2$ copy ratio segmentation data as described in the Supplementary Materials.

This approach detects B-allele frequency (BAF) shifts at germline heterozygous sites, indicative of AI, allowing for detection of chromosomal alterations in low mutant cell fraction settings (14, 15). Germline heterozygous sites with a depth greater than or equal to 10 were included as input for AI analysis. The hidden Markov model of hapLOHseq was used to compute the probability that a set of adjacent markers span a region of AI. An AI event was defined as a continuous set of markers with posterior probabilities exceeding the threshold of 0.85.

Genome Analysis Toolkit (GATK; ref. 16) was used for segmentation of $\log_2$ copy ratio data. SCNAs were called by overlaying HapLOHseq AI and GATK segmentation calls (Supplementary Fig. S5A). For SCNA calls exclusive to GATK, only those with a $\log_2$ copy ratio below -1 and above 0.58 for deletion/amplifications were included in the final call set. This approach allows for the inclusion of balanced amplifications/losses, which do not result in AI, as well as focal SCNAs spanning a modest number of germline heterozygous sites. Genomic regions with posterior probability of AI > 0.85 were included in the final SCNA call set and were classified using GATK segmentation values, and $\log_2$ copy ratios below -0.41 and above 0.32 were called as deleted and amplified, respectively. cnLOH was defined as genomic regions with a $\log_2$ copy ratio between ± 0.15 and a BAF deviation >0.1. Events with a posterior probability of >0.85 and $\log_2$ copy ratio between ± 0.15 and -0.41 or $+0.32$ were defined as undetermined (Supplementary Fig. S4B). An aneuploidy score was calculated for each sample. It was defined as the number of chromosome arms (out of 39) with arm-level aneuploidy, following principles previously used in the analysis of genomic instability (17). A chromosome arm (except for the short arm of acrocentric chromosomes 13, 14, 15, 21, and 22) was categorized as aneuploid when an amplification, deletion, cnLOH, or undeterminable SCNA(s) spanned more than 75% of the chromosome arm. To accommodate for high-confidence AI events, with subtle $\log_2$ copy ratio deviations, an arm-level SCNA was also called in cases where one type of SCNA (amplification, deletion, or cnLOH) plus undeterminable SCNA(s) spanned more than 75% of the arm, but a single type of SCNA did not reach the 75% threshold.

For identification of SCNA patterns suggestive of DNA damage repair deficiencies, we calculated a new and easy to compute score. This complexity score (CS) was calculated by summing the number of chromosome arms with two SCNAs with opposing classification (i.e., gain and loss, or gain cnLOH). Undetermined events and those smaller than 1 Mb were excluded. This chromosome arm–level signature is inferred to have arisen from double-strand breaks, thus higher scores are present in patients with deficiencies in DNA repair.

Statistical analysis

Progression-free survival (PFS) was defined as time period from the start of any treatment (chemotherapy, radiotherapy, or surgery) to date of disease progression (defined by RECIST 1.1 guidelines; ref. 18) or death. Overall survival (OS) was defined as time from tissue sampling (surgery, core biopsy, or EUS-FNA) to death for any reason. Survival curves were estimated using the Kaplan–Meier method. Statistical analyses were performed with SPSS statistical software, version 24 (IBM) or Prism 8 (GraphPad Software, Inc.). All tests were two-sided. Statistical significance was defined as a P value of <0.05. We used bootstrapping to estimate the sampling distribution of the CS score in the DFCI cohort.

Results

Patient cohort and workflow

To analyze the feasibility and impact of epithelial cell enrichment, we utilized samples from either surgically resected primary PDAC ($N = 5$) or CT-guided metastatic core biopsies ($N = 4$, 3 patients) in a pilot "first phase" of this study. The 9 pilot phase samples were obtained from 8 independent patients. Subsequently, for the main ("second phase") study, we assessed 23 cytology samples from 23 patients with PDAC undergoing endoscopic FNAs between April 2017 and November 2018 at MDACC. Patient details and processing workflow for both phases are summarized in Supplementary Table S1 and Supplementary Fig. S1A. Matched blood samples were obtained in 24 of 31 patients (77.4%).

Pilot phase: significance and feasibility of EpCAM enrichment

A major obstacle for genomic characterization of small biopsies, especially using WES, is the limited amount of starting material and the

Published OnlineFirst November 13, 2020; DOI: 10.1158/1078-0432.CCR-20-2667

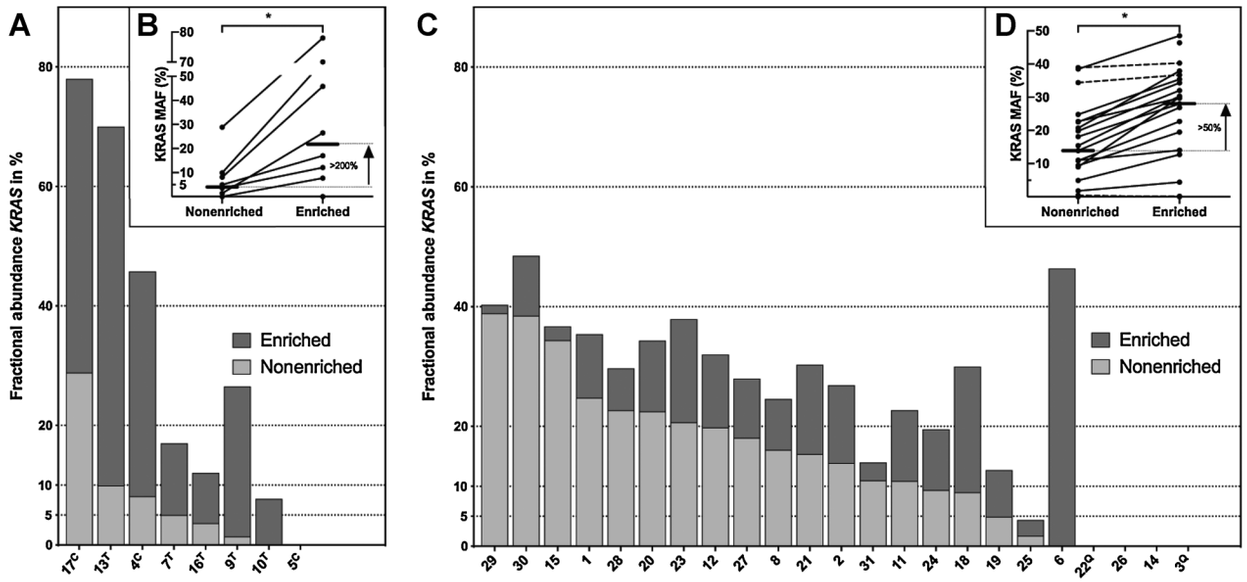

Figure 1.

Detection of mutant *KRAS* in FNAs and core biopsies. **A** and **C,** Fractional abundance of mutant *KRAS* in enriched (dark gray) and nonenriched (light gray) samples measured by ddPCR. Samples of the pilot phase derived from resected tumor specimens ($n = 5$, marked with T) or core biopsies ($n = 3$, marked with **C** are shown in **A** and **B**); one sequential core biopsy was not processed with ddPCR. Samples derived from FNAs in the second study phase ($n = 23$) are summarized in **C** and **D**. **B** and **D,** Lines indicate changes in *KRAS* MAF between nonenriched and enriched samples with a median increase of 95%. Straight lines indicate a percentage increase of >10%, and connected lines show a difference <10%. Samples marked with Q represent *KRAS* mutations in Q61.

generally low tumor cellularity of pancreatic cancer. To overcome this known hurdle, we used a magnetic EpCAM-pulldown approach to enrich for epithelial tumor cells. In the pilot phase, we used five fresh resected tissues samples with a low cellularity (<10%) and four CT- or ultrasound-guided core biopsies (liver and lung metastases, $N = 2$ each; Supplementary Fig. S1A and S1B). All samples were mechanically and enzymatically dissociated into a single-cell suspension before further processing. EpCAM enrichment was performed using an EpCAM-based magnetic pulldown followed by DNA isolation (Supplementary Fig. S1C). ddPCR showed a significant increase in *KRAS* mutant allele frequency (MAF; median, 4.3% vs. 21.7%; $P = 0.049$; **Fig. 1A** and **B**). In 4 patients with a nonenriched *KRAS* MAF falling below the cutoff for inclusion in CLIA reports (<5%), enrichment increased the MAF above this threshold (**Fig. 1A** and **B**). In addition, we compared performance for WES SNV and SCNA calls between EpCAM-enriched samples from resected PDAC and matched archived formalin-fixed paraffin-embedded (FFPE) slides of the matched tumor at resection ($n = 2$). Although this comparison showed only a few alterations in FFPE tissues, a greater number of genomic alterations were observed in the enriched samples, underscoring the value of EpCAM enrichment (Supplementary Table S2; Supplementary Fig. S2A and S2B). For example, in patient 13, sequencing of the FFPE block did not identify any mutations in PDAC driver genes, whereas they were detected in the EpCAM-enriched sample (*KRAS, SMAD4*, and *RNF43*; Supplementary Table S2). In addition, no major AI events were found in the matched FFPE-derived samples compared with the enriched counterpart in both patients (Supplementary Fig. S2A and S2B).

All but one sample (1/9) of this pilot phase (patient 16, resected tumor) passed sequencing quality control (QC), which was therefore excluded from further analysis, with the exception of ddPCR profiling. The genomic landscape of mutations in known PDAC-associated genes in this pilot phase generally matches those previously reported (**Fig. 2**; refs. 3, 4, 19, 20).

Second phase: EUS-FNA biopsies resemble commonly reported PDAC genomic landscapes from high-quality tissue sources

In the second phase of this study, we applied our EpCAM-enrichment strategy to 23 independent real-world EUS-FNA samples collected during routine diagnostic procedures (18/23 with paired PBMC, median of one FNA pass, range 1–2). Comparable with the results of the pilot phase, EpCAM enrichment followed by ddPCR showed a significant increase in *KRAS* MAF (median, 13.9% vs. 28.0%; $P = 0.03$; **Fig. 1C** and **D**). These results were also seen by sequencing as we split up one pooled FNA with two research passes (patient 18) to conduct WES on matched enriched and nonenriched DNA. The median MAF of all overlapping mutations and SCNAs, in the enriched versus the nonenriched samples, increased significantly ($P < 0.001$, Supplementary Table S2; Supplementary Fig. S2C). Only three cases showed either no demonstrable *KRAS* or an MAF below 5% after EpCAM enrichment (range *KRAS* MAF, 0%–4.39%). Nondiagnostic EUS-FNA passes cannot be excluded in these cases as our single research passes were acquired after routine clinical passes and may therefore harbor lower levels of cancer cells (21).

All 23 enriched FNA samples had enough DNA to proceed with library preparation and passed sequencing QC. The genomic landscape of mutations in known PDAC-associated genes generally matched those from previous reports (3, 4, 10, 15). In our cohort, significantly recurrent mutations (>10%) were identified in *KRAS, TP53, CDKN2A, SMAD4, GNAS, RNF43*, and *ARID1A* (**Fig. 2**). Prevalence of *KRAS* mutations using sequencing alone was 82.6% (19/23 patients), whereas combination of both sequencing and ddPCR increased the *KRAS* mutation detection rate to 91.3% (21/23 patients). In order to confirm our methods for calling SNVs and CNVs in

Published OnlineFirst November 13, 2020; DOI: 10.1158/1078-0432.CCR-20-2667

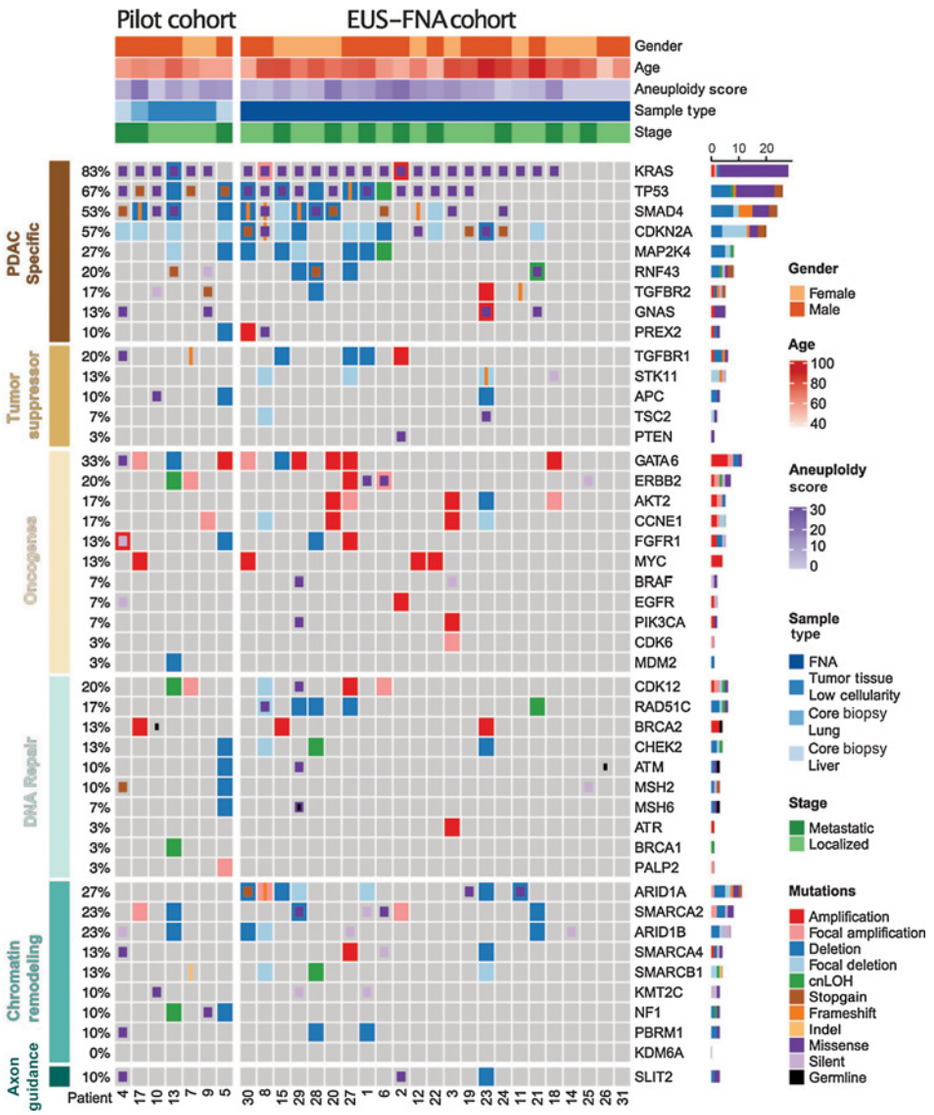

Figure 2.

Genomic alterations identified during the pilot and subsequent study. Heatmap of genomic data for 30 patients (columns) for pilot phase including resected specimens and core biopsies (left side) and for EUS-FNA–derived samples (right side). Heatmap includes SNV (classified as missense, silent, indel, frameshift, stopgain, stoploss, and germline) as well as SCNA (classified as amplifications, deletions, and cnLOH) in selected PDAC driver genes organized by their functional classes. Germline mutations are only shown if identified in a CLIA-certified clinical test (Supplementary Table S3) in addition to our calling algorithm. Patients' clinicopathologic data are shown as tracks at the top. The percentage of PDAC samples with an alteration of any type is noted at the left and the proportions of alterations per genes at the right.

patients that underwent a subsequent resection or core biopsy, we used pregenerated targeted sequencing CLIA laboratory reports as the gold standard for validation. All but one SNV (patient 6: *TP53*) showed a concordance (92.3%) between the CLIA report and our sequencing results (Supplementary Table S3). In addition, comparison of sequencing with ddPCR results for *KRAS* MAF and *GNAS* p.R201C showed significant correlation ($R^2 = 0.93$; $P < 0.0001$; Supplementary Fig. S3A and S3B; Supplementary Table S4).

Although not present in a majority of patients with PDAC, low-frequency, potentially actionable alterations were found in individual cases. Based on knowledge of recently published actionable mutations (2) and by including only highly deleterious SNVs from the COSMIC database and amplifications with more than 3 copies, a total of 5 of 23 EUS-FNA patients (21.7%) showed potentially actionable alterations such as *MYC* amplifications = 1 (SCNA with a level of 5.5), *MTOR* = 1 (nonsense mutation, p.A835S), *BRAF* = 1 (nonsense mutation, p.R509L), *MSH6* = 1 (nonsense mutation, p.P1087R), and *POLE* = 1 (frameshift insertion, p.F699Vfs*11; **Fig. 3A**). These results match prevalent actionable mutations previously reported in 17% to 48% of PDAC cases (19, 20, 22). Potential treatment options for these mutations include GSK525762 for *MYC*-dependent carcinomas; everolimus, VS5584, or LY3023414 for MTOR-mutant tumors; or vemurafenib for *BRAF*-mutant PDACs and agents targeting tumors with mismatch repair defects caused by *MSH6* and *POLE* such as pembrolizumab and nivolumab which have shown response rates of over 30% in patients with noncolorectal cancer (2, 23). Nonetheless, it should be emphasized that estimates for the proportion of actionable mutations in PDAC vary widely depending on the inclusion criterion.

Taken together, we were able to show that EpCAM enrichment of epithelial tumor cells significantly increases MAF and facilitates genomic profiling in PDAC, especially in challenging sample types like EUS-FNA and samples with low overall tumor cellularity.

TMB is correlated with mutations in DNA repair genes

PDAC is known for a relatively modest mutational burden, compared with melanoma or lung cancer (1–4). Matching previous reports, our median mutational burden for (non-) synonymous SNVs (18/23 PBMC paired samples) was 1.63 mutations/Mb (range,

Published OnlineFirst November 13, 2020; DOI: 10.1158/1078-0432.CCR-20-2667

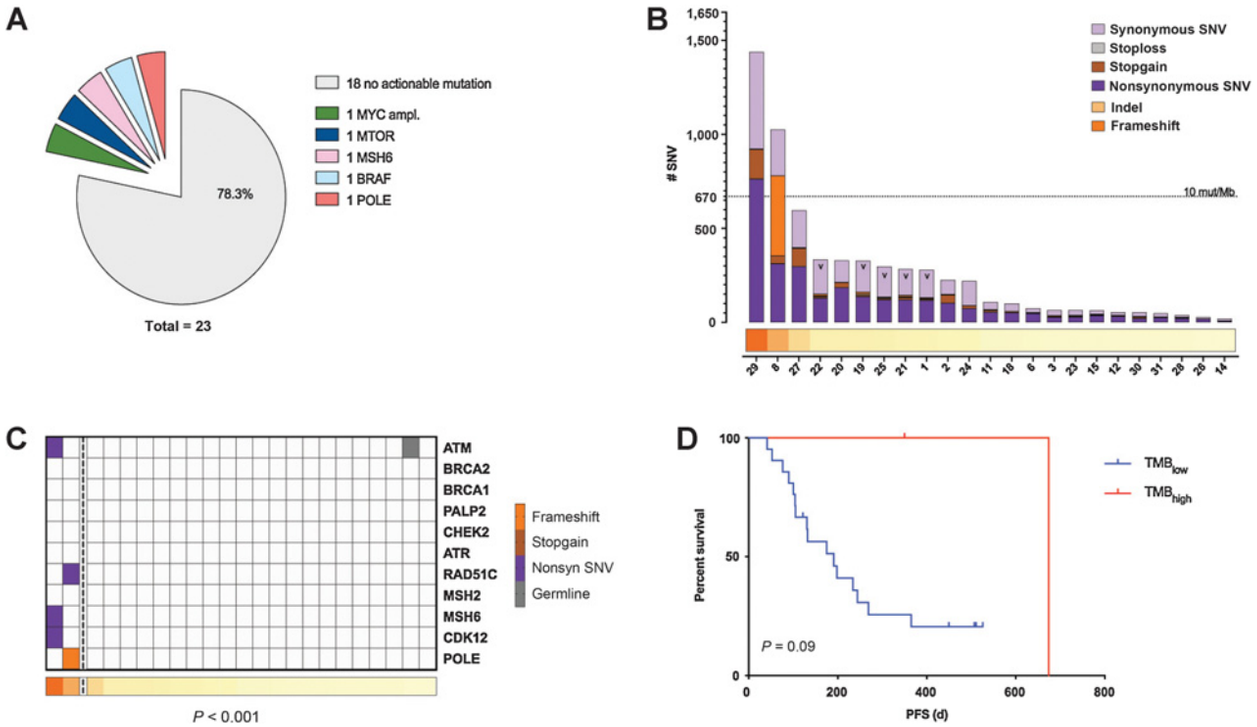

Figure 3.

Clinicopathologic significance of mutational burden (only EUS-FNA cohort, $n = 23$). **A,** Potential actionable alterations based on literature findings (2). Alterations included are deleterious SNVs found in the COSMIC database and gene amplifications with copy number of 3 or greater. **B,** Sum of all somatic mutations (missense, silent, frameshift, indel, stopgain, and stoploss) per patient (column) arranged in decreasing order. TMB_{high} cases are defined as > 670 mutations/patient (>10 SNVs/Mb). Samples without paired PBMC for germline correction are marked with v, and all other samples are FNAs with paired PBMC. **C,** TMB shown as tracks at the bottom with TMB_{high} cases left of vertical dotted line and mutations in DDR genes highlighted ($P < 0.0001$). **D,** Kaplan–Meier curves showing PFS comparing TMB_{high} vs. TMB_{low} ($P = 0.09$).

0.29 mut/Mb–21.46 mut/Mb; ref. 24). TMB was not affected by the presence of matching germline samples, stage, or tissue origin (Supplementary Fig. S3C–S3E).

Two of 23 individuals in our EUS-FNA cohort (8.7%) showed an increased mutational burden (TMB_{high}), defined as carrying more than 10 mutations/Mb by recent Pan-cancer analysis (**Fig. 3B**; ref. 25). Both TMB_{high} patients harbored SNVs in DNA-damage response (DDR) genes or mismatch repair defect genes, whereas the majority of TMB_{low} displayed no mutations in these genes ($P < 0.001$; **Fig. 3C**), which is in line with previously reported results (26). Patient 29 harbored a *MSH6* germline mutation (Lynch syndrome) that has been confirmed by clinical CLIA germline testing as a variant of unknown significance and an additional nonsynonymous mutation (Supplementary Table S3). This patient had an extensive family history of multiple cancers including a mother with breast cancer, a sister with PDAC, a parental cousin with an aggressive melanoma, and two parental cousins with brain tumors. Patient 8 had a COSMIC-annotated frameshift insertion in *POLE* (COSM2001733, p.F699Vfs*11, no

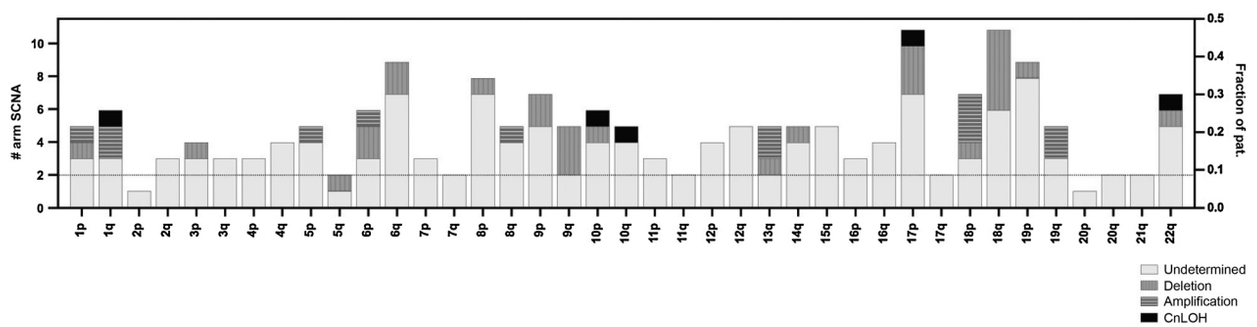

Figure 4.

SCNA(s) across all patients. Arm-level SCNA(s) with classification information (deletion, amplification, cnLOH, or undetermined) per chromosomal arm (left *y* axis) and fraction of patients with events (right *y* axis).

Published OnlineFirst November 13, 2020; DOI: 10.1158/1078-0432.CCR-20-2667

clinical CLIA testing performed) and also reported a family history for cancer (gastrointestinal cancer: mother and grandfather). In our limited EUS cohort, TMB_{high} patients demonstrated a trend toward improved PFS (median PFS, 674 days vs. 191 days; $P = 0.09$; **Fig. 3D**) but not OS (417 days vs. undefined; $P = 0.19$) compared with non-TMB_{high} (Supplementary Fig. S4A).

Prognostic impact of chromosomal alterations in WES

To ensure a rigorous standard for annotating SCNA, we used two independent algorithms: HapLOHseq (14), a powerful tool to analyze the presence of AI in low purity samples, and the GATK standard segmentation pipeline (Supplementary Fig. S4B). The results from these tools were merged to obtain a high-confidence SNCA call set, which was validated by a significant correlation of the *MYC* amplification estimates between sequencing and ddPCR results ($n = 7$, $R^2 = 0.91$; $P < 0.0001$; Supplementary Fig. S5A–S5C).

Consistent with previous studies, deleterious SCNAs were mainly detected in known tumor-suppressor genes such as *CDKN2A* (9/23, 39.1%), *SMAD4* (7/23, 30.4%), *TP53* (7/23, 21.7%), and *ARID1A* (6/23, 26.1%; all $P < 0.05$; refs. 3, 4, 19, 20). Interestingly, *CDKN2A* showed a large number of focal SCNA events (5/9, 55.5%), whereas most other loci showed a mixture of both focal and larger events. Not unexpectedly, amplifications were most commonly centered on established oncogenes such as *GATA6* (5/23, 21.7%) or *MYC* (3/23, 13.0%; **Figs. 2** and **4**; Supplementary Fig. S6A). Mirroring results from previous PDAC publications, at least one arm-level SCNA occurred in 78.3% of patients. The majority of patients harbored multiple SCNAs, most frequently spanning chromosome arms 6q (9/23, 39.1%), 8p (8/23, 34.8%), 9p (7/23, 30.4%), 17p (11/23, 47.8%), 18p (7/23, 30.4%), 18q (11/23, 47.8%), and 19p (9/23, 39.1%; refs. 4, 17; **Fig. 4**; Supplementary Fig. S6).

Genomic instability from SCNA data across cancer types can be estimated using a number of different approaches. For PDAC, structural rearrangements contributing to an "unstable genome" (>200 rearrangements) have been used as a measure of genomic instability (3, 27). We were unable to derive this previously described "unstable genome" phenotype from the exome capture platform (SureSelect, Agilent), as it only covers 71 possible breakpoints. Therefore, other previously proposed quantitative metrics, such as HRD-LST (large-scale state transitions), HRD-LOH, the total SCNA burden, as well as aneuploidy were analyzed (17, 28, 29), and all of these quantitative assessments were readily feasible on EUS-FNA WES data. All scores were significantly correlated with each other, which is why we used aneuploidy in the subsequent analyses (all $P < 0.015$, Supplementary Table S5). In our cohort, aneuploidy score was not affected by patient's gender, primary tumor location, tissue source, or age (Supplementary Fig. S7A–S7D). Somatic *TP53* mutation carriers showed a significantly higher aneuploidy score than patients without a *TP53* mutation (median, 0; range, 0–8 vs. 11; range, 3–22; $P = 0.0002$), as has been previously reported (Supplementary Fig. S7E; ref. 17). The magnitude of aneuploidy measured by the number of aneuploid chromosome arms on WES has previously been used as an indirect measure of genomic instability, the prognostic value of which is an area of active research (17). Correspondingly, studies in many solid tumors (30) showed a correlation of high aneuploidy with later-stage disease and poorer prognosis [e.g., colorectal cancer (31) and esophageal cancer (32)]. We therefore evaluated the prognostic potential of the aneuploidy score. Classification of patients based on the median aneuploidy level into a low-level aneuploidy ($aneuploidy_{low}$: bottom half = 0–7 arm-level events) and high-level aneuploidy ($aneuploidy_{high}$: top half ≥ 8 arm-level events) revealed a significant and deleterious impact on prognosis (**Fig. 5A–C**). $Aneuploidy_{high}$ tumors showed a median PFS of 104.5 days, whereas tumors with low-level aneuploidy experienced a significantly longer PFS of 365 days ($P = 0.009$; **Fig. 5B**). In addition, $aneuploidy_{high}$ showed a trend for worse OS (225 days vs. undefined; $P = 0.06$; **Fig. 5C**). Importantly, the aneuploidy score maintained its prognostic trends also in localized patients (**Fig. 5D** and **E**), which suggested that aneuploidy's prognostic value is not based on advanced tumor stage. Correspondingly, after restricting the analysis to nonsurgically treated patients ($n = 19$) in this group, prognostic impact of aneuploidy remained significant (OS, 286.6 ± 58.8 days vs. 466.9 ± 69.5 days; $P = 0.039$ and PFS, 130.0 ± 51.4 days vs. 317.0 ± 24.4 days; $P = 0.005$). A potential confounder for our analysis may be the inclusion of TMB_{high} samples as these samples demonstrated longer PFS and therefore results have to be interpreted with caution. To further validate the prognostic impact of the aneuploidy score, we used an independent cohort from the DFCI in Boston, MA (20). There are several details that need to be highlighted when comparing the two datasets. In the DFCI cohort: (i) most of the specimens (96%) were taken using core needles or intraoperative biopsies, primarily from metastatic lesions, whereas only 4% of cases were sampled by EUS-FNA with 9% coming from primary pancreatic lesions; (ii) no enrichment of the biopsies was performed and the authors report a median cellularity of 40% (range, 5%–80%); (iii) most of the cohort (91%) and all of the patients with a cellularity >20% were diagnosed with metastatic disease; (iv) no UMI-enhanced sequencing was used for WES.

To minimize bias in the aneuploidy score related to low cellularity samples in the DFCI cohort, we restricted the analysis to specimens with a tumor cellularity of >20% ($n = 52/73$). The median aneuploidy score of the DFCI cohort was 15 (range, 2–33), and only 8 of 52 patients showed an aneuploidy score below 8. This may be due to the advanced stage in the DFCI cohort and mirrors our findings that patients with metastasis show a trend for higher aneuploidy score compared with localized patients [median of 5.5 (range, 0–18) vs. 11 (range, 0–22); $P = 0.07$]. PFS for most patients in the DFCI cohort was unavailable; therefore, we used OS data. Using our cutoffs for $aneuploidy_{high}$ (≥8) and $aneuploidy_{low}$ (≤7), there was no prognostic value for patients with $aneuploidy_{high}$ (median OS in days: 625 ± 35.8 vs. 635 ± 74.8; $P = 0.60$). Because of the differences between the cohorts as detailed above, we then evaluated median aneuploidy score as a cohort-specific cutoff value and found a significantly worse OS survival for $aneuploidy_{high}$ (≥15) patients (313.2 ± 38.4 vs. 792.7 ± 160.8; $P = 0.0013$; Supplementary Fig. S7F).

Collectively, we speculate that increased aneuploidy in localized patients may be associated with more aggressive disease and earlier metastatic spread.

Prediction of platinum response using treatment-naïve EUS-FNA

Therapeutic decisions on first-line therapy in PDAC are currently mostly made on a clinical basis (e.g., performance status), without using biomarkers, unlike established markers for other cancer types, like colon cancer (33). There have been ongoing efforts using genomic or transcriptomic data to predict response to platinum-based therapy. In particular, cancers with *BRCA1/2* mutations or HRD show superior response to platinum-based therapies in multiple cancers, including PDAC (22, 34–36). We therefore evaluated the potential of WES data within our unique EUS-FNA set to predict response to platinum regimens.

Eight patients (4 localized and 4 metastatic) whose EUS-FNA samples were sequenced were treated with platinum-based therapies.

Published OnlineFirst November 13, 2020; DOI: 10.1158/1078-0432.CCR-20-2667

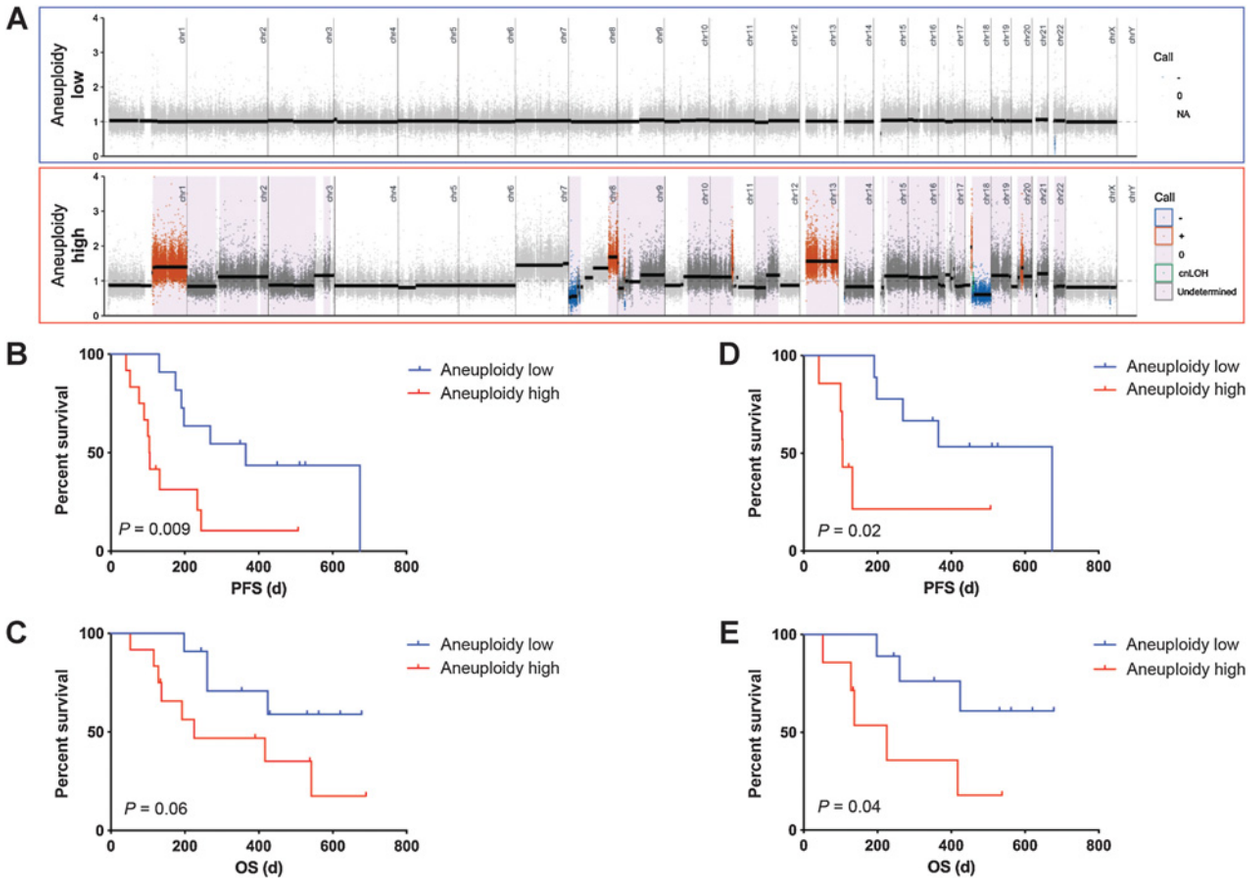

Figure 5.

Prognostic significance of aneuploidy in patient samples. **A,** Exemplary segmentation plots intersected with HapLOHseq calls (lavender background) showing samples classifying into aneuploidy$_{low}$ (≤7 chromosomal arm events) and aneuploidy$_{high}$ (≥8). **B,** Kaplan–Meier curves comparing PFS of patients with low vs. high aneuploidy levels ($P = 0.009$). **C,** Kaplan–Meier curves comparing OS of patients with low vs. high aneuploidy levels ($P = 0.06$). **D,** Kaplan–Meier curves comparing PFS of patients with low vs. high aneuploidy levels for patients with localized tumors only ($P = 0.02$). **E,** Kaplan–Meier curves comparing OS of patients with low vs. high aneuploidy levels in localized patients only ($P = 0.04$). *For this and subsequent figures, HapLOHseq calls shown pass a threshold of posterior probability of AI > 0.85.

Three of these showed a response to FOLF(IRIN)OX—defined as stable disease or partial response based on RECIST 1.1 criteria—whereas 5 patients progressed. None of the patients harbored deleterious SNVs in the following genes: *BRCA1/2, PALB2, FANCM, XRCC4/6, CHEK2, BRIP1*, or *BARD1*, except for 2 patients with *ATM* variants (patients 26 and 29). There was significance between patients with higher TMB and platinum response (8.86 mut/Mb; range, 4.89–21.37 vs. 1.1 mut/Mb; range, 0.79–3.36; $P = 0.04$; **Fig. 6A**), which is in line with former reports (3). Previously proposed parameters including aneuploidy, HRD-LST, and HRD-LOH (17, 29) did not show a significant correlation (**Fig. 6B**; Supplementary Table S5) with platinum response, whereas signature 3 showed a marginal positive association with response ($P = 0.06$), a finding that is in line with previous results (37).

We therefore evaluated our SCNA data for new approaches to predict platinum response which might correlate with HRD or DDR deficiency. Based on the assumption that DDR deficiency and especially an impaired DNA double-strand break repair contribute to HRD, we analyzed the number of chromosomal arms with opposing SCNA segments (e.g., gain and deletion present in the same chromosome arm; **Fig. 6C**) and use the sum of arms exhibiting this pattern to calculate a complexity score (CS). Our assumption is that a higher CS is inversely correlated with DNA double-strand repair capabilities. The CS is novel with regards to the integration of copy-number (segmentation data) with AI calls derived using a haplotype-based approach. However, this approach is similar in concept to using large-scale state transitions as a signature for HRD, which identifies adjacent chromosome segments with different copy-number states (29). Patients with platinum therapy response showed a significantly higher CS than those with progressive disease (CS: 3, range 2–3 vs. 0, range 0–1; $P = 0.04$; **Fig. 6D**). In addition, a high CS showed a trend for better PFS (674 days vs. 175 days; $P = 0.11$; **Fig. 6E**), OS (417 days vs. undefined; $P = 0.14$; Supplementary Fig. S7G), and a positive TMB correlation with tumors harboring a mutation in DDR genes with highest CS ($R^2 = 0.37$; $P = 0.002$; **Fig. 6F**). In addition to the 8 patients treated with a platinum-based therapy, 8 patients of the FNA cohort received a gemcitabine-based regimen. Seven patients were excluded from this analysis due to trial treatment, upfront surgery, side effects, fragility, or patient's choice not to undergo any therapy. When examining CS for chemotherapy prediction, we observe a marginally significant

Published OnlineFirst November 13, 2020; DOI: 10.1158/1078-0432.CCR-20-2667

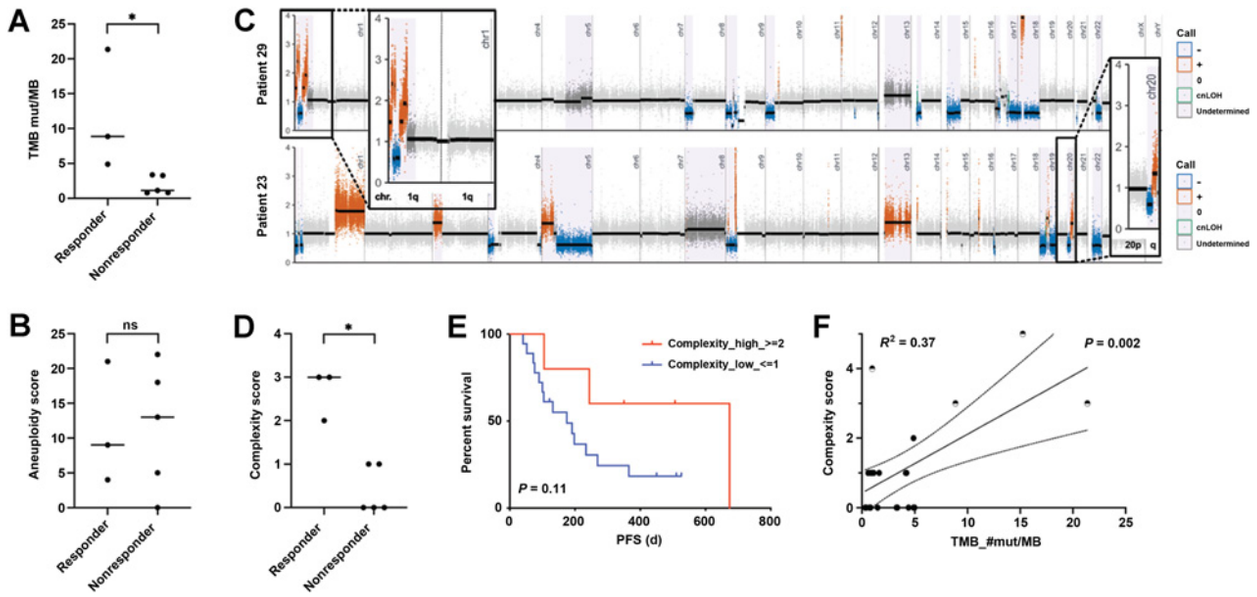

Figure 6.

Predictive value of SCNAs in platinum-based therapy response. **A,** Scattered box plot showing the TMB level of responders vs. nonresponders to platinum-based therapy ($P = 0.04$). **B,** Scattered box plot showing the aneuploidy level of responders vs. nonresponders to platinum-based therapy ($P = 0.73$). **C,** Exemplary segmentation plots of two patients intersected with HapLOHseq calls (lavender background) showing samples with areas highlighted and zoomed in showing chromosomal arms rated positive for CS calculation. **D,** Scattered box plot showing the CS of responders vs. nonresponders to platinum-based therapy ($P = 0.04$). **E,** Kaplan–Meier curves comparing PFS of patients with low vs. high CS ($P = 0.11$). **F,** Linear regression plotting CS vs. TMB ($R^2 = 0.37$, $P = 0.002$), half-filled dots mark samples with alterations in known DDR genes.

association between the CS score and response: median 1.5, range 0–3 for responders and median 1, range 0–1 for nonresponders ($P = 0.07$; Supplementary Fig. S7H). We also attempted to test the predictive value in the DFCI cohort (see above). There were three responders in the dataset (with 1 having an estimated tumor purity of only 4%); this severely restricted power to test for an association between the CS score and response to platinum therapy. However, we do note that patients with *BRCA1/2* mutations (4 germline and 1 somatic) in the DFCI cohort have significantly higher CS scores than patients without these mutations ($P = 0.008$, mean = 3.6 CS for those with a mutation and mean = 0.7 CS for those without). In addition, we performed mutational signature analysis as described previously (13) on FNA samples from treatment-naïve tumors (Supplementary Fig. S8). Herein, signature 3, which is associated with double-strand repair deficiency, showed a positive association with the CS ($R^2 = 0.49$; $P = 0.07$).

Taken together, CS shows potential as a predictive biomarker to estimate platinum responsiveness based on an indirect DDR evaluation even from limited FNA samples.

Longitudinal follow-up of an immune checkpoint–treated patient gives insight into a possible mechanism of resistance

To demonstrate the clinical significance and feasibility of WES from limited clinical biopsies, we interrogated two consecutive endoscopic lung biopsies in a patient (patient 17) with recurrent metastatic PDAC to the lung (both biopsies were included in the pilot phase). The first biopsy [timepoint 1 (T1)] was taken prior to immunotherapy with a PD-L1 antibody (durvalumab) and a STAT3 inhibitor (AZD9150; ref. 38). The second endoscopic biopsy [timepoint 2 (T2)] was taken after progression on aforementioned therapy and prior to initiation of a hypoxia-activated prodrug regime with evofosfamide (39). Before immunotherapy initiation, this patient was diagnosed with a multifocal pulmonary recurrence 2 years after upfront distal pancreatectomy. The recurrent tumor was then treated with capecitabine and oxaliplatin but progressed within a year (**Fig. 7A**).

Comparative analysis of the biopsy taken before immunotherapy treatment (T1) and after progression (T2) revealed new-onset focal deletions of *STK11, TSC2*, and the *CD274* locus (*PD-L1*; **Fig. 7B**). These loci have been previously reported to have a great impact on immunotherapy resistance. *STK11* loss, for example, has been repeatedly linked to the development of immunotherapy resistance in *KRAS*-mutant lung cancer (40), and *PD-L1* loss is associated with adaptive immune resistance in Hodgkin lymphoma and other neoplastic diseases (41). In addition to these focal deletions, chromosome 3q, 10q, 17q, 6p, and 6q also developed new arm-wide SCNAs, indicating LOH at all MHC genes, as evident by high confidence AI calls. Excluding these focal changes, T1 and T2 had overall congruous AI profiles. T1 and T2 biopsies shared focal deletions in major PDAC tumor suppressors such as *SMAD4* and *CDKN2A*, as well as amplifications in *GATA6* and *MYC*. T1 and T2 SNVs in established drivers, *KRAS, SMAD4*, and *TP53*, were also shared (**Fig. 7C**). Only two of the nonoverlapping deleterious SNVs had a COSMIC annotation (CCDC42: p.R104W, COSM4443319 and RCBTB2: p.V347M, COSM6445879); upon inspection and literature review, these do not have a known mechanistic link that would explain the development of immunotherapy resistance. Overall, mutational burden remained roughly the same between T1 and T2 (2.1 mut/Mb vs. 1.6 mut/Mb). As illustrated by this example, paired longitudinal endoscopic biopsies obtained over the course of therapy in patients with PDAC might elucidate genomic alterations that could explain the development of resistance to immunotherapy (or targeted therapies).

Published OnlineFirst November 13, 2020; DOI: 10.1158/1078-0432.CCR-20-2667

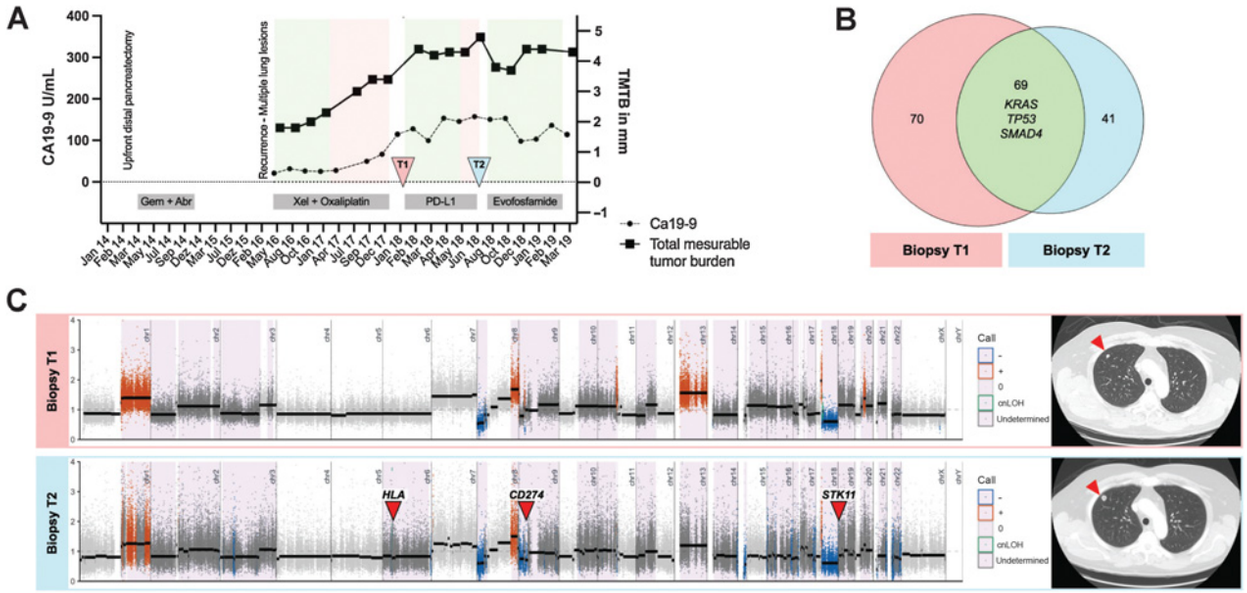

Figure 7.

Longitudinal follow-up of patient 17. **A,** Time course of disease plotting the total measurable tumor burden (TMTB; right *y* axis) and Ca19–9 (left *y* axis) with therapy regime administered at bottom. Green areas mark time periods with stable disease or partial response defined by RECIST 1.1, whereas red areas show progression. Timepoints of tissue sampling (T1 and T2) are indicated by arrows. **B,** Venn diagram plotting overlapping and distinct (non-) synonymous SNVs at T1 ($n = 139$, left) and T2 ($n = 110$, right). **C,** Left: Segmentation plots of T1 and T2 with intersected HapLOHseq calls (lavender background). Red arrows indicate loci that might be associated with acquired resistance to immune therapy. Right: Exemplary CTC images showing an increase of pulmonary metastasis between T1 and T2 (red arrow).

Discussion

Over the past decade, precision oncology has improved clinical outcomes for many patients with solid cancers. Patients with melanoma and breast cancer are now routinely screened for their V600E proto-oncogene B-Raf (*BRAF*; ref. 42) and HER2 status, respectively (43). Targeting these aberrations has alleviated prognosis in both entities. Despite significant efforts, PDAC has proven less susceptible to targeted or immune therapies, mainly due its stroma-dense, immune "cold" tumors that additionally show a remarkable genomic heterogeneity (1–6).

Previous WES, whole-genome sequencing (WGS), and whole transcriptomic approaches in molecular profiling of PDAC have used tissue from multiple imaging-guided core biopsies for DNA and RNA profiling. The amount of tissue from these multiple cores is substantially greater than our "one-pass" EUS-FNA starting material (11, 13, 20, 22). It is also important to mention that multiple EUS-FNA passes are not necessarily associated with an increased amount of neoplastic cells harvest (44, 45) nor with an increased sensitivity of detection (21), and indeed, might increase the associated risk of complications (21, 46). Other sampling techniques such as EUS-FNB have shown promising results for in-depth genetic analysis, but their applicability and widespread use can be constrained by their significant expense (47, 48). In addition, a major advantage of EUS-FNA compared with EUS-FNB is that the former allows for ROSE-rapid on-site cytology assessment that ensures that there is adequate cellularity and a diagnostic specimen. Here, we report our efforts to characterize EpCAM-enriched real-world, limited EUS-FNA. Despite the fact that most patients with PDAC are diagnosed using EUS-FNA, these samples have so far been deemed not suitable for in-depth molecular analysis such as WES (49, 50). To increase the tumor to normal cell proportion, many studies have either enriched their specimens, e.g., laser microdissection (time- and labor-intensive), or excluded low tumor cellularity samples from analysis altogether (2–6, 20). In contrast, we used a simple and fast enrichment method to successfully isolate tumor cells resulting in an improved detection of deleterious mutations.

There is evidence that evaluation of aneuploidy as a marker for genomic instability may be a valid surrogate in metastatic PDAC (22, 51). Aneuploidy demonstrated prognostic significance independent of disease stage within the current study and an independent dataset of patients with pancreatic cancer. This finding is in line with results showing a worse prognosis and later disease stage correlated with increased aneuploidy (3, 24, 32). In this regard, tumors with high aneuploidy have shown increased tumor progression and chemotherapy resistance due to a higher intratumoral heterogeneity and ultimately an elevated capacity for adaptation (52). It is important to mention that aneuploidy seems to be context-dependent and therefore might differently affect distinct tumor types (32).

One of the important clinical questions in PDAC is the susceptibility to platinum-based therapies as one of two first-line regimens, which should ideally be discernible in WES data on limited samples material like EUS-FNA. In light of recent findings, up to 25% of patients with PDAC harbor a genomic footprint of HRD (3), and many of these potential responders might be missed using only "classic" DDR mutations for identification, like *BRCA1/2* or *PALB2* that are present in 5% to 7% of patients with PDAC (53). Other HRD-causing alterations like *BRCA1* promoter hypermethylation or biallelic loss of *PALB2* are even more challenging, if not impossible, to detect by most commonly used targeted sequencing panels (2). In a cohort of patients with breast cancer, over 30% of HRD-positive tumors had no underlying genetic alteration associated with HRD and yet demonstrated platinum susceptibility (35). Within this aforementioned study, HRD has been estimated by a WGS algorithm called

Published OnlineFirst November 13, 2020; DOI: 10.1158/1078-0432.CCR-20-2667

"HRDetect," but the algorithm performed suboptimally with WES data because essential predictor components such as rearrangement signatures and indels analysis are restricted (35, 36).

We identified a relatively facile WES-based scoring system of the "complexity" of SCNA events within a chromosomal arm that predicts platinum response in this cohort of patients with PDAC. This CS analyzes the presence of alternating SCNA events (gains, losses, and cnLOHs > 1M) within a single chromosomal arm boundary. This kind of event pattern can only occur upon a severe disruption of double-strand DNA repair and results in missegregation of "shattered" arm fragments in mitosis. It is relatively easy to calculate using WES data and standard GATK segmentation pipeline which makes it an attractive possible biomarker. We therefore hypothesize that CS may be a marker for increased genomic instability indicating susceptibility to platinum-based treatment. Interestingly, CS positively correlated with increased TMB that by itself also showed a predictive value but did not show a correlation with other SCNA markers, like aneuploidy.

We acknowledge important drawbacks in our study. One downside of our approach is that it requires a freshly acquired aspiration biopsy with dissociated cells as starting material, as we did not attempt WES on archival cytology samples. On the other hand, dissociation of cells from FNAs is a relatively simple procedure when compared with the dissociation of core biopsies which is time consuming. We were also not able to conduct a transcriptional analysis to validate loss or gain of function of genes because EUS-FNA provided sparse material to conduct additional assays. In addition, our WES library design refrained us from analyzing important RNA fusion patterns which are accessible primarily using WGS.

Although significant EpCAM expression is seen in epithelial-derived carcinoma cells when compared with normal epithelial, up to one third of pancreatic cancers may have low to no EpCAM expression (54, 55). This underlines a potential limitation of the EpCAM-enrichment approach of tumor cells and may warrant alternative strategies such as negative selection by targeting cells expressing CD45, CD31, and FAP to clean the sample of immune/blood cells, endothelial cells, and fibroblasts. Based on the minimal amount of cellular material acquired from a single EUS-FNA pass, we were not able to process each pass with multiple selection methods to compare intrapatient accuracy and performance. In addition, with advances and improvements in sampling strategies (like EUS-FNB), enrichment in the context of adequate tissue acquisition may become redundant. Finally, due to the small number of overall patients, the non-CLIA setting of our assay, and the inherent cohort heterogeneity, our conclusions need to be validated in a larger prospective EUS-FNA cohort.

In conclusion, in this proof-of-concept study, we show the importance and ease of EpCAM enrichment for genomic analysis of real-world limited aspiration (EUS-FNA) samples. Using enriched EUS-FNA samples, we were able to perform an in-depth whole high-quality molecular-barcoded WES analysis, reproducing genomic patterns consistent with previous results. We show the prognostic potential of SCNA (namely aneuploidy) for PDAC diagnosis and also identify a novel predictive biomarker (CS) for platinum responsiveness in our cohort. CS may be a relatively facile biomarker for predicting platinum responsiveness in newly diagnosed PDAC not harboring overt mutations in canonical DDR genes.

Authors' Disclosures

A. Semaan reports grants from DFG during the conduct of the study. A. Maitra reports other from Cosmos Wisdom Biotech, Thrive Earlier Detection, and JNJ outside the submitted work. Y.A. Jakubek reports other from Invitae outside the submitted work. No disclosures were reported by the other authors.

Authors' Contributions

A. Semaan: Conceptualization, data curation, investigation, writing-original draft. **V. Bernard:** Conceptualization, methodology. **J.J. Lee:** Conceptualization. **J.W. Wong:** Data curation, formal analysis, methodology. **J. Huang:** Data curation, formal analysis. **D.B. Swartzlander:** Data curation, investigation. **B.M. Stephens:** Data curation. **M.E. Monberg:** Data curation. **B.R. Weston:** Resources. **M.S. Bhutani:** Resources. **K. Chang:** Data curation, formal analysis. **P.A. Scheet:** Supervision, funding acquisition. **A. Maitra:** Supervision, funding acquisition, project administration. **Y.A. Jakubek:** Data curation. **P.A. Guerrero:** Supervision.

Acknowledgments

We thank A.J. Aguirre, B.M. Wolpin, and the Hale Family Research Center at Dana-Farber Cancer Institute for providing an independent dataset used for replication of our results. Most of all we thank the patients and their families. A. Maitra is supported by the MD Anderson Pancreatic Cancer Moon Shot Program, the Khalifa Bin Zayed Al-Nahyan Foundation, and the NIH (U01CA196403, U01CA200468, and P50CA221707). A. Semaan is supported by the German Research Foundation (SE-2616/2–1). V. Bernard is supported by the NIH (U54CA096300, U54CA096297, and T32CA217789). J.J. Lee is supported by the NIH (T32CA009599).

The costs of publication of this article were defrayed in part by the payment of page charges. This article must therefore be hereby marked *advertisement* in accordance with 18 U.S.C. Section 1734 solely to indicate this fact.

Received July 9, 2020; revised September 25, 2020; accepted November 9, 2020; published first November 13, 2020.

References

1. Kleeff J, Korc M, Apte M, La Vecchia C, Johnson CD, Biankin AV, et al. Pancreatic cancer. Nat Rev Dis Primers 2016;2:16022.
2. Collisson EA, Bailey P, Chang DK, Biankin AV. Molecular subtypes of pancreatic cancer. Nat Rev Gastroenterol Hepatol 2019;16:207–20.
3. Waddell N, Pajic M, Patch A-M, Chang DK, Kassahn KS, Bailey P, et al. Whole genomes redefine the mutational landscape of pancreatic cancer. Nature 2015; 518:495–501.
4. Cancer Genome Atlas Research Network. Integrated genomic characterization of pancreatic ductal adenocarcinoma. Cancer Cell 2017;32:185–203.
5. Moffitt RA, Marayati R, Flate EL, Volmar KE, Loeza SGH, Hoadley KA, et al. Virtual microdissection identifies distinct tumor- and stroma-specific subtypes of pancreatic ductal adenocarcinoma. Nat Genet 2015;47:1168–78.
6. Bailey P, Chang DK, Nones K, Johns AL, Patch A-M, Gingras M-C, et al. Genomic analyses identify molecular subtypes of pancreatic cancer. Nature 2016;531:47–52.
7. Tempero MA. NCCN guidelines updates: pancreatic cancer. J Natl Compr Canc Netw 2019;17:603–5.
8. Roy-Chowdhuri S, Chen H, Singh RR, Krishnamurthy S, Patel KP, Routbort MJ, et al. Concurrent fine needle aspirations and core needle biopsies: a comparative study of substrates for next-generation sequencing in solid organ malignancies. Mod Pathol 2017;30:499–508.
9. Gleeson FC, Kerr SE, Kipp BR, Voss JS, Minot DM, Tu ZJ, et al. Targeted next generation sequencing of endoscopic ultrasound acquired cytology from ampullary and pancreatic adenocarcinoma has the potential to aid patient stratification for optimal therapy selection. Oncotarget 2016;7:54526–36.
10. Conroy T, Desseigne F, Ychou M, Bouché O, Guimbaud R, Bécouarn Y, et al. FOLFIRINOX versus gemcitabine for metastatic pancreatic cancer. N Engl J Med 2011;364:1817–25.
11. Bernard V, Semaan A, Huang J, San Lucas FA, Mulu FC, Stephens BM, et al. Single-cell transcriptomics of pancreatic cancer precursors demonstrates epithelial and microenvironmental heterogeneity as an early event in neoplastic progression. Clin Cancer Res 2019;25:2194–205.
12. McKenna A, Hanna M, Banks E, Sivachenko A, Cibulskis K, Kernytsky A, et al. The genome analysis toolkit: a MapReduce framework for

Published OnlineFirst November 13, 2020; DOI: 10.1158/1078-0432.CCR-20-2667

analyzing next-generation DNA sequencing data. Genome Res 2010;20:1297–303.
13. Blokzijl F, Janssen R, van Boxtel R, Cuppen E. MutationalPatterns: comprehensive genome-wide analysis of mutational processes. Genome Med 2018;10:33.
14. San Lucas FA, Sivakumar S, Vattathil S, Fowler J, Vilar E, Scheet P. Rapid and powerful detection of subtle allelic imbalance from exome sequencing data with hapLOHseq. Bioinformatics 2016;32:3015–7.
15. Jakubek Y, Lang W, Vattathil S, Garcia M, Xu L, Huang L, et al. Genomic landscape established by allelic imbalance in the cancerization field of a normal appearing airway. Cancer Res 2016;76:3676–83.
16. Van der Auwera GA, Carneiro MO, Hartl C, Poplin R, Del Angel G, Levy-Moonshine A, et al. From FastQ data to high confidence variant calls: the genome analysis toolkit best practices pipeline. Curr Protoc Bioinformatics 2013;43:11.10.1–11.10.33.
17. Taylor AM, Shih J, Ha G, Gao GF, Zhang X, Berger AC, et al. Genomic and functional approaches to understanding cancer aneuploidy. Cancer Cell 2018;33:676–89.
18. Eisenhauer EA, Therasse P, Bogaerts J, Schwartz LH, Sargent D, Ford R, et al. New response evaluation criteria in solid tumours: revised RECIST guideline (version 1.1). Eur J Cancer 2009;45:228–47.
19. Singhi AD, George B, Greenbowe JR, Chung J, Suh J, Maitra A, et al. Real-time targeted genome profile analysis of pancreatic ductal adenocarcinomas identifies genetic alterations that might be targeted with existing drugs or used as biomarkers. Gastroenterology 2019;156:2242–53.
20. Aguirre AJ, Nowak JA, Camarda ND, Moffitt RA, Ghazani AA, Hazar-Rethinam M, et al. Real-time genomic characterization of advanced pancreatic cancer to enable precision medicine. Cancer Discov 2018;8:1096–111.
21. Mohamadnejad M, Mullady D, Early DS, Collins B, Marshall C, Sams S, et al. Increasing number of passes beyond 4 does not increase sensitivity of detection of pancreatic malignancy by endoscopic ultrasound–guided fine-needle aspiration. Clin Gastroenterol Hepatol 2017;15:1071–8.
22. Aung KL, Fischer SE, Denroche RE, Jang G-H, Dodd A, Creighton S, et al. Genomics-driven precision medicine for advanced pancreatic cancer: early results from the COMPASS trial. Clin Cancer Res 2018;24:1344–54.
23. Marabelle A, Le DT, Ascierto PA, Di Giacomo AM, De Jesus-Acosta A, Delord J-P, et al. Efficacy of pembrolizumab in patients with noncolorectal high microsatellite instability/mismatch repair-deficient cancer: results from the phase II KEYNOTE-158 study. J Clin Oncol 2020;38:1–10.
24. Witkiewicz AK, McMillan EA, Balaji U, Baek G, Lin W-C, Mansour J, et al. Whole-exome sequencing of pancreatic cancer defines genetic diversity and therapeutic targets. Nat Commun 2015;6:6744.
25. Campbell BB, Light N, Fabrizio D, Zatzman M, Fuligni F, de Borja R, et al. Comprehensive analysis of hypermutation in human cancer. Cell 2017;171:1042–56.
26. Humphris JL, Patch A-M, Nones K, Bailey PJ, Johns AL, McKay S, et al. Hypermutation in pancreatic cancer. Gastroenterology 2017;152:68–74.
27. Campbell PJ, Yachida S, Mudie LJ, Stephens PJ, Pleasance ED, Stebbings LA, et al. The patterns and dynamics of genomic instability in metastatic pancreatic cancer. Nature 2010;467:1109–13.
28. Telli ML, Timms KM, Reid J, Hennessy B, Mills GB, Jensen KC, et al. Homologous recombination deficiency (HRD) score predicts response to platinum-containing neoadjuvant chemotherapy in patients with triple-negative breast cancer. Clin Cancer Res 2016;22:3764–73.
29. Popova T, Manié E, Rieunier G, Caux-Moncoutier V, Tirapo C, Dubois T, et al. Ploidy and large-scale genomic instability consistently identify basal-like breast carcinomas with BRCA1/2 inactivation. Cancer Res 2012;72:5454–62.
30. Hieronymus H, Murali R, Tin A, Yadav K, Abida W, Moller H, et al. Tumor copy number alteration burden is a pan-cancer prognostic factor associated with recurrence and death. Elife 2018;7:e37294.
31. Laubert T, Freitag-Wolf S, Linnebacher M, König A, Vollmar B, Habermann JK, et al. Stage-specific frequency and prognostic significance of aneuploidy in patients with sporadic colorectal cancer–a meta-analysis and current overview. Int J Colorectal Dis 2015;30:1015–28.
32. Ben-David U, Amon A. Context is everything: aneuploidy in cancer. Nat Rev Genet 2020;21:44–62.
33. Sveen A, Kopetz S, Lothe RA. Biomarker-guided therapy for colorectal cancer: strength in complexity. Nat Rev Clin Oncol 2020;17:11–32.
34. Goldstein JB, Zhao L, Wang X, Ghelman Y, Overman MJ, Javle MM, et al. Germline DNA sequencing reveals novel mutations predictive of overall survival in a cohort of patients with pancreatic cancer. Clin Cancer Res 2020;26:1385–94.
35. Staaf J, Glodzik D, Bosch A, Vallon-Christersson J, Reuterswärd C, Häkkinen J, et al. Whole-genome sequencing of triple-negative breast cancers in a population-based clinical study. Nat Med 2019;25:1526–33.
36. Davies H, Glodzik D, Morganella S, Yates LR, Staaf J, Zou X, et al. HRDetect is a predictor of BRCA1 and BRCA2 deficiency based on mutational signatures. Nat Med 2017;23:517–25.
37. Shahda S, Timms KM, Ibrahim AA, Reid JE, Cramer HM, Radovich M, et al. Homologous recombination deficiency in patients with pancreatic ductal adenocarcinoma and response to chemotherapy. JCO Precis Oncol 2018;2:1–11.
38. Shastri A, Choudhary G, Teixeira M, Gordon-Mitchell S, Ramachandra N, Bernard L, et al. Antisense STAT3 inhibitor decreases viability of myelodysplastic and leukemic stem cells. J Clin Invest 2018;128:5479–88.
39. Pourmorteza M, Rahman ZU, Young M. Evofosfamide, a new horizon in the treatment of pancreatic cancer. Anticancer Drugs 2016;27:723–5.
40. Skoulidis F, Goldberg ME, Greenawalt DM, Hellmann MD, Awad MM, Gainor JF, et al. STK11/LKB1 mutations and PD-1 inhibitor resistance in KRAS-mutant lung adenocarcinoma. Cancer Discov 2018;8:822–35.
41. Restifo NP, Smyth MJ, Snyder A. Acquired resistance to immunotherapy and future challenges. Nat Rev Cancer 2016;16:121–6.
42. Chapman PB, Hauschild A, Robert C, Haanen JB, Ascierto P, Larkin J, et al. Improved survival with vemurafenib in melanoma with BRAF V600E mutation. N Engl J Med 2011;364:2507–16.
43. Slamon DJ, Leyland-Jones B, Shak S, Fuchs H, Paton V, Bajamonde A, et al. Use of chemotherapy plus a monoclonal antibody against HER2 for metastatic breast cancer that overexpresses HER2. N Engl J Med 2001;344:783–92.
44. Cleveland P, Gill KRS, Coe SG, Woodward TA, Raimondo M, Jamil L, et al. An evaluation of risk factors for inadequate cytology in EUS-guided FNA of pancreatic tumors and lymph nodes. Gastrointest Endosc 2010;71:1194–9.
45. Savides TJ, Donohue M, Hunt G, Al-Haddad M, Aslanian H, Ben-Menachem T, et al. EUS-guided FNA diagnostic yield of malignancy in solid pancreatic masses: a benchmark for quality performance measurement. Gastrointest Endosc 2007;66:277–82.
46. Erickson RA, Sayage-Rabie L, Beissner RS. Factors predicting the number of EUS-guided fine-needle passes for diagnosis of pancreatic malignancies. Gastrointest Endosc 2000;51:184–90.
47. Dreyer SB, Jamieson NB, Evers L, Duthie F, Cooke S, Marshall J, et al. Feasibility and clinical utility of endoscopic ultrasound guided biopsy of pancreatic cancer for next-generation molecular profiling. Chin Clin Oncol 2019;8:16.
48. Vestrup Rift C, Melchior LC, Kovacevic B, Toxvaerd A, Klausen P, Karstensen JG, et al. Next-generation sequencing of endoscopic ultrasound guided microbiopsies from pancreatic cystic neoplasms. Histopathology 2019;75:767–71.
49. Chantrill LA, Nagrial AM, Watson C, Johns AL, Martyn-Smith M, Simpson S, et al. Precision medicine for advanced pancreas cancer: the individualized molecular pancreatic cancer therapy (IMPaCT) trial. Clin Cancer Res 2015;21:2029–37.
50. Varadarajulu S, Tamhane A, Eloubeidi MA. Yield of EUS-guided FNA of pancreatic masses in the presence or the absence of chronic pancreatitis. Gastrointest Endosc 2005;62:728–36.
51. Lohse I, Mason J, Cao PM, Pintilie M, Bray M, Hedley DW. Activity of the novel polo-like kinase 4 inhibitor CFI-400945 in pancreatic cancer patient-derived xenografts. Oncotarget 2017;8:3064–71.
52. Vitale I, Manic G, Senovilla L, Kroemer G, Galluzzi L. Karyotypic aberrations in oncogenesis and cancer therapy. Trends Cancer Res 2015;1:124–35.
53. Golan T, Kindler HL, Park JO, Reni M, Mercade TM, Hammel P, et al. Geographic and ethnic heterogeneity in the BRCA1/2 pre-screening population for the randomized phase III POLO study of olaparib maintenance in metastatic pancreatic cancer (mPC) [Internet]. J Clin Oncol 36:15s, 2018 (suppl; abstr 4115).
54. Trzpis M, McLaughlin PMJ, de Leij LMFH, Harmsen MC. Epithelial cell adhesion molecule: more than a carcinoma marker and adhesion molecule. Am J Pathol 2007;171:386–95.
55. Spizzo G, Fong D, Wurm M, Ensinger C, Obrist P, Hofer C, et al. EpCAM expression in primary tumour tissues and metastases: an immunohistochemical analysis. J Clin Pathol. 2011;64:415–20.

AACR American Association for Cancer Research

Clinical Cancer Research

Defining the Comprehensive Genomic Landscapes of Pancreatic Ductal Adenocarcinoma Using Real-World Endoscopic Aspiration Samples

Alexander Semaan, Vincent Bernard, Jaewon J. Lee, et al.

Clin Cancer Res 2021;27:1082-1093. Published OnlineFirst November 13, 2020.

Published OnlineFirst November 1, 2018; DOI: 10.1158/1078-0432.CCR-18-1955

Translational Cancer Mechanisms and Therapy

Clinical Cancer Research

Single-Cell Transcriptomics of Pancreatic Cancer Precursors Demonstrates Epithelial and Microenvironmental Heterogeneity as an Early Event in Neoplastic Progression

Vincent Bernard[1,2,3], Alexander Semaan[1,3], Jonathan Huang[1,3], F. Anthony San Lucas[4], Feven C. Mulu[1,3], Bret M. Stephens[1,3], Paola A. Guerrero[1,3], Yanqing Huang[5], Jun Zhao[1,3], Nabiollah Kamyabi[1,3], Subrata Sen[1], Paul A. Scheet[4], Cullen M. Taniguchi[5], Michael P. Kim[6], Ching-Wei Tzeng[6], Matthew H. Katz[6], Aatur D. Singhi[7], Anirban Maitra[1,3], and Hector A. Alvarez[8]

Abstract

Purpose: Early detection of pancreatic ductal adenocarcinoma (PDAC) remains elusive. Precursor lesions of PDAC, specifically intraductal papillary mucinous neoplasms (IPMNs), represent a *bona fide* pathway to invasive neoplasia, although the molecular correlates of progression remain to be fully elucidated. Single-cell transcriptomics provides a unique avenue for dissecting both the epithelial and microenvironmental heterogeneities that accompany multistep progression from noninvasive IPMNs to PDAC.

Experimental Design: Single-cell RNA sequencing was performed through droplet-based sequencing on 5,403 cells from 2 low-grade IPMNs (LGD-IPMNs), 2 high-grade IPMNs (HGD-IPMN), and 2 PDACs (all surgically resected).

Results: Analysis of single-cell transcriptomes revealed heterogeneous alterations within the epithelium and the tumor microenvironment during the progression of noninvasive dysplasia to invasive cancer. Although HGD-IPMNs expressed many core signaling pathways described in PDAC, LGD-IPMNs harbored subsets of single cells with a transcriptomic profile that overlapped with invasive cancer. Notably, a proinflammatory immune component was readily seen in low-grade IPMNs, composed of cytotoxic T cells, activated T-helper cells, and dendritic cells, which was progressively depleted during neoplastic progression, accompanied by infiltration of myeloid-derived suppressor cells. Finally, stromal myofibroblast populations were heterogeneous and acquired a previously described tumor-promoting and immune-evading phenotype during invasive carcinogenesis.

Conclusions: This study demonstrates the ability to perform high-resolution profiling of the transcriptomic changes that occur during multistep progression of cystic PDAC precursors to cancer. Notably, single-cell analysis provides an unparalleled insight into both the epithelial and microenvironmental heterogeneities that accompany early cancer pathogenesis and might be a useful substrate to identify targets for cancer interception.

See related commentary by Hernandez-Barco et al., p. 2027

Introduction

Pancreatic ductal adenocarcinoma (PDAC) is the third leading cause of cancer-related deaths in the United States, and most patients present with unresectable disease due to the lack of effective early-detection strategies (1). This reiterates the critical need for understanding the pathogenesis of early neoplasia with the goal of developing biomarkers and molecular targets for cancer interception. The most common cystic neoplasm that is a *bona fide* precursor to PDAC is intraductal papillary mucinous neoplasms (IPMNs), which comprise roughly 40% to 50% of resected lesions that are initially diagnosed as asymptomatic pancreatic cysts (2). Although most IPMNs harbor low-grade dysplasia (LGD), it is imperative to

[1]Department of Translational Molecular Pathology, The University of Texas MD Anderson Cancer Center, Houston, Texas. [2]The University of Texas MD Anderson Cancer Center UTHealth Graduate School of Biomedical Sciences, Houston, Texas. [3]Sheikh Ahmed Pancreatic Cancer Research Center, The University of Texas MD Anderson Cancer Center, Houston, Texas. [4]Department of Epidemiology, The University of Texas MD Anderson Cancer Center, Houston, Texas. [5]Department of Radiation Oncology, The University of Texas MD Anderson Cancer Center, Houston, Texas. [6]Department of Surgical Oncology, The University of Texas MD Anderson Cancer Center, Houston, Texas. [7]Department of Pathology, University of Pittsburgh Medical Center, Pittsburgh, Pennsylvania. [8]Department of Hematopathology, The University of Texas MD Anderson Cancer Center, Houston, Texas.

Note: Supplementary data for this article are available at Clinical Cancer Research Online (http://clincancerres.aacrjournals.org/).

V. Bernard, A. Semaan, J. Huang, and F.A. San Lucas contributed equally to this article.

Corresponding Author: Hector A. Alvarez, The University of Texas MD Anderson Cancer Center, Houston, TX 77030. Phone: 713-745-0838; E-mail: HAAlvarez@mdanderson.org

doi: 10.1158/1078-0432.CCR-18-1955

Published OnlineFirst November 1, 2018; DOI: 10.1158/1078-0432.CCR-18-1955

Translational Relevance

Previous studies on pancreatic cancer precursor lesions have identified commonly mutated oncogenes and tumor suppressors (e.g., *KRAS*, *GNAS*, and *TP53*). On the other hand, little is known about the transcriptomic heterogeneity within both cancer and stromal cells that contribute to invasive disease, particularly at the level of single cells. As efforts toward a precancer atlas of epithelial cancers develop, the ability to perform high-resolution tumor profiling through single-cell transcriptomic studies such as these will allow us to better understand the molecular underpinnings contributing to preneoplastic progression. This is especially relevant for discovery of clinically relevant biomarkers of early-stage disease, as well as potential targets for cancer interception.

distinguish IPMNs that have progressed to high-grade dysplasia (HGD), or harbor an outright invasive component (PDAC). To guide clinicians with identifying IPMNs harboring HGD or PDAC, several radiologic "high risk" or "worrisome features" (so-called Sendai and Fukuoka criteria) have been proposed (3). Although the rate of overdiagnosis and overtreatment has been significantly reduced, these criteria still lack optimal sensitivity and specificity (4). Although patients with noninvasive IPMNs have an excellent prognosis upon surgical resection, once an IPMN develops an invasive component, the probability of long-term survival drops significantly (5). Although we have now elucidated the signature driver mutations (*KRAS* and *GNAS)* that distinguish IPMNs from other pancreatic cysts, these do not reliably distinguish between indolent versus aggressive IPMNs (6, 7). In fact, the overall state of knowledge remains rudimentary, especially with regard to molecular metrics that can identify "aggressive" precancerous lesions that are likely to progress to carcinoma and require intervention from those that are "indolent" and will naturally regress or remain stable. Thus, much remains to be elucidated in terms of biomarkers of IPMN progression and the underlying molecular features of dysplastic cells that predicate to invasive neoplasia.

The application of single-cell DNA and RNA sequencing to cancers has provided unprecedented insights into tumor and microenvironmental heterogeneity present in established cancers. However, the extrapolation of these technologies to the compendium of precursor lesions has been scarce. In the specific context of the pancreas, prior studies have established the transcriptional profiles of normal cell types, such as islet cells, using single-cell approaches (8–10). In this study, we perform the first reported single-cell transcriptomic profiling of cystic precursor lesions of PDAC spanning histologic grades of dysplastic epithelium. Specifically, we demonstrate our ability to generate transcriptomic libraries from >5,400 single cells from surgically resected pancreatic tissues, including 2 IPMNs with LGD, 2 IPMNs with HGD, and 2 PDAC lesions utilizing a droplet-based single-cell RNA-seq methodology (11). Our results demonstrate that epithelial and stromal heterogeneity is evident even within precursor lesions during multistep carcinogenesis and reflect the progressive co-option of the microenvironment toward a tumor-promoting milieu.

Materials and Methods

Cell line and fresh tissue material from surgically resected IPMNs and PDAC

A total of 6 patients were recruited at MD Anderson Cancer Center (MDACC) and University of Pittsburgh Medical Center (UPMC) through informed written consent following institutional review board (IRB) approval at both institutions (PA15-0014, Lab08-0098, Lab05-0080, and Lab00-396). This study was conducted in accordance with Good Clinical Practices concerning medical research in humans per the Declaration of Helsinki. Two PDACs and 1 HGD-IPMN were profiled from MDACC and 2 LGD-IPMNs and 1 HGD-IPMN were profiled from UPMC. A previously established pancreatic tumoroid line (MP81) was also profiled (12). Tumoroid line source was validated through STR DNA fingerprinting and confirmed to be *mycoplasma*-free. Histologic subtypes of IPMN included in this study were gastric (1 LGD-IPMN), intestinal (1 LGD-IPMN), and pancreatobiliary (2 HGD-IPMNs). Tumor cellularity was determined by pathologic review of tissue and compared with yield of cell phenotypes from single-cell RNA-seq.

Preparation of fresh tissue material and dissociation into single cells

Pancreatic tissue was delivered to the laboratory on ice after surgical resection in DMEM, high-glucose, GlutaMAX Supplement, HEPES (Thermo Fisher, 10564011) in 1% bovine serum albumin (Thermo Fisher, B14) in a 15-mL conical tube. Tissue was then transferred to a 35- × 12-mm Petri Dish (Thermo Fisher, #150318), and minced with sterile surgical scalpel to 0.5- to 1.0-mm fragments in approximately 1 mL of the media.

Tissue digestion was performed with Liberase TH Research Grade (Sigma-Aldrich, 5401135001) alone for IPMN samples, or with both Liberase TH Research Grade and Accutase solution for PDAC tissues (Sigma-Aldrich, A6964). For warm digestion with Liberase TH Research Grade, pancreatic tissue fragments were incubated to a final concentration of 10 mg/mL and placed on an incubated orbital shaker at 37°C, 225 RPM for 20 minutes and gently pipetted every 10 minutes. At the end of the digestion period, the fragments (tissue slurry) were gently pipetted and washed to maximize the release of single cells. The tissue slurry was passed through a 100-μm cell strainer followed by a 35-μm cell strainer. The single-cell suspension was transferred to a new 15-mL conical tube and centrifuged for 5 minutes at 400 RCF at 4°C. The supernatant was discarded, and the cell pellet was resuspended in 400 μL of PBS for downstream cell viability analysis and cell counting.

For warm digestion of PDAC tissues, we followed the identical procedure above as the IPMNs, followed by a second digestion period using sterile-filtered Accutase solution, and placed on a shaker at 37°C, 225 RPM for 30 minutes, with gentle pipetting every 10 minutes.

ddSEQ SureCell library preparation

Single-cell transcriptomic amplification and library prep was performed using the SureCell WTA 3′ Library Prep Kit for the ddSEQ System following the manufacturer's recommendations (Illumina, cat. #20014279). Samples were processed across 6 sequential ddSEQ runs. Briefly, single cells were individually partitioned into subnanoliter droplets. Single cells were then lysed and barcoded inside individual droplets, with subsequent

Published OnlineFirst November 1, 2018; DOI: 10.1158/1078-0432.CCR-18-1955

first-strand synthesis. Individual droplets containing barcoded sample cells were disintegrated, purified, and subjected to second strand cDNA synthesis. Purified amplified cDNA was subsequently quantified on a 2200 TapeStation System (Agilent) in order to validate quality of amplification by quantifying the area under the curve in regions between 200- and 5,000-bp range on a D5000 high-sensitivity screentape (Supplementary Fig. S5A). Successful reactions (>2 ng yield) were then fragmented and amplified using Nextera technology for low input cDNA material. Double-sided size selection and library purification was performed utilizing purification beads per the manufacturer's protocol to remove short library fragments. Final library quality and concentration was measured by TapeStation (Supplementary Fig. S5B) as the area under the curve. Libraries were sequenced on across 6 Illumina NextSeq 500 runs.

Single-cell clustering and transcriptomic analyses

Resulting FastQ files were run through the single-cell RNA-seq app on BaseSpace. Briefly, reads were aligned against a reference genome using Spliced Transcripts Alignment to a Reference (STAR), followed by barcode tagging and BAM indexing (13). Count files are generated using gene unique molecular identifier (UMI) counter and with cells passing quality filter based on cells above background and passing knee filter.

To perform the T-SNE clustering and additional downstream analysis, the UMI count files were compiled into sparse matrices and subsequently filtered based on the criteria that each cell must express a minimum of 300 genes and be composed of less than 15% mitochondrial genes. Following filtering, the data are log normalized, scaled, and centered. The output is then analyzed by principal component analysis (PCA). After identifying the number of dimensions to use, the result is clustered in a shared nearest-neighbor algorithm and T-SNE before plotting. The resulting T-SNE plots were colored according to specific features to visually present expression of genes in various clusters. These annotated matrices were also used to find differentially expressed genes between subpopulations. Heat maps organized by annotated clusters were generated by plotting the top 20 differentially expressed genes associating with each cluster. Functions for analysis were provided through the recommended workflow in the SEURAT package (11).

The correlation matrices were created based on the filtered list of cells used in the T-SNE. Matrices were formed through the function "cor" from the stats package. The Pearson correlation coefficients were then plotted in ComplexHeatmap (14). Cells are ordered through hierarchical clustering. For cell-cycle analysis, we defined a cell-cycle characteristic coefficient as the average of the $\log_2(\text{TPM} + 1)$ across genes for a cell from the gene ontology set (version 6.2 MSigDB) related to the G_1, S, G_2, and M phases, respectively (15, 16). These coefficients were then plotted in ComplexHeatmap (13) and hierarchically clustered by cells. All T-SNE and heat maps were run in R v3.4.2.

Results

Concordance of single-cell RNA sequencing to bulk-cell lines

Prior to tissue profiling, we investigated the concordance of bulk and single-cell RNA-seq profiles from a PDAC tumoroid line (MP81) using the droplet-based sequencing technology. Single-cell and bulk-cell RNA libraries were made using Nextera library preparation chemistry. Single-cell RNA-seq was performed at 670 million reads, resulting in 30.4% of the reads mapping to the coding sequence (CDS) regions, and 37.7% mapping to UTR regions with 91,032 reads, 10,800 UMI counts, and a median of 3,293 unique genes detected per cell passing filter. Correlations in gene-expression levels between 2,022 single cells and bulk cell suspension were excellent ($r_s > 0.9$), with total coverage gene counts of 17,507 and 15,185 for single cells and bulk cells, respectively (Supplementary Fig. S1A). We also verified the concordance of gene counts across 2 independent replicates of single-cell library preparation from the same cell line sample. This revealed a high correlation in gene-expression levels ($r_s > 0.9$) with almost identical levels of gene coverage (14,994 and 14,488; Supplementary Fig. S1B).

Preneoplastic epithelium of IPMNs demonstrates both unique and shared transcriptomic signatures with PDAC

We subsequently applied droplet-based single-cell RNA sequencing to study the diverse transcriptional profiles that exist within surgically resected preneoplastic (IPMN) and invasive (PDAC) pancreatic lesions (Supplementary Figs. S1C and S1D, S2 and Supplementary Table S1). Cumulatively, among all of the tissue samples, 5,403 single cells were sequenced. Cells with low expression of genes (<300 genes) and high percentage of mitochondrial genes expressed (>10%) were digitally filtered out, resulting in 3,343 single cells used for the subsequent analysis. Scatter plots of number of UMIs compared with number of genes and abundance of mitochondrial transcripts revealed consistent read depth across single cells between lesions and absence of apoptosis induced transcript batch effects (Supplementary Fig. S1C). The mean number of genes and UMIs detected per cell was 1,101 and 3,194, respectively. After identifying the top variable genes, we performed PCA and determined which principal components (Supplementary Fig. S1D) to use for unsupervised clustering using t-distribution stochastic neighbor embedding (t-SNE; ref. 17), which was implemented using the SEURAT package (Fig. 1A; ref. 11). This analysis identified 10 distinct subpopulations ("clusters") composed of unique stromal and epithelial components classified defined by characteristic gene-expression patterns (Fig. 1B and C; Supplementary Table S2; Supplementary Fig. S3).

We first identified the neoplastic single-cell "clusters" through previously defined signature transcripts for pancreatic epithelial lesions, including *KRT19* and *MUC1*, which were present among all samples types (IPMNs and PDAC) irrespective of grade if dysplasia or invasion (refs. 18, 19; Fig. 2A). We subsequently sought to correlate the histologic grading of the designated "clusters" with known biomarkers of dysplastic progression to cancer. This revealed high expression of transcripts such as *CEACAM6* within subpopulations of HGD-IPMN and PDAC samples, which confirmed previously published data on this marker in bulk RNA analysis and IHC of intact tissues (20, 21). Conversely, we observed high expression of *MUC5AC*, which encodes for an apomucin mostly seen in LGD and downregulated during histologic progression, within the LGD-IPMNs compared with the other sample types (18).

In an effort to identify "cluster-defining" signatures, we profiled the top 25 differentially expressed genes within each of the 10 distinct single-cell "cluster" (Fig. 2B; Supplementary Table S3). Annotation of the resulting transcripts revealed aberrant expression of multiple cancer-related genes even within the LGD-IPMN cells designated as "clusters" LG.Ep1, 2, and 3 (Fig. 1B). These include overexpression of transcripts such as *TFF3* and *REG4*

Published OnlineFirst November 1, 2018; DOI: 10.1158/1078-0432.CCR-18-1955

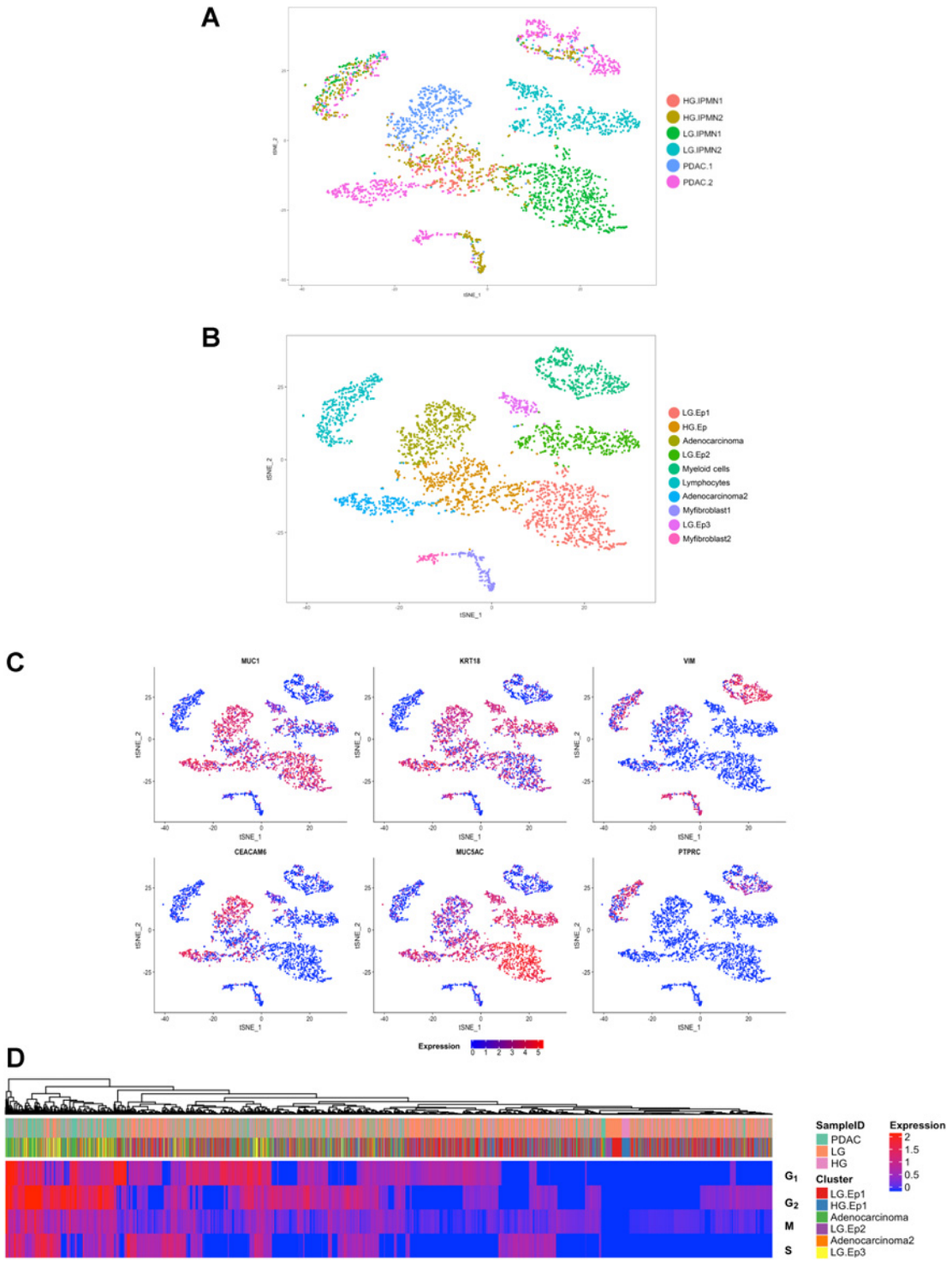

Figure 1.

tSNE plots of all 3,343 cells from 6 lesions included in this study, (**A**) annotated by different tissue samples, (**B**) annotated by unique cell types characterized by gene expression (ductal epithelium = Ep). **C,** Feature plots demonstrating expression of specified genes among clusters on the tSNE. **D,** Clustered heat map of cell-cycle characteristic coefficients per cell within the subpopulations indicated by the header demonstrating a greater proliferative state of PDAC-derived cells.

Published OnlineFirst November 1, 2018; DOI: 10.1158/1078-0432.CCR-18-1955

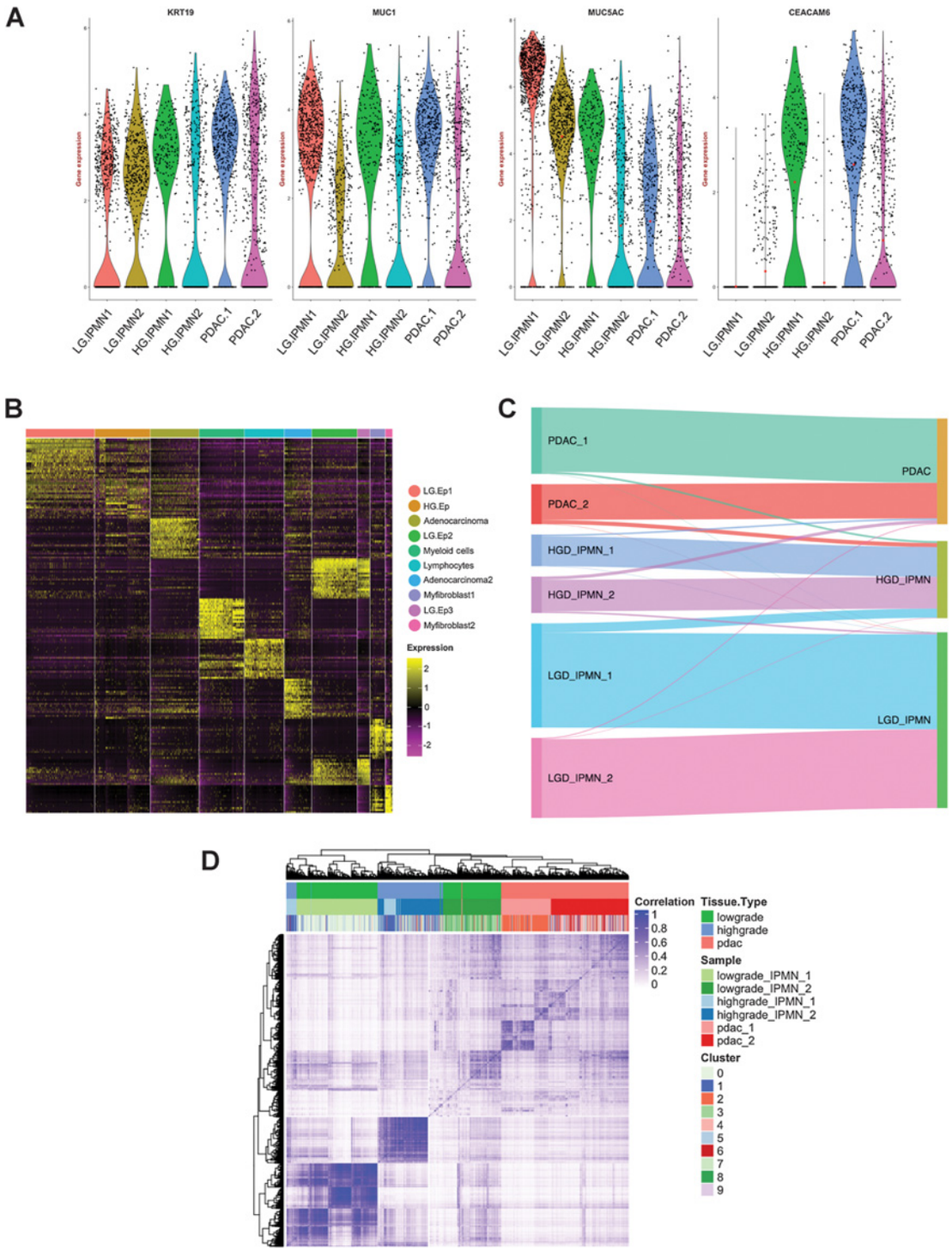

Figure 2.

A, Violin plots of gene expression across lesion types confirm expression of characteristic PDAC and cystic preneoplasia-related markers. **B,** Heat map of the top 20 differentially expressed genes used to identify cell phenotypes across each of the 10 discrete clusters indicated by the header. **C,** Sankey diagram demonstrating epithelial cells profiled from LGD-IPMNs, HGD-IPMNS, and PDAC tissue and where they reside within annotated tSNE clusters. **D,** Correlation heat map of Pearson correlation coefficients of hierarchically clustered individual cells across all lesions, identified by originating lesion type and tSNE cluster.

Published OnlineFirst November 1, 2018; DOI: 10.1158/1078-0432.CCR-18-1955

that have been previously described as upregulated during cancer progression (22, 23). On the contrary, the LGD-IPMN clusters demonstrated persistent expression of putative tumor suppressor genes (TSG) such as *RAP1GAP* that have been shown to suppress tumor invasion and metastases across various cancers (including RAS-mutant neoplasms; refs. 24), while HGD-IPMNs (HG.Ep) revealed downregulation of the aforementioned TSGs, concomitant with higher expression of oncogenic transcripts previously associated with progression to PDAC such as *S100P* and *S100A10*, among others (25–27).

We then investigated whether biological differences could be observed through gene ontology and pathway analyses (IPA: Ingenuity Pathways Analysis) of differentially expressed genes between neoplastic epithelial clusters (Fig. 1B). Several aberrant canonical pathways were identified during the transition from LGD to HGD-IPMNs that are related to previously published core signaling pathways in PDAC, including integrin signaling, signaling by small GTPases, Wnt/B-catenin signaling, axonal guidance signaling, apoptosis, and G_1–S phase regulation (Supplementary Table S4; refs. 28, 29). When comparing the PDAC and LGD lesions, aberrant expression of the same pathways was observed, with the additional deregulation of DNA damage response, TGF-B signaling, and SAPK/JNK signaling. Other aberrant canonical pathways identified during transition from LGD to HGD and PDAC lesions include metabolism related pathways such as oxidative phosphorylation and mitochondrial dysfunction, as well as mTOR signaling (Supplementary Table S5).

Cell-cycle analysis of epithelial cells across lesion types revealed higher proliferative states (G_2–M and S phase) in cells derived from PDAC compared with LGD and HGD lesions (Fig. 1D). Generally, there was a significant proportion of LGD cells with low expression of cell-cycle genes likely representing cells within low proliferative states (G_0 phase). On the other hand, there is a small population of cells derived from LGD lesions (LG.Ep3) with high expression of proliferation-related genes, which may represent a more aggressive subpopulation within this lesional type. This may suggest that even within lesions histologically identified as low grade, there exist rare populations of cells with varying degrees of putative malignant potential. Further, it is important to note that even "adenocarcinoma"-designated clusters contained cells originating from LGD-IPMNs with associated expression of PDAC core signaling pathways and deregulation of TSGs (Fig. 2C). In our particular data set, 1.2% of epithelial cells from LGD-IPMNs were found in adenocarcinoma-related clusters. Additionally, up to 8.9% of cells from LGD-IPMNs tended to cluster with HGD-IPMNs with their respective changes in gene-expression pathways. This suggests that even within IPMNs with otherwise LGD histology, there are cells that phenocopy the transcriptomic features of invasive neoplasia (Supplementary Fig. S2). The expression profiles of such low frequency cells within LGD-IPMNs would likely be missed during bulk RNA sequencing, and further underscores the utility of the single-cell sequencing approach in elucidating the epithelial heterogeneity that exists even within early precursor lesions of PDAC.

Analysis of the cell-to-cell correlations for gene-expression of the 3,343 cells demonstrated relatively higher intratumoral coherence among cells from LGD and HGD lesions compared with those from PDAC (Fig. 2D), a not surprising finding suggesting an increase in intratumoral epithelial heterogeneity during the progression from IPMNs to PDAC (30). Interlesion correlation was better observed in cells derived from stromal components including myeloid and lymphocytic populations, whereby a significant number of populations showed similarities across tissue types (Fig. 1A–C). This suggests the presence of common cancer-associated immune components among lesion types. On the other hand, even though these stromal components tended to cluster with one another (Fig. 1B), correlation heat maps suggested the presence of multiple unique subtypes within the stroma and nonrandom variations during histologic progression to cancer (Supplementary Fig. S4 and results below).

Virtual microdissection of stromal and immune heterogeneity during IPMN progression

In an effort to better identify unique subpopulations of stromal components across lesion types, we opted to perform single-cell digital microdissection of only stromal cells and exclude epithelial components. This resulted in the identification of 7 unique clusters with varying degrees of enrichment across lesions types (Fig. 3A and B). Differential expression of the top 20 genes across clusters allowed us to identify distinct immune and myofibrolast-derived phenotypes within each lesional subtype (Fig. 3C and D).

A high proportion of cytotoxic T cells (measured by CD8, and presence of granzyme- and perforin-related transcripts) were observed in LGD-IPMNs compared with HGD-IPMNs and PDAC. In proportion to other immune subtypes, CD4 T cells also appear to be more highly enriched in LGD-IPMN compared with others and present with generalized activation as defined by expression of *CD69*. We also detected the presence of rare B-cell populations (expressing CD20 and CD19) that are present in both HGD-IPMNs and in LGD-IPMNs, but are completely absent in PDACs. Presence of tumor-infiltrating B cells has recently been described in PanIN lesions with an immunosuppressive role during the initiating stages of PDAC multistep progression and may, in fact, have a similar role in the context of IPMNs based on these findings (10, 31, 32).

Notably, we observed a significantly enriched proportion of myeloid-derived suppressor cells (MDSCs), within the stromal component of PDAC, representing 51% (277/544) of single stromal cells profiled, compared with 2.3% (3/131) and 3.5% (10/281) within LGD-IPMNs and HGD-IPMNs, respectively. These MDSCs resemble the protumorigenic polymorphonuclear MDSCs (PMN-MDSCs) phenotype based on expression of CD11b (*ITGAM*), S100A9, CCL3, and APOE, which has been previously described to be prevalent during cancer progression (33). Among myeloid-derived populations, we also observed cDC2-type dendritic cells (DC), characterized by expression of CD1C, THBD, and *FCER1A* (34). These cells have been shown to have T-cell stimulatory potential and are critical mediators of cross-presentation of tumor antigens mediated through the high-affinity IgE receptor FcεRI (*FCER1A*; ref. 35). This proinflammatory subpopulation appears in greater proportions among LGD and HGD-IPMNs, suggesting a more prevalent predication for antitumor immune response within preneoplastic lesions.

Heterogeneous fibroblast populations across histologic subtypes were also identified, potentially representing distinct stromal functions during tumorigenesis. For example, the fibroblast subtype known as "inflammatory" CAF (iCAF) is characterized by expression of *VIM*, *FAP*, *COL3A1*, *DES*, *IL6*, and *CXCL12* and reduced expression of a-SMA (*ACTA2*; refs. 36, 37). This

Published OnlineFirst November 1, 2018; DOI: 10.1158/1078-0432.CCR-18-1955

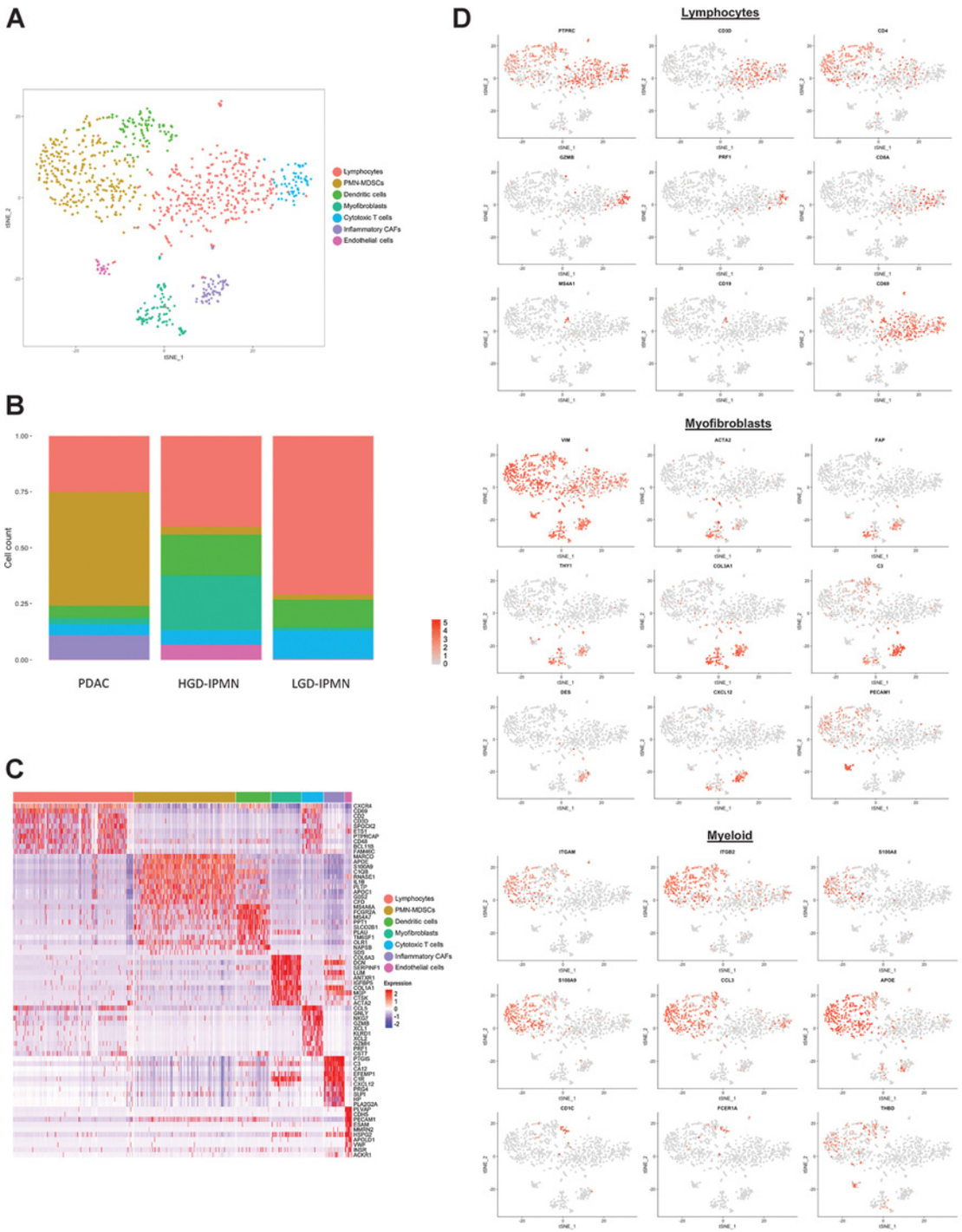

Figure 3.

A, tSNE plot of all stromal cells that were virtually microdissection from entire lesions. Different colors represent annotation of unique cell phenotypes. **B,** Proportion of cell phenotypes enriched in each lesion (PDAC, HG IPMN, and LG IPMN); colors refer to unique cell types in **A**. **C,** Heat map of the top 20 differentially expressed genes used to identify cell phenotypes across clusters. **D,** Feature plots demonstrating expression of specific genes among clusters to identify respective cell types.

subpopulation has been shown to be involved in immunosuppression, growth factor secretion, and promotion of protumorigenic mechanisms facilitating invasion and metastasis (36), which might correlate with its exclusive representation in PDAC-derived clusters, representing 10.5% (58/544) of single stromal cells profiled, and absence within noninvasive IPMNs. A separate compartment of CAFs, described as myofibroblasts ("myCAFs"), with increased alpha-SMA expression and reduced

Published OnlineFirst November 1, 2018; DOI: 10.1158/1078-0432.CCR-18-1955

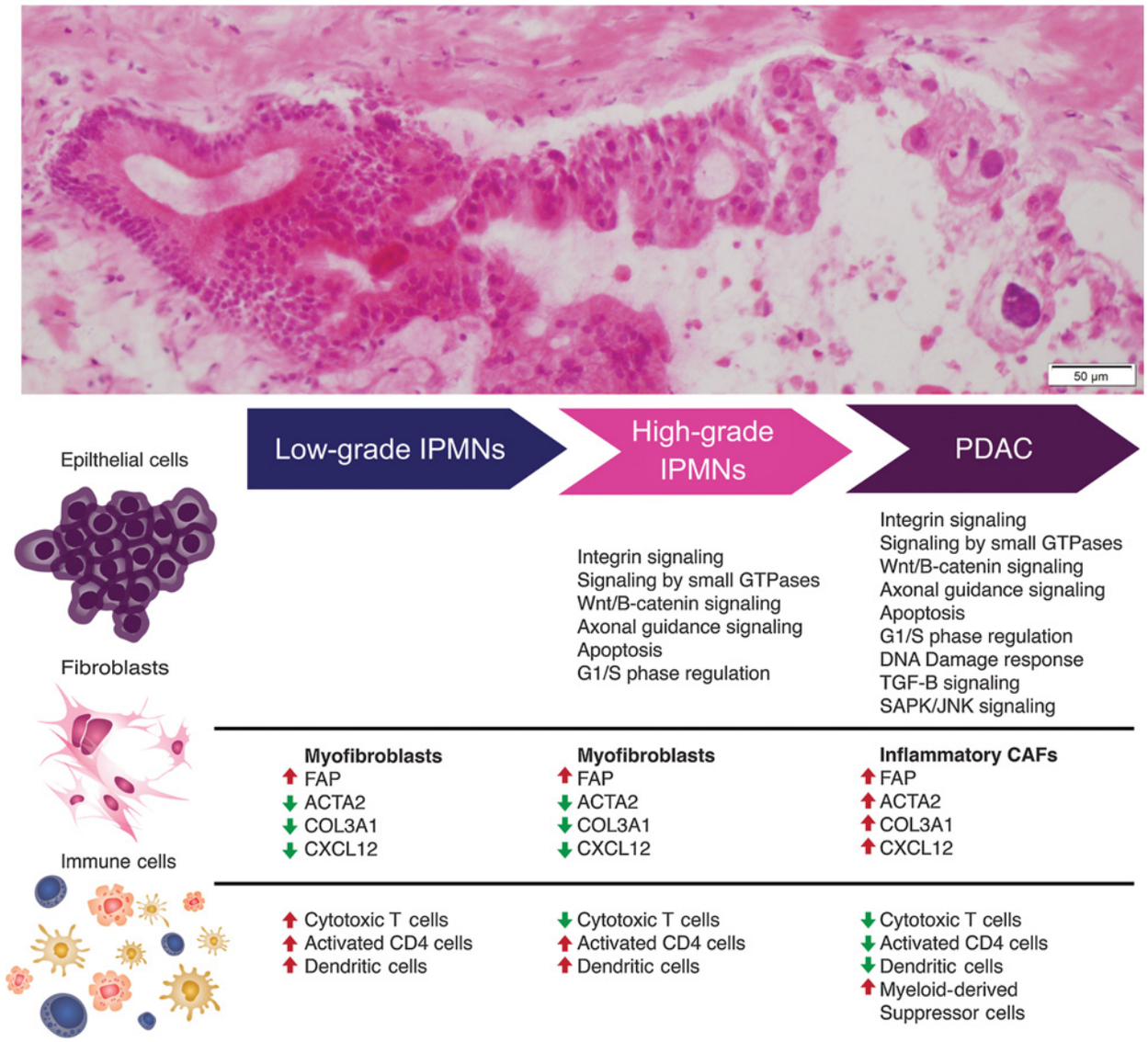

Figure 4.
Schematic representation of evolving molecular and phenotypic signatures during preneoplastic progression of pancreatic cancer.

expression of *CXCL12* and *DES*, was also identified. These myCAFs have been implicated in distinct functions from iCAFs, including secretion of autocrine stromal and endothelial growth factors (36). This population is rare in LGD-IPMNs, but is highly represented in HGD-IPMNs, suggesting that activation of fibroblasts to the myCAF phenotype tends to occur even within noninvasive dysplastic lesions (Fig. 4).

Discussion

Histologically well-established precancerous lesions precede the onset of PDAC by years, if not decades. With an increasing use of diagnostic cross-sectional imaging, incidence of precancerous lesions in the form of pancreatic cysts is rising even in clinically healthy individuals (38–40). In general, approximately 2.4% of the general population undergoing MRI present with a cystic pancreatic lesion with individuals over 70 years having an incidence of up to 10% (41). To guide clinicians, several radiologic guidelines have been reported and progressively updated (3, 42, 43). In general, large, symptomatic main duct IPMNs with enhancing mural nodules show the highest probability of malignant transformation; frequency of invasive IPMNs is 43.1% (range, 11%–81%) and should be surgically treated (3). Yet several other case series of resected IPMNs report a wide range of IPMN-related pancreatic adenocarcinoma (6%–81%; refs. 44–46). A balance between diagnosis of potentially invasive IPMNs and harmful overtreatment of patients is thus crucial in our approach stratification of cystic lesions. In the current study, we describe an approach at profiling the molecular events that occur during pancreatic

Published OnlineFirst November 1, 2018; DOI: 10.1158/1078-0432.CCR-18-1955

carcinogenesis in the context of these cystic precursors (IPMNs) with the goal of understanding the heterogeneity of epithelial and stromal components that might delineate lesions with an aggressive potential. We do this through high-resolution single-cell RNA sequencing of LGD-IPMNs, HGD-IPMNs, and PDACs, which allows us to specifically profile aberrant pathways across multiple cell types. Interestingly, progression from LGD and HGD lesions to invasive PDAC revealed shifts in distinct cell populations encompassing both epithelial and stromal/immune compartments.

Among epithelial populations, we detected expression of transcripts of gastric lineage that have been previously described during IPMN progression and have been correlated with better prognosis, such as *MUC5AC*, as differentially overexpressed in our LGD lesions (47). Although oncogenic transcripts are also expressed at the LGD stage, there appears to be retained expression of tumor suppressor–related pathways, which may help counteract further dysplastic progression of these lesions. Within HGD lesions, differential expression of these tumor suppressor pathways is no longer detected, and we begin to find previously described classic core signaling pathways in PDAC (29, 48).

As a stroma-rich cancer, multiple studies have shown how the diverse tumor microenvironment (TME) plays a crucial role in the development, progression, and immune evasion that exemplifies the biology of PDAC (49, 50). As previously shown by Moffit and colleagues, "virtual microdissection" of stromal genes revealed an "activated" subpopulation of stroma characterized by overexpression of inflammatory pathways (51). Although these findings are further validated within our own study, Moffit and colleagues were not able to distinguish specific contributions of immune and myofibroblast components to this signature. By dissecting specific cell types at the single-cell level, we further delineate this signature to describe the dichotomy of "myCAF" versus "iCAF" fibroblast populations during multistep progression, with the former cells observed (albeit rarely) even in LGD-IPMNs and the latter cells only identified in PDAC samples. Within our analysis, besides expression of many typical CAF markers (*FAP*, *THY1*, and *DES*), the iCAF cells also show a unique expression pattern of the C-X-C motif chemokine ligand 12 (CXCL12; ref. 52). This chemokine and its corresponding receptor (CXCR4) are believed to play a crucial role in many solid cancers and are associated with metastatic spread in breast cancer, lung cancer, and melanoma (53–56). Accumulating evidence also points to a role in PDAC progression, with higher expression of CXCL12 correlating with metastasis, likely by facilitating immune evasion, and increased levels of matrix metalloproteinases leading to cellular invasion (57–60). Within our own study, we find similar trends in the presence of other cellular populations that parallel the emergence of CXCL12-expressing iCAFs, such as a decrease in cytotoxic T-cell and increase in myeloid-suppressive proportions, creating the notorious immune-suppressive TME well described in PDAC.

Myeloid-derived subpopulations also tend to evolve during tumor progression. Composed of multiple clusters expressing CD11b, ITGB2, CD13, CD18, and S100A9, a clear separation based on their individual transcriptomes remains difficult. This high overlap of myeloid-derived subpopulations mirrors recent findings in breast cancer where previously proposed M1 and M2 macrophage-associated genes are frequently expressed within the same cells between these 2 clusters (61). As Azizi and colleagues describe, this suggests that distinct prototypical macrophages may not be prevalent within tumors and may in fact exist within the spectrum of these 2 phenotypes. Among other myeloid-derived populations, we do identify PMN-MDSCs that are known surrogates of prognosis and contribute to immune evasion and tumor progression through neoangiogenesis, migration and invasion, and thus metastatic spread (62, 63). Similar to the elevated proportion of CAFs experienced in more advanced disease, we describe a striking increase in MDSC populations compared with preneoplastic lesions (51% of nonepithelial cell types in PDAC, versus <5% in noninvasive IPMNs). This resembles findings from Kumar and colleagues whereby CAFs are able to actively recruit PMN-MDSCs to tumors, further supporting the role of an "inflammatory CAF" subpopulation in promoting immunosuppression (64). Additional work has described the importance of immune populations during tumorigenesis in the context of IPMNs specifically (65). Spatial characteristics as related to epithelial and cytotoxic T cell, as well as myeloid cell and cytotoxic T-cell proximity, have been shown to be a predictive feature of the presence of HGD. This is believed to be caused by immunosuppressive interactions derived from tumor cells and myeloid cells against cytotoxic T cells, regulating tumor development. With further data supporting the role of myeloid-derived cytotoxic T-cell suppression, immunotherapeutic approaches targeting this cross-talk may serve as a novel strategy at impeding tumor progression (10, 66).

The identification of demonstrable DC populations within LGD and HGD-IPMN microenvironment suggests a proinflammatory phase that is present during the noninvasive precursor states. This is particularly true in LGD-IPMNs where a higher proportion of cytotoxic T cells exist in comparison with other lesion types that may be supported by cDC2 cells through cross-presentation of tumor antigens and T-cell stimulation. Additionally, the presence of these DCs in IPMNs may also provide opportunities for cancer "immune interception," because DC-targeted vaccines have previously shown effectiveness in the context of an myeloid immunosuppressive environment through reduction of PMN-MDSCs (67).

Although single-cell RNA sequencing provides new tools for high-resolution profiling of cell populations, it is not without its limitations, particularly in the context of this study. Although these methodologies are accurate in determining relative abundance of transcripts, they suffer when attempting to capture lowly expressed genes (68). This is mostly of symptom of droplet-based approaches as currently described. Although they allow for high-throughput sequencing of thousands of single cells from a single sample by counting the 3′ end of transcripts, sensitive detection of low to moderately expressed mRNA transcripts is forfeited compared with those methodologies providing full-length transcript data (68–70). As we aimed to profile the complex heterogeneity of these preneoplastic tissues within this study, we prioritized maximizing throughput through a droplet-based approach at the cost of observing an average of 1,101 genes per cell. Sequencing depth is another important consideration, as low read depth would not be optimal for providing detailed transcript information from a single cell that may contain subtle changes gene-expression signatures. But even with increasing sequencing depth, transcript dropout remains a significant limitation where poor mRNA capture and amplification may result in up to 72% of loss transcripts, particularly in genes expressed at low levels (68). It is also important to note that single-cell dissociation of tissues remains a challenging protocol, for 1 thing to maintain viability of cells throughout the process and the other to maintain relative

Published OnlineFirst November 1, 2018; DOI: 10.1158/1078-0432.CCR-18-1955

cell representation as isolation protocols often lead to selective degradation of specific cell types. There also remains the potential for these methodologies to alter expression states and mRNA levels during this process. Further work has demonstrated that this can be ameliorated through RNA-seq of single nuclei which may result in less of a bias of cell populations (19, 71). Further limitations within our own study include the low number of samples profiled. This is mostly a consequence of the relative paucity of freshly resected surgical samples from pancreatic cysts of appropriate cellularity (low-grade cysts are particularly challenging in being paucicellular), as well as the difficulty of obtaining adequate viability following single-cell dissociation in order to create viable cDNA and sequencing libraries. This further exacerbates the fact we could not obtain consistent histologic subtypes in our preneoplastic lesions, which can have a direct impact on transcriptomic heterogeneity.

In conclusion, we describe how the TME may evolve during the multistep progression of IPMNs to PDAC, whereby the noninvasive precursor lesions begin to experience a loss of cytotoxic T cells during dysplastic progression and begin to assimilate immune components such as PMN-MDSCs, with immune-suppressive properties. Additionally, we demonstrate this permissive microenvironment is correlated with appearance of tumor-promoting iCAF stromal cell populations that facilitate immune evasion. Notably, single-cell analysis of IPMNs reveals, for the first time, that even in otherwise histologically innocuous LGD-IPMNs, we find minor populations of cells that transcriptionally phenocopy HGD and PDAC (~9% and ~1% of LGD-IPMN cells, respectively). It is possible that future single-cell analyses on a larger series of LGD-IPMNs might establish a "threshold" that portends aggressive natural history even in the absence of radiologically detectable worrisome features. Although it is important to stress the limited generalizations that can be made from such a small subset of lesions, the ability to detect these gene-expression patterns among single cells provides a primer for uncovering how heterogeneous cell types contribute to tumor carcinogenesis. Leveraging this strategy may thus facilitate elucidation of molecular biomarkers for disease stratification.

Disclosure of Potential Conflicts of Interest

C.M. Taniguchi reports receiving commercial research grants from Galera Therapeutics. A.D. Singhi is a consultant/advisory board member for Foundation Medicine. No potential conflicts of interest were disclosed by the other authors.

Authors' Contributions

Conception and design: V. Bernard, F.C. Mulu, B.M. Stephens, M.H. Katz, A. Maitra, H.A. Alvarez

Development of methodology: V. Bernard, A. Semaan, F.A. San Lucas, F.C. Mulu, B.M. Stephens, C.-W. Tzeng, M.H. Katz, H.A. Alvarez

Acquisition of data (provided animals, acquired and managed patients, provided facilities, etc.): V. Bernard, A. Semaan, F.C. Mulu, B.M. Stephens, J. Zhao, N. Kamyabi, C.M. Taniguchi, M.P. Kim, C.-W. Tzeng, M.H. Katz, A.D. Singhi, H.A. Alvarez

Analysis and interpretation of data (e.g., statistical analysis, biostatistics, computational analysis): V. Bernard, A. Semaan, J. Huang, F.A. San Lucas, Y. Huang, N. Kamyabi, P.A. Scheet, M.H. Katz, A. Maitra, H.A. Alvarez

Writing, review, and/or revision of the manuscript: V. Bernard, A. Semaan, J. Huang, F.A. San Lucas, B.M. Stephens, P.A. Guerrero, N. Kamyabi, S. Sen, C.M. Taniguchi, M.P. Kim, C.-W. Tzeng, M.H. Katz, A. Maitra, H.A. Alvarez

Administrative, technical, or material support (i.e., reporting or organizing data, constructing databases): V. Bernard, B.M. Stephens, H.A. Alvarez

Study supervision: C.M. Taniguchi, H.A. Alvarez

Acknowledgments

This work was supported by the MD Anderson Moonshot Program and the Khalifa Bin Zayed Al-Nahyan Foundation, the NIH (U01CA196403 and U01CA200468 to A. Maitra and in part by U54CA096300 and U54CA096297 to V. Bernard), the Cancer Prevention Research Institute of Texas (RP140106 to V. Bernard and RP170067 to N. Kamyabi and V. Bernard), and the DFG (German Research Foundation; SE-2616/2-1 to A. Semaan).

The costs of publication of this article were defrayed in part by the payment of page charges. This article must therefore be hereby marked *advertisement* in accordance with 18 U.S.C. Section 1734 solely to indicate this fact.

Received June 19, 2018; revised September 18, 2018; accepted October 29, 2018; published first November 1, 2018.

References

1. Siegel RL, Miller KD, Jemal A. Cancer statistics, 2018. CA Cancer J Clin 2018;68:7–30.
2. Salvia R, Crippa S, Partelli S, Armatura G, Malleo G, Paini M, et al. Differences between main-duct and branch-duct intraductal papillary mucinous neoplasms of the pancreas. World J Gastrointest Surg 2010;2:342–6.
3. Tanaka M, Fernandez-Del Castillo C, Kamisawa T, Jang JY, Levy P, Ohtsuka T, et al. Revisions of international consensus Fukuoka guidelines for the management of IPMN of the pancreas. Pancreatology 2017;17:738–53.
4. Heckler M, Michalski CW, Schaefle S, Kaiser J, Buchler MW, Hackert T. The Sendai and Fukuoka consensus criteria for the management of branch duct IPMN – A meta-analysis on their accuracy. Pancreatology 2017;17:255–62.
5. Rezaee N, Barbon C, Zaki A, He J, Salman B, Hruban RH, et al. Intraductal papillary mucinous neoplasm (IPMN) with high-grade dysplasia is a risk factor for the subsequent development of pancreatic ductal adenocarcinoma. HPB (Oxford) 2016;18:236–46.
6. Molin MD, Matthaei H, Wu J, Blackford A, Debeljak M, Rezaee N, et al. Clinicopathological correlates of activating GNAS mutations in intraductal papillary mucinous neoplasm (IPMN) of the pancreas. Ann Surg Oncol 2013;20:3802–8.
7. Matthaei H, Wu J, Dal Molin M, Shi C, Perner S, Kristiansen G, et al. GNAS sequencing identifies IPMN-specific mutations in a subgroup of diminutive pancreatic cysts referred to as "incipient IPMNs". Am J Surg Pathol 2014;38:360–3.
8. Segerstolpe A, Palasantza A, Eliasson P, Andersson EM, Andreasson AC, Sun X, et al. Single-cell transcriptome profiling of human pancreatic islets in health and type 2 diabetes. Cell Metab 2016;24:593–607.
9. Muraro MJ, Dharmadhikari G, Grun D, Groen N, Dielen T, Jansen E, et al. A single-cell transcriptome atlas of the human pancreas. Cell Syst 2016;3:385–94e3.
10. Gunderson AJ, Kaneda MM, Tsujikawa T, Nguyen AV, Affara NI, Ruffell B, et al. Bruton tyrosine kinase-dependent immune cell cross-talk drives pancreas cancer. Cancer Discov 2016;6:270–85.
11. Macosko EZ, Basu A, Satija R, Nemesh J, Shekhar K, Goldman M, et al. Highly parallel genome-wide expression profiling of individual cells using nanoliter droplets. Cell 2015;161:1202–14.
12. Sakellariou-Thompson D, Forget MA, Creasy C, Bernard V, Zhao L, Kim YU, et al. 4-1BB agonist focuses CD8(+) tumor-infiltrating T-cell growth into a distinct repertoire capable of tumor recognition in pancreatic cancer. Clin Cancer Res 2017;23:7263–75.
13. Dobin A, Davis CA, Schlesinger F, Drenkow J, Zaleski C, Jha S, et al. STAR: ultrafast universal RNA-seq aligner. Bioinformatics 2013;29:15–21.
14. Gu Z, Eils R, Schlesner M. Complex heatmaps reveal patterns and correlations in multidimensional genomic data. Bioinformatics 2016;32:2847–9.

Published OnlineFirst November 1, 2018; DOI: 10.1158/1078-0432.CCR-18-1955

15. Liberzon A, Birger C, Thorvaldsdottir H, Ghandi M, Mesirov JP, Tamayo P. The Molecular Signatures Database (MSigDB) hallmark gene set collection. Cell Syst 2015;1:417–25.
16. Subramanian A, Tamayo P, Mootha VK, Mukherjee S, Ebert BL, Gillette MA, et al. Gene set enrichment analysis: a knowledge-based approach for interpreting genome-wide expression profiles. Proc Natl Acad Sci U S A 2005;102:15545–50.
17. Waltman L, Jan van Eck N. A smart local moving algorithm for large-scale modularity-based community detection. Eur Phys 2013;86:471.
18. Jonckheere N, Skrypek N, Van Seuningen I. Mucins and pancreatic cancer. Cancers (Basel) 2010;2:1794–812.
19. Gao R, Kim C, Sei E, Foukakis T, Crosetto N, Chan LK, et al. Nanogrid single-nucleus RNA sequencing reveals phenotypic diversity in breast cancer. Nat Commun 2017;8:228.
20. Duxbury MS, Matros E, Clancy T, Bailey G, Doff M, Zinner MJ, et al. CEACAM6 is a novel biomarker in pancreatic adenocarcinoma and PanIN lesions. Ann Surg 2005;241:491–6.
21. Duxbury MS, Ito H, Benoit E, Ashley SW, Whang EE. CEACAM6 is a determinant of pancreatic adenocarcinoma cellular invasiveness. Br J Cancer 2004;91:1384–90.
22. Terris B, Blaveri E, Crnogorac-Jurcevic T, Jones M, Missiaglia E, Ruszniewski P, et al. Characterization of gene expression profiles in intraductal papillary-mucinous tumors of the pancreas. Am J Pathol 2002;160:1745–54.
23. He XJ, Jiang XT, Ma YY, Xia YJ, Wang HJ, Guan TP, et al. REG4 contributes to the invasiveness of pancreatic cancer by upregulating MMP-7 and MMP-9. Cancer Sci 2012;103:2082–91.
24. Zhang L, Chenwei L, Mahmood R, van Golen K, Greenson J, Li G, et al. Identification of a putative tumor suppressor gene Rap1GAP in pancreatic cancer. Cancer Res 2006;66:898–906.
25. Arumugam T, Simeone DM, Van Golen K, Logsdon CD. S100P promotes pancreatic cancer growth, survival, and invasion. Clin Cancer Res 2005;11:5356–64.
26. Kim GE, Bae HI, Park HU, Kuan SF, Crawley SC, Ho JJ, et al. Aberrant expression of MUC5AC and MUC6 gastric mucins and sialyl Tn antigen in intraepithelial neoplasms of the pancreas. Gastroenterology 2002;123:1052–60.
27. Sitek B, Sipos B, Alkatout I, Poschmann G, Stephan C, Schulenborg T, et al. Analysis of the pancreatic tumor progression by a quantitative proteomic approach and immunhistochemical validation. J Proteome Res 2009;8:1647–56.
28. Bailey P, Chang DK, Nones K, Johns AL, Patch AM, Gingras MC, et al. Genomic analyses identify molecular subtypes of pancreatic cancer. Nature 2016;531:47–52.
29. Biankin AV, Waddell N, Kassahn KS, Gingras MC, Muthuswamy LB, Johns AL, et al. Pancreatic cancer genomes reveal aberrations in axon guidance pathway genes. Nature 2012;491:399–405.
30. Oldfield LE, Connor AA, Gallinger S. Molecular events in the natural history of pancreatic cancer. Trends Cancer 2017;3:336–46.
31. Pylayeva-Gupta Y, Das S, Handler JS, Hajdu CH, Coffre M, Koralov SB, et al. IL35-producing B cells promote the development of pancreatic neoplasia. Cancer Discov 2016;6:247–55.
32. Lee KE, Spata M, Bayne LJ, Buza EL, Durham AC, Allman D, et al. Hif1a Deletion reveals pro-neoplastic function of B cells in pancreatic neoplasia. Cancer Discov 2016;6:256–69.
33. Ouzounova M, Lee E, Piranlioglu R, El Andaloussi A, Kolhe R, Demirci MF, et al. Monocytic and granulocytic myeloid derived suppressor cells differentially regulate spatiotemporal tumour plasticity during metastatic cascade. Nat Commun 2017;8:14979.
34. Villani AC, Satija R, Reynolds G, Sarkizova S, Shekhar K, Fletcher J, et al. Single-cell RNA-seq reveals new types of human blood dendritic cells, monocytes, and progenitors. Science 2017;356. pii: eaah4573.
35. Platzer B, Elpek KG, Cremasco V, Baker K, Stout MM, Schultz C, et al. IgE/FcεRI -mediated antigen cross-presentation by dendritic cells enhances anti-tumor immune responses. Cell Rep 2015. doi 10.1016/j.celrep.2015.02.015.
36. Ohlund D, Handly-Santana A, Biffi G, Elyada E, Almeida AS, Ponz-Sarvise M, et al. Distinct populations of inflammatory fibroblasts and myofibroblasts in pancreatic cancer. J Exp Med 2017;214:579–96.
37. Avery D, Govindaraju P, Jacob M, Todd L, Monslow J, Pure E. Extracellular matrix directs phenotypic heterogeneity of activated fibroblasts. Matrix Biol 2018;67:90–106.
38. Canto MI, Hruban RH, Fishman EK, Kamel IR, Schulick R, Zhang Z, et al. Frequent detection of pancreatic lesions in asymptomatic high-risk individuals. Gastroenterology 2012;142:796–804; quiz e14–5.
39. Nougaret S, Mannelli L, Pierredon MA, Schembri V, Guiu B. Cystic pancreatic lesions: from increased diagnosis rate to new dilemmas. Diagn Interv Imaging 2016;97:1275–85.
40. Klibansky DA, Reid-Lombardo KM, Gordon SR, Gardner TB. The clinical relevance of the increasing incidence of intraductal papillary mucinous neoplasm. Clin Gastroenterol Hepatol 2012;10:555–8.
41. de Jong K, Nio CY, Hermans JJ, Dijkgraaf MG, Gouma DJ, van Eijck CH, et al. High prevalence of pancreatic cysts detected by screening magnetic resonance imaging examinations. Clin Gastroenterol Hepatol 2010;8:806–11.
42. Vege SS, Ziring B, Jain R, Moayyedi P, Clinical Guidelines C, American Gastroenterology A. American gastroenterological association institute guideline on the diagnosis and management of asymptomatic neoplastic pancreatic cysts. Gastroenterology 2015;148:819–22; quize12–3.
43. European Study Group on Cystic Tumours of the P. European evidence-based guidelines on pancreatic cystic neoplasms. Gut 2018;67:789–804.
44. Lee SY, Lee KT, Lee JK, Jeon YH, Choi D, Lim JH, et al. Long-term follow up results of intraductal papillary mucinous tumors of pancreas. J Gastroenterol Hepatol 2005;20:1379–84.
45. Nara S, Onaya H, Hiraoka N, Shimada K, Sano T, Sakamoto Y, et al. Preoperative evaluation of invasive and noninvasive intraductal papillary-mucinous neoplasms of the pancreas: clinical, radiological, and pathological analysis of 123 cases. Pancreas 2009;38:8–16.
46. Sadakari Y, Ienaga J, Kobayashi K, Miyasaka Y, Takahata S, Nakamura M, et al. Cyst size indicates malignant transformation in branch duct intraductal papillary mucinous neoplasm of the pancreas without mural nodules. Pancreas 2010;39:232–6.
47. Yonezawa S, Horinouchi M, Osako M, Kubo M, Takao S, Arimura Y, et al. Gene expression of gastric type mucin (MUC5AC) in pancreatic tumors: its relationship with the biological behavior of the tumor. Pathol Int 1999;49:45–54.
48. Jones S, Zhang X, Parsons DW, Lin JC, Leary RJ, Angenendt P, et al. Core signaling pathways in human pancreatic cancers revealed by global genomic analyses. Science 2008;321:1801–6.
49. Kalluri R. The biology and function of fibroblasts in cancer. Nat Rev Cancer 2016;16:582–98.
50. Chang JH, Jiang Y, Pillarisetty VG. Role of immune cells in pancreatic cancer from bench to clinical application: an updated review. Medicine (Baltimore) 2016;95:e5541.
51. Moffitt RA, Marayati R, Flate EL, Volmar KE, Loeza SG, Hoadley KA, et al. Virtual microdissection identifies distinct tumor- and stroma-specific subtypes of pancreatic ductal adenocarcinoma. Nat Genet 2015;47:1168–78.
52. Shiga K, Hara M, Nagasaki T, Sato T, Takahashi H, Takeyama H. Cancer-associated fibroblasts: their characteristics and their roles in tumor growth. Cancers (Basel) 2015;7:2443–58.
53. Xu C, Zhao H, Chen H, Yao Q. CXCR4 in breast cancer: oncogenic role and therapeutic targeting. Drug Des Devel Ther 2015;9:4953–64.
54. Jiang YM, Li G, Sun BC, Zhao XL, Zhou ZK. Study on the relationship between CXCR4 expression and perineural invasion in pancreatic cancer. Asian Pac J Cancer Prev 2014;15:4893–6.
55. Tsai MF, Chang TH, Wu SG, Yang HY, Hsu YC, Yang PC, et al. EGFR-L858R mutant enhances lung adenocarcinoma cell invasive ability and promotes malignant pleural effusion formation through activation of the CXCL12-CXCR4 pathway. Sci Rep 2015;5:13574.
56. Mitchell B, Mahalingam M. The CXCR4/CXCL12 axis in cutaneous malignancies with an emphasis on melanoma. Histol Histopathol 2014;29:1539–46.
57. Zhang J, Liu C, Mo X, Shi H, Li S. Mechanisms by which CXCR4/CXCL12 cause metastatic behavior in pancreatic cancer. Oncol Lett 2018;15:1771–6.
58. Cui K, Zhao W, Wang C, Wang A, Zhang B, Zhou W, et al. The CXCR4-CXCL12 pathway facilitates the progression of pancreatic cancer via induction of angiogenesis and lymphangiogenesis. J Surg Res 2011;171:143–50.

59. Sleightholm RL, Neilsen BK, Li J, Steele MM, Singh RK, Hollingsworth MA, et al. Emerging roles of the CXCL12/CXCR4 axis in pancreatic cancer progression and therapy. Pharmacol Ther 2017;179:158–70.
60. Feig C, Jones JO, Kraman M, Wells RJ, Deonarine A, Chan DS, et al. Targeting CXCL12 from FAP-expressing carcinoma-associated fibroblasts synergizes with anti-PD-L1 immunotherapy in pancreatic cancer. Proc Natl Acad Sci U S A 2013;110:20212–7.
61. Azizi E, Carr AJ, Plitas G, Cornish AE, Konopacki C, Prabhakaran S, et al. Single-cell immune map of breast carcinoma reveals diverse phenotypic states driven by the tumor microenvironment. Cell 2018;174:1293–308. e36. PMID: 29961579.
62. Gabrilovich DI. Myeloid-derived suppressor cells. Cancer Immunol Res 2017;5:3–8.
63. Gentles AJ, Newman AM, Liu CL, Bratman SV, Feng W, Kim D, et al. The prognostic landscape of genes and infiltrating immune cells across human cancers. Nat Med 2015;21:938–45.
64. Kumar V, Donthireddy L, Marvel D, Condamine T, Wang F, Lavilla-Alonso S, et al. Cancer-associated fibroblasts neutralize the anti-tumor effect of CSF1 receptor blockade by inducing PMN-MDSC infiltration of tumors. Cancer Cell 2017;32:654–68e5.
65. Barua S, Solis L, Parra ER, Uraoka N, Jiang M, Wang H, et al. A functional spatial analysis platform for discovery of immunological interactions predictive of low-grade to high-grade transition of pancreatic intraductal papillary mucinous neoplasms. Cancer Inform 2018;17:1176935118782880.
66. Zhang Y, Velez-Delgado A, Mathew E, Li D, Mendez FM, Flannagan K, et al. Myeloid cells are required for PD-1/PD-L1 checkpoint activation and the establishment of an immunosuppressive environment in pancreatic cancer. Gut 2017;66:124–36.
67. Kiss M, Van Gassen S, Movahedi K, Saeys Y, Laoui D. Myeloid cell heterogeneity in cancer: not a single cell alike. Cell Immunol 2018; 330:188–201.
68. Ziegenhain C, Vieth B, Parekh S, Reinius B, Guillaumet-Adkins A, Smets M, et al. Comparative analysis of single-cell RNA sequencing methods. Mol Cell 2017;65:631–43e4.
69. Svensson V, Natarajan KN, Ly LH, Miragaia RJ, Labalette C, Macaulay IC, et al. Power analysis of single-cell RNA-sequencing experiments. Nat Methods 2017;14:381–7.
70. Picelli S, Bjorklund AK, Faridani OR, Sagasser S, Winberg G, Sandberg R. Smart-seq2 for sensitive full-length transcriptome profiling in single cells. Nat Methods 2013;10:1096–8.
71. Lacar B, Linker SB, Jaeger BN, Krishnaswami SR, Barron JJ, Kelder MJE, et al. Nuclear RNA-seq of single neurons reveals molecular signatures of activation. Nat Commun 2016;7:11022.

Published OnlineFirst November 1, 2018; DOI: 10.1158/1078-0432.CCR-18-1955

Clinical Cancer Research

Single-Cell Transcriptomics of Pancreatic Cancer Precursors Demonstrates Epithelial and Microenvironmental Heterogeneity as an Early Event in Neoplastic Progression

Vincent Bernard, Alexander Semaan, Jonathan Huang, et al.

Clin Cancer Res 2019;25:2194-2205. Published OnlineFirst November 1, 2018.

BJC British Journal of Cancer

www.nature.com/bjc

ARTICLE

Molecular Diagnostics

Characterisation of circulating tumour cell phenotypes identifies a partial-EMT sub-population for clinical stratification of pancreatic cancer

Alexander Semaan[1,2], Vincent Bernard[1,2], Dong U. Kim[1,2,3], Jaewon J. Lee[1,4], Jonathan Huang[1,2], Nabiollah Kamyabi[1,2,5], Bret M. Stephens[1,2], Wei Qiao[6], Gauri R. Varadhachary[7], Matthew H. Katz[4], Yu Shen[6], Francis Anthony San Lucas[8], Peter Gascoyne[9], Hector A. Alvarez[8], Anirban Maitra[1,2] and Paola A. Guerrero[1,2]

BACKGROUND: Limited accessibility of the tumour precludes longitudinal characterisation for therapy guidance in pancreatic ductal adenocarcinoma (PDAC).

METHODS: We utilised dielectrophoresis-field flow fractionation (DEP-FFF) to isolate circulating tumour cells (CTCs) in 272 blood draws from 74 PDAC patients (41 localised, 33 metastatic) to non-invasively monitor disease progression.

RESULTS: Analysis using multiplex imaging flow cytometry revealed four distinct sub-populations of CTCs: epithelial (E-CTC), mesenchymal (M-CTC), partial epithelial-mesenchymal transition (pEMT-CTC) and stem cell-like (SC-CTC). Overall, CTC detection rate was 76.8% (209/272 draws) and total CTC counts did not correlate with any clinicopathological variables. However, the proportion of pEMT-CTCs (prop-pEMT) was correlated with advanced disease, worse progression-free and overall survival in all patients, and earlier recurrence after resection.

CONCLUSION: Our results underscore the importance of immunophenotyping and quantifying specific CTC sub-populations in PDAC.

British Journal of Cancer https://doi.org/10.1038/s41416-021-01350-9

BACKGROUND

Pancreatic ductal adenocarcinoma (PDAC) is projected to be the second leading cause of cancer-related deaths within the next decade and continues to have a dismal 5-year survival rate of 9%.[1] Almost 80% of patients are diagnosed at locally advanced or metastatic stages and current treatment options are mostly limited to cytotoxic agents. Even with seemingly curative resection for patients presenting with localised disease many patients suffer early recurrence, suggesting an underlying propensity for early dissemination and resistance to available treatments.[2]

Elucidation of tumour cell phenotypes as they evolve during therapy can provide predictive insights into emergence of resistance to standard of care therapies in PDAC. A recently applied strategy to profile such dynamic changes in real time has involved the study of disseminated cancer cells, better known as circulating tumour cells (CTCs).[3] As obtaining serial biopsies from primary or metastatic lesions in PDAC is clinically challenging, liquid biopsies have gained traction in recent years for understanding tumour kinetics under therapy. As opposed to circulating tumour DNA (ctDNA) and exosomes, CTCs provide the added benefit of representing the phenotypic characteristics of their tumour of origin.[4]

Classically, CTC isolation has involved the use of epithelial biomarkers such as cytokeratin and epithelial cell adhesion molecule (EpCAM) through immunogenic capture techniques such as CellSearch®, and their enumeration has shown to be a useful clinical prognosticator in breast, prostate, lung and colorectal cancers.[5–8] However, a predictive model utilising CTCs as a biomarker has yet to demonstrate strong evidence for clinical validity in PDAC.[9] Specifically, the role of CTC sub-populations, including those with non-epithelial characteristics, in clinical stratification remains to be elucidated through a comprehensive unbiased approach. Additionally, other CTC phenotypes such as circulating tumour microemboli (CTMs) may represent unique tumour capabilities such as increased metastatic propensity.[10,11] As such, uncovering the dynamic nature of evolving CTC phenotypes correlating to tumour progression and therapeutic response is of clinical importance but poorly characterised, mostly

[1]Department of Translational Molecular Pathology, The University of Texas MD Anderson Cancer Center, Houston, TX, USA; [2]Sheikh Ahmed Center for Pancreatic Cancer Research, The University of Texas MD Anderson Cancer Center, Houston, TX, USA; [3]Department of Gastroenterology and Biomedical Research Institute, Pusan National University Hospital, Pusan National University School of Medicine, Busan, Korea; [4]Department of Surgical Oncology, The University of Texas MD Anderson Cancer Center, Houston, TX, USA; [5]Department of Bioengineering, Rice University, Houston, TX, USA; [6]Department of Biostatistics, The University of Texas MD Anderson Cancer Center, Houston, TX, USA; [7]Department of Gastrointestinal Medical Oncology, The University of Texas MD Anderson Cancer Center, Houston, TX, USA; [8]Deparment of Hematopathology, The University of Texas MD Anderson Cancer Center, Houston, TX, USA and [9]Advance Electrofluidic System Ilc, Houston, TX, USA

Correspondence: Paola A. Guerrero (paguerrero@mdanderson.org)

These authors contributed equally: Alexander Semaan, Vincent Bernard, Dong U. Kim

Received: 22 May 2020 Revised: 20 January 2021 Accepted: 4 March 2021
Published online: 30 March 2021

due to a limitation of current enumeration strategies that only utilise epithelial and hematopoietic markers, restricting the definition of a CTC and potentially biasing its quantification. Ultimately, whether certain sub-populations of CTCs may be more clinically relevant than others remains undetermined.[12,13]

In order to perform a comprehensive phenotypic characterisation of PDAC CTCs, we used an epitope-independent isolation approach utilising a microfluidics-based dielectrophoresis enrichment strategy, followed by a multiplexed immunostaining assay.[14–16] This approach provides the opportunity to profile the morphologic and phenotypic characteristics of these cells while bypassing the enrichment of epithelial cells. We evaluated its capability for the isolation of CTCs with different phenotypes and their clinical significance in a longitudinal cohort of PDAC patients.

METHODS

Study population

Between April 2015 and January 2018, 74 patients were consented at MD Anderson Cancer Center (MDACC) under protocol number PA14-0867 and PA11-0670. Cohort details are shown in Table 1. The study was performed in accordance with standard ethical guidelines approved by the institutional review board (IRB) and in accordance with the Declaration of Helsinki. All patients had clinically and histologically confirmed localised or metastatic PDAC.

Cell Lines

Human pancreatic cell lines PANC-1, MIAPaCa-2 and HPAFII, Cancer associated fibroblast-19 (CAF-19) and Human brain microvascular endothelial cells (HBMEC) were used as controls. All cell lines were authenticated using a short tandem repeat (STR) DNA test.

Table 1. Patient demographics and clinicopathological characteristics.

Cohorts characteristics	Patients
Total patient number	74
Peripheral blood samples	272
Mean age	62.1 years (range 31–82 years)
Gender	
Men	42 (56.8%)
Women	32 (43.2%)
Median follow-up time per patient	15.4 months
Localised disease	41 (66.4%)
Metastatic	33 (45.6%)
Localised group: neoadjuvant treatment	36/41 (87.8%)
AJCC staging	
I	9 (12.2%)
II	22 (29.7%)
III	10 (13.5%)
IV	33 (44.6%)
Metastasis side	
Liver	23 (69.7%)
Lung	7 (21.2%)
Others (peritoneum, distant lymph nodes)	3 (9.1)
Tumour location	
Head	56 (75.7%)
Tail/Body	18 (24.3%)
Treatment status	
Baseline treatment-naïve	65
Baseline treated (palliative and neoadj.)	9

Blood sample collection and processing

Whole-blood samples were collected in acid citrate dextrose tubes (BD, Franklin, Lakes NY) and processed within 4 h of phlebotomy. Upon arrival, whole blood was centrifuged at 2500 × *g* for 10 mins, plasma was removed and peripheral blood mononuclear cells (PBMCs) were isolated using Lymphocyte Separation Medium (Corning, Corning, NY) and centrifugation at 620 × *g* for 30 min. PBMCs were stored at −80 °C in CryoStor® CS10 (Stemcell, Vancouver, Canada).

Microfluidic device and sample preparation

Circulating tumour cells were isolated utilising dielectrophoresis-field flow fractionation (DEP-FFF).[14,17] The underlying concept of isolation takes advantage of the difference in "crossover frequency" (a parameter that depends on cell size and membrane surface area) of different cell types. Cells can be manipulated by a heterogeneous alternating electric field generated by electrodes in a low conductivity suspending medium. Below a field crossover frequency, cells are repelled from electrodes and above that frequency they are attracted to them. The crossover frequency for different cell types depends sensitively on their sizes and membrane surface areas. To isolate CTCs, we choose a suspension conductivity and electric field frequency to attract CTCs towards electrodes while repelling PBMCs.[14,16] In our long, flat DEP-FFF chambers, a low conductivity, isotonic elution medium flows at a constant rate of 1.2 mL/min. The specimen is injected from a slit to form a 25-µm layer adjacent to it. Ions and non-ionic molecules exchange by diffusion between the adjacent specimen and elution flows, reducing the conductivity near the cells while maintaining their tonicity. Further along the chamber, the cells pass over a microelectrode array energised at the frequency chosen to attract CTCs and repel PBMCs. A 20-µm layer of the flow closest to the electrode surface, and containing the CTCs, is then skimmed off into culture medium and kept on ice. The chambers are installed vertically to eliminate the influence of gravity in positioning the cells.

In order to deplete ions enough for DEP separation, a running buffer containing 181 mM D-Mannitol (Sigma–Aldrich, St. Louis, MO), 67 mM Dextrose (Sigma–Aldrich), 1 mg/mL Kolliphor P188 (Sigma–Aldrich), 12.5% OptiPrep (Sigma–Aldrich) and 9 mM HEPES (Corning) was used. Buffy coats were thawed and resuspended in 0.46 mL of DMEM (Thermo Fisher, Carlsbad) supplemented with 10% FBS (Corning) and penicillin/streptomycin (Corning). 0.1 mL of 1 mg/ml DNase (StemCell) was added and samples were incubated at room temperature for 5 min. 0.44 mL of Cell density correction buffer (87 mM D-Mannitol, 170.4 mM Dextrose, 2.3 mg/mL Kolliphor P188, 20% OptiPrep and 22.7 mM HEPES) was added and samples were loaded into a 1 mL syringe. Samples were injected into the microfluidic device at a constant rate of 25 ul/min and a DEP current of ~0.2 A. The eluate parameters were: flow rate of ~1.2 mL/min, frequency of 45–90 kHz, conductivity of 20–40 ms/m.

Immunofluorescence and ImageStream

Samples collected through the microfluidic device were stained with antibodies against EpCAM conjugated to PE Cy7 (eBiosciences, San Diego, CA), CD133 conjugated to PE (Miltenyi Biotec, Bergisch Gladbach, Germany) and CD45 conjugated to Alexa 700 (Thermo Fisher). Then samples were fixed with 4% paraformaldehyde and permeabilised with 0.1% Triton X-100 (Sigma–Aldrich). This was then followed by staining with anti-vimentin conjugated to eFluor 615 (eBiosciences) and anti-CK conjugated to FITC (Thermo Fisher). Finally, DAPI was added and samples were analysed through Amnis ImageStream Mark II imaging Flow Cytometer (Millipore Sigma, Burlington, MA). In order to establish a reliable pipeline to classify all clinical samples, we first analysed well-characterised PDAC cell lines (PANC-1, MIAPaCa-2 and HPAFII) through this process. Once an expression threshold was

determined (after compensation and gating), the same scheme was applied to clinical samples.

Predictive value of CTCs and statistical analysis

Regarding the CTC counts, receiver operating characteristic (ROC) curves and corresponding area of the curve (AUC) were utilised to identify the threshold values for predicting progressive disease. The Youden index was used to determine the cut point with the optimised sensitivity and specificity. The distribution of each continuous variable was summarised by its mean, standard deviation median, interquartile range. The distribution of each categorical variable was summarised in terms of its frequencies and percentages. Continuous variables were compared between two groups by Wilcoxon rank sum test, or by Kuskal-Wallis test if there are more than two groups. Survival curves were estimated using the Kaplan–Meier method, where overall survival is defined as time period from initial diagnosis to death of any reason, and the survival time was censored if the patient was alive at the last follow-up time. Progression-free survival was defined as time from day of first therapy to progression based on most recent RECIST 1.1 criteria or censored at the last follow-up. Log rank tests were used to compare the time-to-event variables between groups. The Cox proportional hazards regression model was used to evaluate the association between patient prognostic variables and overall survival or progression-free survival. If a continuous variable is highly skewed, the appropriate transformation (e.g. log transformation) was applied before modelling. The variables with $p \le 0.2$ under univariate analyses were included into the initial multivariable Cox model. Backward model selection was used to remove variables from the model until all remaining variables were statistically significant with $p < 0.05$. Statistical analyses were performed with SPSS statistical software, version 24 (IBM, Armonk, NY), Prism 8 (GraphPad Software, Inc, San Diego, USA) and SAS (SAS Institute Inc, Cary, NC). Statistical significance was defined as a p-value of <0.05.

RESULTS

Dielectrophoretic based isolation of heterogeneous CTC sub-populations

DEP-FFF enables epitope-independent isolation of viable CTCs based on physical cell properties including the diameter and surface rigidity.[14–16] This allows for the capture of distinct sub-populations of CTCs within an hour of blood processing time. In order to demonstrate our capture efficiency, we performed spike-in experiments utilising a PDAC cell line, PANC-1, into healthy human peripheral blood mononuclear cells (PBMCs). Spike-ins of 10, 100, 200, 500, 1000 and 1,200 ($n = 3$ replicates for each) cells revealed recovery rates of up to 91% (average recovery rate 89.1%) with high linearity ($R^2 = 0.9873$, Fig. 1a). Our ability to capture and characterise multiple unbiased CTC sub-populations was also tested by adding different PDAC cell lines with known phenotypes of interest, including epithelial (HPAFII), mesenchymal (MIAPaCa-2) and stem cell-like (PANC-1 spheroids) subtypes. These cell lines were successfully "re-identified" following DEP isolation, where cells were stained with anti-CD45, EpCAM, pan-cytokeratin (PanCK), vimentin and CD133 antibodies, as well as DAPI (Fig. 1b). Based on characterisation of isolated PDAC cells using DEP and imaging flow cytometry with distinct epithelial, mesenchymal and stem-cell markers, we defined four distinct sub-populations in the peripheral blood of patients with PDAC using expression of markers listed above—epithelial (E-CTC),

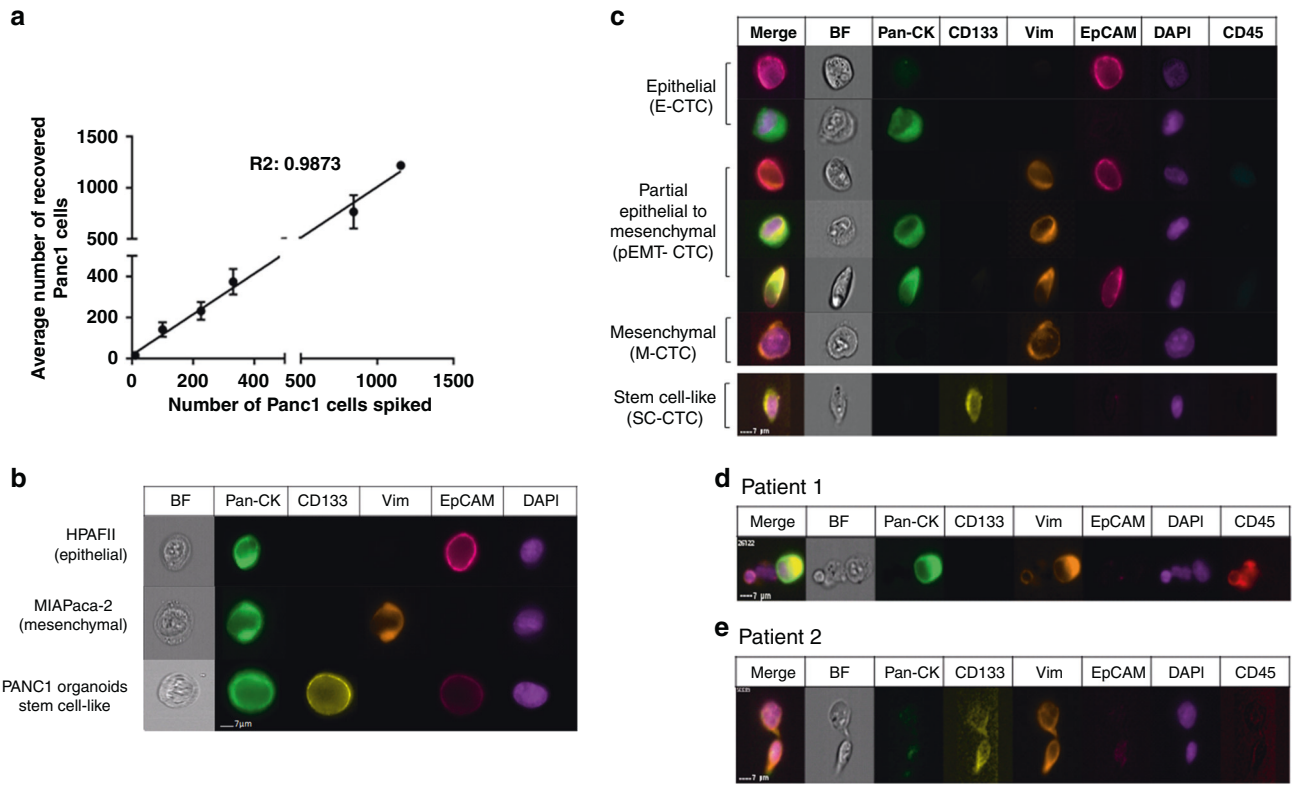

Fig. 1 Capture efficiency of epitope-independent microfluidics device. a Scatter plot showing known cell numbers added to PBMC and number of cells recovered from DEP-FFF, **b** Brightfield and immunofluorescence images of marker proteins of different cell lines recovered using DEP-FFF and analysed by imagestream flow cytometry. BF Brightfield, Pan-CK pan-cytokeratin, Vim vimentin, EpCAM epithelial cell adhesion molecule, DAPI 4′,6-Diamidin-2-phenylindol and CD45 Protein tyrosine phosphatase, receptor type C. Brightfield and immunofluorescence images of CTC populations (**c**) CTCs lymphocytes (**d**) and CTC–CTC clusters (**e**) identified in PDAC patients by ImageStream.

mesenchymal (M-CTC), bi-phenotypic or partial epithelial-mesenchymal transition (pEMT-CTC) and stem cell-like (SC-CTC) —based on markers of interest (Table 2). CTCs were further curated based on characteristic size (>14 µm) and distinct nuclear structure covering >80% of the cell surface (Fig. 1c). In addition to single CTCs, this technique was able to isolate CTCs associated with lymphocytes as well as clusters of CTCs (Fig. 1d, e).

Patient characteristics

A total of 74 patients (mean age 62.1 years, range 31–82 years) with histologically proven PDAC between April 2015 and January 2018 were enrolled in the study (Table 1). From these patients, 272 peripheral blood samples were collected and processed through DEP (median number of blood draws/patient = 3.0, range 1–9). The median follow-up time for all patients was 15.4 months (range 0–43.1 months). Longitudinal follow-up samples were obtained during routine clinical follow-up appointments for patients enrolled in the protocol before administration of chemotherapy and together with clinically necessary blood draws. The cohort was stratified into two groups: 41 out of 74 (55.4%) with localised disease and 33 out of 74 (44.6%) patients with metastatic disease. In the localised disease group, 36 of 41 received neoadjuvant treatment (87.8%), of which 27% (10/36) progressed under treatment and therefore did not receive surgery. Twenty-two patients underwent resection of the primary tumour (22/41, 53.6%) with mostly R0 resections (18/22, 78.6%). In addition, 4/41 (9.8%) patients underwent surgical exploration without resection due to intraoperative diagnosis of metastasis and 5/41 (12.2%) patients did not receive an operation due to comorbidities. In the metastatic disease group, 22/33 (67.7%) progressed on therapy during a median follow-up of 6.2 months (range 0–23.5 months). In patients with metastatic disease, baseline draws were untreated in 8/33 (24%) of cases while 25/33 were treated (75%). In addition, 21/33 (64%) have progression samples collected. The average number of draws was 3.8 (1–7 range) and the average time between draws was 80.5 days (26–294 range).

Table 2. Defined subtypes to classify patient-derived CTCs.

Phenotypes identified	Markers
E-CTC	$CD45^-$, $EpCAM^+$ and/or $Pan\text{-}CK^+$, $DAPI^+$
pEMT-CTC	$CD45^-$, $EpCAM^+$ and/or $Pan\text{-}CK^+$, Vim^+, $DAPI^+$
M-CTC	$CD45^-$, $EpCAM^-$, Vim^+, $DAPI^+$
SC-CTC	$CD45^-$, $CD133^+$, $DAPI^+$

CTC counts in overall PDAC cohort

Overall CTC detection rate across all samples, and including single CTCs and clusters, was 76.8% (209/272 samples, range 0–692 cells/7.5 ml of blood). Mean number of CTCs per 7.5 ml of blood was 29 ± 70.6 (range 0–692). Across all samples, mean numbers of CTCs were as follows: E-CTC: 3.5 ± 1.1 cells/7.5 ml (12.2%), M-CTC: 9.3 ± 1.5 cells/7.5 ml (31.9%), pEMT-CTC: 13.8 ± 2.1 cells/7.5 ml (47.7%) and SC-CTC: 2.4 ± 0.5 cells/7.5 ml (8.2%) (Fig. 2a).

In treatment naïve patients at baseline ($n = 65$), mean total CTC number was 41.2 ± 62.7 and per sub-type: E-CTC-1.5 ± 0.6 cells/7.5 ml (3.7%), M-CTC 13.8 ± 2.9 cells/7.5 ml (33.5%), pEMT-CTC 21.0 ± 4.05 cells/7.5 ml (51.1%) and SC-CTC 4.8 ± 2.1 cells/7.5 ml (11.7%) (Fig. 2b). CTC clusters were identified in 32/65 (49.2%, range 0–18 clusters) treatment-naive patients with a mean

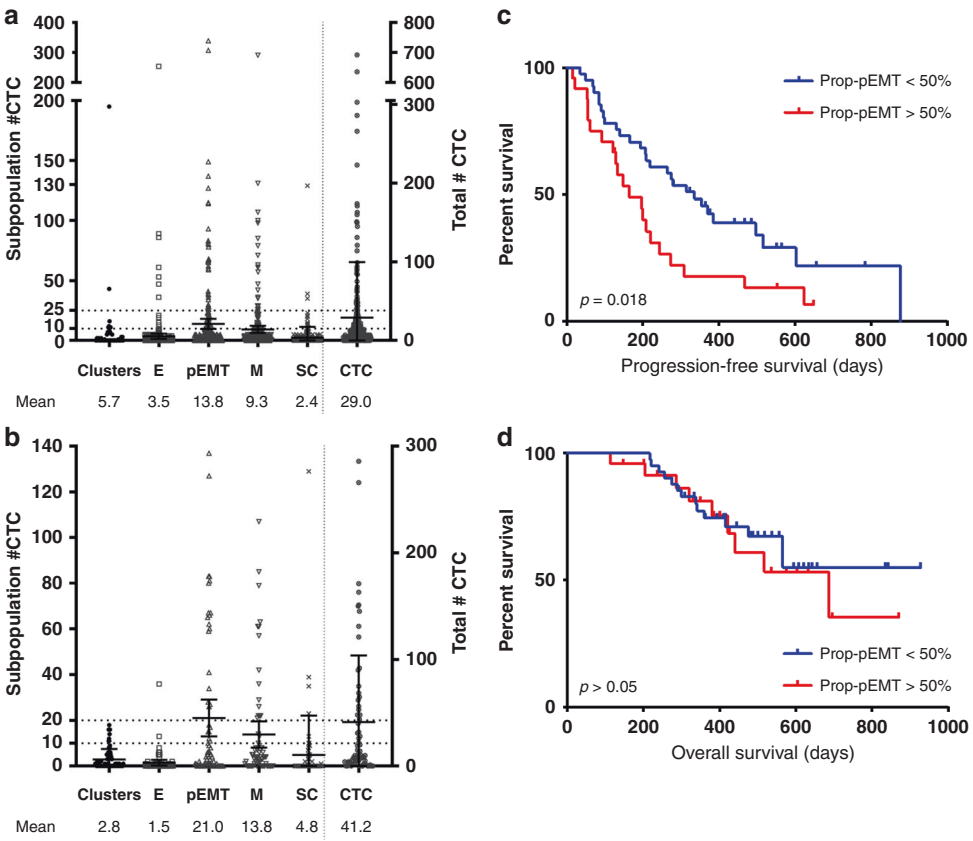

Fig. 2 Number of CTCs identified in PDAC patients. a Scatter plot showing total counts in five phenotypically distinct populations across all collected samples ($n = 272$) or at baseline treatment naïve status ($n = 65$). **b** Last column shows all counts. Prognostic value of CTCs at baseline treatment-naïve status ($n = 65$). **c** Progression-free survival comparing patients with more vs. less than 50% Prop-pEMT ($p = 0.018$). **d** Overall survival comparing patients with more vs. less than 50% Prop-pEMT ($p = 0.63$).

2.6 ± 12.6 cells/7.5 ml in all draws and 2.8 ± 4.6 cells/7.5 ml in BTN patients only (Fig. 2a, b).

Notably, there was no difference in total CTC counts at baseline ($n = 65$) based on tumour location, stage and size (all $p > 0.05$, Supplementary Table 1, Supplementary Fig. 1A-D). However, the proportion of pEMT-CTC relative to total CTC count ("Prop-pEMT") was significantly higher in M1 vs. M0 patients (mean 52.4% vs 28.4%, $p = 0.004$, Supplementary Fig. 1E, Supplementary Table 1). Additionally, "Prop-pEMT" increased with stage (stage I: 24.4 ± 26.9%, stage II: 28.5 ± 23.5%, stage III: 32.4 ± 35.1%, stage IV: 52.0 ± 33.5%, $p = 0.0024$, Supplementary Fig. 1F, Supplementary Table 1) and with distal tumour location (head: 33.5 ± 29.1%, tail/body: 54.2 ± 35.2%, $p = 0.04$) Supplementary Fig. 1G Supplementary Table 1).

Liquid biopsies of all patients ($n = 139$) while on therapy demonstrated that those with progressive disease based on RECIST criteria, compared to those with blood draws on therapy but without progression had significantly more total CTCs ($p = 0.0162$), E-CTCs ($p = 0.0489$), M-CTCs ($p = 0.0087$) and higher Prop-pEMT ($p = 0.0410$) (Supplementary Fig. 2 and Supplementary Table 2).

Baseline treatment-naïve (BTN, $n = 65$) patients with a higher proportion of pEMT-CTC ≥ 50% showed a significantly worse progression-free survival (PFS) compared to patients with a lower pEMT-CTC proportion on univariate analysis ($p = 0.020$, Fig. 2c, Supplementary Table 3B, 4). On multivariate analysis, proportion of pEMT-CTC remains significantly associated to poorer PFS (HR 1.98, 95% CI 1.05–3.73, $p = 0.036$) after adjusting for other factors (Supplementary Table 3A-C). Proportion of pEMT-CTC showed no impact on overall survival in BTN patients (Fig. 2d). In addition, disease stage had a significant impact on PFS (p-value = 0.009), but was not a significant factor (p-value = 0.190) in the multivariable model after adjusting for pEMT-CTC, log transformed SC, and age (Supplementary Table 3C). No other subgroup showed a significant prognostic value at BTN status (all, $p > 0.05$; Supplementary Table 3A-B and Supplementary Table 5) including total pEMT counts at different cut-offs (Supplementary Table 6).

CTC counts in localised disease

Among patients with localised disease, mean CTC counts (including single CTCs and clusters) dropped significantly following resection across total, pEMT, EMT subgroups and clusters (Fig. 3a–f), but did not drop to zero in any patient. Among resected patients, seven (7/22, 31.8%) had an early recurrence within 12 months after surgical resection. Patients with "Prop-pEMT" > 50% in preoperative blood draws ($n = 22$) were at higher risk for an early recurrence (4/7 (57.1%) versus 1/15 (6.7%), $p = 0.02$, Fig. 3g). Similarly, patients with preoperative "Prop-pEMT" >50% showed a worse overall survival (OS) after resection (677 days versus not reached $p = 0.01$, Fig. 3h). None of the other CTC sub-populations showed a significant impact on early recurrence rate or OS (all $p > 0.05$, Supplementary Table 7).

CTC counts in metastatic disease

In treatment naïve patients with M1 disease ($n = 29$), the presence of at least one pEMT-CTC at baseline was significantly associated with decreased overall survival compared to patients with undetectable pEMT-CTCs (325.2 ± 28.0 days vs. 731.0 ± 67.8 days, $p < 0.001$, Fig. 3i). Liquid biopsies of M1 patients while on therapy ($n = 132$) demonstrated that those with progressive disease had significantly more M-CTCs (13.5 ± 23.0 cells/draw vs. 4.2 ± 10.3 cells/draw, $p = 0.005$).

Molecular characterisation of different CTC sub-populations

To further characterise isolated CTCs, we performed droplet digital PCR (ddPCR) for mutant *KRAS* as previously described,[18] in captured cells from a patient with metastatic PDAC following progressive disease in the liver. Cells were isolated by DEP-FFF from a single draw at the time of progression. They were then stained as described and FACS sorted in either pools of 10 cells prior to amplification (CTC-2, Vim^+ and CTC-3, Vim^+), or amplified as single cells (CTC-1, $E^+/CK^+/Vim^{+/-}$) depending on the number of cells captured. Whole-genome amplification of sorted cells was performed with the REPLI-g Single Cell Kit (Qiagen) per the manufacturer's protocol. In addition, three pools of 10 CD45+ cells were also isolated and amplified and used as wild-type control and paired tumour tissue from the metastatic side was used as positive control (Table 3). Mutant *KRAS* was detected in all three CTCs (mutant allele fraction (MAF) 1.27, 84.3 and 78.4, respectively) and in the tumour sample (MAF 50.22) while all three CD45+ cells were *KRAS* negative. Additionally, to better characterise the M phenotype and exclude other cell populations that also expressed Vimentin, $CD31^+/Vim^+$ and FAP^+/Vim^+ cells were analysed in three clinical samples (Supplementary Fig. 3). In all three cases, we did not detect a single FAP^+/Vim^+ or $CD31^+Vim^+$ cells instead, we detected ~1% of CD45− cells expressing CD31 or FAP in combination with Vim and CK.

DISCUSSION

In visceral tumours, such as PDAC, repeated tumour sampling for therapy monitoring and molecular profiling is rarely performed in the clinical setting due to their invasive nature and cost. Thus, strategies involving liquid biopsies have gained traction for their minimally invasive approach in cancer diagnosis, prognostication, therapy stratification and measuring response to therapy. In this study, we interrogated if longitudinal characterisation of CTC sub-populations may better resolve the prognostic and predictive utility of this liquid biopsy compartment. We also describe CTC phenotypes that may be most relevant to metastasis and chemoresistance, which have been previously correlated with the presence of cancer stem cells or cells with epithelial-mesenchymal transition (EMT) profiles.[19,20]

Biased immunogenic capture of CTCs based on epithelial markers potentially excludes cells that have biological implications in the process of metastasis and chemoresistance.[21,22] Even among epithelial markers typically used for CTC capture, such as EpCAM or cytokeratins, there is no consensus regarding specific marker(s) that may more effectively identify clinically relevant CTCs. Utilising DEP-FFF, which allows for isolation of particles based on their physical properties, we isolated CTCs through an antigen independent approach. In doing so, we effectively isolated phenotypically distinct CTC populations that may be grouped into four major sub-populations based on our multiplexed immunostaining assay: E-CTC, M-CTC, pEMT-CTC and SC-CTC

Similar to previous work,[23–26] the most common sub-population of PDAC CTCs expressed a combination of epithelial and mesenchymal markers (pEMT-CTC), representing neoplastic cells arrested in a "bi-phenotypic" state as they are shed from their tumour of origin.[21,22,27] Increasing evidence suggests that EMT is a highly dynamic process, inclusive of intermediate cell states ("pEMT"), such that only a minority of cancer cells transition to a pure mesenchymal state.[22,27,28] Notably, neoplastic cells with a partial-EMT phenotype show greater invasiveness and therapeutic resistance,[22] which coincides with our findings of this CTC sub-population correlating with both stage at presentation, as well as with progression on therapy. Specifically, we demonstrate that "prop-pEMT" (the proportion of CTCs with pEMT phenotype overall CTCs) are higher in patients with metastases at diagnosis. Additionally, whereas there are no effective methods for stratification of early recurrence risk in resectable PDAC, we demonstrate that a high "prop-pEMT" at the time of surgery is correlated with early recurrence. Importantly, CTC numbers rarely dropped to zero even after complete surgical resection, which is in-line with recent studies.[5,25] This raises the concern that micro-

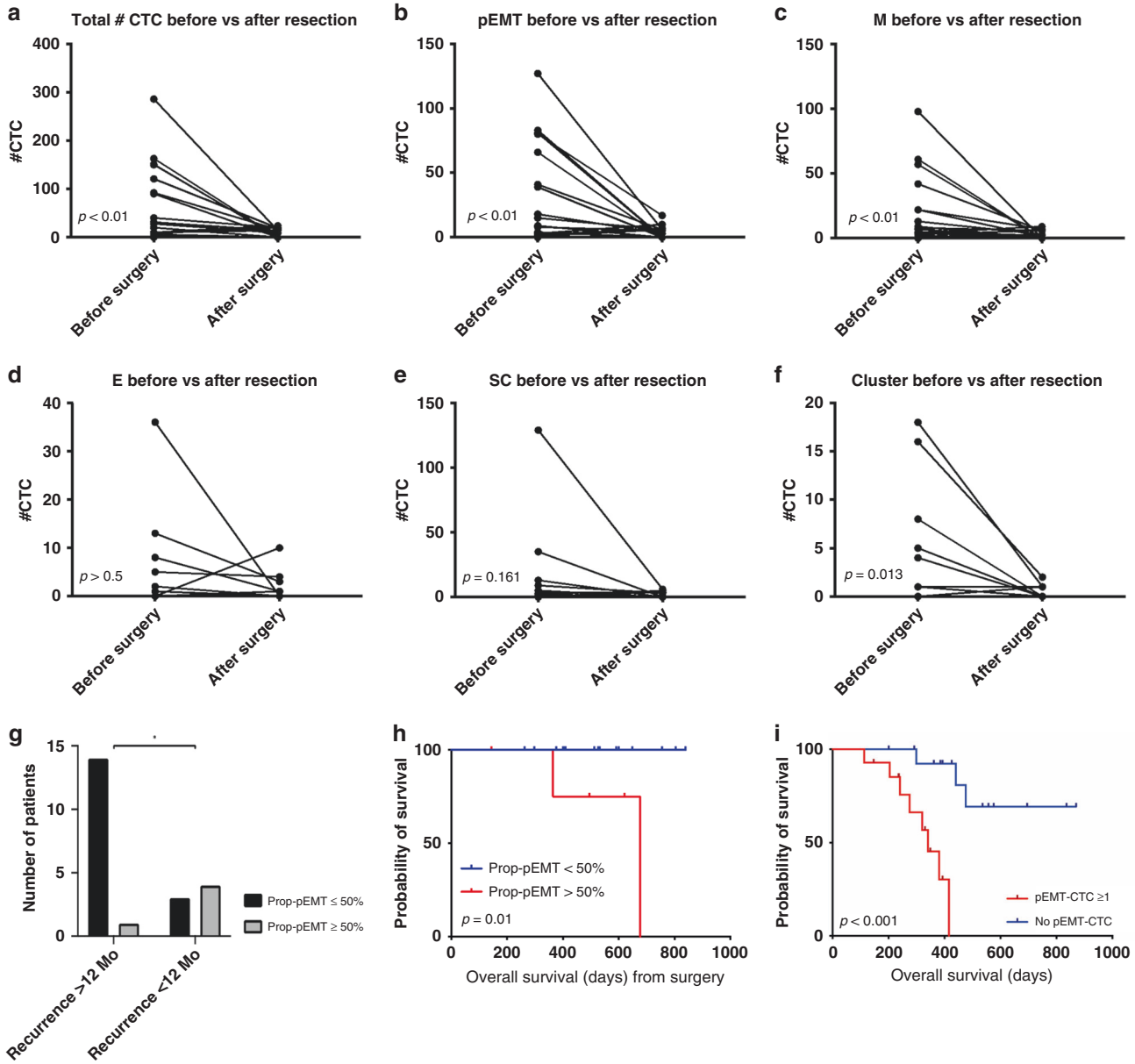

Fig. 3 Comparison of total counts in sub-populations. a total CTCs, **b** pEMT-CTC, **c** M-CTC, **d** E-CTC, **e** SC-CTC, **f** CTC clusters before and after surgery ($n = 22$). Prognostic value of CTCs at draw closest to surgery. **g** Bar graph plotting Prop-pEMT ≥ 50% vs. recurrence status (Fisher exact test, $p = 0.021$). **h** Kapla–Meier plot (overall survival from surgery) comparing patients with vs. without 50% Prop-pEMT ($p = 0.01$). **i** Overall survival comparing patients with at least one pEMT-CTC vs none ($p < 0.001$).

Table 3. Molecular characterisation of CTC by ddPCR.

Sample	Number of cells	Phenotype	MAF mutant *KRAS* by ddPCR
CTC-1	10	$CD45^{-}/Vim^{+}$	1.27
CTC-2	10	$CD45^{-}/Vim^{+}$	84.3
CTC-3	1	$CD45^{-}/E+/CK+/Vim^{+/-}$	78.4
Positive control	Pellet	Tissue	50.22
Negative control 1	10	CD45+	WT
Negative control 2	10	CD45+	WT
Negative control 3	10	CD45+	WT

metastatic lesions may have already been established even in patients with apparently curative resection and begun releasing CTCs themselves. Additionally, once overt metastasis is detectable, we show that a single EpCAM/vimentin co-expressing cell, representing a specific pEMT status, in treatment-naive patients is associated with a significantly worse overall survival. As previously described, we also did not detect differences in CTC total counts across PDAC stages, which may depict the aggressive nature of PDAC and its ability to metastasise from its onset.[2,26]

While most clinical correlates of adverse outcome were associated with pEMT-CTCs, we identified at least one parameter associated with the population of $Vim^{+}/EpCAM^{-}$ CTCs (M-CTC). This M-CTC sub-population was significantly higher at radiographic progression compared to non-progression in metastatic patients under treatment. CTCs predominantly expressing vimentin have been associated with a worse prognosis or aggressive disease in other cancer types[6,7] while vimentin only expressing CTCs are seen in rarer numbers in the context of PDAC.[5,25,26] Taken together with pEMT-CTCs as described above, the presence of these two populations may portend a dynamic picture of CTCs that exist in the spectrum of EMT and the ability for tumours to adapt to chemotherapeutic pressures.

Among weaknesses of our study, we understand the limits of our characterisation approach in that only a certain number of markers can be included within the Imagestream analysis. We attempted to maximise our approach by including as many conjugated markers as we could reliably and consistently use. As such, we are insightful of the fact that the markers selected may not necessarily be sensitive or specific enough to characterise the entire population of these CTC subtypes. For example, we could only include CD133 and Vimentin as markers to characterise 'stem cell-like" and mesenchymal populations, respectively. We believe that further studies should be able to take a more comprehensive approach to populations, like those of stem cells by including markers such as CD44, CD24, ALDH and RORγ.[29] Additionally, we have not fully characterised the size limit of our device in terms of its ability to isolate CTC clusters and thus feel it is important to interpret these results with caution.

In conclusion, our study identifies at least four distinct sub-populations of CTCs within a single blood draw of PDAC patients. Although such CTC subtypes have been previously described individually,[13,19] our study provides a comprehensive characterisation of such populations at baseline treatment naïve status and during longitudinal follow-up. Of all CTC sub-populations, we have isolated in PDAC through an antigen independent retrieval method, the pEMT phenotype showed the greatest predictive and prognostic value in both resectable and metastatic disease. The biological underpinnings of this pEMT sub-population warrants further study to understand the cellular mechanisms driving their aggressive potential and therapeutic resistance, particularly in contrast to M-CTCs. Our detailed phenotypic characterisation of CTCs is important as specific sub-populations, rather than total CTC number, in circulation may have greater clinical relevance and provide insights into treatment response.[20]

ACKNOWLEDGEMENTS

Not applicable.

AUTHOR CONTRIBUTIONS

A.M., P.A.G., H.A. Study Design: A.M., P.A.G., H.A., A.S., V.B., D.U.K. Provision of clinical samples and information: B.S., G.R.V., M.H.K. Samples processing: A.S., V.B., P.G., D.U.K. Microfluidics device design: P.G., F.A.S.L. Sample isolation: A.S., V.B., P.A.G., D.U.K., N.K. Samples staining and cytometry: A.S., V.B., P.A.G., D.U.K. Data analysis: J.H., F.A.S.L., J.J.L., W.Q., Y.S. P.A.G. Manuscript writing: A.S., V.B. All authors read and approved the final manuscript.

ADDITIONAL INFORMATION

Ethics approval and consent to participate The study was performed in accordance with standard ethical guidelines approved by the institutional review board (IRB), protocol numbers PA11-0670 and PA15-0014 at MD Anderson Cancer Center, and in accordance with the Declaration of Helsinki. Patients provided their informed consent to participate in this study.

Data availability All data generated and analysed during the current study are available from the corresponding author on reasonable request.

Competing interests A.M. receives royalties for a pancreatic cancer biomarker test from Cosmos Wisdom Biotechnology, and this financial relationship is managed and monitored by the UTMDACC Conflict of Interest Committee. A.M. is also listed as an inventor on a patent that has been licensed by Johns Hopkins University to Thrive Earlier Detection. The remaining authors declare no competing interests.

Funding information This research was supported in part by the Cancer Prevention and Research Institute of Texas (CPRIT) (No. RP160517), NCI P50 CA221707, U01 CA196403 and U01 CA200468 to A.M. N.K. was supported by the CPRIT Research Training Program (No. RP170067). V.B. was supported by the CPRIT Research Training Program (Nos. RP140106 and RP170067) and NCI (Nos. T32CA217789-03 and U54CA096297). J.J.L. was supported by the National Institutes of Health (NIH) (No. T32CA009599). A.S. was supported by the German Research Foundation (SE-2616/2-1). D.U.K. was supported by the National Research Foundation of Korea (NRF) grant funded by the Korea government (MSIT) (No. 2018R1C1B5086234).

Supplementary information The online version contains supplementary material available at https://doi.org/10.1038/s41416-021-01350-9.

Publisher's note Springer Nature remains neutral with regard to jurisdictional claims in published maps and institutional affiliations.

REFERENCES

1. Siegel, R. L., Miller, K. D. & Jemal, A. Cancer statistics. *CA Cancer J. Clin.* **69**, 7–34 (2019).
2. Rhim, A. D., Mirek, E. T., Aiello, N. M., Maitra, A., Bailey, J. M., McAllister, F. et al. EMT and dissemination precede pancreatic tumor formation. *Cell* **148**, 349–361 (2012).
3. Pecot, C. V., Bischoff, F. Z., Mayer, J. A., Wong, K. L., Pham, T., Bottsford-Miller, J. et al. A novel platform for detection of CK+ and CK− CTCs. *Cancer Discov.* **1**, 580–586 (2011).
4. Siravegna, G., Marsoni, S., Siena, S. & Bardelli, A. Integrating liquid biopsies into the management of cancer. *Nat. Rev. Clin. Oncol.* **14**, 531–548 (2017).
5. Wei, T., Zhang, X., Zhang, Q., Yang, J., Chen, Q., Wang, J. et al. Vimentin-positive circulating tumor cells as a biomarker for diagnosis and treatment monitoring in patients with pancreatic cancer. *Cancer Lett.* **452**, 237–243 (2019).
6. Satelli, A., Batth, I., Brownlee, Z., Mitra, A., Zhou, S., Noh, H. et al. EMT circulating tumor cells detected by cell-surface vimentin are associated with prostate cancer progression. *Oncotarget* **8**, 49329–49337 (2017).
7. Satelli, A., Brownlee, Z., Mitra, A., Meng, Q. H. & Li, S. Circulating tumor cell enumeration with a combination of epithelial cell adhesion molecule- and cell-surface vimentin-based methods for monitoring breast cancer therapeutic response. *Clin. Chem.* **61**, 259–266 (2015).
8. Chemi, F., Rothwell, D. G., McGranahan, N., Gulati, S., Abbosh, C., Pearce, S. P. et al. Pulmonary venous circulating tumor cell dissemination before tumor resection and disease relapse. *Nat. Med.* **25**, 1534–1539 (2019).
9. Nagrath, S., Jack, R. M., Sahai, V. & Simeone, D. M. Opportunities and challenges for pancreatic circulating tumor cells. *Gastroenterology* **151**, 412–426 (2016).
10. Kamyabi, N., Huang, J., Lee, J. J., Bernard, V., Semaan, A., Stephens, B. et al. A microfluidic device for label-free isolation of tumor cell clusters from unprocessed blood samples. *Biomicrofluidics* **13**, 044111 (2019).
11. DiPardo, B. J., Winograd, P., Court, C. M. & Tomlinson, J. S. Pancreatic cancer circulating tumor cells: applications for personalized oncology. *Expert Rev. Mol. Diagn.* **18**, 809–820 (2018).
12. Court, C. M., Ankeny, J. S., Sho, S., Hou, S., Li, Q., Hsieh, C. et al. Reality of single circulating tumor cell sequencing for molecular diagnostics in pancreatic cancer. *J. Mol. Diagn.* **18**, 688–696 (2016).
13. Lapin, M., Tjensvoll, K., Oltedal, S., Javle, M., Smaaland, R., Gilje, B. et al. Single-cell mRNA profiling reveals transcriptional heterogeneity among pancreatic circulating tumour cells. *BMC Cancer* **17**, 390 (2017).

14. Shim, S., Stemke-Hale, K., Tsimberidou, A. M., Noshari, J., Anderson, T. E. & Gascoyne, P. R. Antibody-independent isolation of circulating tumor cells by continuous-flow dielectrophoresis. *Biomicrofluidics* **7**, 11807 (2013).
15. Shim, S., Stemke-Hale, K., Noshari, J., Becker, F. F. & Gascoyne, P. R. Dielectrophoresis has broad applicability to marker-free isolation of tumor cells from blood by microfluidic systems. *Biomicrofluidics* **7**, 11808 (2013).
16. Gascoyne, P. R. & Shim, S. Isolation of circulating tumor cells by dielectrophoresis. *Cancers* **6**, 545–579 (2014).
17. Balasubramanian, P., Kinders, R. J., Kummar, S., Gupta, V., Hasegawa, D., Menachery, A. et al. Antibody-independent capture of circulating tumor cells of non-epithelial origin with the ApoStream(R) system. *PLoS ONE* **12**, e0175414 (2017).
18. Allenson, K., Castillo, J., San Lucas, F. A., Scelo, G., Kim, D. U., Bernard, V. et al. High prevalence of mutant KRAS in circulating exosome-derived DNA from early-stage pancreatic cancer patients. *Ann. Oncol.* **28**, 741–747 (2017).
19. Aktas, B., Tewes, M., Fehm, T., Hauch, S., Kimmig, R. & Kasimir-Bauer, S. Stem cell and epithelial-mesenchymal transition markers are frequently overexpressed in circulating tumor cells of metastatic breast cancer patients. *Breast Cancer Res.* **11**, R46 (2009).
20. Liu, H., Sun, B., Wang, S., Liu, C., Lu, Y., Li, D. et al. Circulating tumor cells as a biomarker in pancreatic ductal adenocarcinoma. *Cell Physiol. Biochem.* **42**, 373–382 (2017).
21. Alix-Panabieres, C. & Pantel, K. Challenges in circulating tumour cell research. *Nat. Rev. Cancer* **14**, 623–631 (2014).
22. Aiello, N. M. & Kang, Y. Context-dependent EMT programs in cancer metastasis. *J. Exp. Med.* **216**, 1016–1026 (2019).
23. Porter, R. L., Magnus, N. K. C., Thapar, V., Morris, R., Szabolcs, A. Neyaz, A. et al. Epithelial to mesenchymal plasticity and differential response to therapies in pancreatic ductal adenocarcinoma. *Proc. Natl Acad. Sci. USA* **116**, 26835–26845 (2019).
24. Ting, D. T., Wittner, B. S., Ligorio, M., Vincent Jordan, N., Shah, A. M., Miyamoto, D. T. et al. Single-cell RNA sequencing identifies extracellular matrix gene expression by pancreatic circulating tumor cells. *Cell Rep.* **8**, 1905–1918 (2014).
25. Gemenetzis, G., Groot, V. P., Yu, J., Ding, D., Teinor, J. A., Javed, A. A. et al. Circulating tumor cells dynamics in pancreatic adenocarcinoma correlate with disease status: results of the Prospective CLUSTER Study. *Ann. Surg.* **268**, 408–420 (2018).
26. Poruk, K. E., Valero, V. 3rd, Saunders, T., Blackford, A. L., Griffin, J. F., Poling, J. et al. Circulating tumor cell phenotype predicts recurrence and survival in pancreatic adenocarcinoma. *Ann. Surg.* **264**, 1073–1081 (2016).
27. Nieto, M. A., Huang, R. Y., Jackson, R. A. & Thiery, J. P. Emt: 2016. *Cell* **166**, 21–45 (2016).
28. Aiello, N. M., Maddipati, R., Norgard, R. J., Balli, D., Li, J., Yuan, S. et al. EMT subtype influences epithelial plasticity and mode of cell migration. *Dev. Cell* **45**, 681–95 e4 (2018).
29. Lytle, N. K., Ferguson, L. P., Rajbhandari, N., Gilroy, K., Fox, R. G., Deshpande, A. et al. A multiscale map of the stem cell state in pancreatic adenocarcinoma. *Cell* **177**, 572–86 e22 (2019).